UNIVERSITÉ DU LUXEMBOURG

PhD-FSTM-2021-023
The Faculty of Sciences, Technology and Medicine

DISSERTATION

Defence held on 26/04/2021 in Esch-sur-Alzette

to obtain the degree of

DOCTEUR DE L'UNIVERSITÉ DU LUXEMBOURG

EN SCIENCES DE L'INGÉNIEUR

by

Patrick PEREIRA DIAS
Born on 5th April 1990 in Luxembourg (Luxembourg)

DRY-STACKED INSULATION MASONRY BLOCKS BASED ON MISCANTHUS CONCRETE

Dissertation defence committee

Dr. Danièle WALDMANN, dissertation supervisor
Professor, Université du Luxembourg

Dr. Frank SCHOLZEN, Chairman
Professor, Université du Luxembourg

Dr. André LECOMTE, Vice – chairman
Professor, Université de Lorraine

Dr. Marc OUDJENE, Member
Professor, Université de Laval

Dr. Romain TRAUCHESSEC, Member
Université de Lorraine

ACKNOWLEDGMENT

The present thesis entitled “Dry-stacked insulation masonry blocks based on Miscanthus concrete” was elaborated during my PhD at the Faculty of Science, Technology and Medicine (FSTM) of the University of Luxembourg. The experimental tests were mainly carried out at the Laboratory of Solid Structures (LSS) of the University of Luxembourg. The realisation of the present work, as well as the writing and the defence were carried out in the period from the 1st September 2016 to the 30th April 2021.

First, I want to express my sincere gratitude to Prof. Dr.-Ing. Danièle Waldmann for offering me this unique opportunity for accepting me as a scientific collaborator in her research group. Furthermore, I want to thank her for the continuous guidance, the permanent availability, the trust put on my work, her professionalism including a lot of constructive advices and especially for her comprehension considering personal reasons.

Moreover, I my sincere thanks go also to my thesis supervision committee (CET), specifically Prof. Dr. –Ing. Frank Scholzen, Professor of Mechanical Engineering from the FSTM at the University of Luxembourg and Prof. Dr. –Ing. André Lecomte, Professor at the Department of Chemistry and Physics of Solids and Surfaces (Institut Jean Lemour) of the University of Lorraine for acting as Chairman respectively Vice-Chairman in my dissertation defence committee. Their remarks during our yearly meetings were very valuable and allowed me to improve my dissertation in different ways. Moreover, I also want to thank Prof. Marc Oudjene, Professor in the department of civil engineering from the

University of Laval (Québec, Canada) and Dr. Romain Trauchessec from the Department of Chemistry and Physics of Solids and Surfaces (Institut Jean Lemour) of the University of Lorraine for accepting to be part of the jury members of my defence.

Moreover, I am deeply thankful to the management board of Contern S.A., especially to Carlo Spina and Kahtan Watfa from Contern S.A. for the supply of the Miscanthus, the valuable feedback and the help in different experimental tests, which were very valuable to achieve my research goals. I would also like to express my gratitude to Zornitza Tosheva, Research specialist from the Department of Physics and Materials Science of the FSTM at the University of Luxembourg for supplying and help on the scanning electron microscopic analysis.

I am also very thankful to the support team from the structural laboratory of the University of Luxembourg, namely Gilbert Klein, Marc Seil, Claude Collé, Logan Freitas, Vicente Reis Adonis, Ed Weyer, Ken Adam, Markus Schlienz, Cédric Bruyère and Grace Ligbado for sharing their professional and private knowledge, which allowed me to distract from the daily work. I would like to express my deepest gratitude to Marc Seil and Gilbert Klein for their extremely amicable and beneficial help, their support to improve the tests and their flexibility to help and give precise and good advises. Furthermore, I would like to thank to the staff members of the University of Luxembourg for their administrative help, especially Marielle Mabille, Mike Hansen, Shayan Weber and Suzanne Biwer. I am also very thankful to the team of the informatics support, especially to Antoine Zoccolo, Clément Linnig and Mickael Pilato for their availability and their kindness.

I want also to express my deepest gratitude to my PhD and Post-doc colleagues, Dr. –Ing. Vishojit Bahadur Thapa, Dr. –Ing. Dolgion Erdenebat, Dr. –Ing. Michael Weiler, Dr. -Ing. Gael Chewe Ngapeya, Dr. –Ing. Laddu Bhagya Jayasinghe, Dr. –Ing. Thanh Tung Nguyen, Lorenc Bogoviku, Hooman Eslami, Tarik Camo and Sinan Kaassamani for the numerous laughing escapades, the very nice lunch breaks, the professional and private advices and the kindness giving throughout my PhD. You were all in a way or another important.

Moreover, I would like to thank the students Joe Steines, Michael Gonçalves Dantas, Yannick Zimmer, Mike Paulus, Elma Arifi, Vanessa Jesuino Kammer, Magdalena Ivanova, Fabienne Leclerc, Cristiano Monteiro, Céline Tavares, Kim Rech and Michel Almeida Silva for their active contribution to the success of this work through their semester projects, Bachelor and Master's theses under my personal supervision.

In particular, I want to thank all my friends, especially to Dany, Gil, Tiago, David and Sidnei. Furthermore, I would like to express my deepest gratitude to my parents and sister for their moral and unconditional support over many years. Without the happiness provoked by all of you, this work would

not have been possible. The deepest acknowledgment goes especially to my wife and our two young daughters Laura and Lydia. We had many difficult moments and it was very difficult for all of us, but with your help, I managed to conclude this work.

I really thank you all for the support in one way or the other!

Luxembourg, the 28th February 2021

Patrick Pereira Dias

ABSTRACT

The present dissertation entitled "Dry-stacked insulation masonry blocks based on Miscanthus concrete" is carried out at the University of Luxembourg and financed by CONTERN Lëtzebuerger Beton. The principal aim of this project is to valorise the sustainability in the construction sector and improve the circular economy by using Luxembourgish Miscanthus to produce a masonry block. The latter should include bearing and thermal properties. Besides, a dry-stacked system should be adopted. The imposed aims are reached by developing a masonry block based on two materials connected by a dovetail connection. Furthermore, a dry-stacked system is adopted using a horizontally and vertically tongue-groove system. The present research demonstrates the approach performed to achieve these goals.

The process to reach the described aims is divided in five major steps. The first step consists of an analysis on the needed amount of mixture components with the aim of achieving the highest possible load-bearing capacity of concrete based on Miscanthus aggregates. It can be concluded that the variation of the amount of components affects the density, which has an increasing parabolic relation with the load-bearing capacity of the specimens. Furthermore, the long-term deformations considering shrinkage of Miscanthus concrete achieve in average 2350 $\mu m/m$, which is the double of a lightweight concrete. However, comparing the long-term deformations of Miscanthus concrete with Hemp-concrete a benefit of at least 50 % can be considered.

Secondly, a machine-learning tool is applied to predict the compressive strength by introducing the mixture components and avoiding the need of creating time-consuming and costly experimental tests. Furthermore, it is possible to analyse the impact of each individual component on the load-bearing

capacity. This tool has the ability of optimising the mixture according to the needs in compressive strength.

Next, a Miscanthus concrete mixture is used to manufacture rectangular masonry blocks and an analysis on their geometrical height and roughness imperfections is performed experimentally and numerically on the load-bearing capacity of walls and single masonry blocks. The roughness was investigated by measuring the contact surface. Accordingly, an exponential relation is identified between the applied compressive strength and the contact surface. The height imperfections show a low impact on the load-bearing capacity of the wall. This statement is also validated in the numerical calculation. Finally, an increase of the relation height to length of a wall reduces linearly the maximum achieved compressive strength.

The next step consists of investigating the use of a Mycelium-Miscanthus composite for insulation purposes and analyse different properties. The scanning electron microscopic analysis allows investigating the bond between Mycelium and Miscanthus. It can be concluded that the Mycelium webs enter the Miscanthus fibre and holds in the way the specimen together. Furthermore, a density of 122 kg/m^3 and a thermal conductivity of 0.09 W/mK is measured in this bio composite, which is higher than a conventional insulation material. Besides, a fire resistance of category EI15 according to EN13501-2:2003 is measured. These results show a promising capacity of this composite as a building insulation.

The last phase of this project consists of creating an interaction between all the parts by applying the investigated material properties into one masonry block with a geometry able to be applied in a dry-stacked masonry wall. The latter is applied by introducing a horizontal and vertical tongue-groove system in the masonry block. This block is divided in two parts, a bearing and insulation material, which are connected by a dovetail connection. A sensitivity analysis is performed in the wall by varying different properties of the masonry block, such as the thickness of the bearing and the insulation part, the angle of the dovetail connection or the position of tongue-groove system. An increase of the width of the bearing part has an increasingly linear impact on the load-bearing capacity. However, an increase of the thickness of the insulation part does not show any impact on the maximum achieved compressive strength. Furthermore, the impact of the geometrical imperfections like height and roughness are analysed. Subsequently, the needed thickness of the masonry block is calculated based on the imposed thermal transmittance value. A total thickness of the masonry block of 77 cm was determined. Therefore, it can be concluded that the thermal conductivity of the insulation part has to be improved to reduce the needed thickness of the masonry block.

Finally, this thesis assesses the use of Miscanthus fibres in a masonry block, which has a bearing and insulation capacity. Furthermore, the tongue-groove system of the masonry block and the low Young's Modulus of the Miscanthus mixture allow its application in a dry-stacked wall in the construction sector.

Keywords – Miscanthus x giganteus; Miscanthus lightweight concrete; Pre-treatment of Miscanthus fibres; Compressive strength; Shrinkage; Machine learning; Gaussian process regression; Dry-stacked masonry; load-bearing capacity; roughness; contact surface; height differences; Mycelium; Thermal insulation; Bio-composite

KUERZFAASUNG

Dës Dissertatioun mam Titel "Dry-stacked insulation masonry blocks based on Miscanthus concrete" gëtt op der Uni Lëtzebuerg duerchgefouert a finanzéiert vun CONTERN Lëtzebuerger Beton. D'Haaptzil vun dësem Projet ass d'Nohaltegkeet am Bausecteur ze valoriséieren an d'kreeslafwirtschaft ze verbesseren andeems lëtzebuerger Miscanthus benotzt gëtt fir e Mauerblock ze produzéieren. Dësen soll droend a isolatiounsfähegkeeten enthalen. Ausserdeem sollt en dréchent gestapelt Mauersystem adoptéiert ginn. Déi imposéiert Ziler ginn erreecht duerch d'Entwécklung vun engem Mauerblock baséiert op zwee Materialien verbonne mat enger Schwalbenschwanzverbindung. Den dréchen gestapelt Mauersystem gëtt mat engem horizontale a vertikale Nut-Feder-System ugeholl. Déi aktuell Fuerschung demonstréiert d'Approche fir dës Ziler z'erreechen.

De Prozess fir déi beschriwwenen Ziler z'erreechen ass a fënnef Schrëtt gedeelt. Den éischte Schrëtt besteet aus enger Analyse iwwer déi néideg Quantitéit u Mëschungskomponenten mam Zil déi héchst méiglech Tragkraaft vu Beton op Basis vu Miscanthus Aggregaten z'erreechen. Et kann ofgeschloss ginn datt d'Variatioun vun der Menge u Komponenten d'Dicht beaflosst, déi eng wuessend parabolesch Relatioun mat der tragender Kapazitéit vun den Exemplairen huet. Ausserdeem erreechen déi laangfristeg Deformatiounen duerch d‘Schwinden vu Miscanthus Beton am Duerchschnëtt ëm 2350 $\mu m/m$, wat d'Duebelt vun engem Liichtbeton ass. Vergläicht een die laangfristeg Deformatiounen vu Miscanthus Beton mat Hanf-Beton, kann e Benefice vun op d'mannst 50% berécksiichtegt ginn.

Zweetens gëtt e Maschinneléiereinstrument ugewannt fir d'Kompressiounsstäerkt virauszesoen andeems d'Mëschungskomponente agefouert ginn. Dëst huet den Virdeel en Besoin un Zäitverbrauchend an deier experimentell Tester ze vermeiden. Ausserdeem ass et méiglech den Impakt vun all eenzel Komponent

op déi tragend Kapazitéit ze analyséieren. Dësen Tool huet d'Fäegkeet d'Mëschung ze optimiséieren je no de Bedierfnesser an der Drockkraaft.

Als nächstes gëtt eng Miscanthus Betonmëschung benotzt fir rechteckeg Mauerbléck ze fabrizéieren. Den Impakt vun hir geometresch imperfektiounen (Héicht a Rauegkeet) gëtt experimentell an numeresch op der tragender Kapazitéit vu Maueren an eenzege Mauerbléck analyséiert. D'Rauegkeet gët ënnersicht andeems d'Kontaktoberfläche gemoosst gët. Deementspriechend gëtt eng exponentiell Bezéiung tëscht der ugewandter Drockkraaft an der Kontaktfläch identifizéiert. D'Héichtenonreegelméissegkeeten weisen e klengen Impakt op d'Tragfähegkeet vun der Mauer. Dës Ausso gëtt och an der numerescher Berechnung validéiert. Schlussendlech reduzéiert eng Erhéijung vun der Bezéiung tëschent der Héicht an der Längt vun enger Mauer déi maximal erreechten Drockkraaft.

De nächste Schrëtt besteet aus der Untersuchung iwwer de Gebrauch vun engem Mycelium-Miscanthus Komposit fir Isoléierungszwecker a verschidden Eegeschaften ze analyséieren. D'Scannenelektronmikroskopesch Analyse erlaabt d'Verbond tëscht Mycelium a Miscanthus z'ënnersichen. Et kann ofgeschloss ginn datt d'Mycelium Weben an d'Miscanthus Faser erakommen an esou den specimen zesummen hält. Ausserdeem gëtt eng Dicht vun 122 kg/m^3 an eng Wärmeleedung vun 0,09 W/mK an dësem Biokomposit gemooss, wat méi héich ass wéi e konventionellt Isoléiermaterial. E Feierwidderstand vun der Kategorie EI15 geméiss EN13501-2:2003 gët an dem Biokomposit gemooss. Dës Resultater weisen eng villverspriechend Kapazitéit vun dësem Komposit als Gebaiisolatioun.

Déi lescht Phase vun dësem Projet besteet aus enger Interaktioun tëscht all Deeler ze kreéieren andeems d'ënnersicht Materialeegeschaften an ee Mauerblock mat enger Geometrie applizéiert ginn, déi an enger dréchen gestapelt Mauerwand applizéiert ka ginn. Déi lescht gëtt ugewannt andeems en horizontal a vertikal Nut-Feder-System am Mauerblock agefouert gët. Dëse Block ass an zwee Deeler opgedeelt, e Droenden an en Isoléierenden, déi duerch eng Schwalbenschwanzverbindung verbonne ginn. Eng Sensibilitéitsanalyse gëtt an der Mauer duerch verschidden Eegeschafte vum Mauerblock gemaach, wéi d'Déckt vum Droenden an d'Isolatiounsdeel, de Wénkel vun der Schwalbenschwanzverbindung oder der Positioun vum Nut-Feder-System. Eng Erhéijung vun der Breet vum Droenden deel huet d‘Auswierkung déi tragend Kapazitéit z‘erhéijen. Den Isolatiounsdeel awer weist mat enger Erhéijung vun der Déckt keen Impakt op déi maximal erreecht Drockkraaft. Ausserdeem gouf den Impakt vun de geometresche Onreegelméissegkeeten wéi Héicht a Rauegkeet analyséiert. Als läscht gëtt déi néideg Déckt vum Mauerblock berechent op Basis vum imposéierten Wärmedurchgangskoeffizient. Eng Gesamtdéckt vum Mauerblock vu 77 cm gouf festgeluecht. Dofir kann et ofgeschloss ginn datt d'Wärmeleitfäegkeet vum Isoléierungsdeel muss verbessert ginn fir déi néideg Déckt vum Mauerblock ze reduzéieren.

Schlussendlech beurteelt dës Dissertatioun d'Benotzung vu Miscanthus Faseren an engem Mauerblock deen Droend- an Isolatiounskapazitéiten huet. Den nidderegen E-Modul vun der Miscanthus Mëschung an d‘Nut-Feder-System vum Mauerblock erlaabt seng Uwendung an enger dréchen gestapelter Mauer am Bausecteur.

Schlësselwierder – Miscanthus x giganteus; Miscanthus liicht Beton; Virbehandlung vu Miscanthus Faseren; Drockkraaft; Schwinden; Maschinnel léieren; Gaussesche Prozess Regressioun; Dréchen gestapelt Mauerwierk; Tragfäegkeet; Rauegkeet; Kontakt Uewerfläch; Héichten Differenz; Mycelium; Isolatioun; Bio-Komposit

SOMMAIRE

Le présent mémoire intitulé "Dry-stacked insulation masonry blocks based on Miscanthus concrete" est réalisé à l'Université du Luxembourg et financé par CONTERN Lëtzebuerger Beton. L'objectif principal de ce projet est de valoriser la durabilité dans le secteur de la construction et d'améliorer l'économie circulaire en utilisant le miscanthus luxembourgeois pour produire un bloc de maçonnerie. Ce dernier devrait inclure des propriétés portantes et thermiques. En outre, un système de pose à sec devrait être adopté. Les objectifs imposés sont atteints par le développement d'un bloc de maçonnerie basé sur deux matériaux reliés par un assemblage à queue d'aronde. En outre, un système d'empilement à sec est adopté en utilisant un système de rainure et languette horizontale et verticale. La présente recherche démontre l'approche adoptée pour atteindre ces objectifs.

Le processus pour atteindre les objectifs décrits est divisé en cinq étapes. La première étape consiste en une analyse de la quantité nécessaire de composants du mélange dans le but d'obtenir la plus grande capacité portante possible du béton à base de granulats de miscanthus. On peut conclure que la variation de la quantité de composants affecte la densité, qui a une relation parabolique croissante avec la capacité portante des échantillons. En outre, les déformations à long terme en tenant compte du retrait du béton de miscanthus atteignent en moyenne 2350 $\mu m/m$, soit le double d'un béton léger. Cependant, en comparant les déformations à long terme du béton de miscanthus avec celles du béton de chanvre, on peut considérer un bénéfice d'au moins 50 %.

Ensuite, un outil d'apprentissage machinal est appliqué pour prédire la résistance à la compression en introduisant les composants du mélange. Ceci a l’avantage d’éviter la nécessité de créer des tests expérimentaux longs et coûteux. En outre, il est possible d'analyser l'impact de chaque composant

individuel sur la capacité de charge. Cet outil a la capacité d'optimiser le mélange en fonction des besoins en matière de résistance à la compression.

Ensuite, un mélange de béton au miscanthus est utilisé pour fabriquer des blocs de maçonnerie rectangulaires et une analyse de leurs imperfections géométriques (hauteur et rugosité) est effectuée expérimentalement et numériquement sur la capacité portante des murs et des blocs de maçonnerie seuls. La rugosité a été étudiée en mesurant la surface de contact. En conséquence, une relation exponentielle est identifiée entre la résistance à la compression appliquée et la surface de contact. Les imperfections en hauteur montrent un faible impact sur la capacité de charge du mur. Cette affirmation est également validée dans le calcul numérique. Enfin, une augmentation de la relation entre la hauteur et la longueur d'un mur réduit linéairement la résistance maximale à la compression.

L'étape suivante consiste à étudier l'utilisation d'un composite Mycélium-Miscanthus à des fins d'isolation et à analyser différentes propriétés. L'analyse au microscope électronique à balayage permet d'étudier la liaison entre le mycélium et le miscanthus. On peut conclure que les toiles de mycélium entrent dans la fibre de miscanthus et maintiennent l'échantillon ensemble. De plus, une densité de 122 kg/m^3 et une conductivité thermique de 0,09 W/mK sont mesurées sur ce composite biologique, ce qui est supérieur à un matériau d'isolation conventionnel. En outre, une résistance au feu de la catégorie EI15 selon la norme EN13501-2:2003 est mesurée. Ces résultats montrent une capacité prometteuse de ce composite en tant qu'isolant de bâtiment.

La dernière phase de ce projet consiste à créer une interaction entre toutes les parties en appliquant les propriétés des matériaux étudiés dans un bloc de maçonnerie avec une géométrie permettant l’application dans un mur de maçonnerie empilé à sec. Cette dernière est appliquée par l'introduction d'un système de rainure et de languette horizontal et vertical dans le bloc de maçonnerie. Ce bloc est divisé en deux parties, un matériau porteur et un matériau isolant reliés par un assemblage à queue d'aronde. Une analyse de sensibilité est effectuée sur le mur en faisant varier différentes propriétés du bloc de maçonnerie, telles que l'épaisseur de la partie porteuse et de la partie isolante, l'angle de la connexion en queue d'aronde ou la position du système de rainure et languette. Une augmentation de la largeur de la partie porteuse a un impact de plus en plus linéaire sur la capacité de charge. En revanche, une augmentation de l'épaisseur de la partie isolante n'a pas d'incidence sur la résistance maximale à la compression obtenue. En outre, l'impact des imperfections géométriques telles que la hauteur et la rugosité est analysé. Ensuite, l'épaisseur nécessaire du bloc de maçonnerie est calculée sur la base de la valeur de transmission thermique imposée par la norme. Une épaisseur totale du bloc de maçonnerie de 77 cm a été déterminée. On peut donc conclure que la conductivité thermique de la partie isolante doit être améliorée pour réduire l'épaisseur nécessaire du bloc de maçonnerie.

Enfin, cette thèse évalue l'utilisation des fibres de miscanthus dans un bloc de maçonnerie, qui a une capacité portante et isolante. De plus, le système languette-rainure du bloc de maçonnerie et le faible module de Young du mélange de miscanthus permettent son application dans un mur empilé à sec dans le secteur de la construction.

Mots clés – Miscanthus x giganteus; Béton léger au miscanthus; Prétraitement des fibres de miscanthus; Résistance à la compression; Retrait; Apprentissage machinal; Régression du processus gaussien; Maçonnerie empilée à sec; Capacité portante; Rugosité; Surface de contact; Différences de hauteur; Mycélium; Isolation thermique; Composite biologique

KURZFASSUNG

Die vorliegende Dissertation mit dem Titel "Dry-stacked insulation masonry blocks based on Miscanthus concrete" wurde an der Universität Luxemburg durchgeführt und von CONTERN Lëtzebuerger Beton finanziert. Das Hauptziel dieses Projekts ist es, die Nachhaltigkeit im Bausektor aufzuwerten und die Kreislaufwirtschaft zu verbessern, indem luxemburgischer Miscanthus zur Herstellung eines Mauersteins verwendet wird. Dieser soll tragende und thermische Eigenschaften aufweisen. Außerdem soll ein trocken gestapeltes System verwendet werden. Die auferlegten Ziele werden durch die Entwicklung eines Mauersteins erreicht, der auf zwei Materialien basiert, die durch eine Schwalbenschwanzverbindung verbunden sind. Darüber hinaus wird ein trocken gestapeltes System mit einem horizontalen und vertikalen Nut-Feder-System verwendet. Die vorliegende Arbeit demonstriert die Vorgehensweise zur Erreichung dieser Ziele.

Der Prozess zur Erreichung der beschriebenen Ziele ist in fünf Hauptschritte unterteilt. Der erste Schritt besteht aus einer Analyse der benötigten Menge an Mischungskomponenten mit dem Ziel, eine möglichst hohe Tragfähigkeit des Miscanthus-Betons zu erreichen. Es wurde festgestellt, dass sich die Variation der Menge der Komponenten auf die Dichte auswirkt, die einen parabolischen Zusammenhang mit der Tragfähigkeit der Probekörper aufweist. Weiterhin erreichen die Langzeitverformungen unter Berücksichtigung des Schwindens von Miscanthus-beton im Mittel 2350 $\mu m/m$, was dem Doppelten eines Leichtbetons entspricht. Vergleicht man jedoch die Langzeitverformungen von Miscanthus-Beton mit denen von Hanf-Beton, so kann man von einem Vorteil von mindestens 50 % ausgehen.

Zweitens wird ein Machine-Learning-Tool zur Vorhersage der Druckfestigkeit eingesetzt, indem die Mischungskomponenten eingeführt werden. Dies hat den Vorteil lange Erstellungszeit und

kostenintensive experimentelle Tests zu vermeiden. Darüber hinaus ist es möglich, den Einfluss jeder einzelnen Komponente auf die Tragfähigkeit zu analysieren. Dieses Werkzeug hat auch die Fähigkeit, die Mischung entsprechend den Anforderungen an die Druckfestigkeit zu optimieren.

Folgend wird eine Miscanthus-Betonmischung zur Herstellung von rechteckigen Mauersteinen verwendet. Eine Analyse der Auswirkung ihrer geometrischen Unregelmäßigkeiten (Höhe und Rauigkeit) wird experimentell und numerisch auf die Tragfähigkeit von Wänden und einzelnen Mauersteinen durchgeführt. Die Rauigkeit wurde durch Messung der Kontaktfläche untersucht. Demnach wird ein exponentieller Zusammenhang zwischen der aufgebrachten Druckfestigkeit und der Kontaktfläche identifiziert. Die Höhenunregelmäßigkeiten zeigen einen geringen Einfluss auf die Tragfähigkeit der Wand. Diese Aussage wird auch in der numerischen Berechnung bestätigt. Schließlich reduziert eine Vergrößerung des Verhältnisses Höhe zu Länge einer Wand die maximal erreichte Druckfestigkeit.

Der nächste Schritt besteht darin, die Verwendung eines Myzel-Miscanthus-Verbund für Dämmzwecke zu untersuchen und verschiedene Eigenschaften zu analysieren. Die rasterelektronenmikroskopische Analyse ermöglicht die Untersuchung der Bindung zwischen Myzel und Miscanthus. Es kann festgestellt werden, dass die Myzel-Vliese in die Miscanthus-Faser eindringen und so den Probekörper zusammenhalten. Weiterhin wird in diesem Bio-Verbundwerkstoff eine Dichte von 122 kg/m^3 und eine Wärmeleitfähigkeit von 0,09 W/mK gemessen. Diese ist jedoch höher als herkömmliche Dämmstoffe. Des Weiteren wird ein Feuerwiderstand der Kategorie EI15 nach EN13501-2:2003 gemessen. Diese Ergebnisse zeigen eine vielversprechende Kapazität dieses Bioverbunds als Gebäudedämmung.

Die letzte Phase dieses Projekts besteht darin, eine Interaktion zwischen allen Teilen zu schaffen, indem die untersuchten Materialeigenschaften in einem Mauerstein mit einer Geometrie angewendet werden, die in einer trocken gestapelten Mauer angewendet werden kann. Letzteres wird durch die Einführung eines horizontalen und vertikalen Nut-Feder-Systems in den Mauerstein erreicht. Der Mauerstein besteht aus zwei Einzelteilen, ein Trag- und ein Dämmmaterial, die durch eine Schwalbenschwanzverbindung verbunden sind. Es wird eine Sensitivitätsanalyse in der Wand durchgeführt, indem verschiedene Eigenschaften des Mauersteins variiert werden, wie z. B. die Dicke des Trag- und des Dämmstoffteils, der Winkel der Schwalbenschwanzverbindung oder die Position des Nut-Feder-Systems. Eine Vergrößerung der Breite des tragenden Teils hat einen zunehmend linearen Einfluss auf die Tragfähigkeit der Wand. Eine Erhöhung der Dicke des Dämmteils zeigt hingegen keinen Einfluss auf die maximal erreichte Druckfestigkeit. Weiterhin wird der Einfluss der geometrischen Unregelmäßigkeiten wie Höhe und Rauigkeit analysiert. Anschließend wird eine erforderliche Gesamtdicke des Mauersteins von 77 cm auf der Grundlage des vorgegebenen

Wärmedurchgangskoeffizienten berechnet. Daraus wurde geschlossen, dass die Wärmeleitfähigkeit des Dämmstoffs verbessert werden muss, um die erforderliche Dicke des Mauersteins zu reduzieren.

Schließlich wird in dieser Arbeit die Verwendung von Miscanthus-fasern in einem Mauerstein beurteilt, der eine Trag- und Dämmfähigkeit aufweist. Darüber hinaus ermöglichen das Nut-Feder-System des Mauersteins und der niedrige Elastizitätsmodul der Miscanthus-Mischung eine Anwendung als Trockenbauwand im Baubereich.

Schlüsselwörter – Miscanthus x giganteus; Miscanthus-Leichtbeton; Vorbehandlung von Miscanthus-Fasern; Druckfestigkeit; Schwinden; Maschine-learning; Gauß‘sche Prozessregression; Trockenmauerwerk; Tragfähigkeit; Rauigkeit; Kontaktfläche; Höhenunterschiede; Myzel; Wärmedämmung; Bio-Verbundstoff

RESUMO

A presente dissertação intitulada “Dry-stacked insulation masonry blocks based on Miscanthus concrete” foi realizada na Universidade do Luxemburgo e financiada pela CONTERN Lëtzebuerger Beton. O objetivo principal deste projeto é valorizar a sustentabilidade no setor da construção e melhorar a economia circular, usando Miscanthus produzido no Luxemburgo para produzir blocos de alvenaria. Este último deve incluir propriedades com capacidade de carga e térmicas. Além do mais, deve ser adotado um sistema de empilhamento a seco. Estes objetivos serão alcançados através do desenvolvimento de um bloco de alvenaria composto por dois materiais e ligados por uma cauda de andorinha (“dovetail connection”). Também pretende-se adotar um sistema de empilhamento a seco, utilizando um sistema de entalhe horizontal e vertical. A presente pesquisa demonstra a abordagem realizada para atingir esses objetivos.

O processo para atingir os objetivos descritos está dividido em cinco etapas principais. A primeira etapa consiste numa análise da quantidade necessária de componentes de mistura, com o objetivo de alcançar a maior capacidade de carga possível de betão com base em agregados de Miscanthus. Pode concluir-se que a variação da quantidade de componentes afetou a densidade assemelhando-se a uma parábola em relação à capacidade de carga das amostras. Além disso, as deformações a longo prazo considerando a retração do betão Miscanthus atingem em média 2350 $\mu m/m$, que é o dobro de um betão leve. No entanto, comparando as deformações de longo prazo do betão Miscanthus com o betão cânhamo, pode ser considerado um benefício de pelo menos 50%.

Em segundo lugar, uma máquina de aprendizagem é aplicada para prever a resistência à compressão, introduzindo os componentes da mistura e evitando a necessidade de criar testes experimentais

demorados e dispendiosos. Além disso, é possível analisar o impacto de cada componente individual na capacidade de carga. Esta ferramenta tem ainda a capacidade de otimizar a mistura de acordo com as necessidades de resistência à compressão.

Em seguida, uma mistura de betão Miscanthus é usada para fabricar blocos de alvenaria retangulares e uma análise das suas imperfeições geométricas e rugosidade é realizada experimental e numericamente sobre a capacidade de carga de paredes e blocos de alvenaria simples. A rugosidade foi investigada através da medição da superfície de contato. Consequentemente, é identificada uma relação exponencial entre a resistência à compressão aplicada e a superfície de contato. As imperfeições de altura mostram um baixo impacto na capacidade de carga da parede. Esta afirmação também é validada no cálculo numérico. Finalmente, um aumento da relação altura-comprimento de uma parede reduz linearmente a resistência à compressão máxima alcançada.

O próximo passo consiste em investigar o uso de um compósito Micélio-Miscanthus para fins de isolamento e analisar as diferentes propriedades. A análise microscópica eletrônica de varrimento permite investigar a ligação entre o Micélio e Miscanthus. Conclui-se que as teias de micélio entram na fibra de Miscanthus e prendem o espécime no seu conjunto. Além disso, uma densidade de 122 kg/m^3 e uma condutividade térmica de 0,09 W/mK é medida neste compósito, que é maior do que um material de isolamento convencional. Também é medida uma resistência ao fogo da categoria EI15 de acordo com EN13501-2:2003. Estes resultados mostram uma capacidade promissora desse compósito como isolante de edifícios.

A última fase deste projeto consiste em criar uma interação entre todas as partes, aplicando as propriedades do material investigado num bloco de alvenaria com uma geometria passível de ser aplicada em uma parede de alvenaria empilhável a seco. Esta última é aplicada através da introdução de um sistema de um sistema horizontal e vertical de entalhes no bloco de alvenaria. Este mesmo bloco é dividido em duas partes, uma parte de apoio e outra de isolamento, que são conectados por uma ligação em cauda de andorinha. É realizada uma análise de sensibilidade na parede variando diferentes propriedades do bloco de alvenaria, como a espessura da parte de portadora e da parte de isolamento, o ângulo da conexão da cauda de andorinha ou a posição do sistema de encaixe de entalhes. Um aumento da largura da parte portadora tem um impacto crescente linear na capacidade de suporte de carga. No entanto, um aumento da espessura da parte de isolamento não mostra qualquer impacto na resistência à compressão máxima alcançada. Além disso, o impacto das imperfeições geométricas como a altura e rugosidade é analisada. Subsequentemente, a espessura necessária do bloco de alvenaria é calculada com base no valor de transmitância térmica imposta pela norma. Foi determinada uma espessura total do bloco de alvenaria de 77 cm. Portanto, pode-se concluir que a condutividade térmica da parte de isolamento deve de ser melhorada para reduzir a espessura necessária do bloco de alvenaria.

Finalmente, esta tese avalia a utilização de fibras de Miscanthus em um bloco de alvenaria, que possui capacidade de carga e isolamento. Para além disso, o sistema de entalhes do bloco de alvenaria e o baixo módulo de elasticidade da mistura de Miscanthus permitem a sua aplicação numa parede empilhável a seco no setor da construção.

Palavras-chave – Miscanthus x giganteus; betão leve Miscanthus; Pré-tratamento de fibras de Miscanthus; Resistência à compressão; Encolhimento; Aprendizagem maquinal; Regressão do processo Gaussiano; Alvenaria empilhável a seco; capacidade de carga; rugosidade; superfície de contato; diferenças de altura; Micélio; Isolamento térmico; composto biológico

TABLE OF CONTENTS

For

My wife

&

children

For

My parents

&

Sister

Chapter 1 GENERAL

1.1 MOTIVATION

The atmosphere layer is being reduced more and more due to the high amount of produced greenhouse gases, which consist mostly of methane (CH_4), nitrous oxide (N_2O) and carbon dioxide (CO_2). According to different sources, the construction sector is responsible for 39 % of the worldwide CO_2 emissions and 36 % of the energy used in the Globus. Therefore, the need to increase the sustainability in the construction sector is urging more and more to reduce the CO_2 emissions and the huge energy consumption.

The highest impact of the CO_2 emissions from the construction sector are based on extraction, processing, manufacturing and transportation of building materials. Multitudes of studies are being performed to reduce the consumption of energy and the CO_2 emissions. One solution to achieve this aim is to diminish the use of raw and non-renewable resources like sand and gravel in concrete. Due to their substantial exploitation, the available resources are decreasing considerably. Furthermore, strict governmental regulations are constraining the opening of new quarries and forcing a big change in construction activities. Accordingly, in Europe a directive is proposed to achieve a zero net carbon emission in 2050, known as the European Green Deal, which aims to accomplish a sustainable EU economy in the construction sector.

One solution to this problem is the use of natural resources in the building sector, which would reduce the environmental footprint, the energy use and the carbon emissions. The filler of a concrete could be replaced by a plant-based filler with good acoustic and thermal properties. In the present work, the C_4- plant Miscanthus is used to replace sand and gravel in concrete creation.

Miscanthus is a sustainable solution to be used as filler and very interesting due to its properties. It can grow up to 4 m with a high yield and has a very low need of fertilisation and pesticide input. Due to its phytoremediation, this plant contributes to a depollution of industrial wasteland. The water use of Miscanthus contributes to a surface stabilisation of the soil and in the meantime prevents soil erosion, water movement or metal transportation due to wind. In addition to its positive impact on biodiversity, it has an advantageous CO_2 balance comparing to the extraction of raw or non-renewable materials. Furthermore, this plant can grow under European climate, which encourages a circular economy. All the presented assets cause the Miscanthus plant to be very interesting economically and ecologically.

1.2 SCOPE AND AIMS

The main focus of this research work is to develop a sustainable masonry block based on Miscanthus fibres. The masonry block should have a bearing capacity and good thermal properties to achieve the thermal transmittance value of U = 0.13 W/m^{2}K imposed by the "Règlement grand-ducal du 23 juillet 2016 modifiant le Règlement grand-ducal du 30.11.2007 concernant la performance énergétique des bâtiments d'habitations" based on the European directive 2010/31/UE. In the presented research work, the value of U = 0.13 W/m^{2}K is aimed using two materials in one masonry block connected by a dovetail connection. One material comprises the bearing capacity and the other thermal properties. Furthermore, no mortar should be applied in the joints of the masonry blocks. Therefore, a modular principle is used by adapting the geometry of the masonry blocks.

The approach to achieve the presented aims is divided in several phases. First, a bearing material based on Miscanthus is analysed by varying its components and aiming for the highest load-bearing capacity in prisms (4x4x16 cm) and cubes (15x15x15 cm). Next, all the experimental results are bundled and the experimentally achieved load-bearing capacity is optimised using a machine learning tool. In the following, a rectangular masonry block (40x20x10 cm) is created and the load-bearing capacity is analysed, as well as the height differences and the roughness of the masonry blocks. Finally, a material based on Mycelium and Miscanthus fibres is investigated to be used as the thermal part of the masonry block.

Furthermore, it has to be specified that the techniques and analysis presented in this research work are limited to the used materials. Identical results cannot be guaranteed if similar materials are used. In this case, a new investigation should be performed and compared to the actual results to verify their accordance.

1.3 CONTENTS AND STRUCTURE OF THE THESIS

This doctoral thesis is based on an accumulation of four publications. During the writing preparation of the present work, one publication is accepted and peer-reviewed and three are submitted in top-ranked journals. A general overview of the ten chapters of this thesis is shown in **Fig. 1-1**. **Chapter 1** and **Chapter 2** are based on an introduction to the present thesis. In **Chapter 1**, the motivation, the objectives and the structure of the thesis are presented to give a shorten vision of the whole work. Furthermore, the title of the four publications are given and a coherence between the different publications is performed. **Chapter 2** consists of an introduction to the analysis performed in the framework of this thesis.

Chapter 3 comprises a literature review on the raw materials as well as on the techniques and principles used. The first part of this chapter analyses the Miscanthus plant in detail and compares it to different Miscanthus species and their respective use in different sectors. Next, the fibrous concrete is analysed by investigating different fibrous materials in a cementitious matrix. Besides, a study on Mycelium is performed by analysing the fungus and listing different species as well as the use of Mycelium for insulation purposes. Thereafter, a general overview of masonry blocks is presented as well as their use in a dry-stacked wall and their connection to an insulation material. This chapter is concluded with a section analysing the application of Machine learning in the definition and optimisation of a concrete mixture.

Chapter 4 reflects the published content of the research paper entitled as “Optimisation of the mechanical properties of Miscanthus lightweight concrete”.

Chapter 5 presents the submitted research paper entitled as “Machine learning in mix design of Miscanthus lightweight concrete”.

Chapter 6 reflects the second submitted research paper entitled as “Analysis of the geometrical imperfections of a dry-stacked masonry block based on Miscanthus”.

Chapter 7 presents the second accepted research paper entitled as “Investigation of Mycelium-Miscanthus composites as building insulation material”.

In **Chapter 8** the application of a masonry block consisting of a bearing and insulation part and connected with a dovetail connection is numerically analysed on a dry-stacked wall. The geometry and the wall dimensions are varied and the impact on the load-bearing capacity is analysed.

The two last sections **Chapter 9** and **Chapter 10** consists of a conclusion of the whole work and an outlook for possible future research works.

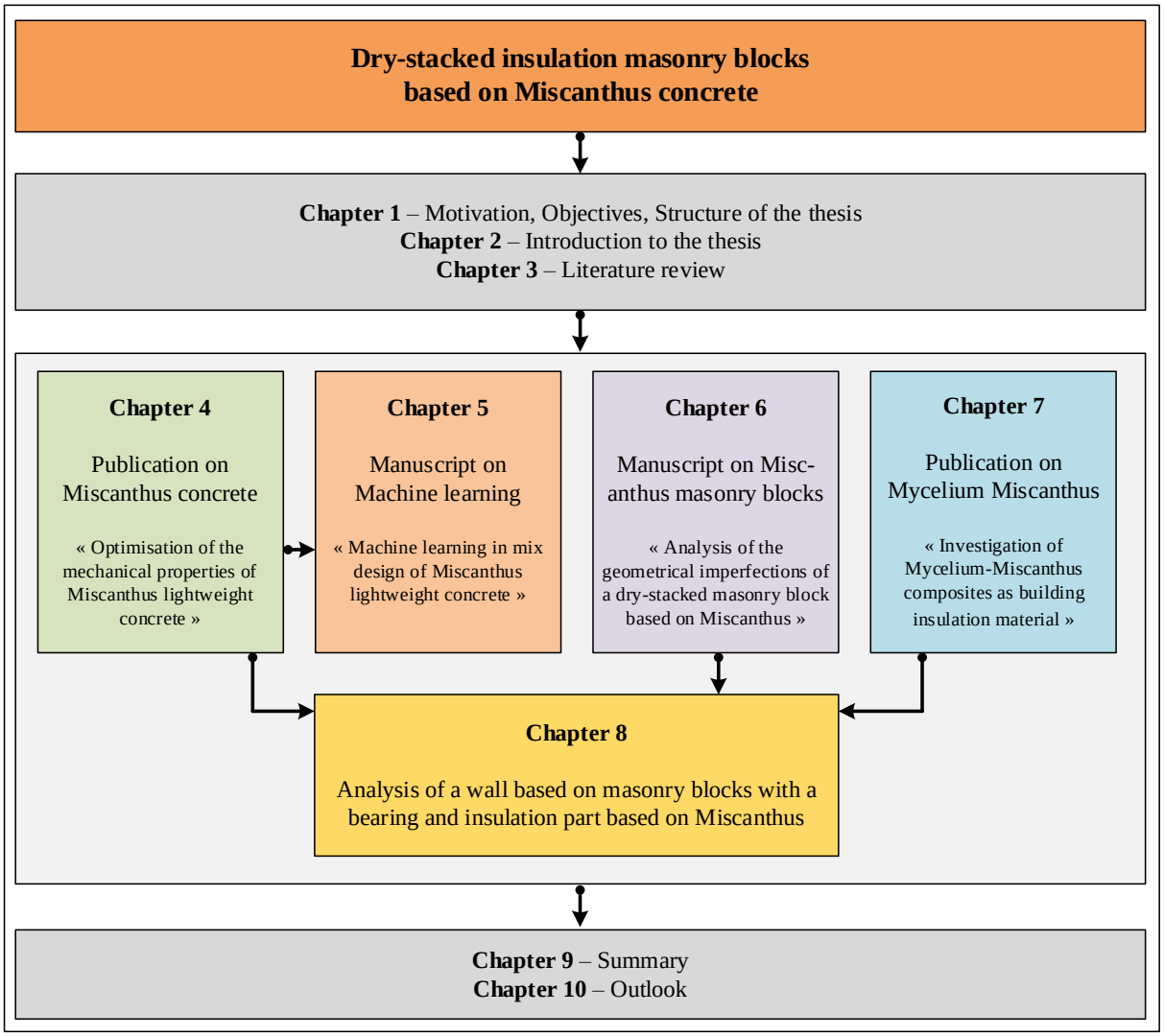

Fig. 1-1: General overview of the thesis' structure

1.4 PRESENTATION OF THE RESEARCH PAPERS AND THE LINKS BETWEEN EACH PUBLICATION

In this section, the principal points of the four publications are presented. As previously stated, currently one research paper is published and the three others are submitted and under review. The research paper "Optimisation of the mechanical properties of Miscanthus lightweight concrete" was published in the journal Construction and Building materials in October 2020 under following direct link: https://doi.org/10.1016/j.conbuildmat.2020.119643. Finally, a link between the research papers and the objective of the current research work is stated.

1.4.1 PUBLICATION ON MISCANTHUS MIXTURES

The first research paper entitled as "Optimisation of the mechanical properties of Miscanthus lightweight concrete" consists of analysing different lightweight concrete mixtures based on Miscanthus fibres. The mixtures were based on seven components, which includes the Miscanthus fibres, cement, a silicate sealant and water. The optimisation of the mix was performed by varying the amount of Miscanthus, cement and water/cement ratio. The load-bearing capacity of all the mixes was analysed on prisms and cubes. Furthermore, the impact of a pre-treatment of the Miscanthus fibres, prior to use, is analysed on the load-bearing capacity and on the long-term deformations using shrinkage drains. In addition, an SEM analysis is performed on the Miscanthus fibres and on the solid lightweight concrete based on Miscanthus fibres to analyse their microstructure and the impact of the different variations. Finally, the Young's Modulus is calculated using the measured compressive strength and density of each specimen.

The highest load-bearing capacity of 19.3 MPa was reached by prisms based on the mixture using pre-treated Miscanthus fibres and with a W/C ratio of 0.8. The calculated Young's Modulus was of 9.9 GPa and the shrinkage drains achieved a long-term deformation of 2244 $\mu m/m$ after a curing time of 480 days. Furthermore, the load-bearing capacity showed to be very dependent on the analysed shape of the specimen.

1.4.2 MANUSCRIPT ON MACHINE LEARNING

The second manuscript entitled "Machine learning in mix design of Miscanthus lightweight concrete" aims to predict the compressive strength of a Miscanthus lightweight concrete using a machine-learning tool. In this work, the algorithm of Gaussian process regression is used. The prediction performed by this approach is based on ten input variables and one output variable, the compressive strength. The input data consists of six mix constituents of concrete, water/cement ratio, pre-treatment condition of Miscanthus fibres, curing time and form of specimen. This input data was based on experimental data and was introduced along with the achieved compressive strength in the regression learner. 414 sets, consisting of the input and the output variables, were used in the Gaussian process regression.

Different kernel functions can be adopted in the Gaussian process regression. Therefore, using the predicted compressive strength a comparison between the squared exponential and the rational quadratic kernel function was performed. The latter showed to be more accurate and with a minimum of errors considering the predicted compressive strength.

Furthermore, a graphical user interface created in MATLAB was created. The advantage of this app is the possibility of predicting the compressive strength of Miscanthus lightweight concrete by introducing

the input data. This technique allows the user to optimise the mixture by varying the components and avoid costly experimental analysis.

1.4.3 MANUSCRIPT ON MISCANTHUS MASONRY BLOCKS

The third manuscript consists of the submitted research paper entitled as “Analysis of the geometrical imperfections of a dry-stacked masonry block based on Miscanthus”. In this manuscript, masonry blocks based on Miscanthus lightweight concrete are analysed as well as their suitability to be used in dry-stacked walls. Since the publication on Miscanthus mixtures (previous section) concluded that the load-bearing capacity was shape-dependent, this manuscript starts with an analysis on the compressive strength of the masonry blocks based on different mixture composition and procedure. Furthermore, the contact area of the blocks is analysed at different loads using a two-sheet paper (FUJIFILM). Next, a dry-stacked masonry wall of 80 x60 cm is built and the load-bearing capacity as well as the contact surfaces are analysed. In addition, the height differences of the masonry blocks are measured.

A load-bearing capacity of 5.42 MPa was achieved by the masonry block based on the mixture with a W/C ratio of 0.7 and an adapted mixture procedure. The gradual loading of a masonry block allowed concluding that an exponential relation could be established between the contact area and the applied load. The small wallets achieved a load-bearing capacity of 4.84 MPa and no sudden failure or the wall could be observed, which is very advantageous considering safety aspects.

Furthermore, a sensitivity analysis on the material properties is performed on a numerical model validated by the experimental results. The numeric model allowed studying different aspects considering the height differences and roughness imperfections. Due to the very low height differences of the masonry blocks, the load-bearing capacity was in average reduced by only 2.5 %. However, the roughness had a higher impact on the achieved compressive strength, which was reduced by a maximum of 31 %. Finally, it could be concluded that due to the low Young’s Modulus of lightweight concrete based on Miscanthus, the masonry block are suitable to be used on a dry-stacked masonry wall.

1.4.4 PUBLICATION ON MYCELIUM MISCANTHUS INSULATION

The second accepted paper is entitled “Investigation of Mycelium-Miscanthus composites as building insulation material”. The main objective of this paper is to achieve an insulation material based on Miscanthus. Therefore, a composite based on a self-growing Mycelium and Miscanthus is analysed. Due to the low density of the bio-composite, a low thermal conductivity is expected. Furthermore, the use of these biomaterials contributes to reduce the environmental footprint of a building insulation used in the construction sector.

The analysis starts with a variation of the proportions of the Miscanthus and Mycelium to determine the composite with the lowest density. Furthermore, a microscopic analysis is performed using scanning electron microscopy to identify the geometry of the Mycelium in the composite and the bond between Mycelium and Miscanthus. In addition, the quality of this material was assessed measuring its thermal conductivity, which achieved values between 0.0882 and 0.104 W/mK, its compressive strength and water absorption. Furthermore, a render was applied on the bio-composite and the fire resistance was measured on composites with and without render. According to the standard EN13501-2:2003, the material could be categorised into the category of EI 15. Finally, using the presented results it could be concluded that the joint between Miscanthus and Mycelium was suitable to be used as a sustainable insulation material in the construction sector.

1.5 COHERENCE BETWEEN THE PAPERS AND THE OBJECTIVES

The main objective of this dissertation is to analyse the suitability of using Miscanthus as a bearing and insulation masonry block on a dry-stacked wall. First, the bearing part of the masonry block is analysed by investigating the load-bearing capacity of Miscanthus lightweight concrete. This is performed in detail in the publication on Miscanthus mixtures, where the highest load-bearing capacity is aimed. Next, the manuscript on Machine learning was created using all the data on the prisms and cubes based on different mixtures. This manuscript allowed predicting and improving the load-bearing capacity of a prism or cube after a specific curing time. However, the prediction performed in the manuscript on Machine learning was limited on prismatic and cubic shapes. Therefore, a precise mixture analysis based on the results from the publication on Miscanthus mixtures was performed for the masonry blocks in the manuscript on Miscanthus masonry blocks. The fourth manuscript on Mycelium Miscanthus insulation was performed to analyse the suitability of this composite as the insulation part of the principal objective of this thesis, which was the masonry block based on Miscanthus with bearing and insulation capacities.

Chapter 2 INTRODUCTION

Concrete is the most used material in the building sector. Currently most structures in constructions either contain environmentally harmful components or are made of non-renewable resources. The concrete production contributes to up to 8 % of the global CO_2 emissions. Furthermore, the high rate of extraction of raw materials, water consumption and transport lead to a negative environmental impact. These statistics reveal the need for innovative and sustainable building materials for different kinds of structural applications.

The European Parliament pushes the realisation of these concepts by issuing the directive 2010/31/EU of 19 May 2010 on the energy performance of buildings, which requests that by 31st December 2020 all new building have to meet the conditions of a nearly zero-energy building. Luxembourg also adopted this directive in the national regulation "Règlement grand-ducal du 23 juillet 2016 modifiant le Règlement grand-ducal du 30.11.2007 concernant la performance énergétique des bâtiments d'habitations" and limited the heat transfer coefficient for exterior walls with insulation to 0.13 W/m^{2}K for nearly zero-energy residential buildings. These requirements obliged the construction and manufacturing industries to adopt a new sustainable way of thinking. Furthermore, the action plan presented by the European Green deal to achieve by 2050 a zero net emissions of greenhouse gases proposes different strategies, such as deconstruction, circular economy and the use of environmental-friendly technologies and products.

Currently many investigations and experiments are carried out to achieve these targets by increasing the attractiveness and the use of "green" and organic materials. A very promising organic material is the Miscanthus x giganteus plant, due to its high yield, good biomass, low greenhouse gas emissions and low need for fertilizers during its growth period. Therefore, in this work the potential of masonry blocks based on Miscanthus lightweight concrete is studied. The Miscanthus fibres in the matrix act as a

reinforcement of the lightweight concrete. Furthermore, due to the connection between the fibres and the matrix, the fibres prevent a brittle failure of the block, which is very interesting considering safety aspects.

The main objective of this dissertation consists of developing a masonry block based on Miscanthus lightweight concrete with a thermal transmittance value, preferably, below 0.13 W/m^2K. Therefore, the approach of using two parts based on different materials and connected by a dovetail connection has been investigated. One part consists of a bearing material based on Miscanthus lightweight concrete. This part is designed as structural element to support the vertical loads. The second part, which is connected by a dovetail connection to the first part, should have good insulation properties and has the highest impact on the aimed low thermal transmittance value. Furthermore, the geometry of the masonry blocks are adapted for a modular building following the concept of design for deconstruction. This concept has the advantage of reducing the need for a component like cement mortar in the joints. In addition, it has among others the advantages of increasing the construction speed, which reduces the labour cost, and reducing the material waste in the construction site. These advantages cause the construction based on modular principal to be environmentally friendly and sustainable.

The approach to achieve the main objective of this dissertation is divided in four steps. First, a mixture based on Miscanthus lightweight concrete is experimentally investigated. The aim of this step is to achieve the highest possible load-bearing capacity and simultaneously use the highest amount of Miscanthus. Therefore, the different components of the mixture are varied and their impact on the load-bearing capacity is analysed. Furthermore, all relevant parameters of the mixture, such as the components, the curing time or the pre-treatment of Miscanthus were implemented in a Machine-learning tool to optimise and improve the mixture considering the compressive strength.

Secondly, masonry blocks with a rectangular geometry (40x20x10 cm) were produced and analysed to investigate the suitability of the previously defined mixtures in a masonry block shape. This was performed on a single masonry block and on a dry-stacked wall. Furthermore, the impact of the geometrical imperfections, like roughness and height differences, on the load-bearing capacity was analysed experimentally and numerically. The non-linear numerical model was first calibrated based on the experimental tests of the single masonry block and the dry-stacked wall. Next, a sensitivity analysis to analyse the impact on the achieved compressive strength was performed on the numerical model of the single masonry block by varying among others the material laws and the roughness. The height differences of the masonry blocks were implemented in the numerical wall. Furthermore, different dimensions of the wall were investigated to analyse their impact on the load-bearing capacity of the system.

The third part of the dissertation was focused on the elaboration of an insulation material based on Miscanthus. Therefore, Miscanthus fibres were merged with Mycelium and their application as an insulation was analysed. First, the suitability of the junction between Mycelium and Miscanthus was investigated by varying the components used. Next, the impact of the starch used in the mixture is examined. The spider web structure of the connection between the Mycelium and the Miscanthus is analysed using a scanning electron microscopy (SEM). Next, the compressive strength and water absorption capacity of the specimens is approached. Finally, the most important step of this part of the study is the analysis of the thermal conductivity of the bio-composite and its fire resistance.

The fourth and last step of this research is the combination of the previous created steps. First, the geometrical shape of the masonry block considering the modular principle was numerically generated with the bearing and the insulation part of the masonry block connected by a dovetail connection. Next, a dry-stacked masonry wall is generated and a parameter analysis on the geometry of the single masonry block is performed by varying the thickness of both parts and analysing their impact on the load-bearing capacity. Finally, an analysis on the height of the wall in relation to the thickness of the masonry block is created and their impact on the achieved compressive strength is investigated.

Chapter 3 LITERATURE REVIEW

The literature review is divided in five major parts. It starts with an analysis on the Miscanthus, where different species are approached and the similarity to hemp is stated. Next, fibrous concrete is analysed making a difference between non-sustainable and sustainable fibres. One of the most important advantages of the fibres in a cementitious matrix is their action as a reinforcement, which forces the failure of a specimen to be ductile, as can be noticed in **Fig. 3-1**. This is followed by an investigation on the numerous species of Mycelium and an examination is performed on the Ganoderma resinaceum. This section is finalised by approaching the existent composites between Mycelium and sustainable fibres.

Thereafter, the masonry blocks are treated by starting with generalities and continuing to a connection between a bearing and an insulation material to constitute a masonry block, whose application is first analysed on a conventional wall and next on a dry-stacked wall. The latter will be discussed according to the existing system and the drawbacks due to roughness and height imperfections. Finally, the application of machine learning tools is analysed and more precisely in the engineering sector to predict different properties from concrete mixtures.

Fig. 3-1: Fractured specimen showing the ductile failure behaviour of Miscanthus lightweight concrete

3.1 MISCANTHUS

The C-4 plant Miscanthus will be discussed in the following section starting by a general overview of the different species and leading to a detailed discussion about Miscanthus x giganteus. Furthermore, the similarities between the Miscanthus x giganteus and hemp will be presented.

3.1.1 SPECIES OF MISCANTHUS

The name Miscanthus was defined in 1856 by Andersson. According to the European conception, the genus Miscanthus is subdivided in 17-20 different species, primary native from Southeast Asia [1]. Due to their high biomass, Miscanthus x giganteus, Miscanthus sacchariflorus, Miscanthus sinensis, Miscanthus condensatus and Miscanthus floridulus are very interesting for breeding [2]. The genesis of Miscanthus x giganteus, which contains 57 chromosomes, was generated by a random crossbreeding in Japan between Miscanthus sacchariflorus, with 76 chromosomes, and Miscanthus sinensis with 36 chromosomes [1].

Miscanthus is also widely used due to its high power source. Its energy is usually extracted by gas extraction, liquidation or incineration. The latter are mostly used in Austria, where a decentralised heating is preferred [3] and a specific cases a mobile ash grate for Miscanthus is attached to these boilers [4]. In England, Miscanthus is also used in central heating and can reach a power of up to 2-5 MW [5].

Pude [2] analysed the morphological differences between the four Miscanthus species, Miscanthus x giganteus, Miscanthus sacchariflorus, Miscanthus sinensis and Miscanthus. Robustus. He compared the height of the stem, its diameter the amount of leaves per stem and the bulk density. The Miscanthus x

giganteus species showed to achieve the highest stem dimensions with the lowest amount of leaves and the lowest bulk density of 91.7 kg/m^3. Furthermore, Pude [2] also analysed physical parameters of Miscanthus lightweight concrete by using distinctively the four species of Miscanthus. Here anew the Miscanthus x giganteus species achieved the highest load-bearing capacity of 0.74 MPa. Since, the aim of this work is to use the Miscanthus fibres as an aggregate for lightweight concrete, the species Miscanthus x giganteus is chosen for further development.

3.1.2 MISCANTHUS X GIGANTEUS

3.1.2.1 MORPHOLOGY OF MISCANTHUS X GIGANTEUS

The crossbreeding plant Miscanthus x giganteus was imported from Japan to Denmark in the 1930s by the plant collector Aksel Olsen [6]. About 30 years later several debates were conducted to create a Miscanthus production in Denmark for the cellulose industry, where the main problem constituted in generating a suitable propagation method for the establishment of larger stocks. Later the Miscanthus x giganteus plants was spread in Europe by the Institute of Landscape Plants in Hornum as a new renewable raw material [2]. Nowadays, it is widely used in different environments like riverbanks, volcanic deserts, mountain areas and agricultural land. However, since it is a recent species in Europe the cultivation and use of this species is still being adapted [7].

During the past 15 years, the tall perennial grass Miscanthus x giganteus is extensively planted in Europe. The cultivation of this plant is based on rhizomes (**Fig. 3-2**), which are plant at a depth of 2-5 cm. It can be planted in autumn or spring. However, both seasons could kill the plant, one is the cold winter and the other one can be the drought. Nowadays, it is usually performed in spring because in case of drought the rhizomes can be irrigated. 3-4 weeks after cultivation, the rhizomes start budding and 3-4 weeks later the first leaves start to show up.

Fig. 3-2: Rhizome of Miscanthus x giganteus [8]

During the first year, the Miscanthus x giganteus plant will only grow 70-100 cm and will not be harvested. In the following year, the plant starts to in late spring and can achieve a height of 2.5-3.0 m. During winter the shoots and leaves freeze. The latter falls, covers the ground and reacts as crop protection and fertilisation. Mid of April the shoots dry to achieve about 20 % of humidity and are harvested for the first time by cutting the stems. 6 weeks later the plant has already 70 cm. At the end of the growing phase it can achieve up to 3-4 m high (**Fig. 3-3**) [9, 10], which would mean that a dry matter of 15-17 t/ha could be harvested. During the first two years, a special attention should also be given to the weed control that could harm and reduce the growing effectiveness of Miscanthus. In the upcoming years the harvested dry weight is increased [11] and can achieve up to 24 t/ha per year [6] for the following 18 years depending on the harvesting region [12, 13]. During this period the Miscanthus x giganteus plant needs less care and its propagation is carried out vegetative [14].

This species of Miscanthus has important advantages during its growing phase after the second year. Partly due to the falling frozen leaves in winter, the Miscanthus plant has a high tolerance to cold. Generally, it has a high resistance to pesticides and accordingly also to diseases. Another advantage is the low need in ash, water and minerals [15]. The performed water use of the plant results in a surface stabilisation of the soil, which impedes soil erosion, metal transportation due to wind and water movement [16]. Furthermore, it can grow on barren and contaminated grounds and simultaneously cleaning them by reducing its contamination [16, 17]. All these advantages make this plant to be very interesting economically and ecologically [7, 14, 18].

Fig. 3-3: Grown Miscanthus x giganteus [19]

The particularity of the Miscanthus x giganteus is in the stem and is principally composed of four types of tissue layers, which are subdivided in three regions (**Fig. 3-4**) [20]. The epidermis (Ep) is the outer ring covering and protecting the whole stem and surrounding the first region, which is based on vascular bundles (Vb) and the sclerenchyma ring (Sc.). The middle region is constituted by vascular bundles and parenchyma (Pa) and the inner ring contains mostly parenchyma tissues, which are responsible for the

photosynthesis procedure and the commutation of gases [20, 21]. In total about 62 % of the mass is the parenchyma ring [2]. It consists of simple thin-walled cells with inner air spaces, which is also considered as the porous nature. As presented in **Fig. 3-5** the parenchyma section covers a high percentage of the cross-section of the Miscanthus fibre.

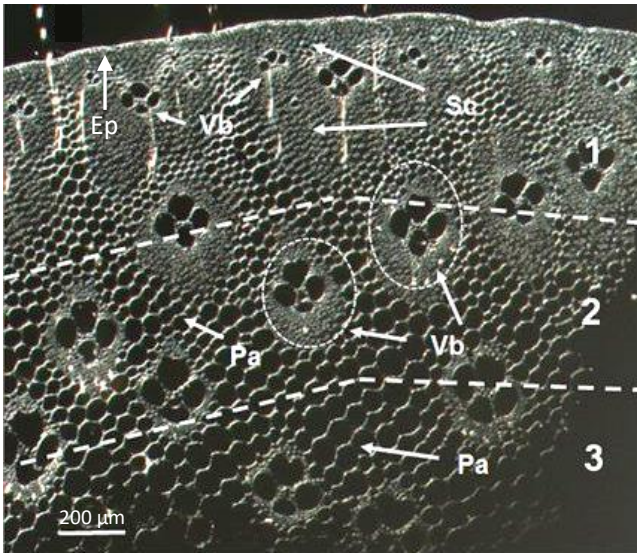

Fig. 3-4: Cross-section of a Miscanthus x giganteus stalk (adapted from B. Chabbert et al. [20])
Ep = epidermis, Sc = sclerenchyma ring (outer ring), Vb = vascular bundles and Pa = parenchyma ring

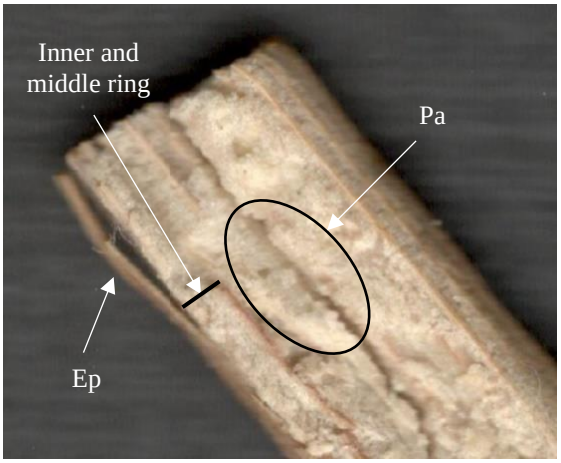

Fig. 3-5: Scanned Miscanthus fibre with designation of the different sections

Pude et al. [22] analysed different chemical parameters of the Miscanthus fibres. They concluded that the mass percentage of Miscanthus x giganteus consists of 40 % of cellulose, 16.2 % of lignin and 1.8 % of silicon. They determined the position of the highest lignin content being the epidermis as well as the sclerenchyma ring by using phloroglucinsaline acid, which colours the lignin in red. The lignin also affects the strength of the material [2]. Therefore, they concluded that the sclerenchyma and the parenchyma ring have the highest influence on the strength of the material. Furthermore, the high

parenchyma quantity of Miscanthus could even substitute polystyrene due to its high amount of air voids [23].

The aim of this dissertation is to use the Miscanthus fibres in a lightweight concrete mixture; therefore, a very important aspect is the water absorption of Miscanthus. This physical parameter showed to vary by 200-358.2 % of the mass percentage [22]. This high difference was dependent on the harvesting time of the Miscanthus x giganteus fibres. Since cement reacts in the first minutes after pouring water, Görtz et al. [24] claims that the Miscanthus fibres should be added in this time-lapse to ensure a good link between the materials. Therefore, the absorption velocity of Miscanthus x giganteus is of high interest for a further mixing with cement. In the first 30 seconds, the fibres absorbed water with a velocity of 16.2 mm/min and reduced it in the upcoming moments until reaching a minimum of 4 mm/min [2] after 20 min. During this time, the absorbed water achieved a height of 29.7 mm in a fibre with a diameter of 8.8 mm. In relation to other Miscanthus species, the Miscanthus x giganteus had the highest water absorption velocity.

3.1.2.2 USAGE OF MISCANTHUS X GIGANTEUS

Aside Miscanthus x giganteus being a promising sustainable material for the building sector, it is also widely used in the agricultural area for mulch or bedding of animals and as mulch for pathways [6, 25]. In addition, it is also broadly used for bioenergy production by direct combustion, gasification or as chopped material [15, 26]. The advantage of using Miscanthus is principally the reduction of green gas emissions, which provides a sustainable solution to climate and energy policies. Furthermore, if the plant is grown on a degraded land, it reduces the interest of deforestation in relation to the production of biofuels [27].

In this dissertation, the Miscanthus x giganteus fibres are used, due to their promising properties of insulation and strength, as an aggregate in a lightweight concrete [28]. According to Pude [2] Miscanthus x giganteus is the most suitable to be used as aggregate for lightweight concrete, not only for its Young's modulus which varies between 2-8 GPa in the stem [29], but also due to its high parenchyma content. Nowadays, sustainable lightweight concretes are performed using wood chips, which are mostly based on Beech wood (**Fig. 3-6** left) and Bark wood of conifers (**Fig. 3-6** right). The latter has the drawback that it has to be dried and sorted prior to use. Due to this needed pre-treatment, this material becomes very capital-intensive and loses the attraction of being a sustainable material. The Beech tree has a similar cellulose content (47.7 %) [30] as Miscanthus x giganteus but only 15 % of the mass is parenchyma, which is 4 times less than the parenchyma content of Miscanthus x giganteus.

Fig. 3-6: European beech tree (left) [31]; Bark conifer (pine) (right) [32]

A lightweight concrete using Miscanthus fibres was produced by Pude et al. [22]. They used 1000 cm^3 of fibres, the binder consisted on 250 g of cement and 50 g of lime and a water amount of 250 ml was added. Prior to use the fibres were pre-treated by immersing them in water for 3.5 hours. Next, they were put in a filter for 3 hours and used in the mixture. In average, a load-bearing capacity of 0.45 MPa was achieved using Miscanthus x giganteus. During curing time, a water-loss of 11 % of the mass percentage is measured after 3 days and about 50 % after 17 days [2]. In average, the Miscanthus concrete had a permanent water binding of 38 % considering the mass percentage. Pude [2] and Pude et al. [22] concluded that achieved load-bearing capacity was dependent on the diameter of the fibres, the cellulose content, the water-loss and the permanent water binding of the Miscanthus concrete.

A lightweight concrete based on Miscanthus aggregates was also analysed by Waldmann et al. [33] by investigating the impact of the pre-treatment of Miscanthus, the W/C ratio and cement content of the mixture on the achieved load-bearing capacity after a curing time of 14 days. The analysed pre-treatments consisted of $CaCl_2$, chalk, $MgCO_3$ or no pre-treatment at all. The highest compressive strength of 0.8 MPa was reached using the $CaCl_2$. The W/C ratio was varied between 0.7 and 1.6. A maximum of 1.4 MPa compressive strength was achieved using a W/C ratio of 1.6. Another variation performed by Waldmann et al. [33] was the cement content from 75-449 kg/m^3. The highest load-bearing capacity of 6 MPa was reached by the mixture using the highest amount of cement and a W/C ratio of 1.1.

Açikel [34] analysed the mechanical properties (compressive, splitting and tensile strength and Young's Modulus) of several cementitious mixtures based on Miscanthus fibres. The amount of cement in the mix varied from 350-450 kg/m^3 with a constant w/c ratio of 0.5. The amount of Miscanthus fibres varied from 0-6 % (vol. %). After creating the mixture, the consistency was verified using a slump test and a slump of 70-110 mm was measured. All the measurements were performed according to the Turkish

Standards TS EN 12390. The compressive strength, the splitting strength and the Young's Modulus were measured on cylinders with a diameter of 15 cm and a height of 30 cm, after a curing time of 7 and 28 days. The tensile strength was performed on beams with the dimensions of 5x15x75 cm.

The cement amount in the mixes had the highest impact on the results of the compressive, splitting and tensile strength and Young's Modulus. Due to the low fibre amount, the achieved results were almost not impacted by this variation, independent from the curing time. The compressive, resp. the splitting strength achieved by Açikel [34] after a curing time of 28 d varied between 29-37 MPa resp. 2.5-3.3 MPa. The Young's Modulus of the mixtures varied from 37.3 to 40.6 GPa.

In addition to the presented studies, Miscanthus x giganteus can also be very interesting economically by encouraging local farming of Miscanthus [35, 36]. This would benefit the local economy, aside from reducing the travel distances of the fibres and the CO_2 emissions. In addition, replacing the aggregates of concrete by a sustainable fibre would reduce the depletion of natural resources such as sand and gravel, which is already a global issue [37].

3.1.3 SIMILARITIES TO OTHER SUSTAINABLE FIBRES

In the following sections, different sustainable fibres, wood, hemp, coir, jute, flax, bamboo and wheat straw, will be presented according to their chemical composition. Their mechanical behaviour in cementitious mixtures will be analysed. Furthermore, Miscanthus and hemp will be compared due to their structure similarities. In addition, a life cycle assessment of these two plants will be presented.

3.1.3.1 SUSTAINABLE FIBRES IN CEMENTITIOUS MIXTURES

According to R. Pude et al. [22], who analysed different Miscanthus genotypes as sustainable fibres in concrete, stated that one of the factor that impacted the most the load-bearing capacity was the cellulose and the lignin content of the fibres. Miscanthus x giganteus had in average 40% of cellulose and 15 % of lignin. Vo and Navard [38] analysed these properties for different sustainable fibres (**Table 3-1**). The lignin content of all the presented fibres were lower than the one from Miscanthus x giganteus, except for the coir and the wheat straw. The contrary was for the cellulose content; all the fibres had a higher cellulose percentage except the coir and the wheat straw.

Sustainable fibre	Cellulose (%)	Lignin (%)
Coir (extracted from coconut)	36 – 43	41 – 45
Flax	60 – 81	2 – 3
Hemp	70 – 78	3.7 – 5
Jute	51 – 72	5 – 13
Wood cell fibres	94 – 99	Very low
Bamboo*	74	10
Wheat straw**	28 – 39	16 – 25

Table 3-1: Proportion of cellulose and lignin [38]; *[39]; **[40]

In addition to the chemical composition of the materials, O. Faruk et al. [41] analysed the mechanical properties, more precisely the Young's Modulus of bamboo (11-17 GPa), jute (26.5 GPa), flax (27.6 GPa) and hemp (70 GPa) fibres. A Young's modulus of 3.1-4.3 GPa was measured by Munawar et al [42] for coconut fibres. All these fibres achieved a higher Young's Modulus than Miscanthus fibres (2-8 GPa) [43]. Next, the fibres were used as aggregate in a cementitious mixture (**Table 3-2**). It is clear that independent from the type of fibres, a higher wt. % of fibres in the matrix resulted in a lower compressive strength [44-51].

H. Ramaswamy et al. [44] mixed 1% in vol. of bamboo, coir and jute fibres to cement, sand and coarse aggregate using the proportions 1:3.58:2.87 and a W/C ratio of 0.65. This proportion of fibres allowed the matrix to achieve a compressive strength of 6.86 MPa (jute), 8.33 MPa (bamboo) and 10.3 MPa (coir) after a curing time of 28 days.

L. Arnaud and E. Gourlay [45] analysed different hemp concrete mixtures by varying the type of hydraulic lime and the atmospherically conditions during curing. They concluded that the specimens cured in an environment of 20 °C, a relative humidity of 50 % and using a NHL 3.5 lime achieved the highest compressive strength of 0.33 MPa. Furthermore, they stated that a higher relative humidity of 75 and 98 % reduced the compressive strength by 45-55 %. Different types of hemp shives were also analysed by C. Niyigena et al. [52] and similar compressive strength was achieved (0.13 – 1.07 MPa).

S. Elfordy et al. [46] analysed a mixture based on hemp and lime by projecting it and adding the water just before projection to reduce the absorption time of the fibres. They reached with this technique a compressive strength of 0.85 MPa. Furthermore, the weight percentage of hemp in the mix induced a low thermal conductivity of (0.18 - 0.55 W/mK). A similar observation was performed by E. P. Aigbomian et al. [47], which achieved with sawdust and waste paper a compressive strength of 0.80 MPa and a thermal conductivity of 0.046 to 0.069 W/mK.

A hemp concrete based on different composition of the biomass was analysed by P. B. De Bruijn et al. [48]. They varied the amount of cement and lime in the hemp mix. The composition of the used aggregates were hemp dust, hemp shives and hemp fibres. The highest compressive strength of 0.83 MPa was achieved using cement and lime together.

V. Dubois et al. [49] analysed a hemp concrete replacing the cement by quarry fines. Moreover, they analysed the impact of the relation binder/aggregate, lime proportions and the W/C ratio on the compressive strength. The mixture using a binder/aggregate relation of 5.5 with 30 % of lime and a W/C ratio of 0.45 achieved the highest compressive strength of 2.10 MPa.

Merta and Tschegg [50] analysed a fibre concrete based on a mixture with cement, fly ash and aggregates (0-4, 4-8 and 8-16) using the proportions 1:0.15:7.47 and a W/C ratio of 0.67. The weight percentage of the hemp fibres and wheat straw was 0.19 %. The mixture with hemp fibres achieved a higher compressive strength (34.6 MPa) than the mixture with wheat straw (31.7 MPa). Furthermore, according to Merta et al. [53] the durability of hemp fibers depends on the alkaline environment of the cement matrix, which affects the loss of tensile strength due to aging.

A mixture based on hemp shives, an hydraulic binder and water was analysed by Niyienga et al. [51]. A weight percentage of hemp shives of 17.9 % with a water/binder ratio of 1.2 and shiv/binder ratio of 0.48 and achieved a compressive strength of 0.11 – 1.1 MPa. They concluded that even with a W/B ratio of 1.2 the binder did not get the required water amount to react due to the high water absorption of the hemp shives.

An additional study on natural hemp concrete was performed by Awwad et al. [54] by analysing the mechanical (compressive strength, flexural, splitting tensile and Young's Modulus) and the thermal properties of hemp concrete. Lastly a slump test was done. The creation of the specimen as well as the testing of them was performed according to the standard ASTM (American Society for Testing Materials). The mixtures with hemp fibres were compared to a reference mixture (control) and to a polypropylene mix. Awwad et al. varied the amount of hemp (0.5-1.0 vol. %) and coarse aggregate (0-30 vol. %) in the mix to analyse its impact on the mechanical and thermal results (**Table 3-3**). Therefore, different shapes of specimens were used. The flexural test was performed on beams (15x15x53cm), the compressive strength, the splitting tensile and the Young's Modulus was measured on cylinders (15x30cm) and the thermal conductivity of the materials was measured on blocks of 30x30x5cm.

Reference	Sustainable fibres	Amount of fibres [wt. %]	Compressive strength [MPa]
[44]	Jute	n.g. (1 % in vol.)	6.86
	Bamboo	n.g. (1 % in vol.)	8.43
	Coir	n.g. (1 % in vol.)	10.3
[45]	Hemp shives	14.3 – 15.9	0.22 – 0.33
[46]	Hemp shives	16.0	0.18 – 0.85
[47]	Sawdust 75% waste paper	n.g.	0.80
[48]	Hemp composition	10.4 – 12.4	0.15 – 0.83
[49]	Hemp straw	9.6 – 11.6	0.90 – 2.10
[50]	Hemp fibres	0.19	34.6
	Wheat straw	0.19	31.7
[51]	Hemp shives	17.9	0.13 – 1.07
[54]	Hemp fibres		

Table 3-2: Type and amount of fibres in the cementitious matrix and their achieved compressive strength (n.g. = not given)

Mix no.	Mix type	Fibers (vol.%)	Aggregate reduction (vol.%)	Cylinders	Beams	Blocks
1	Control	–	–	15	6	1
2	0.5% Polypropylene	0.5	–	15	6	1
3	0.5% Hemp	0.5	–	15	6	1
4	0.5% Hemp – 10% coarse	0.5	10	15	6	1
5	0.5% Hemp – 20% coarse	0.5	20	15	6	1
6	0.5% Hemp – 30% coarse	0.5	30	15	6	1
7	0.75% Hemp – 10% coarse	0.75	10	15	6	1
8	0.75% Hemp – 20% coarse	0.75	20	15	6	1
9	0.75% Hemp – 30% coarse	0.75	30	15	6	1
10	1% Hemp – 10% coarse	1	10	15	6	1
11	1% Hemp – 20% coarse	1	20	15	6	1
12	1% Hemp – 30% coarse	1	30	15	6	1

Table 3-3: Mixtures perpared by Awwad et al. [54] to analyse the mechanical and thermal properties

The mixtures presented by Awwad et al. are based on cement, medium coarse aggregate and sand in the proportions 1:2.2:2.03 and a w/c ratio of 0.68. The proportion of hemp in the mixtures varied between 0.5 and 1 % (vol. %). The proportion of the coarse aggregate varied between a reduction of 10 to 30 % (vol. %).

The compressive strength was measured after a curing time of 3, 7 and 28 days by Awaad et al. [55]. The reference mixture achieved a compressive strength of 23.4 MPa after a curing time of 28 days (**Table 3-4**). Independent from the curing time, the compressive strength decreased with an increase in the volume ratio of hemp. A decrease of the compressive strength was also observed with a higher reduction of the coarse aggregates, except for the mixture using a 1 % of hemp at a curing time of 3 and 7 days.

Mix no.	Mix type	3 Days		7 Days		28 Days	
		MPa	Difference to control (%)	MPa	Difference to control (%)	MPa	Difference to control (%)
1	Control	11.9	–	19.4	–	23.4	–
2	0.5% Polypropylene	11.5	−3	16.1[a]	−17	20.4[a]	−13
3	0.5% Hemp	12.9[a]	+8	15.6[a]	−20	18.9[a]	−19
4	0.5% Hemp – 10% coarse	9.8[a]	−17	14.3[a]	−26	17.5[a]	−25
5	0.5% Hemp – 20% coarse	8.9[a]	−25	12.6[a]	−35	16.7[a]	−29
6	0.5% Hemp – 30% coarse	8.3[a]	−30	11.4[a]	−41	17.8[a]	−24
7	0.75% Hemp – 10% coarse	10.2[a]	−14	12.7[a]	−34	20.1[a]	−14
8	0.75% Hemp – 20% coarse	8.7[a]	−26	12.2[a]	−37	17.1[a]	−27
9	0.75% Hemp – 30% coarse	7.6[a]	−36	11.9[a]	−39	17.9[a]	−23
10	1% Hemp – 10% coarse	9.1[a]	−23	12.6[a]	−35	18.9[a]	−19
11	1% Hemp – 20% coarse	9.4[a]	−21	13.4[a]	−31	18.2[a]	−22
12	1% Hemp – 30% coarse	9.6[a]	−19	14.0[a]	−28	16.8[a]	−28
	SEM[b]	0.21		0.45		0.66	

[a] Significantly different to the control result.
[b] SEM is the standard error of mean.

Table 3-4: Compressive strength after a curing time of 3, 7 and 28 days[54]

The flexural tests performed by Awaad et al. [54] were carried out after a curing time of 7 and 28 days on beams using a 4-point bending test with a span distance of 45 cm and a two-point load on the middle strip of the beam. During testing, the deformation of the beam was measured on the centre of the beam using an electronic gage. After a curing time of 7 days, the highest flexural load of 21.5 kN was attained by the mixture using the highest amount of hemp and the lowest of coarse aggregates (1 % Hemp – 30 % coarse) (**Fig. 3-7**). After a curing time of 28 days, the highest flexural strength was reached by the control mixture (26 MPa). A very interesting point claimed by Awwad et al. was the high ductility of the mixtures containing hemp, which made this material very interesting concerning safety aspects. In contrast, the control and the polypropylene mixtures showed a brittle failure after reaching their maximum load. Thus, they concluded that the fibres had a low impact on the achieved flexural strength but a very important point on the ductile behaviour of the samples. As expected, the first cracks appeared on the tensile zone and the fibres prevented a sudden failure by bridging the cracks and acting as a sustainable reinforcement.

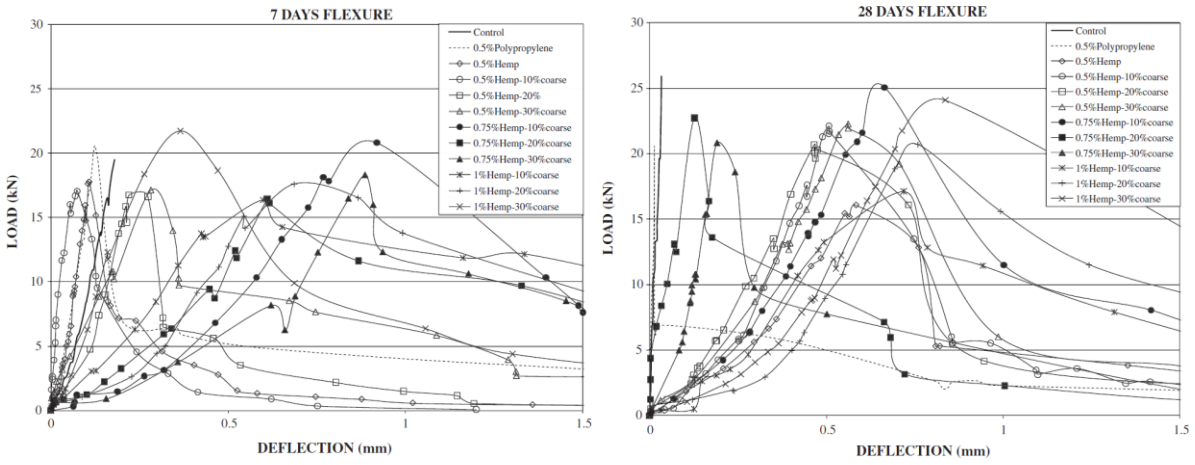

Fig. 3-7: Load-deflection curves after a curing time of 7 and 28 days [54]

Awwad et al. [54] measured the Young's Modulus on cylinders of all the presented mixtures and compared them to the reference mixture (**Table 3-5**). They concluded that due to the low Young's

Modulus of the fibres the achieved Young's Modulus was always lower for the mixtures containing fibres. Furthermore, they also claimed that the ductile behaviour of the hemp concrete was also related to the achieved Young's Modulus, which was reduced up to 37 % compared to the control mixture.

Mix no.	Mix type	28 days			
		$E_{measured}$ (MPa)	$E_{calculated}$[a] (MPa)	Difference $E_{measured}$ to $E_{calculated}$ (%)	Difference to control (%)
1	Control	23,754	22,335	+6	0
2	0.5% Polypropylene	21,818*	20,416	+7	−8
3	0.5% Hemp	22,004	19,923	+10	−7
4	0.5% Hemp – 10% coarse	18,935*	18,501	+2	−20
5	0.5% Hemp – 20% coarse	17,304*	17,888	−3	−27
6	0.5% Hemp – 30% coarse	21,543*	17,812	+21	−9
7	0.75% Hemp – 10% coarse	14,920*	19,847	−25	−37
8	0.75% Hemp – 20% coarse	20,679*	17,982	+15	−13
9	0.75% Hemp – 30% coarse	16,134*	18,397	−12	−32
10	1% Hemp – 10% coarse	18,966*	19,035	0	−20
11	1% Hemp – 20% coarse	16,960*	18,192	−7	−29
12	1% Hemp – 30% coarse	17,088*	16,893	+1	−28
	SEM[b]	457.5			

* Significantly different to the control result.
[a] $E_{calculated} = 33 \cdot w^{3/2} \cdot \sqrt{f'c}$, where w = unit weight in (lb/cu.ft) and f'c = compressive strength in (psi).
[b] SEM is the standard error of mean.

Table 3-5: Young's modulus after a curing time of 28 days [54]

The splitting tensile strength of the control mixture achieved 2.3 MPa after a curing time of 28 days. An increase of the hemp content showed to reduce the splitting tensile strength. However, in addition to the increase of the hemp content, a reduction of the coarse aggregate resulted to be favourable considering the achieved splitting tensile strength. Therefore, Awwad et al. concluded that considering the splitting tensile strength an addition of fibres to the mix could compensate a reduction of the coarse aggregates.

Awwad et al. also compared the thermal conductivity of the mixtures to the control mixture without any fibres (**Table 3-6** (left)). The lowest thermal conductivity of 1.221 W/mK was achieved by the mix 0.75 %Hemp - 30 % coarse, which was 35 % lower than the control mixture. The latter also achieved the highest slump deformation at fresh state (**Table 3-6** (right)). The slump was generally decreased with an increase of the fibre amount in the mix. A minimum slump of 70 mm was achieved using the mixture with the highest amount of hemp fibres. The same slump value was achieved by Açikel [34] for a concrete based on Miscanthus aggregates.

Mix no.	Mix type	28 days	
		λ (W/m K)	Difference to control (%)
1	Control	1.885	0
2	0.5% Polypropylene	1.608	−15
3	0.5% Hemp	1.866	−1
4	0.5% Hemp – 10% coarse	1.504	−20
5	0.5% Hemp – 20% coarse	1.912	+1
6	0.5% Hemp – 30% coarse	1.661	−12
7	0.75% Hemp – 10% coarse	1.746	−7
8	0.75% Hemp – 20% coarse	1.418	−25
9	0.75% Hemp – 30% coarse	1.221	−35
10	1% Hemp – 10% coarse	1.226	−35
11	1% Hemp – 20% coarse	1.232	−35
12	1% Hemp – 30% coarse	1.414	−25

Mix no.	Mix type	Slump (mm)
1	Control	250
2	0.5% Polypropylene	220
3	0.5% Hemp	70
4	0.5% Hemp – 10% coarse	110
5	0.5% Hemp – 20% coarse	140
6	0.5% Hemp – 30% coarse	175
7	0.75% Hemp – 10% coarse	65
8	0.75% Hemp – 20% coarse	110
9	0.75% Hemp – 30% coarse	140
10	1% Hemp – 10% coarse	70
11	1% Hemp – 20% coarse	70
12	1% Hemp – 30% coarse	70

Table 3-6: (left) Young's modulus after a curing time of 28 days; (right) slump results at freshly state mix [54]

Alves Fidelis, et al. [56] analysed jute fibres on a pull-out test on specimens with a width of 50 mm and a variable thickness between 5 and 10 mm. Two mortars with a different kind of binder were created.

The first binder consisted of cement and the second binder consisted of 50 % of metakaolin and 50 % of cement. The mixture of the first mortar was cement, sand and water using the proportions 1:1.2:0.48. The second mixture based on the metakaolin and cement included also sand and water with the proportions 1:1.2:0.44, where 1 was the binder constituted of 50 % of metakaolin and cement. The jute fibres, with a diameter of 0.785-0.804 mm were divided in two categories, the uncoated and the coated with a styrene-butadiene polymer. The fibres were not mixed to the mortars but were placed forehand into the moulds. The mortars were then poured into the mould to create the specimen. The achieved pull-out force was affected by the coating, the mortar and the curing time. The mixtures based on the metakaolin-cement binder achieved and using the coated fibres achieved the highest pull-out force of 0.7 kN after a curing time of 28 days. However, a curing time of 365 days reduced the pull-out force to 0.53 kN.

It can be concluded that the presented mixtures had different proportions particularly considering the amount of the respective sustainable fibre used. However, in addition to the proportions of the components, the cellulose content of the fibre used was an important criterion but also the orientation of microfibris in the cell wall of the fibre [57].

3.1.3.2 SIMILARITIES BETWEEN MISCANTHUS AND HEMP

In this section, the similarities between Miscanthus and hemp are analysed in two steps. First, their structure is compared using the technique of scanning electron microscopy. Next, a life cycle assessment of both fibres will be considered and compared.

3.1.3.2.1 SEM

According to Merta and Tschegg [50], the stem of Miscanthus has a similar structure as hemp, which includes the hollow inner parts comparable to honeycomb structure and the outer core, known as epidermis (**Fig. 3-8** [21] and **Fig. 3-9** [58]). Klímek et al. [21] substituted wood in particleboards by Miscanthus stalks and observed a reduction in the mechanical properties. By performing an SEM analysis on Miscanthus stalks (**Fig. 3-8**) Klímek et al. concluded that the soft parenchyma, which corresponds to 62 % of the mass [2], was the principal cause for the mechanical failures. Merta and Tschegg [50] compared the fracture energy of concrete based on hemp fibres and Miscanthus fibres. They concluded that due to high tensile strength and fineness of the hemp fibres, its fracture energy was 60 % higher than the one achieved by the concrete based on Miscanthus aggregates.

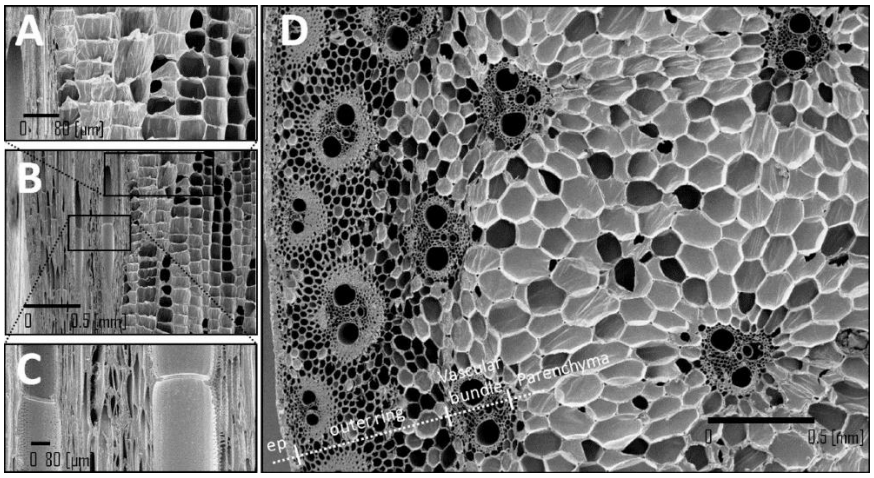

Fig. 3-8: Microscopic structure of a Miscanthus stalk, A-C: longitudinal, D: transverse cross-section (D) [21]

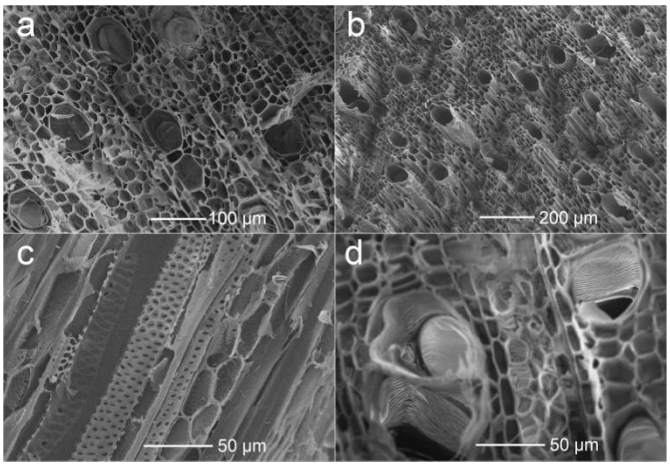

Fig. 3-9: Microscopic structure of hemp; a-b: full view, c-d: longitudinal and cross-section, adapted from [58]

3.1.3.2.2 LIFE CYCLE ASSESSMENT

Ip and Miller [59] conducted a life cycle assessment for hemp-lime wall. The functional unit was 1 m^2 with a thickness of 30 cm. The hemp mixture was based on 30 kg hemp, 50 kg lime-binder and a W/B ratio of 1.5. The lifetime of the structure was set to 100 years. The complete system boundary is shown in **Fig. 3-10** which includes the inputs and the outputs of the process map. The analysis showed that due to the carbon sequestration, based on more than 50 % in hemp shives, a negative net greenhouse gas emission (-48.45 kg CO_{2e}) could be measured in a wall with a thermal transmittance values of U=0.1 W/m^2K (**Table 3-7**) [59]. The savings of CO_2 in hemp are due to its photosynthesis and carbonation, which are above its emissions.

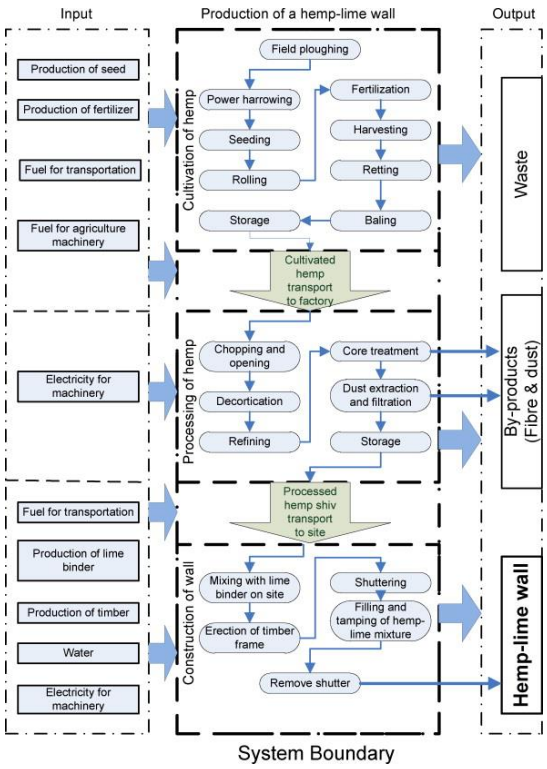

Fig. 3-10: Process used for the life cycle assessment of a wall using hemp fibres [59]

Construction	U-value (W/m^2K)	Net greenhouse gas emissions (kg CO_{2e})	
		without carbon sequestration	with carbon sequestration
300 mm hemp–lime wall, no rendering	0.19	46.63	-36.08
300 mm hemp–lime wall, 30 mm lime–sand rendering both sides	0.189	69.25	-26.52
30 mm lime rendering 550 mm hemp–lime 30 mm lime rendering	0.10	107.29	-48.45

Table 3-7: Greenhouse gas emissions for different wall finishing [59]

Fernando et al. [60] analysed the environmental impact of using Miscanthus for combined heat power production using as a system boundary the emissions caused in the agricultural process, the transport and during manufacturing (**Fig. 3-11**). The savings were based on three categories, the power provision, the fuel provision for heat and the fuel combustion heat. The analysis results in Miscanthus saving more than emitting and thus being beneficial for the environment. Fernando et al. also investigated the use of Miscanthus for other power productions (larger combined heat power production, for domestic heat production, etc.) and achieved always overall greenhouse gas savings.

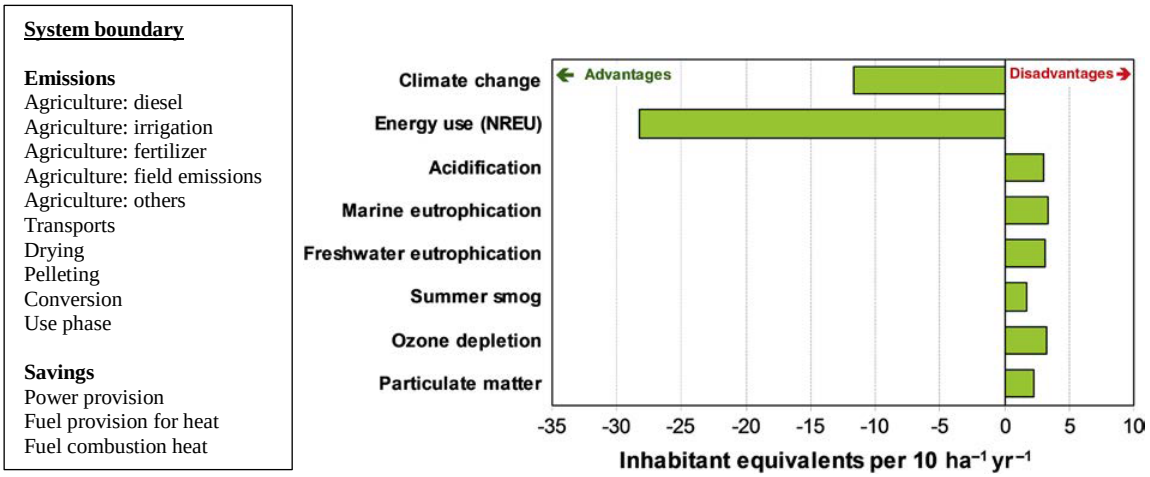

Fig. 3-11: Process used for the life cycle assessment of Miscanthus to small combined heat power [60]

Perić et al. [61] analysed Miscanthus plant as a heat producer and categorised several impacts. One of them is the water depletion, which resulted in a negative impact considering greenhouse gas emissions. The negative result of water depletion could retracted to the high water use during planting and growing of Miscanthus. Nevertheless, similar to Fernando et al. [60], Perić et al. concluded that a high power could be extracted from the plant with a global positive saving of greenhouse gas.

The use of the Miscanthus fibres and hemp cannot be compared on the presented studies due to different reasons like the different functional unit. However, the savings presented are mostly due to the fibres. Therefore, it can be stated that Miscanthus and hemp are very advantageous and ecological considering greenhouse gas savings.

3.1.4 PATENTS

In Europe several patents on the use of sustainable fibres for a concrete mixture are active or on demand. In addition to the plant, they all use a cementitious paste and other additives. In the following sections, a focus on the claims, which envelop the mixtures as well as the materials used, will be laid.

3.1.4.1 CONSTRUCTION MATERIAL ON A PLANT BASIS AND METHOD FOR THE PRODUCING OF THIS CONSTRUCTION MATERIAL (M. FREUDIGER 2002)

The granted patent of M. Freudiger 2002 [62] was applied by NAWARO AG from Switzerland with the application number of EP 1554228 B1. M. Freudiger claimed in this patent that different mixtures were made based on several mix components, which consist of M1, M2, M3 and a plant basis (PB), to analyse the construction material based on plant aggregates. M1 is considered as the binder consisting of cement and M2 is the mineraliser. The final mixtures is achieved by merging M1 and M2. The weight proportions proposed by M. Freudiger 50-90 % of M1 and 10-50 % of M2. The mineraliser M2 is based on two chemical compositions, calcium carbonate $CaCO_3$ and magnesium carbonate $MgCO_3$. The

weight proportions of the two chemical compositions are 60-95 % of $CaCO_3$ and 5-40 % $MgCO_3$. In addition to M1 and M2, M3 is added to the mixture, which consisted of gypsum with starch in a quantity of 200 kg/m^3.

The two mixtures on a PB presented by M. Freudiger consist of a composition of sustainable fibres. The first is a mix of 85 % of Miscanthus with 15 % of softwood. The second PB mix is miscanthus, softwood and hemp with the weight proportions of 75%, 20% and 5%. The water quantity stated by M. Freudiger is 300 litres and 2/3litre of sodium hydroxide per 1000 litres of mixing water is added to the mixing water.

The mixing procedure presented by M. Freudiger is composed of a first mix of M2 using the $CaCO_3$ and $MgCO_3$. Next, the mixture M3 (gypsum with starch) is added to M2 as well as the binder M1. Lastly, the PB and the mixing water are added.

In addition to the mixture, M. Freudiger patented also four elements based on the presented mixture. The first element consists of a sound-insulating element (**Fig. 3-12**) with the form of a panel provided with sound-insulating fins for increasing the sound absorbing surface area. The panel (1) has a thickness of 25cm (h) and is divided in two layers. A supporting layer (3) of 10cm (g) with a static function and an average density of 1250kg/m^3 and a layer (4) of 500kg/m^3 for sound absorption. The latter has a continuous layer with a thickness of 5 cm (f) and on top of it are fins starting with 10 cm (d) downwards to 6 cm (a).

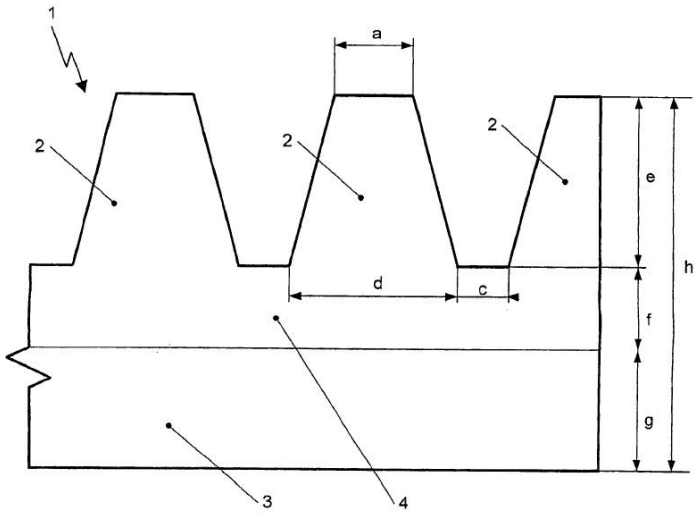

1 : Panel
2 : Sound absorption
3 : Supporting layer
4 : Absorber layer
a : 6 cm
c : 3 cm
d : 10 cm
e : 10 cm
f : 5 cm
g : 10 cm
h : 25 cm

Fig. 3-12: Sound-insulating panel element

Another element presented in the claims is a cuboidal slope reinforcement block (5) (**Fig. 3-13**) with sound-absorbing fins (2) provided (6) on the opposite side of the soil. The blocks contain a tenon (8) and a mortise (9) to provide a form fitting. Several slope reinforcement blocks (5 and 6) can be put

together to form a slope reinforcement wall (10) by form fitting interconnections. Later the wall will be inclined by the angle α of 10° with respect to the perpendicular. Below the elements, a foundation (11) is created to absorb the vertical forces. The horizontal forces of the wall (10) are absorbed using geo fleece mats (13) and tension bands (14).

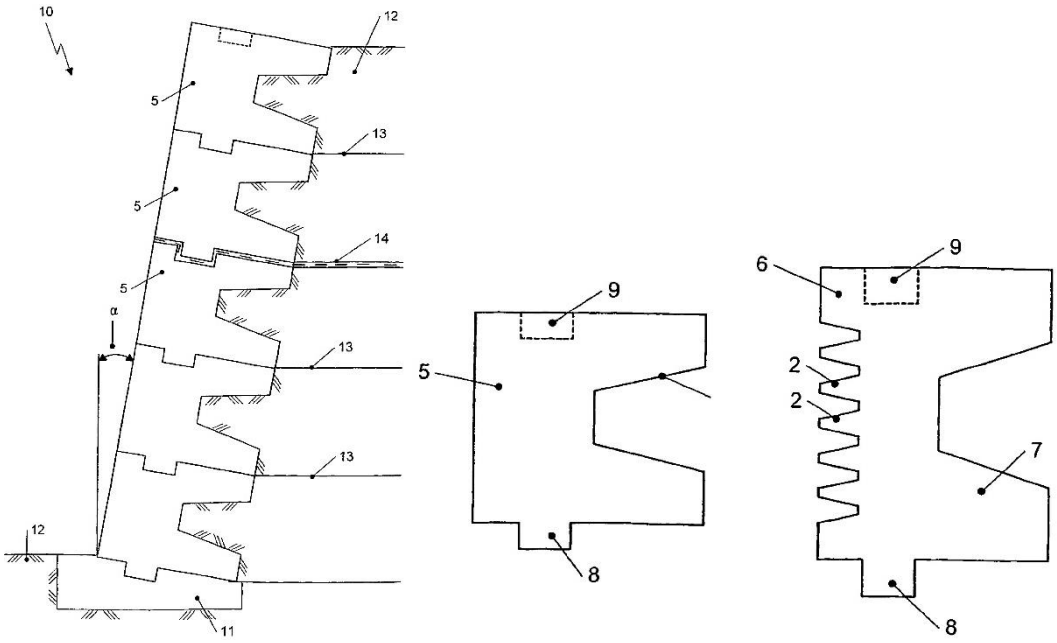

Fig. 3-13: Inclined wall with block elements (left); block elements (right)

The third element presented by M. Freudiger is a ceiling element with a length of 3,5m and reinforced with hemp ropes with a diameter of 12mm and at an interval of 10cm. At every 30 cm interval, a hemp rope with a diameter of 8 mm is used. A last structural element is a timber framing which fulfils the structural function and a plant-based construction material is added to fulfil a thermal insulation and a noise protection.

3.1.4.2 BUILDING MATERIAL WITH A PLANT FILLER (H. HÖHN, 2004)

The granted patent of H. Höhn 2004 [63] was applied by Miscanthus-Nawaro-Innovations S.A. from Luxembourg with the application number of EP 1765742 B1.

The mixture procedure patented by H. Höhn [63] is divided in the following steps. First, a predetermined amount of dry vegetable aggregate milled into particles, with a specific weight of 120-140 kg/m^3, are poured into the mixer. Next, a mineraliser and water are poured into the mixer and mixed for about 1 min. The used mineraliser consists of calcium carbonate $CaCO_3$ and magnesium carbonate $MgCO_3$, with the weight ratio 60:40 to 70:30. In addition to the mineraliser auxiliary materials, like SiO_2, Al_2O_3 Fe_2O_3 or SO_3, can be added in a weight ratio to the mineraliser of 95:5 to 99:1. Finally, the binder is added to the mix and blended for 4-5 minutes.

The amounts patented by H. Höhn [63] consist of 220-260 kg of binder per m^3 of vegetable aggregate. The binder contains a Portland cement grade 52.5 and calcium hydroxide with a weight ratio of 44:56. A fixed value is set for the mineraliser and the mixing water as 100-130 kg, resp. 300-350 litres.

The vegetable aggregate presented is not limited to the use of one plant but is based on a concept of different possibilities. First, it can be Miscanthus fibres with a length from 0 to 35mm. Another possibility is a mixture of Miscanthus fibres and pine wood chips. The length of these fibres, respectively chips lies in a range from about 0 to 40mm. The weight ratio between Miscanthus and pinewood is of about 50:50 - 80:20. One more possibility of the vegetable aggregate is a mixture of Miscanthus fibres, pine wood chips and round pine wood pellets, with a diameter of the round pine wood pellets lying in a range of 6 to 8mm. The Miscanthus fibres and pinewood have a weight ratio of 30:70 and the weight ratio between the chips and the round pellets is of 35:65.

H. Höhn [63] patented the use of the mixture on a building element or part of a building, like an outer wall for residential buildings or a rapid building panel. Other patented elements are an absorption layer for sound absorbing walls, an indoor and/or outdoor plaster and a heat insulation plaster.

3.1.4.3 BUILDING MATERIAL WITH PLANT FILLER (H. HÖHN 2007)

H. Höhn patented in 2007 an additional work on Miscanthus [64] by the applicant Miscanthus-Nawaro-Innovations S.A. from Luxembourg with the application number of this patent is EP 2069255 B1.

Two mixing procedures are presented in this patent. The first method consists of first inserting 1 m^3 of the plant-based aggregate with a specific weight of 70 to 160kg/m^3 in the mixer. Next, 40-80 kg of mineraliser, which consists of (white) hydrated lime based on more than 70 wt.-% of calcium hydroxide $Ca(OH)_2$ and optionally magnesium hydroxide $Mg(OH)_2$, is poured into the mix. Lastly, the 200-280kg cement-based binder and the 250-400 litre of mixing water are introduced and the whole mixture is mixed together.

The second method is divided in two steps. First, the plant-based aggregate, the mineraliser and a proportion of the mixing water are mixed together for 0.2-3 minutes. Next, the remaining water and the binder are poured into the mixture and all the components are mixed together.

The plant-based aggregate can be coming from several plants or from a composition of them. The plants mentioned by H. Höhn [64] are listed in **Table 3-8**. Depending on the plant a specific weight of 70 to 160kg/m^3 is given. The plant can be set as fibres, shavings, grains, slivers or other particles and the moisture of the plant should be between 5 to 25%.

Another patent-reserved object are the building materials listed in **Table 3-9**. These building materials are made from a ready-to-use mixture based on the mixture composition and the mixture procedure presented earlier.

Miscanthus and other kinds of reed	Jerusalem artichoke	Straw
Wood, for example softwood	Hemp	Palm panicles
Grasses, such as switchgrass and ryegrass	Flax	Mixtures of them

Table 3-8: Patented plant-based aggregate

Lightweight concrete	Lightweight render	External walls for residential buildings
Lightweight mortar	Heat-insulating render	Absorption layers for noise control walls
Lightweight screed	Rapid construction slabs	

Table 3-9: Patented building materials

3.1.4.4 Material or dry blend with vegetable aggregate (J. Peters 2008)

The patent of J. Peters from 2008 [65] is published with a European search report. The applicant of this patent is Miscanthus-Nawaro-Innovations S.A. from Luxembourg and the application number o is EP 2154117 A1.

As the patents from Freudiger and Höhn [62-64], J. Peters directed his patent also to building materials and ready-to-use mixtures with a vegetable aggregate in form of crushed particles. The mixture composition includes also a cement-binder and a mineraliser. The latter is a composition of amorphous or crypto and finely crystalline silicone. The silicon consists of a conventional silicon, silicon-aluminium, silicon-iron or silicon-aluminium-iron carrier of natural or artificial-industrial origin. J. Peters claims that the mineraliser is not only limited to the previously listed components but can also be based on the materials in **Table 3-10**. The mineraliser is used as a fin grain with sizes in a range of 0 to 0,2mm. The binder is based on cement with grades of 42,5R and 52,5R.

The concrete mixture of vegetable aggregate, binder, mineraliser and mixing water is not specified. However, a weight ratio between the components is stated. The water binder ratio is between 0.6 and 2.5 and the weight ratio between the binder and the mineraliser can go from 50:50 to 99:1. The amount of binder and mineraliser is dependent on the amount of plant-based aggregate used. Per m^3 of the vegetable aggregate, 50-300kg of binder and 1-300kg mineraliser are used.

Coal ash	Brick flour	trass
Wood ash	Brunt shale	Radiolarites
Boiler slag	Tempered phonolite	Gaize
Boiler ash	Bauxite	Tripel
Iron silicate slag	Red mud	Volcanic ash
Gout dusts	Quartz powder	Metakaolin
Expanded clay flour	Si sludge	Diatomaceous earth
Expanded clay sands	Rhyolites	Tuffs
Glass flour/glass waste artificially and original, such as obsidian and perlite		

Table 3-10: Patented materials to be used as a mineraliser

The possible aggregates patented by J. Peters are listed in **Table 3-11** and should have a water content of 20-60 % and a dry weight of 10-350kg/m^3. Furthermore, a composition of the different listed aggregates is included. However, no precise proportions are claimed.

Miscanthus	Softwoods	Switchgrass
Hemp shavings	Hardwood	Reed
Hemp fibres	Straw	Bamboo

Table 3-11: Patented vegetable aggregates

Finally, J. Peters claims that the use of the mixture to create a building material is also patent-registered. The building materials that are affected are walls of brick stones or of prefabricated wall elements as well as sound-absorbing materials, heat insulating components, plaster, mortar, screed, beds and filling material for filling compartments.

3.1.4.5 Construction material with filler of vegetable origin (I. Höhn and H. Höhn 2008)

The patent of I. Höhn and H. Höhn 2008 [66] is published with a European search report. The applicant of this patent is Höhn Inge and Höhn Heribert from Luxembourg and the application number of this patent is EP 2 177 489 B1.

I. Höhn and H. Höhn patented two mixture procedures based on plant additives and their use in the building sector. The mixture proportions are based on 1 m3 of plant additive. The specific weight of the plant additive should be in a range of 70 to 160kg/m^3 and can be one species or a composition of the ones presented in **Table 3-12**. The particles of the plant additive could be fibres, shavings, grains or others with a residual moisture of the plant additive between 5 and 15%.

The amount of the mineraliser depends on the binder used. A Portland cement of grade 52.5 induces a usage of 20 % of mineraliser, whereas a binder based on Portland limestone cement 52,5 induces a use of 10 % of the mineraliser. The latter consists of gypsum-containing stone and 30% of the mineraliser are in a powder form. The mixing water for the mixtures has be in a range of 250 to 400Litres.

The first procedure consists of putting all the components together and mix it. The second procedure consists of putting the plant additive, the mineraliser and some of the tempering water together and mix it for 0.2-3 mintues. Lastly, the binder and the remaining water are added to the mixture and mixed all together. In addition, to the mixture procedure I. Höhn and H. Höhn patented also the use of this mixture on different lightweight, thermal building materials as listed in **Table 3-13**.

Miscanthus and other reed species	Jerusalem artichoke	Straw
Wood, such as coniferous wood	Hemp fibres	Palm panicles
Grasses, such as switchgrass and ryegrass	Hemp shives	Mixtures of them
Sugar cane	Flax	

Table 3-12: Patented plant additives [66]

Lightweight concrete	Lightweight plaster	External walls for residential buildings
Lightweight mortar	Thermal insulation plaster	Absorption layers for sound insulation walls
Lightweight screed	Rapid construction boards	

Table 3-13: Patented building materials [66]

3.1.4.6 AGRO-SOURCED LIGHTWEIGHT CONCRETE AND USE THEREOF (F. JACQUEMOT AND P. ROUGEAU 2013)

The patent of Jacquemot and Rougeau 2013 [67] is published without a European search report. The applicant of this patent is the Centre d'Etudes et de Recherches de l'Industrie du Beton Manufacture from France and the application number of this patent is EP 2724996 A2.

The mixture presented by Jacquemot and Rougeau is composed of a binder consisting of cement and a mineral additive, a curing accelerator, water and an agro-sourced aggregate. The latter can be one or a composition of the species presented in **Table 3-14**. The cement in the binder is one defined in the norm EN 197-1 and the mineraliser can be limestone, siliceous, blast furnace slags, fly ash, silica fume and metakaolin or a mixture of these components. The proportion in the binder between cement and the mineral additive is 1:1-8. The water/binder ratio is ranged between 0.3 and 1. The curing accelerator is calcium chloride $CaCl_2$ and its proportions in relation to the binder are 3.5-7 %. Lastly, the proportion between the agro-sourced aggregate and the binder is 2-3.5:1.

Hemp boon	Sorghum	Wood aggregates
Flax shives	Miscanthus	Lignocellulosic aggregates

Table 3-14: Patented agro-sourced aggregates [67]

From the presented patents in this work, Jacquemot and Rougeau [67] were the only patenting the achieved compressive strength by specimens based on the previously presented mixture. They claim that a specimen based on the patented mixture should be established in a mould by vibro-compaction. The curing period and the demoulding of the specimen should be performed in an environment of 20°C and a relative humidity of 65 %. The specimen treated under these conditions achieve a compressive strength of 1.5-10 MPa after a curing time of 7 days or 3-15 MPa after a curing time of 28 days. The dry-weight of the specimens should be in a range from 600 to 1400kg/m^3. The specimens in question are construction materials listed in **Table 3-15**.

Masonry block	Wall element	Floor block
Masonry thermal brick	Thermal brick element	

Table 3-15: Patented building materials [67]

In conclusion, the patents presented are very similar and cover the usage of Miscanthus in a concrete mixture. However, except for the patent from Jacquemot and Rougeau, no results on the load-bearing capacity was given by the inventors, which induces that the patents might not be based on achieved results and are therefore, not considered in this work.

3.2 DIFFERENT FIBROUS CEMENTITIOUS MIXTURES

Other than agro-sourced fibres, steel, synthetic, ceramic and carbon fibres are also widely used in in cementitious mixtures. Therefore, in comparison to bio-based concrete the following section presents the use and the advantages of different non-agro-sourced fibres in a cementitious matrix.

3.2.1 STEEL FIBRES

Steel fibres are very popular to be used in concrete due to their high mechanical performance. These fibres are used in different geometries and surface structure (**Fig. 3-14**) to adapt to the needed bond anchorage. They can be straight or corrugated and a hook can be integrated on the end of each fibre. The usual dimensions of steel fibres are a length of 25 to 60 mm and a diameter from 0.4-1.5 mm. The fibre production are usually milled out of a rolling steel block, cut from steel plates or extracted from cold drawn steel wires [68]. Furthermore, the use of steel fibres increase the ductility of the concrete by preventing a premature development of major cracks [69-72].

Fig. 3-14: Steel fibres used in concrete [69]

Holschemacher et al. [69] used different types of steel fibres (**Fig. 3-14**) in combination with a steel bar reinforcement in concrete. They concluded that the highest load-bearing capacity was achieved using the highest amount of steel fibres (60 kg/m^3) and no steel bar reinforcement Furthermore, the behaviour of the steel reinforced fibre concrete was more ductile than without steel fibres. An identical observation was performed by Fanella and Naaman [70] who also proposed an analytical solution to predict the stress-strain behaviour of a steel fibre reinforced concrete.

3.2.2 SYNTHETIC FIBRES

The designation of synthetic fibres is based on synthetic polymers like, glass, polyethylene and polypropylene fibres (**Fig. 3-15**), which can be considered as micro or macro fibres [68]. The shape of the used fibres are similar to the steel fibres [73]. The micro fibres usually consist of monofilament or fibrillated fibres and have a length of 5-20 mm with a diameter of 0.03 mm or less. The macro fibres are mostly embossed or wavy polypropylene fibres with a size of 30-70 mm and a diameter varying between 0.5-1 mm. Rezania et al. [74] claimed that using 0.5 % (wt. %) of glass fibres (**Fig. 3-16**) increased generally the tensile and the flexural strength of shotcrete.

Fig. 3-15: Synthetic fibres used in concrete (macro fibres top and micro fibre bottom) [73]

Fig. 3-16: Glass fibres used in concrete [74]

3.2.3 CERAMIC FIBRES

Ceramic fibres (**Fig. 3-17**) are interesting due to their resistance to high temperature and chemical aggressions. However, the manufacture process and the high cost are a big drawback of these fibres [68]. Su et al. [75] analysed the mechanical properties (flexural, compressive and splitting tensile strength) of ceramic reinforced concrete and stated that the use of 0.3 % (vol. %) of fibres increased the all the properties by 8-15 % compared to the mixture without any fibres.

Fig. 3-17: Ceramic fibres used in concrete [75]

3.2.4 CARBON FIBRES

Carbon fibres (**Fig. 3-18**) are based on polyacrylonitrile or petroleum coal and have a tensile strength comparable to high strength steel fibres. Due to the high price and the environmental impact, the usage of these fibres is very limited [68]. Akihama et al. [76] analysed the tensile strength of carbon reinforced concrete using 3-5 % (vol. %) of carbon fibres and achieved a tensile strength of 7.8-13.7 MPa at a strain of 1.1%.

Fig. 3-18: Carbon fibres used in concrete [77]

3.3 MYCELIUM

A fungus is a known term and there are thousands of species around the world. It is often put into relation to a conventional mushroom that can be found in diverse places, like forests. However, the mushroom is only the fruiting body of the fungus with the purpose of producing spores for reproduction. The nutrients for the mushroom are collected by a web, also known as Mycelium. Dependent on the species, some fungus may never produce a mushroom because they are only based on Mycelium. In the following sections, a junction between Mycelium and Miscanthus will be presented with first an introduction to the different Mycelium species that can be merged to Miscanthus and followed by using Mycelium for insulation purposes.

3.3.1 DIFFERENT SPECIES OF MUSHROOM

An innumerable amount of fungal species can be found in the world and in the daily life of a human. One of these species is e.g. the Penicillium species that is used in the production of cheese, salamis, wine, beer or for medical purposes [78-80]. The fungus is divided in two parts, the mycelium, which is underground, and the visible fruiting body also known as mushroom. According to Schultheis [78], harvesting the Mushroom is not harmful for the fungi if the biotope, which is the tiniest part of the biosphere, is not damaged.

One important species that can be found in nature is the Mycorrhizal fungi. It grows with most of the trees in a forest. The fungi settles in the root of the trees and supply them with nutriments. In return, the trees nourish the Mycelium with sugar. This fungus maximises the use of the fertiliser for the trees, keeps a healthy root system and improves the drought resistance. Due to all these advantages, this fungus is also injected in plants or trees before being planted. This process allows also speeding up the increase of trees [78].

Another very important species in the forest is the Saprophyte fungi. His nutrients are mostly dead organic materials. This process allows creating a sort of recycling and cleaning of the forest because

they first decompose the organic material to extract the nutrients, which they use for growing and reproduction [78].

Another fungus that performs a more aggressive recycling in forest is the Parasitic fungi. In contrast to the Saprophyte fungi, the Parasitic fungi search for a weak point in a tree and assaults it. The fungi starts to spread into the tree by digesting the root cell and at the point when it starts to be on the surface, the tree is already dead [81]. After the death of the tree, the fungus continues to live inside of it for up to 20 years [78].

A very active fungus in the medical sector is the Ganoderma resinaceum (**Fig. 3-19**). It is used to improve different malfunctions in the human body, like lung, kidney, spleen and stomach function. Chen et al. [82] compared the Ganoderma resinaceum to the Ganoderma lucidum, which is a well-known mushroom species, and concluded that both have a very similar fruiting body, spore morphology and triterpenoid species. Furthermore, they concluded that the Ganoderma resinaceum could also be used for breeding new materials.

Fig. 3-19: Fruiting body of the Ganoderma resinaceum [82]

3.3.2 MYCELIUM WITH SUSTAINABLE FIBRES FOR INSULATION PURPOSES

As previously stated a fungus can be used in numerous sectors. This concerns also the building area. Due to the very fine filaments of Mycelium, it becomes very interesting to be used in this sector for insulation purposes.

Due to stricter regulations, the importance of insulation of a building increases more and more. However, conventional insulations are mostly based on synthetic compounds, like polystyrene, polyurethane, plastic-based fibres and foams. The manufacturing of these insulations is often expensive and complicated. Furthermore, during production toxic substances are emitted and a high amount of energy is needed, which results is a high carbon footprint. This signifies that the current insulation products are

not sustainable neither environmental friendly. Therefore, several studies are being performed to develop a new environmental-friendly bio-based insulation, which often requires less energy to be produced and leads to a lower carbon footprint than conventional insulation materials. A product that is suitable to respect the listed points are bioenergy crops [83-85].

A very interesting crop for this purpose is the C4 plant Miscanthus x giganteus due to its high resistance (section 3.1) and efficiency to grow in different European climates [86]. High yield of Miscanthus makes this plant very interesting. It has a high water use efficiency and needs generally a low amount of fertilizers. Furthermore, the fact of being able to absorb a large amount of CO_2 from the environment induces the crop to be very sustainable [87-89].

In addition to the different applications of Miscanthus presented in section 3.1, it can also be used for insulation purposes due to its high insulation capacity [86, 90, 91]. A low-cost insulation particleboard panel with a low density and thermal conductivity was developed by Eschenhagen et al. using Miscanthus and Sunflower stalk [86]. A new insulating bio-composite based on Miscanthus and recycled textile fibres bundled with chitosan was also analysed by El Hage et al. [90]. Due to the low thermal conductivity of Miscanthus (0.04 W/mK) [91], El Hage et al. achieved thermal conductivities varying from 0.069-0.09 W/mK, which is equivalent to a conventional insulation material.

Due to the properties of fungus Ganoderma resincaeum and its biological origin, Mycelium is a good green alternative to be used in the building sector, such as building insulation [92, 93]. Due to the low thermal conductivity (0.08 W/mK) and density (57-99 kg/m^3) [94], Yang et al. [95] analysed the characteristics of a Mycelium bio-form and concluded that it has better properties than the conventional expanded polystyrene foam. Therefore, it can be concluded that a bio-composite based on Mycelium-Miscanthus has a large potential as a building insulation material.

3.4 MASONRY BLOCKS

Since decades, the masonry block is a high importance in the building section. The masonry block can be used in different ways. In the following section, the conventional use of a masonry block using mortared joints will be introduced, followed by an introduction to a dry-stacked system of masonry blocks and its geometrical imperfections. The section will be concluded by the use of a masonry block with an insulation on dry-stacked walls.

3.4.1 GENERALITIES

The technique of using mortar between stones in the building sector was already performed by the Romans 200 B.C. In 1900, the first hollow block was patented by Harmon S. Palmer in the United States.

This was the start for many companies to start to produce manually their own masonry blocks. Today, this process is completely automated and improved to speed up the production [96]. Furthermore, the design of the masonry blocks is also adapted to the actual regulations.

Nowadays, the masonry blocks are not only based on concrete but different fibres are added for reasons, like weight or sustainability. Soto Izquierdo et al. [97] analysed masonry blocks (**Fig. 3-20**) based on sisal reinforced concrete on their compressive strength and compared them to masonry blocks based on plain concrete.

The two mixtures that were analysed by Soto Izquierdo et al. were based on the proportions 1:3.6:2.4, cement:sand:coarse aggregates, with a w/c ratio of 0.45. In one mixture, 1 % (vol. %) of sisal fibres was added to the mixture and the other mix was used as reference.

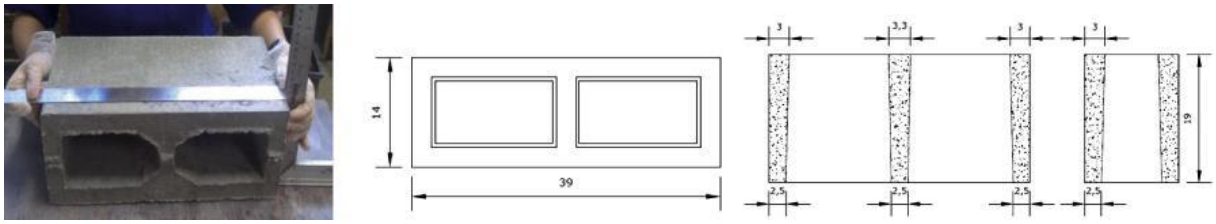

Fig. 3-20: Hollow concrete block and its dimensions [97]

Soto Izquierdo et al. performed compressive strength tests on prisms (L=39 cm, W = 14 cm, H = 19 cm) and two superposed masonry blocks connected by a 1 cm thick mortar joint. In addition, the load-bearing capacity of walls, with the dimensions of L = 79 cm, W = 14 cm, H = 99 cm and a mortar joint of 1 cm between all blocks, was measured.

The density of the masonry blocks based on the fibrous concrete was, due to the sisal fibres, lower than the density of the masonry blocks based on plain concrete. In average, this induced a 20 % lower load-bearing capacity of the masonry blocks based on fibrous concrete (**Fig. 3-21**). However, as presented on the previous sections, the fibrous concrete had a higher ductility.

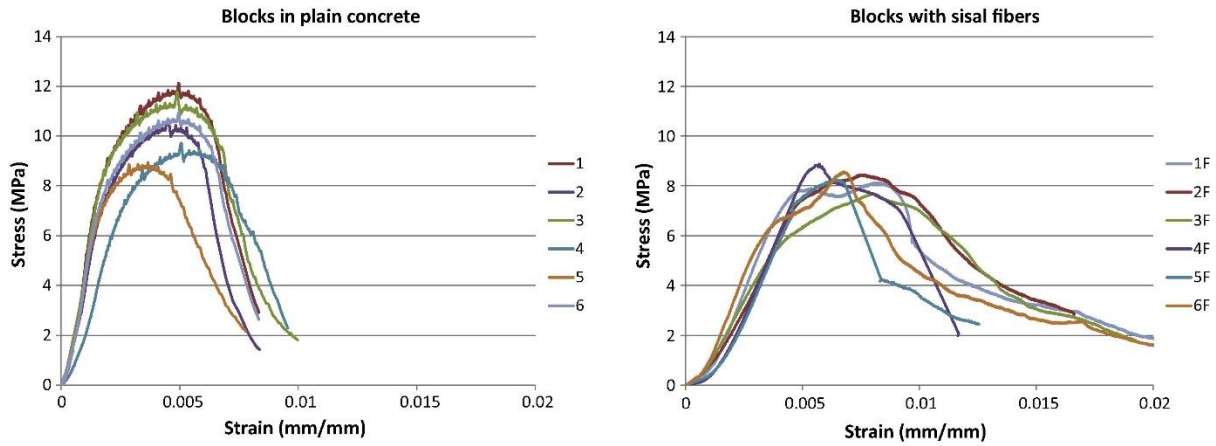

Fig. 3-21: Stress-strain distribution achieved by masonry blocks based on plain concrete and on sisal fibres concrete [97]

The importance of the ductility was visible at failure, where a sudden failure occurred on the masonry blocks based on plain concrete due to the rapidly spreading cracks. In contrast, the masonry blocks based on the fibrous concrete failed progressively as the fibres were bridging the strength in the cracks. Hence, this situation permitted the masonry block to remain as a single piece without any sudden failure.

The analyses performed on the superposed masonry blocks was identical as the one for the masonry blocks. The difference in the compressive strength of the fibrous blocks to the non-fibrous concrete block was lower (18 %) but as before they achieved a higher ductility. The walls analysed by Soto Izquierdo et al. showed that independent from the mixture used for the masonry blocks, a similar compressive strength (3.1 MPa) was achieved by both [97].

In addition to the compressive strength analysis, Awaad et al. [98] considered also the water absorption and the thermal conductivity of masonry blocks based on hemp concrete and compares them to masonry blocks based on a reference mixture without hemp.

Four mixtures were created, one reference mixture using fine and medium aggregates with cement and water and three others on which hemp fibres were added to the mix. The proportions of the reference mixture was 1:13 for aggregates based on cement. A w/c ratio of 0.3 was used for all the mixtures. The first hemp mixture had the same proportions as the reference mixture and 1 % (wt. %) of hemp was added to the mix. The second and the third hemp mixture had a proportion of 1:11.2, resp. 1:7.8 with a hemp addition of 1.7 %, resp. 3.6 % (wt. %) [98].

The specimens were tested after a curing time of 14 and 28 days. The reference mixture achieved a compressive strength of 11.7 MPa after 14 days and 12.7 MPa after 28 days. The first hemp concrete mixture with 1 % of hemp achieved a 58.1% lower compressive strength after a curing time of 14 days and 39.4 % after a curing time of 28 days. A higher amount of hemp in the mix induced also a bigger difference to the reference mixture. The mixture with 3.6 % of hemp had a compressive strength of 77.8 % lower after 14 days and 73.2 % lower after 28 days [98].

The water absorption test showed that an amount of 3.1 % of hemp in the mixture induced a 41 % higher water absorption of the masonry blocks compared to the reference mixture. The measured thermal conductivity of the specimens based on the reference mixture (1.248 W/mK) was 21 % higher than the thermal conductivity of the specimens based on hemp mixture containing 1.7 % of fibres. This fact shows the importance of the fibres concerning the insulation properties of a masonry block [98].

3.4.2 DRY-STACKED WALL

Dry-stacked wall is a very old and economical technique that was performed using stones of different sizes before the invention of mortars. One of the oldest examples of dry-stacked stones are the Megalithic stone temples of Malta, which date from 4000 B.C. [99]. Nowadays, due to new regulations the technique of a dry-stacked wall is becoming more and more interesting. The fact of omitting mortar in the horizontal joints has the advantage of increase the labour speed and more proper construction sites [100, 101]. Furthermore, a deconstruction of the wall can be considered, which could lead to a reuse of the block and adopt the strategy of circular economy. These advantages favoured the use of interlocking systems. The latter can be classified in two categories: the geometrical and the non-geometrical mechanism [100]. The geometrical category does not need any external application because it can be added during manufacturing, such as a dovetail connection, a tongue and groove arrangement or a post-tensioned technique [102]. The second category needs an external application on the masonry block before or during the application of the masonry blocks on the wall, such as grouting the prisms or insert synthetic strips between the blocks. In the following section, different existing systems based on the modular principle are presented. This discussion is concluded by an analysis on the geometrical imperfections of the masonry block designed for dry-stacked wall.

3.4.2.1 EXISTING SYSTEMS

A dry-stacked system, also known as modular principle, is a system where an upper and lower masonry block interlock with the adjacent blocks due to their geometry. This kind of blocks can be used in different situations. In Luxembourg, one of the usage presented by a company is as formwork block, which can be reinforced and grouted. It is also designed to divide spaces for storage of raw materials or other solids in- or outside [103].

Ali et al. [104] analysed the load-bearing capacity and shear strength of dry-stacked masonry blocks based on coconut fibres and reinforced with ropes based on coconut fibres. The aim was to achieve a masonry block as cost efficient as possible to use it in poor earthquake regions.

Ali et al. analysed 4 types of blocks based on the same material and geometry (**Fig. 3-22**). The different types of blocks consisted of a standard block, a bottom part, which was used as a base, a top part and a half block. The length of the full blocks was of 40 cm and two holes were inserted in the blocks to place a longitudinal rope based on coconut fibres to restrict the displacement of the blocks and still allowing an energy dissipation during an earthquake situation. The mixture used for the masonry blocks was based on cement:sand:aggregates with proportions of 1:4:2. In addition to this mixture, 1 % (wt. %) of 5 cm long coconut fibres with a w/c ratio of 0.64 were added.

Fig. 3-22: Left to right: Standard, bottom, top and half block based on coconut fibre [104]

The compressive strength test was performed on single standard blocks and on walls based on different types of blocks. The tested walls were divided in two parts, one was based on 3 superposed standard blocks and the second consisted of one bottom, one standard and one top block. Furthermore, Ali et al. determined the Young's Modulus and the Poisson's ratio of the four types of masonry blocks and the Young's Modulus of the two types of walls based on the achieved compressive strength.

The compressive strength of the single standard masonry block achieved 16.5 MPa (**Fig. 3-23**), which was 4 % higher than the load-bearing capacity of the wall based on standard masonry blocks. However, the corresponding axial strain is higher on the wall, due to the small gap between the blocks, than on the single standard block. Ali et al. claims that the reason for these occurrences are the slenderness of the wall, which is in this case 2.9. The Young's Modulus and the Poisson's ratio are based on the stress-strain distribution of the performed tests.

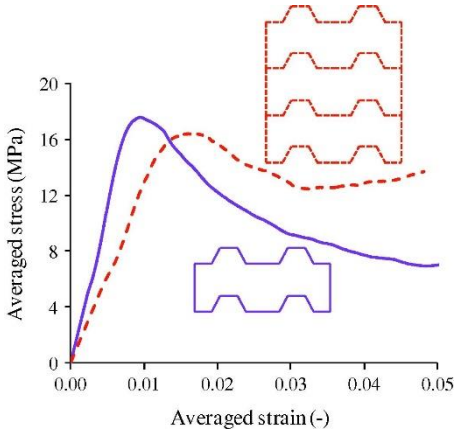

Fig. 3-23: Stress-strain distribution of a single masonry block and a wall based on the standard geometry [104]

The four types of masonry blocks were compared based on the compressive strength, the Young's Modulus and the Poisson's ratio. The highest load-bearing capacity was achieved by the standard and the bottom block, 16.5 MPa resp. 17.0 MPa. The top and half block achieved a 47.5 – 53.1 % lower compressive strength compared to the standard masonry block. The cracks in all the four types of masonry blocks started in the smaller bearing area, which consisted of the lateral interlocking keys and propagated upwards. The highest Young's Modulus (2.34 GPa) and Poisson's ratio (0.015) was measured on the standard masonry blocks.

Next, the wall based on standard blocks (W-SB) was compared to the wall based on one bottom, standard and top block (W-BST) (**Fig. 3-24**). The W-BST achieved a maximum load of 697 kN, which is 83.8 % higher than the W-SB. The higher capacity of the W-BST was due to a better distribution of the load on the bottom and the top block. The W-SB started to crack at the lower interlocking keys of the lower standard block and reduced therefore the capacity of the system. This did not occur on the W-BST, due to a higher contact area with the floor and a better distribution of the loads less cracks appeared in the system.

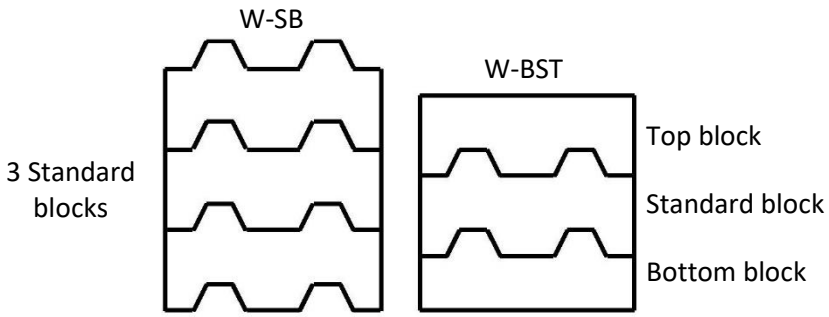

Fig. 3-24: Wall based on 3 standard blocks (W-SB) (left); Wall based on a bottom, standard and top block (W-BST) (right) [104]

The shear capacity was measured in- and out-of-plane (**Fig. 3-25**). The in-plane shear capacity was measured by applying a load parallel to the longitudinal joints. In contrast, the out-of-plane shear capacity was measured parallel to the transversal joints. The shear strength of the in-plane loaded system was of 2.65 MPa, which was 25 % smaller than the shear strength achieved by the out-of plane system.

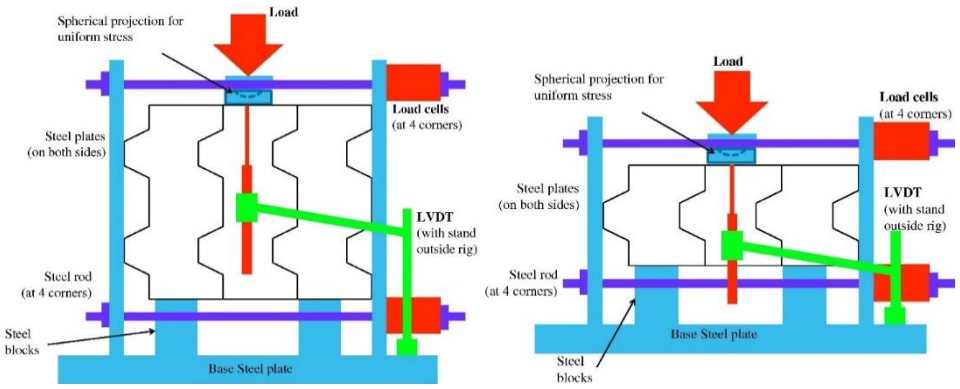

Fig. 3-25: Loading of in-plane shear capacity (left); loading of out-of-plane shear capacity (right) [104]

A dry-stacked interlocking stabilized earth block (ISEB) is analysed by Ben Ayed et al. [105], by measuring the compressive strength. The material composition of the ISEBs was red earth, sand and 8 % of ordinary Portland cement. The design of the blocks considered the standards presented in the African Regional Organization for Standardization (ORAN) and had the dimensions of 24 x 22 x 11 cm (**Fig. 3-26**).

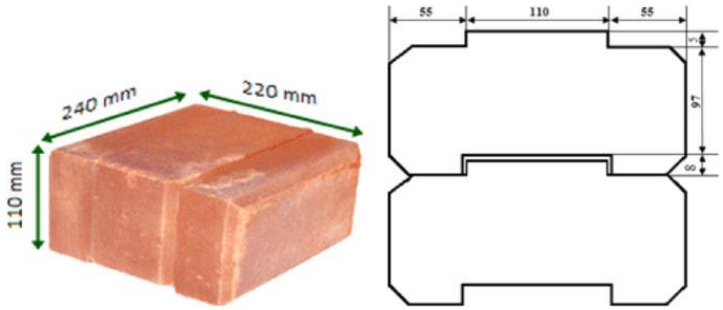

Fig. 3-26: Dimensions of the ISEB and two superposed blocks of ISEBs [105]

Three systems were analysed, one single block, two interlocking blocks and three interlocking blocks. The heels of the blocks that were in contact with the press were cut off to achieve a complete contact between the press and the respective system. The highest load-bearing capacity was achieved by the system of one block (11.9 MPa). The system with the two and three interlocking blocks achieved a 64 %, resp. 77 % lower compressive strength, due to the cracks that appeared in the positions of the modular principle.

Jaafar et al. [106] compared grouted and un-grouted dry-stacked masonry blocks by analysing their load-bearing capacity. The masonry blocks had a length of 30 cm and a height of 20 cm (**Fig. 3-27**). The compressive strength was analysed on walls with a height of 3 rows and a length of one block. A full block was used for the first and the third row and two half blocks were used for the middle row. The upper surface of the top block and the lower surface of the bottom block were grinded and the web of the top block was capped to achieve a complete contact between the external load application and the wall. The tests using the grouted masonry blocks were performed 28 days after being filled.

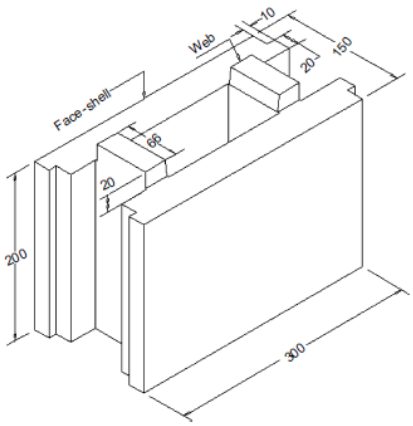

Fig. 3-27: Dimensions of the dry-stacked masonry blocks [106]

The un-grouted walls achieved a maximum load of 268.4 kN, which 31.7 % lower than the maximum load of the grouted system. The grouted interior allowed the masonry blocks to obtain a higher contact area. The grout also reduced the deformation at the beginning of the load application. However, at 57 % of the maximum load of the grouted masonry blocks, the bond between the grout and the block started

to crack and resulted in larger deformations of the wall. The web inside the masonry blocks split independent from the grout status. The difference was the instant of splitting, which was earlier for the un-grouted walls. The cause of this splitting was different for both walls. The webs of the un-grouted wall cracked due to bending effects, while the webs of the grouted wall split due to the laterally expanding grout. Independent form the situation of the web, the final failure of the walls occurred when the first cracks appeared on the face-shells.

The modular principle of two interlocking system is based on the geometry and can be different from case to case. Anand and Ramamurthy [100] compared two dovetail systems. Two concretes with the proportions 1:2:4:0.55 and 1:3:5:0.6 (cement:sand:coarse aggregate:w/c) were used to create the masonry blocks. Two connection concepts were analysed and were based on a dovetail connection. The first concept was to insert a dovetail (I-shape) on all blocks. The second concept was based on the negative of the first concept. These two approaches were compared by evaluating their axial and eccentric load-bearing capacity as well as on their bending resistance. The latter was subdivided in tension parallel to bed joint and a tension normal to bed joint (**Fig. 3-28**). Independent from the system both resulted in a high-efficiency factor for the compressive strength (0.62-0.77) as well as for the eccentric-to-axial capacity ratio compared to the conventional masonry. Furthermore, the bending resistance normal to the bed joint of both masonry blocks with the different dovetail connections was comparable to the one of a mortar-bedded wall.

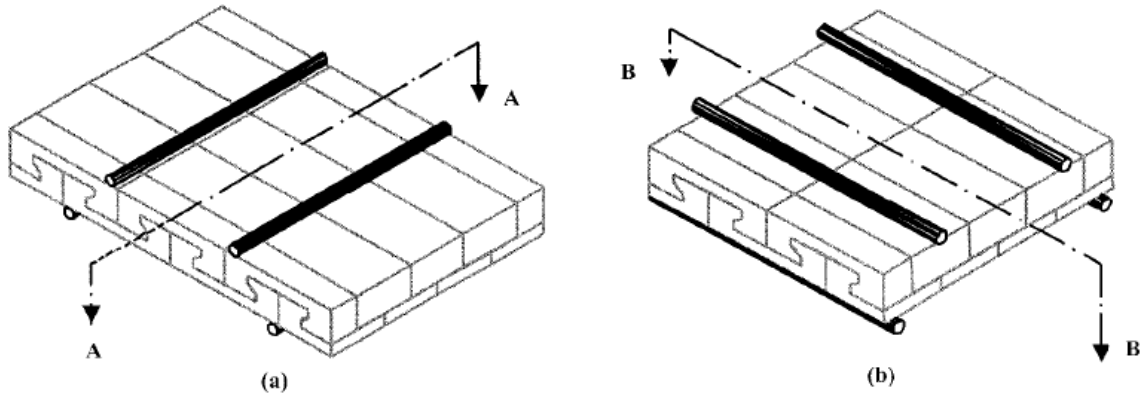

Fig. 3-28: Bending loading (a) tension parallel to bed joint; (b) tension normal to bed joint (adapted from [100])

Kohail et al. [102] compared to different interlocking systems (Sparlock system and Azar system, **Fig. 3-29**) to a conventional system (conventional block, **Fig. 3-29**). The latter achieved the highest compressive strength (12.1 MPa), which was 75 % and 44 % higher than the Sparlock, resp. the Azar block. Kohail et al. also used the blocks as a stacked system by differing them with grouted and un-grouted masonry blocks. As previously, the highest load-bearing capacity was achieved by the conventional blocks. Independent from the masonry block system, the un-grouted blocks achieved in average a 3-15 % higher compressive strength compared to the grouted one.

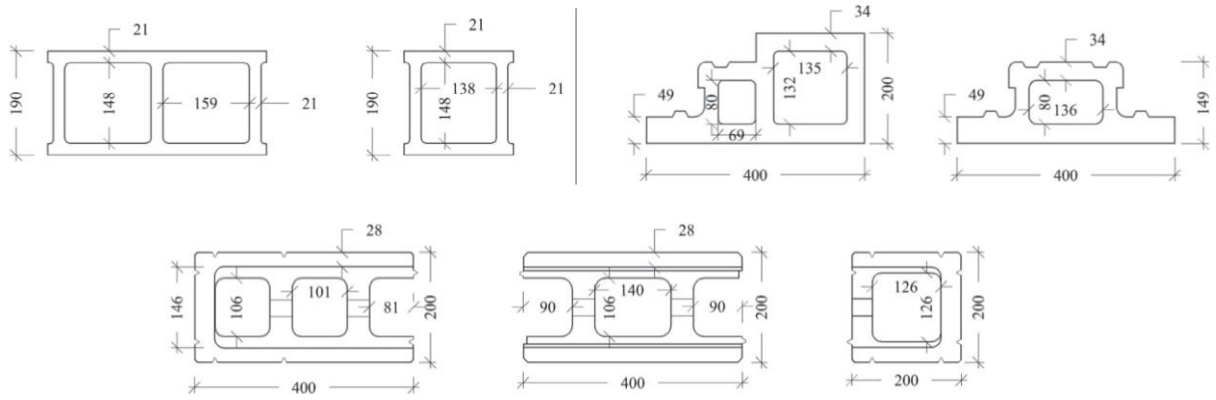

Fig. 3-29: Geometry and dimensions of the three analysed blocks, conventional block (left, top), Sparlock system (right, top) and Azar system (middle, bottom) (unit: mm) [102]

3.4.2.2 IMPERFECTIONS OF A MASONRY BLOCK

As presented the load-bearing capacity of a dry-stacked masonry block is dependent on the modular principle but also on the geometrical imperfections, such as the height difference and the surface roughness. Chewe et al. [107] analysed the impact of these imperfections numerically and analytically and compared them to the experimental tests performed by Agaajani [108]. Therefore, they analysed single masonry blocks and masonry panels of different heights. According to Agaajani [108], the height distribution of the masonry blocks followed a Gaussian law of +/- 2 mm. According to Chewe et al. [107], the height imperfections of each block have a high impact on the load-bearing capacity and can be distinguished in 5 load percolation cases (**Fig. 3-30**). Each case is represented by a single masonry block, whose top surface is full or half loaded. The different percolation are according to the bottom surface, which depends on the interlocking block. This observation was based on the useful section of each masonry block, which is statistically reduced based on an increase in the wall height and length.

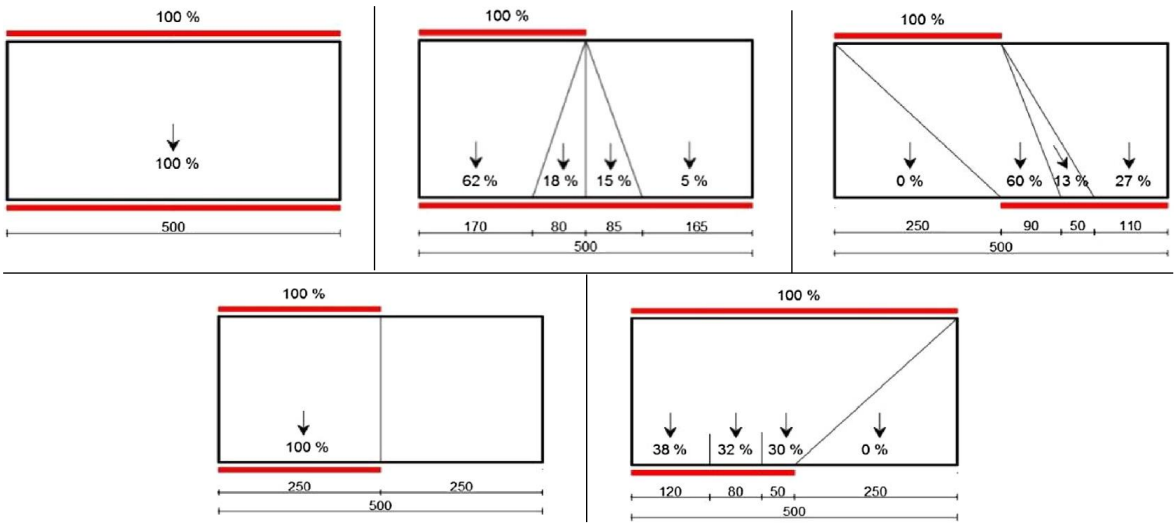

Fig. 3-30: 5 cases of the load percolation [107]

The relation between an increase of the useful section and the load-bearing capacity was analysed by Chewe and Waldmann [109] by introducing a contact layer on top of each masonry block. The latter was composed of two face-shells, which were connected by two web faces, similar to the masonry block of Jaafar et al. [106] (**Fig. 3-27**). The aim of the contact layer was to reduce the impact of the imperfections on the load-bearing capacity due to its low stiffness [110]. Therefore, 4 contact layers based on different materials with a Young's Modulus of 3-11.5 GPa. The advantage of the low Young's Modulus is to alleviate the punctual peak stresses. However, the drawback of this technique is that significant lateral deformations are generated.

Chewe and Waldmann [109] compared the achieved load-bearing capacity of a dry-stacked wall of 100 x 83 cm based on the masonry blocks with their respective contact layer to a dry-stacked wall with the same dimension and using masonry blocks without any contact layer. The observed crack were divided in three categories. The first category consisted of face-shells cracks. The cracks between the face-shell and the web were considered as the second type of cracks and the third category was a spalling around the bed-joint interfaces. The wallets using masonry blocks with a contact layer in the bed joint achieved in average a load-bearing capacity of 4.83 MPa, which was 32 % higher than the load-bearing capacity of the dry-stacked wall using masonry blocks without contact layer.

According to the standard EN 1996-1-1 [111], the load-bearing capacity of a conventional wall can be determined using the compressive strength of the mortar and the masonry block. This claim was expanded by Chewe and Waldmann [109] for the use of dry-stacked masonry walls. They adapted the load-bearing capacity by implementing a factor for the roughness and for the height imperfections in the equation of the standard EN 1996-1-1. As for Agaajani [108], the measurement of 100 masonry blocks performed by Chewe and Waldmann resulted also in a Gaussian distribution with a mean elevation of 200.2 mm and a standard deviation of 1.0 mm. The asperity height of the roughness of the masonry blocks was evaluated by the rate of the actual area in contact. The contact area of the masonry blocks was measured using Prescale FUJIFILM strips in the joints of three stacked masonry blocks. The strips were evaluated and Chewe and Waldmann concluded that a masonry block without contact layer showed a net contact area of 23 %. The latter and the load-bearing capacity were increased by using a contact layer between the blocks and increase the net contact surface [112, 113]. However, the increase of contact area and accordingly the load-bearing capacity is dependent on the material of the contact layer [109, 114].

In the following section, different measurement techniques of the contact area of a masonry block are presented and analysed. The section after following presents a precise calculation of the contact area considering the asperities of the roughness.

3.4.2.2.1 CONTACT AREA OF A MASONRY BLOCK

As previously stated the geometrical imperfections, more precisely the height differences and roughness of a masonry block, have a high impact on the load-bearing capacity of a dry-stacked masonry wall [107]. In this section, different approaches of measuring the height imperfections will be presented.

Ben Ayed et al. [105] analysed the contact area between two superposed interlocking stabilized earth blocks (ISEB) (**Fig. 3-26**). The blocks were designed to have a contact on the lateral heels of each block (**Fig. 3-31**). The selected technique of Ben Ayed et al. consisted of first painting the interfaces with a black colour and next, inserting a specific plain white paper between two blocks. The contact points coloured the paper and showed the contact area. Next, the paper is scanned and the amount of black pixels is counted, using MATLAB, to get the total contact area, in percentage, between the two interlocking blocks.

Fig. 3-31: Determination of the contact area using plain white paper [105]

Two cases were distinguished to define the contact area. The first case was the contact area between two blocks due to self-weight and the second case was to analyse the relation between the contact area and the applied load. The contact area due to self-weight was in average 23.3 % of the entire available surface (24 x 22 cm). An increase of the load induced a linear increase of the contact area. A contact of 50 % was achieved at load-bearing capacity. The remaining 50 % consisted of the void space between the blocks.

A different technique to determine the contact area between interlocking dry-stacked masonry blocks was presented by Zahra and Dhanasekar [115] using matrix based tactile surface sensors (MBTSS). The dry-stacked prism was based on half and full concrete interlocking masonry blocks (**Fig. 3-32**).

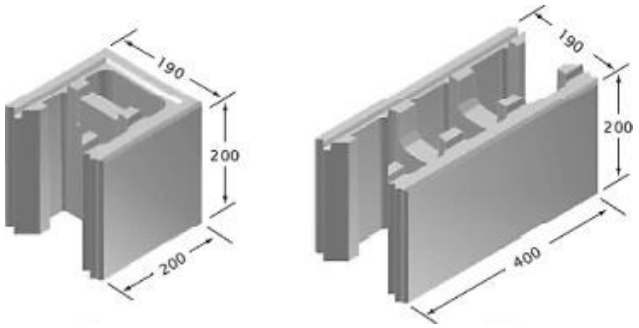

Fig. 3-32: Half and full hollow concrete interlocking block [115]

The contact area was measured on the outer face-shells of the masonry blocks. The sensors were placed on the surface of the face-shells and connected to an equipment to record the real-time contact surface in relation to the applied load (**Fig. 3-33**). The failure load was expected to be 200 kN. However, a maximum load of 100 kN was applied on the dry-stacked prisms.

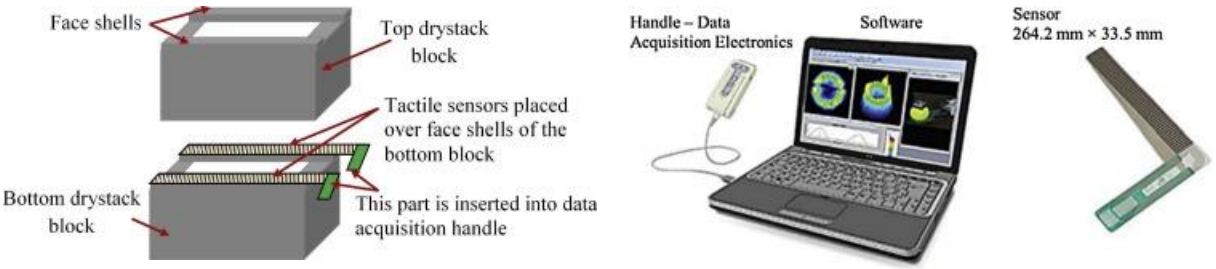

Fig. 3-33: Position of the sensors and MBTSS equipment [115]

During the load application, the real-time contact is recorded using the MBTSS equipment and the stress at different points are shown in a coloured scale (**Fig. 3-34**). The contact of both face-shells are superposed and shown at the same time to instantaneous identify the peak strength. The real-time recording created was seen as a movie and could therefore be split in frames to extract the momentary contact area.

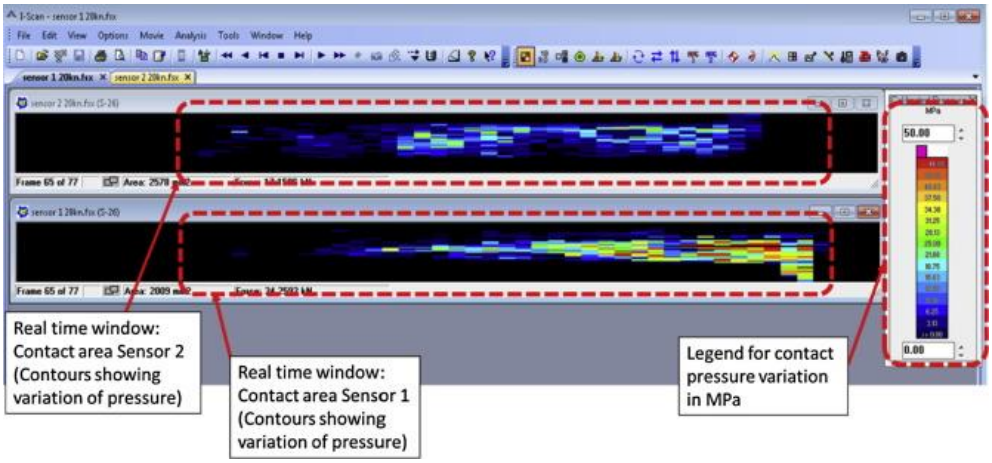

Fig. 3-34: Real-time recording of the actual stress [115]

Next, Zahra and Dhanasekar analysed the contact area over time (**Fig. 3-35** - left) of the four performed tests and 3 phases could be extracted. The first phase consisted of very low contact areas due to the peaks of the roughness. The second phase was composed of an almost vertical increase of the contact area due to the application of the load, which was due to crushing of the peaks of the roughness. The third and last phase consisted of an almost horizontal increase of the contact area since 85-95 % of the surface of the face-shells was in contact. Furthermore, due to the roughness of the surface of the masonry blocks a non-uniform contact pressure was observed.

Next, the relation between the contact area and the applied load is analysed. It could be stated that the highest increase of the contact area with up to 60 % occurred in the application of the first 20 kN. A continuous increase of the load to 80 kN, increased the contact area to 88 %. At the final steps, the impact of the closed gaps and interstices on the contact area started to be more important, which was characterised by a sudden increase of the contact area up to 90 - 95 %.

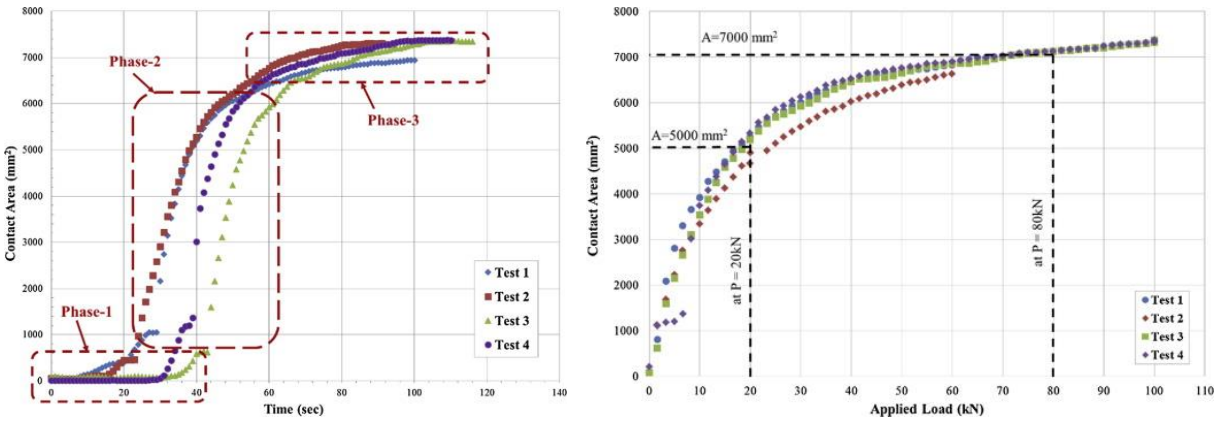

Fig. 3-35: Relation between contact area and time (left); relation between contact area and applied load (right) [115]

The non-uniform distribution was validated by analysing the contact pressure at each measured point of the surface (**Fig. 3-36**). At a load of 20 kN, resp. 100 kN a maximum stress on a contact point of 34 MPa, resp. 77 MPa was observed. Furthermore, Zahra and Dhanasekar observed that some points of the roughness kept at a very high pressure and did not crush. They claimed that this occurrence could be explained by a coarse aggregate present on that place.

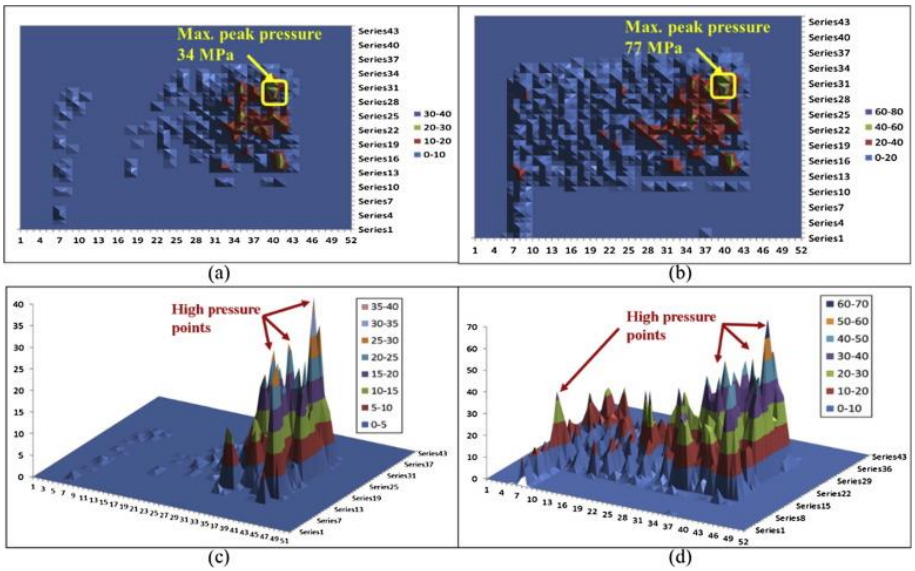

Fig. 3-36: Pressure distribution at each measure point, top figures in 2D for a load of 20 and 100 kN and bottom figures in 3D for a load of 20 and 100 kN [115]

3.4.2.2.2 ROUGHNESS

In 1966, Greenwood and Williamson [112] claimed that independent from the materials, the surfaces are rough on a microscopic scale. Consequently, the net contact area is highly reduced between two surfaces. Different models have been studied to assess the real contact area between two superposed surfaces, but no precise solution could be presented [116].

The contact between two nominally smooth surfaces was analysed by Zhao et al. [117], who divided the contact status in an elastic-plastic and fully plastic situation. They concluded that the asperities could be assumed spherical and the roughness was based on a Gaussian distribution.

Pasaribu and Schipper [118] developed a deterministic model based on a rough surface against a flat-layered surface. The aim of this model was to analyse the contact area and the load carried by each asperity. The asperities were assumed spherical and that there was no interaction between them. Each asperity i was based on its radius β_i and its height z_i. The latter is based on the mean plane as presented in **Fig. 3-37**.

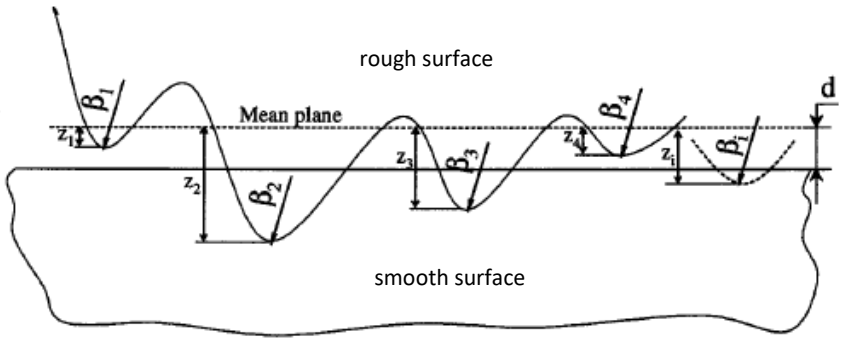

Fig. 3-37: Definition of the asperities of the rough surface (top) and contact to the smooth surface (bottom) [118]

The distance between the two surfaces d defines if an asperity from the rough surface is in contact with the smooth surface, which is the case if $z_i > d$. However, if $z_i < d$ there is no contact between the respective asperity from the rough surface and the smooth surface. The local indentation depth ω_i was defined according to eq. 3-1 by assuming the smooth surface does not deform, which induces that only the asperities would deform.

$$\omega_i = z_i - d \qquad \text{(eq. 3-1)}$$

Passaribu and Shipper [118] considered that the contact status could be elastic, elastic-plastic, or fully plastic. Furthermore, they stated that the status was dependent on the indentation depth of each asperity. According to Greenwood and Williamson [112] and [119], the transition from elastic to elastic-plastic occurs at the critical indentation depth ω_{ci} as defined in eq. 3-2. ω_{ci} is dependent on the radius of the asperity β_i, the hardness H of the material and the reduced elastic modulus E^* of the two surfaces in contact as defined in eq. 3-3. The latter is based on the Young's Modulus of both materials (E_1 and E_2) and on the Poisson's ratio (ν_1 and ν_2) of each material.

$$\omega_{c1} = 0.89\beta_i \left(\frac{H}{E^*}\right)^2 \qquad \text{(eq. 3-2)}$$

$$E^* = \frac{E_1 E_2}{E_1(1-\nu_2^2) + E_2(1-\nu_1^2)} \qquad \text{(eq. 3-3)}$$

The next transition would be from elastic-plastic to fully plastic and would occur at the critical indentation depth ω_{c2} as defined in eq. 3-4, which is dependent on a constant $c = 54$ presented by Zhao et al. [117].

$$\omega_{c2} = c \times \omega_{c1} \qquad \text{(eq. 3-4)}$$

The contact area A_i is dependent on the contact status (elastic e, elastic-plastic ep, fully plastic p) of each asperity and is defined in eq. 3-5. The contact area at an elastic situation A_{ie}, at an elastic-plastic status A_{iep} and at a fully plastic situation A_{ip} are defined in eq. 3-6, eq. 3-7 and eq. 3-8.

$$A_i(\omega_i) = \begin{cases} A_{ie}(\omega_i), & if\ \omega_i < \omega_{ci}(\omega_i) \\ A_{iep}(\omega_i), & if\ \omega_{c1}(\omega_i) < \omega_i < \omega_{c2}(\omega_i) \\ A_p(\omega_i), & if\ \omega_{c2}(\omega_i) < \omega_i \end{cases} \qquad \text{(eq. 3-5)}$$

$$A_{ie}(\omega_i) = \pi\beta_i\omega_i \quad \text{(eq. 3-6)}$$

$$A_{iep}(\omega_i) = \pi\beta_i\omega_i\left[1 - 2\left(\frac{\omega_i - \omega_{c1}}{\omega_{c2} - \omega_{c1}}\right)^3 + 3\left(\frac{\omega_i - \omega_{c1}}{\omega_{c2} - \omega_{c1}}\right)^2\right] \quad \text{(eq. 3-7)}$$

$$A_{ip}(\omega_i) = 2\pi\beta_i\omega_i \quad \text{(eq. 3-8)}$$

The load P_i carried by the area of each asperity can is dependent on the contact status of each asperity and is defined in eq. 3-9. The load carried at an elastic situation P_{ie}, at an elastic-plastic status P_{iep} and at a fully plastic situation P_{ip} are defined in eq. 3-10, eq. 3-11 and eq. 3-12.

$$P_i(\omega_i) = \begin{cases} P_{ie}(\omega_i), & if\ \omega_i < \omega_{ci}(\omega_i) \\ P_{iep}(\omega_i), & if\ \omega_{c1}(\omega_i) < \omega_i < \omega_{c2}(\omega_i) \\ P_p(\omega_i), & if\ \omega_{c2}(\omega_i) < \omega_i \end{cases} \quad \text{(eq. 3-9)}$$

$$P_{ie}(\omega_i) = \frac{4}{3}E\beta_i^{0.5}\omega_i^{1.5} \quad \text{(eq. 3-10)}$$

$$P_{iep}(\omega_i) = A_{iep}\left[H - 0.6H\frac{\ln(\omega_{c2}) - \ln(\omega_i)}{\ln(\omega_{c2}) - \ln(\omega_{c1})}\right] \quad \text{(eq. 3-11)}$$

$$P_{ip}(\omega_i) = A_{ip}H \quad \text{(eq. 3-12)}$$

The total contact area A_{tot} as well as the total carried load P_{tot}, are defined as the summation of the area resp. the carried load of each singular asperity and are defined in eq. 3-13 resp. eq. 3-14.

$$A_{tot} = \sum_i A_i \quad \text{(eq. 3-13)}$$

$$P_{tot} = \sum_i P_i \quad \text{(eq. 3-14)}$$

The presented deterministic contact model is intended for a rough surface against a smooth surface. Pasaribu and Shipper [118] compared this model with the experimental results of Sherbiney and Halling [120] and the numerical calculations of Tang and Arnell [121]. Both models consisted of the contact of a single spherical asperity to a flat-layered surface. Pasaribu and Shipper concluded that extending the single asperity model to the proposed deterministic model was in agreement with the experimental and the numerical models. The deterministic model gives the possibility of analysing the contact area and the carried load more accurately by considering the radius of each asperity. The radius of each asperity

β_i can be calculated using the 3-point peak criterion (3PP criterion) proposed by Pogačnik and Kalin [122] (**Fig. 3-38**). They claimed that an asperity is not perfectly spherical and therefore, proposed a model to extract one radius for each asperity connecting the peak point and its two nearest neighbour points with a circumcircle based on the mathematical equation of a circle (eq. 3-15). Furthermore, they evolved the 3PP criterion to a 5PP and 7PP criterion by implementing more criteria in a 2D model.

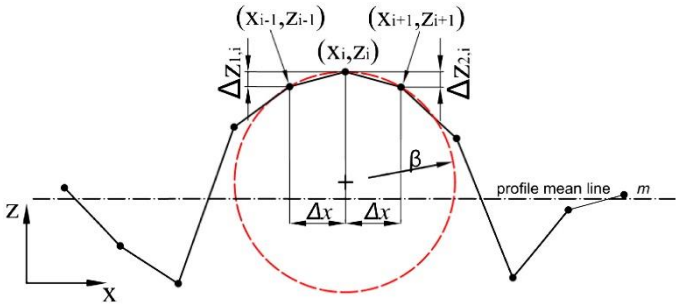

Fig. 3-38: 3-point peak criterion (3PP criterion) [122]

$$Ax^2 + Ay^2 + Bx + Cy + D = 0 \qquad \text{(eq. 3-15)}$$

The coordinates of the three asperity points and passing through the circle are introduced into the eq. 3-15 and the coefficients A, B, C and D are determined using the determinants in relation to the coordinates of the three asperity points. Finally, the radius of each asperity can be determined based on the four coefficients (A, B, C and D) as presented in eq. 3-16.

$$r = \sqrt{\frac{B^2 + C^2 - 4AD}{4A^2}} \qquad \text{(eq. 3-16)}$$

As a conclusion, the contact area and the carried load of a surface could be determined using the deterministic model presented by Pasaribu and Shipper and the radii definition of the asperity proposed by Pogačnik and Kalin.

3.4.1 CONNECTION TO INSULATION MATERIAL

The low thermal transmittance value in a wall imposed by the Luxembourgish standard (U=0.13 W/m^{2}K) [123] in accordance to the European directive 2010/31/UE affected the approach of manufacturing masonry blocks. Furthermore, the fact of the increasing labour price intensifies the need of a masonry block with bearing capacities and a good thermal conductivity. This aim can be approached using different techniques, which are presented in this section.

The biggest problem in a masonry block are the thermal bridges from the outside to the inside of a building. The thermal resistance of a block can be improved by integrating as many closed air gaps as

possible in block to reduce the amount of thermal bridges per block. This technique was analysed by Pierzchlewicz [124] by varying the hole configuration of a concrete masonry block and analysing its thermal conductivity (**Fig. 3-39**). The major difference between the types of blocks analysed was the position of the holes. Type 1 and 2 had aligned holes, while Type 3-5 had staggered holes, which increases the heat flow path from the outside to the inside. Another difference in the 6 types analysed by Pierzchlewicz were the dimensions of the holes and of the complete block. The blocks of type 1 and 2 with aligned holes achieved a thermal conductivity value between 0.87-0.92 W/mK. The fact of staggering the hole position reduced the thermal conductivity of the concrete masonry blocks based on type 3-6 to 0.57-0.68 W/mK. Pierzchlewicz concluded that integrating holes in a concrete masonry block reduces the thermal conductivity by up to 52.5 % compared to a solid concrete block (1.2 W/mK). The thermal conductivity of these blocks could be improved by reducing the thickness of the holes to a minimum, which would reduce the convection effect within these holes [125].

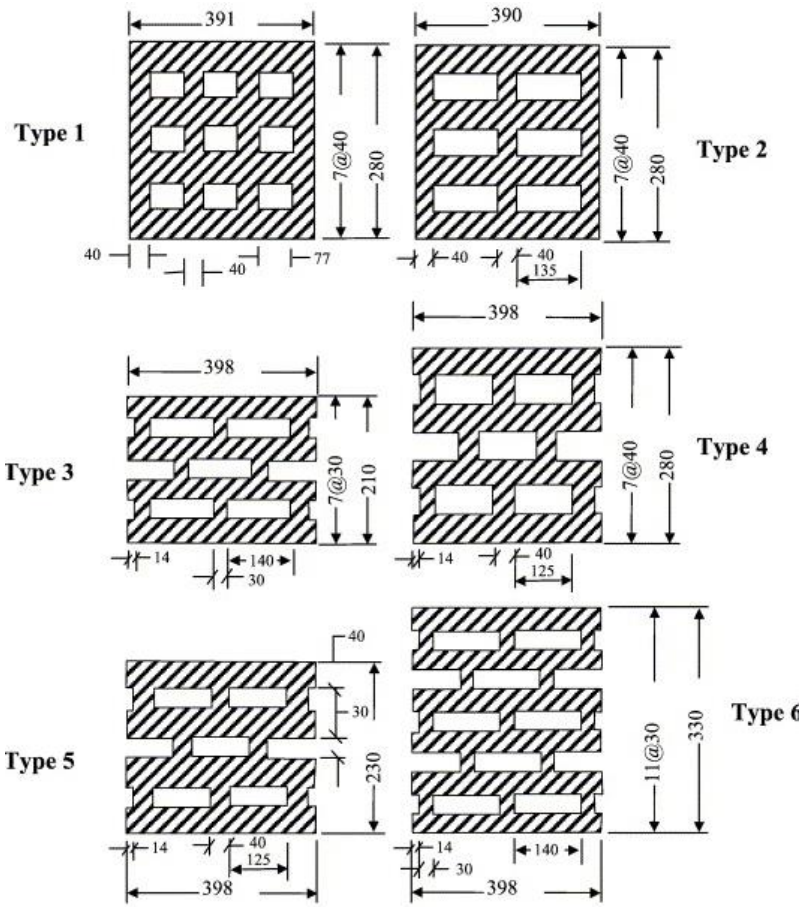

Fig. 3-39: Hollow blocks analysed by Pierzchlewicz [124]

Zukowski and Haese [126] analysed a similar block as Pierzchlewicz with the difference that the hollow blocks were based on porous clay. The holes in the block were filled with perlite to reduce the thermal conductivity of the block (**Fig. 3-40**). The density of the porous clay and the perlite was of 1400 kg/m^3 and 120 kg/m^3 with a thermal conductivity value of 0.410 W/mK resp. 0.046 W/mK. An average thermal

conductivity of 0.09 W/mK was measured using three temperature differences $\Delta\theta$ of 20, 25 and 30°C. Furthermore, they concluded that the masonry block based on porous clay with a density of 653.2 kg/m^3 had a heat capacity of 855.1 J/kgK.

Fig. 3-40: Clay block filled with perlite [126]

Al-Jabri et al. [127] compared a hollow block (PolyBlock 1) and a bearing block linked by a dovetail connection to an insulation (PolyBlock 2) to an ordinary concrete block (**Fig. 3-41**). The PolyBlock 1 was based on polystyrene beads used as lightweight aggregates. The PolyBlock 2 was from a commercial manufacture and no precise details on the material composition are presented by the authors. Al-Jabri et al. analysed the thermal conductivity and the compressive strength of these 3 types of blocks. The masonry block PolyBlock 1 had a density of 798 kg/m^3, which was 44 % lower than the density of the PolyBlock 2 (1418 kg/m^3) and 33 % lower than the ordinary masonry blocks (1168 kg/m^3). The compressive strength of PolyBlock 1 and 2 was of 3.3 and 10.2 MPa, while the compressive strength of the ordinary blocks varied from 5-15 MPa. The thermal conductivity of the PolyBlock 1 and 2 reached a value of 0.626, resp. 0.616 W/mK, which was in average 61 % lower than the thermal conductivity of the ordinary block (1.6 W/mK). So, Al-Jabri et al. concluded that considering the compressive strength and the thermal conductivity the masonry block PolyBlock 2 was the most suitable.

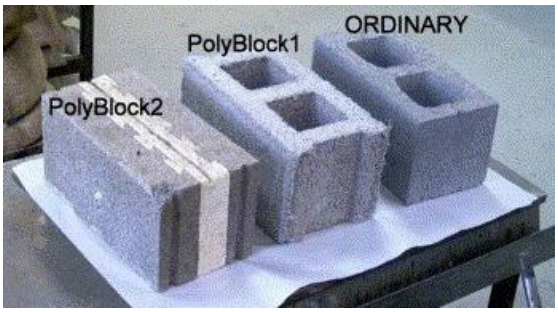

Fig. 3-41: Blocks analysed by Al-Jabri et al. [127]

As previously presented, there are different ways to link a bearing material with an insulation material. In **Fig. 3-42** different commercially manufactured masonry blocks are presented. The first block (a) consists of three parts, two bearing and one insulation part, which are all connected by a dovetail

connection to avoid thermal bridges. The two bearing parts consist of a lightweight concrete with expanded clay as aggregates and the insulation part consists of a polystyrene. The thermal transmittance value of this block is of 0.11 W/m^{2}K. However, these blocks have a low load-bearing capacity of 3 MPa. The second presented block (b) is used as a formwork block. The two outer parts of the block are based on a wood-cement mixture and are connected. This connection leads to thermal bridges between the outside and the inside of the masonry block. However, an insulation is inserted in one part of the block to reduce its thermal transmittance value, which can vary from 0.17-0.30 W/m^{2}K depending on the thickness of the applied insulation. The open space visible in **Fig. 3-42** (b) is filled with a steel reinforcement and concrete. The two other blocks (c) and (d) are based on lightweight concrete with an expanded polystyrene insulation. The two blocks have the same dimensions of 40x20x20 cm. The biggest difference between them is their connection to the insulation. Block (c) connects the bearing parts to the insulation part by a dovetail connection, as Block (a), and achieves a thermal transmittance value of 0.375 W/m^{2}K. Block (d) is a full block with cavities filled with the expanded polystyrene. However, the thermal transmittance is higher (0.64 W/m^{2}K) due to the heat flow that occurs from one side to the other in the masonry block.

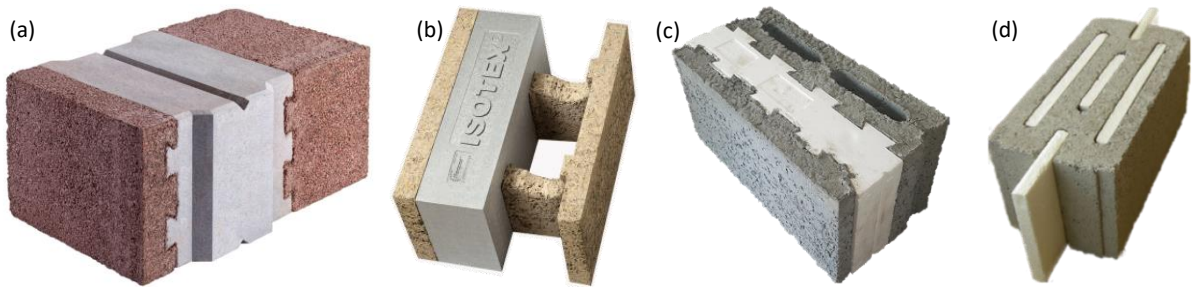

Fig. 3-42: Different commercialised masonry blocks with improved insulation properties; (a) [128]; (b) [129]; (c) (d) [130]

In conclusion, it can be stated that there are numerous approaches to achieve a masonry block with good bearing and insulation properties. Furthermore, the most promising results were achieved by separating the bearing and the insulation part. Therefore, this work will present a dovetail connection between one bearing and one insulation material based on Miscanthus.

3.5 MACHINE LEARNING

In this section, the literature on machine learning is studied to predict the compressive strength of a concrete mixture based on the imposed components. Different techniques can be used to develop an accurate and reliable model to optimise a mixture to the needed compressive strength. The use of the tool of machine learning is increasing for mixture design and optimisation. This artificial intelligence allows adopting a self-learning based on a defined input and output dataset [131]. The most used

techniques applied in the construction section, more precisely the definition of the compressive strength, are the artificial neural networks (ANNs) [132-134], the fuzzy logic [135, 136] and the regression analysis [137-139].

3.5.1 ARTIFICIAL NEURAL NETWORK

The technique of artificial neural networks came up in the 1980s in the cognitive and computer science research [140]. These algorithms were mostly used in the biological data-mining sector, which clearly enhanced the pattern analysis of this technique. The development of this technique is based on the operating mode of how to learn and how to deduce the output data from an input dataset. Nowadays, the ANNs are also used in civil engineering sector due to its high system performance.

Yeh [141] used the ANNs technique to predict and optimise the workability and strength of high-performance concrete. Therefore, the mixture proportions of eight variables (cement, fly ash, blast furnace slag, water, superplasticizer, coarse aggregate, fine aggregate and age of testing) were introduced and varied. Similarly, the compressive strength of lightweight concrete was predicted by Alshihri et al. [142], which based and validated his findings on experimental tests performed in laboratory. Ni and Wang [132] used the ANN but on a single-layer model to predict the compressive strength of concrete after a curing time of 28 days. Bingol et al. [143] used ANNs also to predict the compressive strength of lightweight concrete but with the condition of using pumice aggregates that were previously subjected to high temperatures. A different method of using the ANNs model was adopted by Das et al. [144] to predict the mix proportions of concrete. They manually varied the hidden-layer neurons until achieving an optimal value for the output results.

3.5.2 FUZZY LOGIC

The machine-learning technique of fuzzy logic is based on a degree of truth. The results obtained from this technique are between 0 and 1. The fuzzy logic technique is not seen as a statistical model but mainly as a possibility theory [145]. This approach does not assess its accuracy of the predictions, because it does not verify the correctness of its output data [146]. The reasoning of the fuzzy logic technique to convert the input data into output consists of first measuring the strength of each imposed rule, followed by resolving the consequences of each rule and finalising by merging all this data with the input data [147]. The fuzzy logic technique is not so widely used in civil engineering applications because the results can be compared to an uncertain and imprecise human reasoning [148].

Topcu and Saridemir [135] used the fuzzy logic technique in the civil engineering sector but in combination with the ANNs. They assembled the data of 180 specimens based on 52 mixes and predicted the compressive strength of concrete using nine parameters, which included fly ash.

3.5.3 REGRESSION ANALYSIS

The oldest and one of the most used multivariate technique is the regression analysis [149]. This technique uses all the input variables to perform one prediction. Different regression analysis can be performed. One of the most known and used approach in the regression analysis is the linear regression, which aims for a linear combination between the predictors to achieve a response.

One of the easiest algorithm to be understood is the linear regression, which induces a lower need of computational process and time compared to other algorithms. The latter is also the reason for it to be one of the most widely used approaches to define a relationship between a response and a number of independent predictors [150].

These techniques are also used in civil engineering sector. Chopra et al. [137] used the mix proportions of the laboratory experimental tests and predicted the compressive strength of concrete with and without fly ash replacing the amount of cement after a curing time of 28, 56 and 91 days. Another use of the linear regression was performed by Huang et al. [151], which predicted the bond strength of a fibre reinforced polymer using a multiple linear regression.

Omran et al. [152] compared different approaches based on the regressions analysis to predict the compressive strength of concrete containing three materials to replace ordinary cement, fly ash, Haydite aggregate and Portland limestone cement. The ensemble models and the bootstrap aggregating techniques achieved a good prediction performance. However, the most accurate results were achieved using the Gaussian process regression.

The advantage of the Gaussian process regression being able to be used in different fields is due to its efficient, probabilistic and nonparametric approach, which allows modelling nonlinear and complex functional mappings [153]. This technique is able to describe the distribution of the predictors over functions, which are principally based on a mean function and a covariance function. The latter is based on a given function that designates the influence of each parameter. This possibility allows handling nonlinear data in a precise and optimal way using the Gaussian process regression [153]. This technique was also adopted by Pal and Deswal [154], which raised the reliability of the response based on the input data. Furthermore, the Gaussian process technique allows some precise fitting functions by varying the used kernel function.

Chapter 4 OPTIMISATION OF THE MECHANICAL PROPERTIES OF MISCANTHUS LIGHTWEIGHT CONCRETE (PUBLICATION ON MISCANTHUS MIXTURES)

4.1 ABSTRACT

In this paper, Miscanthus fibres are used to develop lightweight concrete. The amount of Miscanthus and cement, as well as the water/cement ratio, are varied to analyse the behaviour of the mixture concerning the physical and mechanical properties. The Miscanthus was anteriorly pre-treated with a silicate sealant or a cement-based fluid. The current paper analyses the impact of the pre-treatment of the Miscanthus fibres on the compressive strength as well as on the long-term deformations. The specimens with a pre-treatment based on a silicate sealant reached a compressive strength of 19.3 MPa, which is higher than the compressive strength of a conventional LC 16/18, a Young's Modulus above 9.9 GPa and a shrinkage deformation of 2244 $\mu m/m$. Nevertheless, considering the density the pre-treatment showed not to be beneficial.

Keywords – Miscanthus x giganteus; Miscanthus lightweight concrete; Pre-treatment of Miscanthus fibres; Compressive strength; Shrinkage.

4.2 INTRODUCTION

The replacement of aggregates by Miscanthus in concrete formulations aims to reduce the depletion of natural resources such as natural sand and gravel, which are continuously diminishing at some regions of the world due to significant exploitation [37]. This scarcity of natural resources is especially visible in highly developed countries, where opening new quarries become more problematic due to strict governmental regulations. In addition, the use of the Miscanthus plant is a sustainable solution as this plant is among others cultivated for depollution of industrial wasteland.

The Miscanthus x giganteus (Mxg) plant originates from tropical and subtropical regions [155], and its first cultivation in Europe was in the 1930s. Since 1989, field trials have been performed with this plant to investigate its biomass potential. This plant can grow up to 4 m, and the low need for fertilisation and pesticide inputs makes this grass economically and ecologically very interesting. Moreover, this plant decreases water pollution on soil organisms and increases its fertility [17]. These advantages, in addition to the positive impact on biodiversity, render phytoremediation of industrial soils possible. However, during the first winter, the plant presents a narrow genetic base and a low firmness [155]. In the following years, the plant can develop a considerable growth and can achieve a mass production of about 10 to 30 t dry weight per ha per year, considering European climatic conditions and still depending on the different regions [12, 13].

The cross-section of Miscanthus is composed of four types of tissue layers and is subdivided into three regions (**Fig. 4-1**). The outer zone comprises the epidermis (Ep), the sclerenchyma (Sc) and small vascular bundles (Vb). Ep represents the protective outer coating of the cross-section. Sc embodies the outer cell ring, which supports the structural framework of the plant. The Vb consist of supportive and protective tissues and are heterogeneously distributed over the whole cross-section. The intermediate zone is composed of vascular bundles and parenchyma (Pa). The inner region mostly accommodates parenchyma tissues, which are mainly responsible for the photosynthesis process and the commutation of gases [20, 21].

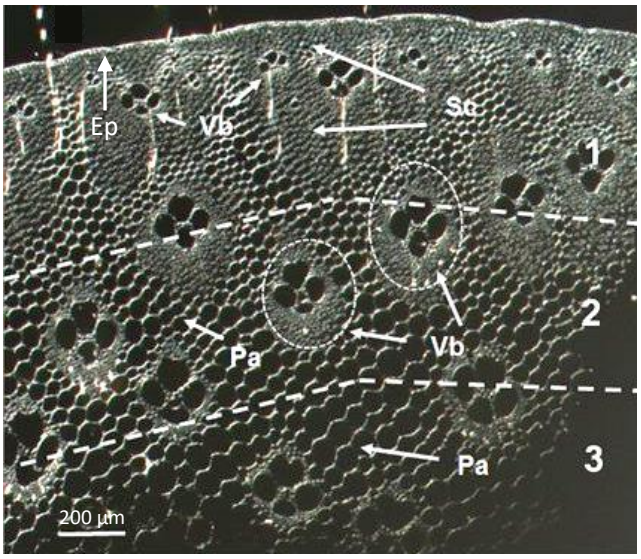

Fig. 4-1: Cross-section of a Miscanthus x giganteus stalk (adapted from B. Chabbert et al. [20])
Ep = epidermis, Sc = sclerenchyma ring (outer ring), Vb = vascular bundles and Pa = parenchyma ring

Nowadays, the use of natural fibres is continuously increasing. The C4-plant Mxg is, e.g. used for energy and biofuel production [156] or as deep litter bedding for horses on account of their high water absorption capacity (in average 304 % [22, 157]). Also, the trend of using natural fibres for lightweight concrete (LC) has grown [158]. Therefore, investigations are carried out on bamboo, jute, flax, hemp, Miscanthus and wood fibres to develop renewable construction materials [52, 62-67, 84, 159-161].

K. Kaack et al. [43] determined the material properties of Miscanthus stems including the flexural rigidity (1-3.5 Nm^2), the moment of inertia (18 000-35 000 m^4) and the Young's Modulus (2-8 GPa). They concluded that the mechanical characteristics mostly depend on the number of subdivisions of the primary stem (internodes) [43]. For comparison to the Young's Modulus of Miscanthus with other natural fibres, O. Faruk et al. [41] analysed the Young's Modulus of bamboo (11-17 GPa), jute (26.5 GPa), flax (27.6 GPa) and hemp (70 GPa) fibres.

Concrete mixtures based on lightweight aggregates are conceived using different binders and component variations. H. Ramaswamy et al. [44] constituted mixtures based on jute, coir and bamboo fibres using weight proportions of 1:3.58:2.87 (cement:sand:coarse aggregate), a w/c ratio of 0.65 and 1% (in vol.) of fibres. After a curing time of 28 days, a compressive strength of 6.86 MPa (jute), 8.33 MPa (bamboo) and 10.3 MPa (coir) have been achieved. Furthermore, an LC based on hemp fibres, with a fibre length of 7-8 mm, was investigated by L. Arnaud and E. Gourlay [45]. They analysed the impact of four hydraulic limes on the compressive strength (**Table 4-1** (A1 – A4)). The investigated binders were NHL 3.5 (Mix A1), NHL 3.5 Z (Mix A2), NHL 2 (Mix A3) and a pre-formulated lime-based binder based on air lime (75%), hydraulic lime (15%) and pozzolanic lime (10%) (Mix A4). In addition to these variations, the effect of different curing conditions was examined by alternating the relative humidity

(RH) of the environment (RH = 30%, 50%, 75% and 98%). The highest compressive strength was reached by the specimens cured in an atmosphere of 20°C and an RH of 50% (**Table 4-1** (A1 – A4)). L. Arnaud and E. Gourlay [45] state that a higher RH (75 and 98%) had with a reduction of 45-55% a negative impact on the compressive strength due to the impediment of carbon dioxide diffusion from the binder. From these four limes, the mixtures using NHL 3.5 and the pre-formulated binder showed the highest compressive strength (**Table 4-1** (A2, A4)). C. Niyigena et al. [52] analysed different types of hemp shives and achieved similar compressive strength (0.13 – 1.07 MPa) as L. Arnaud and E. Gourlay [45].

Lit.	Mix name	Light-weight aggregate type	Aggregate		Cement		Lime		Water		Compr. strength [MPa]
			[kg/m³]	[wt.%]	[kg/m³]	[wt.%]	[kg/m³]	[wt.%]	[kg/m³]	[wt.%]	
[44]	-	Jute	n.g.		n.g.		n.g.		n.g.		6.86
	-	Bamboo	n.g.		n.g.		n.g.		n.g.		8.43
	-	Coir	n.g.		n.g.		n.g.		n.g.		10.3
[45]	A1	Hemp shives	n.g.	14.3	n.g.	-	n.g.	34.8	n.g.	50.9	0.18
	A2	Hemp shives	n.g.	15.4	n.g.	-	n.g.	37.7	n.g.	46.9	0.31
	A3	Hemp shives	n.g.	15.9	n.g.	-	n.g.	38.9	n.g.	45.2	0.22
	A4	Hemp shives	n.g.	14.3	n.g.	-	n.g.	34.8	n.g.	50.9	0.33
[46]	B1	Hemp shives	n.g.	16.0	n.g.	-	n.g.	34.0	n.g.	50.0	0.18 – 0.85
[47]	C1	Sawdust 75% waste paper	n.g.		n.g.		n.g.		n.g.		0.80
[48]	D1	Hemp composition	n.g.	12.0*	n.g.	-	n.g.	42.7*	n.g.	45.3*	0.20(1)
	D2		n.g.	12.4*	n.g.	-	n.g.	37.6*	n.g.	50.0*	0.15(1)
	D3		n.g.	12.0*	n.g.	10.8*	n.g.	29.2*	n.g.	48.0*	0.44(1)
	D4		n.g.	11.7*	n.g.	20.9*	n.g.	20.2*	n.g.	46.4*	0.83(1)
	D5		n.g.	10.4*	n.g.	47.4*	n.g.	-	n.g.	42.2*	0.55(1)
[49](2)	E1	Hemp straw	152.9	11.6	688.1	52.0	-	-	481.7	36.4	0.90
	E2		130.8	9.7	719.2	53.1	-	-	503.5	37.2	1.02
	E3		152.9	11.6	584.9	44.2	103.2	7.8	481.7	36.4	1.42
	E4		130.8	9.7	611.3	45.1	107.9	8.0	503.5	37.2	1.91
	E5		130.8	9.7	503.5	37.2	215.8	15.9	503.5	37.2	1.51
	E6		152.9	11.5	481.7	36.1	206.4	15.5	481.7	36.2	1.47
	E7		129.3	9.6	498.0	37	213.4	15.8	498.0	36.9	1.30
	E8		129.3	11.1	498.0	42.5	213.4	18.2	320.1	27.4	2.10
[22]	F1	Mxg (2002)	55.6 – 81.5	9.2 – 12.9*	250.0	39.6 – 41.3*	50.0	7.9 – 8.3*	250.0	39.6 – 41.3*	0.44 – 0.61
	F2	Mxg (2003)	81.0 – 86.5	12.8 – 13.6*	250.0	39.3 – 39.6*	50.0	7.9*	250.0	39.3 – 39.6*	0.33 – 0.44
	F3	M. sacchari-florus (2002)	109.5 – 123.1	16.6 – 18.3*	250.0	37.1 – 37.9*	50.0	7.4 – 7.6*	250.0	37.1 – 37.9*	0.26 – 0.30
	F4	M. sacchari-florus (2003)	123.9 – 142.5	18.4 – 20.6*	250.0	36.1 – 37.1*	50.0	7.2 – 7.4*	250.0	36.1 – 37.1*	0.39 – 0.44
	F5	M. sinensis (2002)	74.4 – 77.6	11.9 – 12.4*	250.0	39.8 – 40.0*	50.0	8.0*	250.0	39.8 – 40.0*	0.23 – 0.31
	F6	M. sinensis (2003)	62.9 – 85.2	10.3 – 13.4*	250.0	39.4 – 40.8*	50.0	7.9 – 8.2*	250.0	39.4 – 40.8*	0.24 – 0.35
	F7	M. robustus (2002)	76.0 – 88.5	12.1 – 13.9*	250.0	39.2 – 39.9*	50.0	7.8 – 8.0*	250.0	39.2 – 39.9*	0.22 – 0.35

	F8	M. robustus (2003)	62.3 – 85.6	10.2 – 13.5*	250.0	39.3 – 40.8*	50.0	7.9 – 8.2*	250.0	39.3 – 40.8*	0.23 – 0.28
[162](3)	G1	Mxg (pre-soaked fibres)	17.4 – 25.0	1.0 – 1.5*	918.6	54.4 – 54.6*	229.7	13.6 – 13.7*	515.3	30.5 – 30.7*	13.4 – 17.6
	G2		34.8 – 50.0	2.3 – 3.3*	816.6	53.4 – 54.0*	204.2	13.4 – 13.5*	458.0	30.0 – 30.3*	6.8 – 11.0
	G3		52.2 – 75.0	3.9 – 5.5*	714.5	52.2 – 53.1*	178.6	13.0 – 13.3*	400.8	29.3 – 29.8*	2.3 – 5.2
	G4	Mxg (cement impregnated fibres)	17.4 – 25.0	1.0 – 1.5*	918.6	54.4 – 54.6*	229.7	13.6 – 13.7*	515.3	30.5 – 30.7*	23.1 – 28.2
	G5		34.8 – 50.0	2.3 – 3.3*	816.6	53.4 – 54.0*	204.2	13.4 – 13.5*	458.0	30.0 – 30.3*	16.0 – 24.1
	G6		52.2 – 75.0	3.9 – 5.5*	714.5	52.2 – 53.1*	178.6	13.0 – 13.3*	400.8	29.3 – 29.8*	10.8 – 16.9

n.g.: not given;
*: calculated values obtained by dividing the weight of the component by the total weight of the mixture;
(1): compressive strength for a curing time of 126 days;
(2): cement replaced by quarry fines;
(3): lime replaced by ground granulated blast furnace slag.

Table 4-1: Different Mixture compositions per kg/m^3, per wt. % and achieved compressive strength for a curing time of 28 days.

Moreover, S. Elfordy et al. [46] used a different method to manufacture hemp concrete. It consisted of projecting the mixture to a wall or mould through a pipe. The difference here is that the water is only added to the dry-mix (lime and hemp straw) just before it is projected (using a Y-branch pipe). This process gives less time to the fibres to absorb water, and hence less water is needed. By using this method, S. Elfordy et al. [46] reached a compressive strength of 0.85 MPa (**Table 4-1** (B1)). Furthermore, the high mass of lightweight aggregate (16 wt.% of hemp shives) led to low densities and thus, low thermal conductivities were measured (0.18 - 0.55 W/mK). Very low thermal conductivities (0.046 to 0.069 W/mK) were also reached by E. P. Aigbomian et al. [47] developing a lightweight concrete using woodchip aggregates which resulted in a compressive strength of 0.80 MPa (**Table 4-1** (C1)).

P. B. De Bruijn et al. [48] created a hemp concrete using aggregates based on dust (4 wt. %), shives (62 wt. %) and fibres (35 wt. %). Besides, the amount of lime presented in **Table 4-1** (D1 – D5) is a combination of hydrated (25 – 40 %) and hydraulic lime (60 – 75 %). It is good to mention that the mixture using cement and lime reached the highest compressive strength (0.83 MPa). A different hemp concrete was established by V. Dubois et al. [49] using quarry fines instead of cement. They analysed the impact of the relation binder/aggregate (B/A = 4.5, B/A = 5.5) on the compressive strength, the variation of the lime proportions in the binder (0, 15 and 30 %) and the W/C ratio (0.45, 0.7) (**Table 4-1** (E1 – E8)). They conducted compressive strength tests on cylinders (h=220 mm and d=110 mm) and achieved a maximum stress of 2.10 MPa (B/A = 5.5, Lime proportion = 30 %, W/C = 0.45).

Further investigations on concrete mixtures based on Miscanthus were performed by R. Pude et al., Y. Chen et al. and L. Chupin et al. [22, 162, 163]. R. Pude et al. [22] analysed four genotypes of Miscanthus stems (harvested in 2002 and 2003) for their suitability as lightweight concrete aggregates (**Table 4-1** F1 – F8). During the mixing procedure, they measured a pH-value of 11-12 on the mixture and the outer ring of the stem. These values imply that the cement paste had moved up to the outer ring. R. Pude et al. [22] concluded that when embedding Miscanthus with cement, the calcium settles mostly on the sclerenchyma of the Miscanthus fibre. The highest compressive strength (0.61 MPa) was achieved using Mxg from 2002. According to R. Pude et al. [22], the reason for this result is the high cellulose content of the fibres (37.9 – 42.0% of dry matter).

L. Chupin et al. [163] compared the use of rhizomes and stems of Mxg as aggregates for LWC. For the mixture prepared with the stem fibres reached almost the double of the tensile strength of the mix with rhizomes. Besides, the Young's Modulus of the mix with the stem fibres was 3.5 – 4 times higher (900 – 1000 MPa) than the mix based on the rhizomes fibres (257 MPa) [163]. Also, L. Chupin et al. measured a higher cellulose proportion for the stem (47.5 % CWR) than for the rhizome (26.9 – 30.7 % CWR). This measurement supports the statement of R. Pude et al. [22] that a high cellulose content has a positive impact on the bond between plant and cement paste.

Furthermore, Y. Chen et al. [162] developed multiple mixtures (**Table 4-1** (G1 – G6)) using three different lengths of Miscanthus fibres (Powder, 0-2 mm and 2-4 mm). Long strands (2-4 mm) reduced the workability and increased the porosity of the matrix. According to Y. Chen et al. this occurrence also has a positive impact on the acoustic properties since more energy could be absorbed. Furthermore, due to the high water absorption of the fibres [22, 50], Y. Chen et al. analysed the impact of two kinds of pre-treatments on the compression strength, one based on a water saturation of the fibres and the second on impregnation with a cement suspension. The latter presented at least a 45% higher compressive strength after 28 days than the mixtures containing pre-soaked Miscanthus fibres.

The research in this paper aims to develop a concrete mixture using the highest possible amount of Mxg aggregates to create a Miscanthus lightweight concrete that can be used for load-bearing applications on masonry blocks. Except for the mixtures given by Y. Chen et al. [162], no mix could be found in literature that could be used as a load-bearing material. Therefore, the authors examine the physio-chemical processes regarding variations of the mixture components, pre-treatment and long-term deformations. Furthermore, a relation between the compressive strength and the densities has been analysed. Due to the high water absorption capability of the fibres, an investigation on the need of a pre-treatment is carried out. Simultaneously, long-term deformation measurements in shrinkage drains have been performed and analysed by taking into account the type of pre-treatment.

4.3 MATERIALS AND EXPERIMENTS

4.3.1 RAW MATERIALS

The current study is performed on Mxg fibres, which were produced by Luxemburgish farmers. Its separation was performed during the harvest process by cutting the stem in threads of a length of 4 to 6 cm. Furthermore, these strands were used within concrete mixtures to create a bearing material, which can be compared to lightweight concrete.

The Miscanthus concrete mixtures consisted of six components (**Table 4-2)**. The binders were hydraulic lime (NHL 3.5) and cement (CEM I, 42.5R). Instead of increasing the amount of cement, calcium chloride ($CaCl_2$) was used as a mineraliser to increase the compressive strength at an early stage [33, 164-166]. $CaCl_2$ dissolves easily in water, changes the rate of hydration of the mixture, reduces the setting time by 50% and accelerates the hardening procedure of the binder [164, 165]. This stimulation avoided excessive water absorption by the fibres. The amount of $CaCl_2$ was fixed at $12.7\ kg/m^3$. Since the amount of chlorine, according to EN 206:2013 [167], has to be limited for a masonry block, an analysis of the total amount of chlorine in the mixtures is performed. Besides, a superplasticiser (MasterGlenium® ACE 456) is used due to its advantages of accelerating the cement hydration, reducing the water absorption of the cement composite [160] and improving the rheology of the mixture. In the presented mixes, the amount of superplasticiser stayed constant at $5.6\ kg/m^3$. This last represents 1 % of the mass of cement for all the mixtures, except for the section of the cement variation. Besides, due to the high absorption capacity of Miscanthus [162], the fibres were pre-treated before their application in the mixture with a silicate sealant, which is environmentally friendly and diminishes the penetration of water in the threads.

Component	**Density (kg/m^3)**[1]
Miscanthus x giganteus	120
Pure and natural hydraulic lime (NHL 3.5)	740
Cement (CEM I, 42.5R)	3100
$CaCl_2$ (Particle size 2-5mm)	710
Superplasticizer ACE 456	1060
Silicate sealant (liquid)	1100

Table 4-2: Components and their density

[1] The density shown for the Miscanthus, hydraulic lime, $CaCl_2$ and superplasticizer are the bulk density measured in laboratory. The density presented for the cement is the particle density and the density exhibited for the silicate sealant was given by the supplier.

4.3.2 CHARACTERISATION OF THE MIXTURES

The studied mix design (**Table 4-3**) is composed of the materials given in **Table 4-2**. In total five series of compositional mix designs were examined, namely the variation of the amount of Miscanthus, the amount of cement, the W/C ratio, the applied pre-treatment and the density. The effect on the mechanical performance of the hardened specimens in comparison to the reference mixture was evaluated. The reference mixture Ref is composed of 150 kg/m^3 of Mxg, 592 kg/m^3 of cement and 324 kg/m^3 of lime and prepared with a W/C ratio of 0.7 resulting in a pre-determined density of 1 500 kg/m^3. The length of the used Mxg fibres ranged from 40 - 60 mm with a cross-section of 2 - 6 mm. Similar to the observations reported by Mansur and Aziz [168] on jute fibres, the dimensions of the Mxg fibres influenced (decreased) considerably the workability of the mixture. Furthermore, the reference mixture Ref can be compared to a conventional lightweight concrete.

For the first series, the amount of Mxg was varied from 71 to 579 kg/m3 (A1-A4) with a constant W/C ratio of 0.7. The second series comprises the variation of cement content from 150 to 1645 kg/m^3 (B1-B3) with a constant amount of Miscanthus and W/C ratio of 0.7. The creation of the mixtures was planned in wt. % of cement: for mixture B1 20 wt. %, for mixture B2 30 wt. %, for mixture Ref 40 wt. % and for mixture B3 50 wt. %. Although, this leads especially for mixture B3 to a unusual high cement volume, these variations were kept for study purposes but have to be cautiously considered. Subsequently, the W/C ratio was varied from 0.5 to 0.9 (C1-C4) by varying the amount of water, whereas all the other components remained constant in weight. These variations were studied to analyse the impact of the different constituents on the density and on the resulting mechanical performance of the hardened specimens after 28 days of curing. Furthermore, based on the experimental data, the Young's modulus is calculated according to EN1992-1-1:2004 – 11.3.2 [169] using the ultimate load and the density of the specimens. These calculations are experimentally verified using three cylinders (d=15cm and h=30cm) and are based on the mixture which achieved the highest compressive strength.

Moreover, the impact of the pre-treatment on the compressive strength was examined. Two pre-treatments of the fibres were analysed and compared to a non-pre-treated (NPT) mixture (D1-D2 **Table 4-3**). The pre-treatment was applied to limit water penetration into the fibres. One pre-treatment consisted on covering the Miscanthus fibres with a silicate sealant (S), and the other one was based on a cement, quartz and calcium hydroxide solution (CQCH). The pre-treatment procedure was completed when the fibres were saturated. The final series of mixtures studied the impact of the density variation by varying the compacting intensity (E1-E2). This was performed during the casting procedure, where the taskperson used the hand compaction method by rodding a higher or lower material volume into the mould. The precise filling procedure will be explained on the following section. Finally, all the variations are compared to the reference mixture.

Sample ID	Miscanthus [kg/m³] [1]	Cement [kg/m³] [1]	W/C ratio	L/C ratio	Pre-treatment [2]
Reference mixture					
REF	150	592	0.7	0.55	S
Miscanthus variation					
A1	**71**	592	0.7	0.55	S
A2	**238**				
A3	**338**				
A4	**579**				
Cement variation					
B1	150	**150**	0.7	2.17	S
B2		**302**		1.07	
B3		**1645**		0.20	
W/C ratio variation					
C1	150	592	**0.5**	0.55	S
C2			**0.6**		
C3			**0.8**		
C4			**0.9**		
Pre-treatment variation					
D1	150	592	0.7	0.55	**CQCH**
D2					**NPT**
Mass variation					
E1	150	592	0.7	0.55	S
E2					

[1] The value given in kg/m³ is a theoretical value and cannot be used to create 1 m³ of the presented mixture.

[2] Distinction between the three pre-treatments:

- S Silica sealant
- CQCH Cement Quartz Calcium Hydroxide
- NPT No Pre-Treatment

Table 4-3: Variation of the analysed mixtures

This research aims to use the mixture, which presents the highest compressive strength as well as the lowest shrinkage deformation, within a load-bearing masonry block. However, due to the use of cement and the mineraliser $CaCl_2$, the amount of chlorine in each mixture has to be verified. The European standard EN 206:2013-5.2.8 [167] imposes a regulation for the allowable chloride content in function of the application field of the concrete. Within the framework of the current, the developed mixture is meant to be used within a load-bearing masonry block, so that direct contact with steel reinforcement can be excluded. Thus, the total amount of chlorine should not exceed 1,0 % of the binder mass.

4.3.3 MIXTURE PREPARATION AND FILLING PROCEDURE

The mixtures were realised using a rotating pan mixer (Zyklos, ZK 150 HE). First, the water volume is subdivided into two equal parts (W1 and W2), and the first half of the water volume W1 is mixed to the superplasticiser and the mineraliser. Meanwhile, a dry mixture is set up using the Mxg and the lime. In the next step, the water volume W1 is poured, followed by the cement, and finally the remaining water volume W2 is added to the ongoing mixture. The mixing procedure takes about 7.5 min. The development was performed under laboratory conditions and ambient temperatures of 22 ± 4°C.

After that, the moulds were filled according to the standard EN 196-1:2005-05 by filling them only to half before vibration. Next, the remaining part of the form is filled and anew vibrated. Each test series was composed out of three prisms. The series from the reference mix, from the Miscanthus variations and from the cement variations were also used to conceive three cubes per mixture. Monitoring of the weight was performed during the moulding procedure to guarantee a production of specimens with similar densities leading to similar compressive strength. The moulds, three prisms of 4 x 4 x 16 cm each and three cubes of 15 x 15 x 15 cm each, were placed on a scale during pouring so that it was possible to fill them and simultaneously control the total filling weight. After that, also shrinkage drains (6 x 10 x 100 cm) (**Fig. 4-2** & **Fig. 4-13**) were cast and wrapped with cellophane.

All the forms are demoulded after 1 day and wrapped with cellophane foil to avoid desiccation and moisture loss. The prismatic and cubic forms were cured for 28 days, whereas the cellophane is removed after 13 days. Before the compression test, the forms are weighted to measure the density according to EN 12390-7. The compressive strength is measured on three specimens, and a mean value is calculated.

The shrinkage of the mixture is measured using shrinkage drains, which are equipped by a linear variable displacement transformer (LVDT) also known as a displacement transducer with a maximum deviation of 0.2 % for 10 mm (**Fig. 4-2**). Simultaneously, the environmental conditions of the shrinkage drains are registered by continuous measurement of the temperature and the relative humidity. In this paper, the influence of the pre-treatment of the Mxg fibres on shrinkage behaviour is analysed and compared to a

theoretical shrinkage ratio of a lightweight concrete according to the standard EN 1992-1-1:2004 – 3.1.4 [170]. The theoretical shrinkage ratio is calculated using the material properties of a lightweight concrete presented in the EN 1992-1-1:2004 – 11 [169] and the temperature data recorded from the performed measurement.

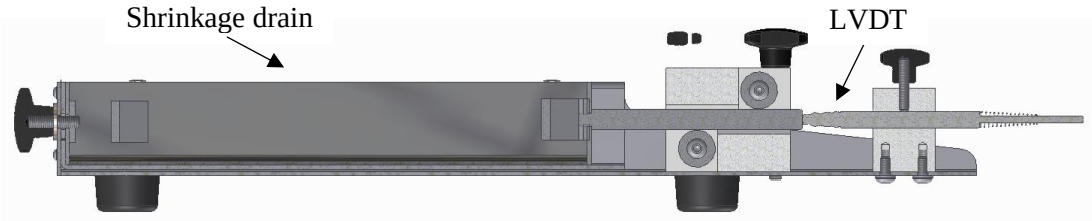

Fig. 4-2: Shrinkage drain [171]

4.4 Results and Discussion

4.4.1 Quantity of chlorine in the mixture

The used mineraliser $CaCl_2$ consists of 64.61 % of pure chlorine. Since the EN 206:2013-5.2.8 [167], which imposes a limit of the chlorine of 1.0 % for the current application, does not specify if the maximum allowed chlorine in a mixture includes the chlorine of the cement, the worst case is assumed, and it has been added to the chlorine of the molecule $CaCl_2$. The cement that has been used in this study comprehends two types of dust, which contain chlorine. In average, each kg of this cement consists of 0.05% chlorine. The total weight of chlorine in the mixture can be defined by summing up the chlorine from the $CaCl_2$ and the cement and relate it to the weight of the binder (cement + lime) that is used in the mixture.

In **Fig. 4-3**the chlorine content (in %) of each mixture is represented. The achieved amount of chlorine is defined on the vertical axis, and the mixtures are represented on the horizontal axis. The upper part of each bar represents the chlorine in the cement, whereas the lower part characterises the chlorine in the CaCl2. This last also has the most substantial influence on the total chlorine content of the mixture. Finally, a straight line representing the imposed limit by the EN 206:2013-5.2.8 is presented.

The highest impact on the chlorine content of a mixture is due to the $CaCl_2$. However, except for the variations B1 and B2 all the created mixtures respect the EN 206:2013-5.2.8. Therefore, it can be concluded that the mixtures respect the limits imposed by the EN 206:2013-5.2.8 and can be used for the production of masonry blocks.

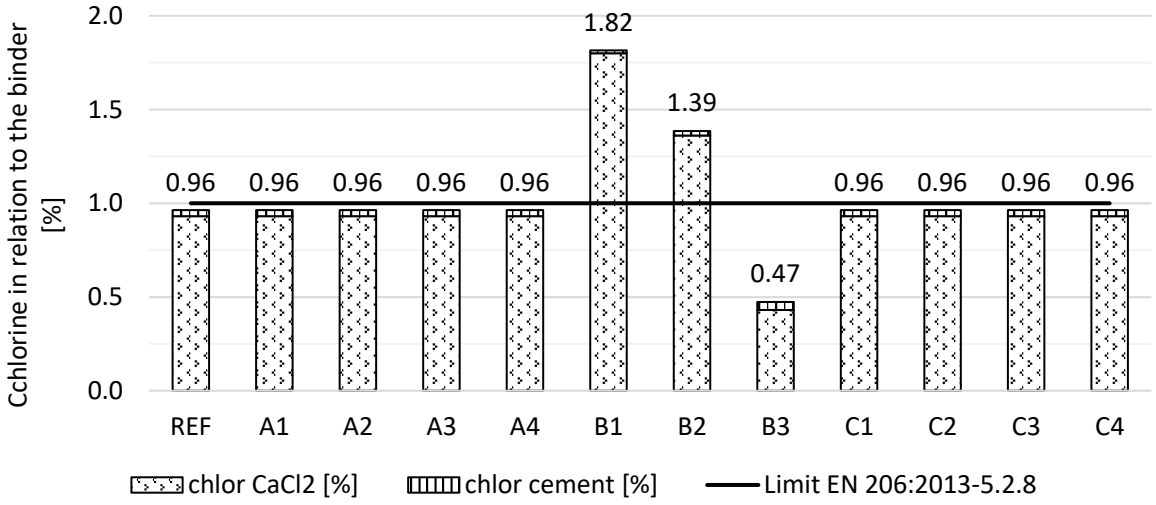

Fig. 4-3: Chlorine content as a percentage of the binder content of each mixture

4.4.2 DENSITY AND COMPRESSIVE STRENGTH

The measured density and compressive strength are summarised in **Table 4-4** for the prismatic shapes and in **Table 4-5** for the cubic shapes. Since the results are mean values out of three specimens, the standard deviation is determined. In order to compare the density and the compressive strength of the mixtures, a relative difference to the reference mixture is calculated. The mixtures A4 and B1 could not be analysed as they crumbled already while stripping the specimens out of the mould. This effect can be explained by the 1:1 ratio between the amount of Mxg and cement used, which leads to a shortage of cement in the mixture.

Variation	**Mix**	**Prisms**					
		Density [kg/m³]	**Standard deviation**	**Relative diff. [%]**	**Compressive strength [MPa]**	**Standard deviation**	**Relative diff. [%]**
Reference	Ref	1221.2	40.8	-	11.7	2.62	-
Miscanthus	A1	1249.4	32.1	+2.3	13.0	2.06	+10.9
	A2*	749.8	2.5	-38.6	2.4	0.11	-79.8
	A3*	593.2	6.1	-51.4	0.8	0.03	-92.9
Cement	B2*	639.9	7.2	-47.6	0.7	0.11	-94.3
	B3*	1017.0	0.5	-16.7	5.3	0.11	-54.6
W/C-ratio	C1	835.7	11.1	-31.6	1.9	0.13	-84.1
	C2	1124.6	50.0	-7.9	9.5	2.32	-19.1
	C3	1339.4	6.9	+9.7	19.3	0.45	+64.1
	C4	1233.3	2.2	+1.0	14.9	0.50	+27.4
Pre-treatment	D1	1309.6	47.1	+7.2	18.8	2.97	+60.5
	D2	1214.5	40.3	-0.5	14.5	4.15	+23.4

Mass	E1*	1060.7	26.9	-13.1	8.0	0.68	-31.9
	E2	1313.3	47.7	+7.5	18.8	1.10	+60.6
* Results are mean values based on two measurements							

Table 4-4: Results of the density, compressive strength, standard deviation and the relative difference based on the reference mixture for the prisms

Variation	Mix	Cubes					
		Density [kg/m³]	**Standard deviation**	**Relative diff. [%]**	**Compressive strength [MPa]**	**Standard deviation**	**Relative diff. [%]**
Reference	Ref - Cu	1399.1	12.9	-	13.8	1.18	-
Miscanthus	A1 - Cu	1523.6	63.5	+8.9	25.3	8.56	+83.6
	A2 - Cu	831.0	11.9	-40.6	2.1	0.08	-85.1
	A3 - Cu	621.8	17.7	-55.6	0.4	0.07	-97.4
Cement	B2 - Cu	688.4	4.5	-50.8	0.3	0.02	-97.9
	B3 - Cu	1309.0	31.4	-6.4	12.4	0.69	-9.8

Table 4-5: Results of the density, compressive strength, standard deviation and the relative difference based on the reference mixture for the cubes

4.4.2.1 MISCANTHUS VARIATION

Considering the Miscanthus variation, it is obvious that a reduction of the amount of Mxg to 71 kg/m^3 has a beneficial impact on the compressive strength. Furthermore, it can be noticed that on the one hand, halving the amount of Mxg from 150 to 71 kg/m^3 increases the density by 2.3% (**Table 4**). The compressive strength is increased by 10.9% for the prismatic specimens (**Table 4**) and by 83.6% for the cubic specimens (**Table 4-5**). This difference can be explained by the increased shape of the cubes and the low ratio between the Miscanthus and the cement (0.12:1). On the other hand, increasing the Mxg from 150 to 338 kg/m^3 (mix A3) reduces the density by 51.4% (prisms), resp. 55.6% (cubes). Furthermore, the achieved compressive strength is below 1 MPa, independent from the shape of the specimen.

In general, an increase in the amount of Miscanthus leads to a clear decrease in the density (**Fig. 4-4**) and the compressive strength (**Fig. 4-5**). It also has to be mentioned that independent from the mix; the cubes had a higher density, as well as a higher standard deviation, than the prisms. This occurrence could be due to higher compaction during the filling procedure, which is to some extent depending on the person in charge. The difference in the density decreases with an increasing amount of Miscanthus. The trend of the compressive strength behaves differently. For the mix using a low amount of Miscanthus (A1), the cubic specimens present almost the double compressive strength than the prismatic ones. Nevertheless, increasing the amount of Miscanthus reduces the difference, and from one point upwards

(150kg/m^3 of Miscanthus), the compressive strength of the cubic samples is even lower than the one of the prismatic ones (**Fig. 4-5**). However, the difference between both shapes remain small (0.3 – 0.4 MPa).

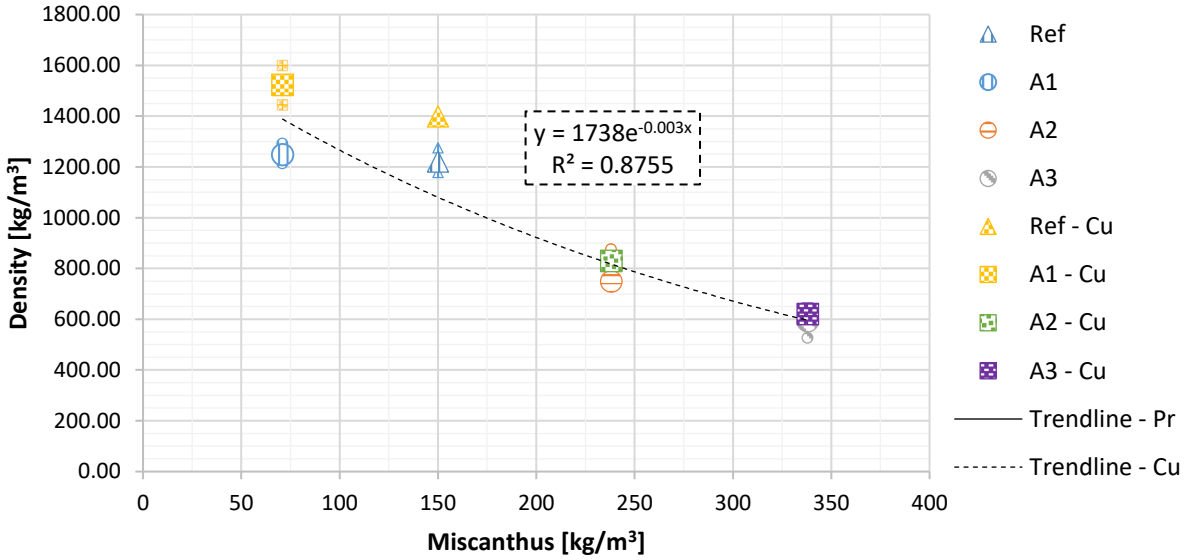

Fig. 4-4: Density of prisms and cubes in function of the amount of Miscanthus in the mixture (The big markers correspond to the mean value of the small markers)

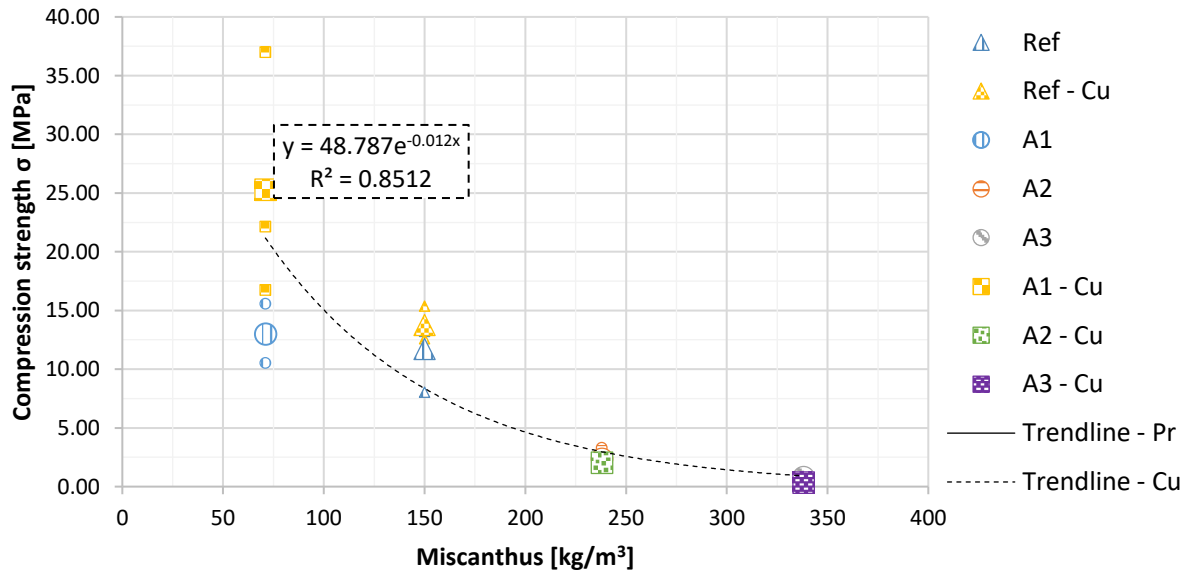

Fig. 4-5: Compressive strength of prisms and cubes in function of the amount of Miscanthus in the mixture (The big markers correspond to the mean value of the small markers)

4.4.2.2 CEMENT VARIATION

The densities of the cement mixes (B2-B3) (**Table 4-4** for prisms and **Table 4-5** for cubes) are lower than the density of the reference mixture. It can be observed that the relative difference of the density of

mix B3 (higher amount of cement compared to the reference mixture) is different for prisms (-16.7%) and cubes (-6.4%). However, a similarity in the density can be noticed for the mixture B2 (-47.6% for prisms and -50.8% for cubes). The impact of the reduction of the cement amount can also be observed by visual comparison (Ref mix (a-b) **Fig. 4-6**; B2 mix (c-d) **Fig. 4-6**).

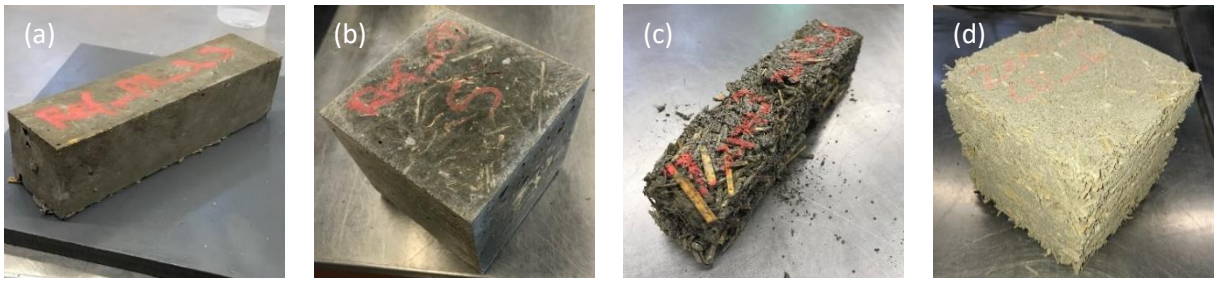

Fig. 4-6: (a) - (b) specimens from mixture Ref and (c) - (d) specimens from mixture B2

Moreover, the variation of cement amount results in a decrease in the compression strength compared to the reference mixture (Ref). The fact of increasing the amount of cement and implying with this a reduction of the compressive strength was unexpected. Therefore, a microstructural analysis is performed on the mixture B3 using SEM (**Fig. 4-7**). Due to the low ratio between Mxg and the cement (0.09:1), this mixture is very close to a standard mixture for normal concrete where W/C ratios of 0.3 – 0.4 are usual. Using here such a high W/C ratio of 0.7 implies a very liquid cement paste and provokes the formation of air voids, which were visualised using SEM. These cavities disrupt the bond between the Mxg and the cement, which leads then to a reduction of the compressive strength (prisms -54.6% and cubes -9.8%). Similar to mix A1, the difference of the compressive strength between prisms and cubes is due to the low ratio between Miscanthus and cement (0.09:1).

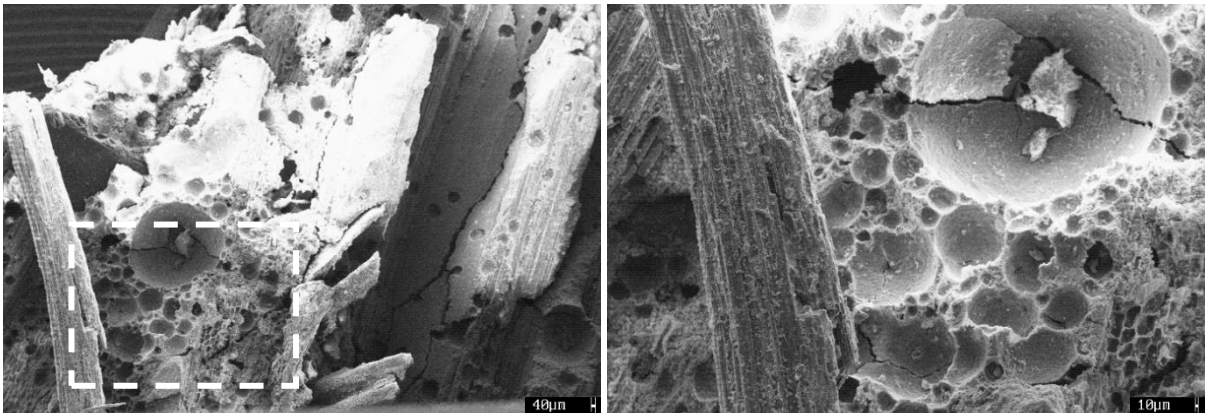

Fig. 4-7: SEM of the mixture B3 at a range of 40 µm and the marked region at a range of 10 µm

The compressive strength reached by the cubes on the mix B3 is also due to the higher availability of hydration products. Therefore, it can be assumed that the water inside the cube is released slower than this is the case for the prismatic shape. Hence, a slower release of water corresponds to a slower loss of weight, a slower diminution of the density and a longer hydration process of the cement in the mixture.

Contrarily, the lower compressive strength of the cubes compared to the prisms (mix B2) is due to the higher Mxg cement ratio (0.50:1). The strands of the Mxg are composed of many air voids, as observed by P. Klímek et al. [21], and thus reduce the density and the achieved compressive strength. Thus, a faster decrease of the weight happens during the curing process, which implies a faster decrease in the density. Therefore, it can be concluded that the difference between the compression strength is related to the airtightness of the specimen and the ratio between the Mxg and the cement.

4.4.2.3 W/C RATIO VARIATION

Moreover, decreasing the W/C ratio leads in principle to a reduction of the density and of the compressive strength. The relative difference of the mixture C2 to the mix Ref is -7.9% for the density and -19.1% for the compressive strength. Since the Miscanthus fibres present a high water absorption [22, 50], reducing the W/C ratio results in less water available for the cement reaction. During hydration, the water, which is first absorbed by the fibres is released afterwards during the fifth hydration phase of cement (steady-state phase) [172], and partly reacts with the non-hydrated cement particles and partly evaporates. Nonetheless, a continued decrease of the W/C ratio (mix C1) shows a relative difference of -31.6% for the density and -84.1% for the compressive strength.

An increase of the W/C ratio represents a gain on the density (+9.7% on C3 mix and +1.0% on C4 mix) and on the compressive strength (+64.1% on C3 mix and +27.4% on C4 mix). Nevertheless, mix C4 shows that the used water amount exceeds the saturation point of the Miscanthus fibres and the water needed for the cement hydration, which implicates bleeding of the mixture.

Furthermore, it is visible on the prismatic specimens, that decreasing the W/C ratio of the mixture Ref results in a decrease of the compressive strength. However, increasing the W/C ratio to 0.8 produces the highest compressive strength presented in this paper for the prismatic samples with 19.3 MPa. The increase of the compressive strength is confirmed by a visible decrease of the porosity with an increase of the W/C ratio (**Fig. 4-8**). Nonetheless, a further increase of the W/C ratio to 0.9 reduces the compressive strength (14.9 MPa). As for the mixture B3, a microstructural analysis (SEM) is performed on the mix C4 which makes void spaces induced by earlier existent air bubbles visible (**Fig. 4-9**). Furthermore, a crack in the binder is becoming apparent, which is a consequence of the shrinkage process in the microstructure of the mix. This perturbation of the bond between the cement matrix and the Mxg fibres results in a reduction of the compressive strength by 4.4 MPa compared to the C3.

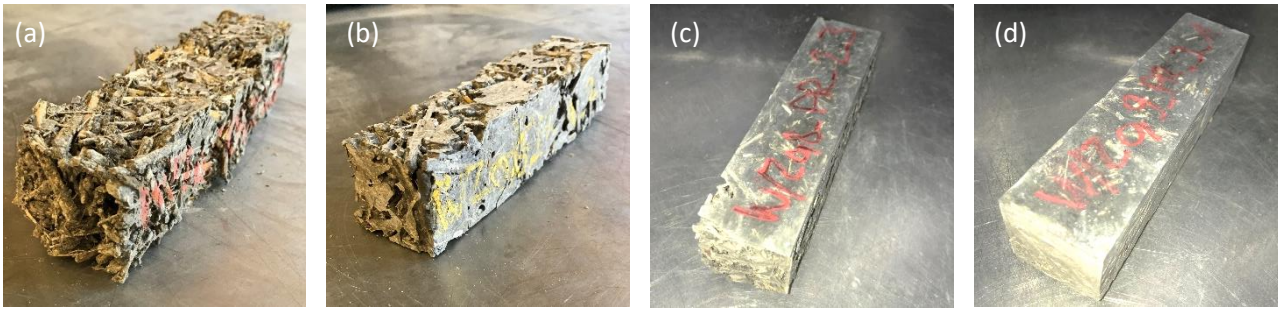

Fig. 4-8: Prisms of the mixtures (a) C1; (b) C2; (c) C3; (d) C4

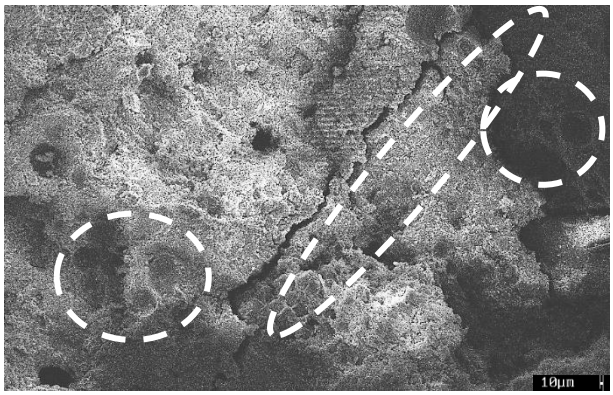

Fig. 4-9: SEM of the mixture C4 pointing out the void spaces and a crack

Nevertheless, a W/C ratio below 0.7 (mix C1 and C2) does not provide sufficient water for the cement reaction as one part of the water is absorbed by the Mxg and is therefore not available for the cement hydration. This lack of water induces the specimen to have high porosity ((a-b) **Fig. 4-8**). The remaining water, which is then used by the cement to react, is not enough for total hydration and leads to a reduction of the compressive strength.

4.4.2.4 Relation between the density and the compressive strength

Furthermore, the relation between the compressive strength and the density is analysed for all mixes of the prismatic and cubic specimens (**Fig. 4-10**), and a parabolic regression can be observed with an increasing density. A similar observation was done by Sagmeister [173] for a lightweight concrete without fines. It is noticeable that with an increasing density of the Mxg concrete, the compressive strength of the prisms is converging to the results of Sagmeister. The differences vary from 5 to 50 % by increasing the density. It is perceptible that a higher density implies a higher compressive strength. This statement can be verified by comparing the mixture Ref, E1 and E2 since they have the same composition. The difference was made during casting, where a density increase of 100 kg/m^3 for the prisms signified that 25g more material was used per prism. It is observable that the highest results were obtained by mixture E2 and the lowest by mixture E1. These findings induce that the compactness of the mixture during casting has a high impact on the compressive strength after a curing time of 28 days.

However, it is very challenging to obtain the same density for the same mixture when producing the mixtures manually, since this is mostly dependent on the personal approach of the person in charge of this task. Nonetheless, it is possible to predict an approximation of the compressive strength of the mixtures after 28 days of curing in function of the weight of the prisms at casting. Furthermore, it can be noticed that the shape of the specimen influences the achieved compressive strength. The shape has an impact on the compressive strength, which reaches a difference of 65.2% considering a low density of 600 kg/m^3, whereas this impact is gradually reduced to 38.1% for a higher density of 1300 kg/m^3.

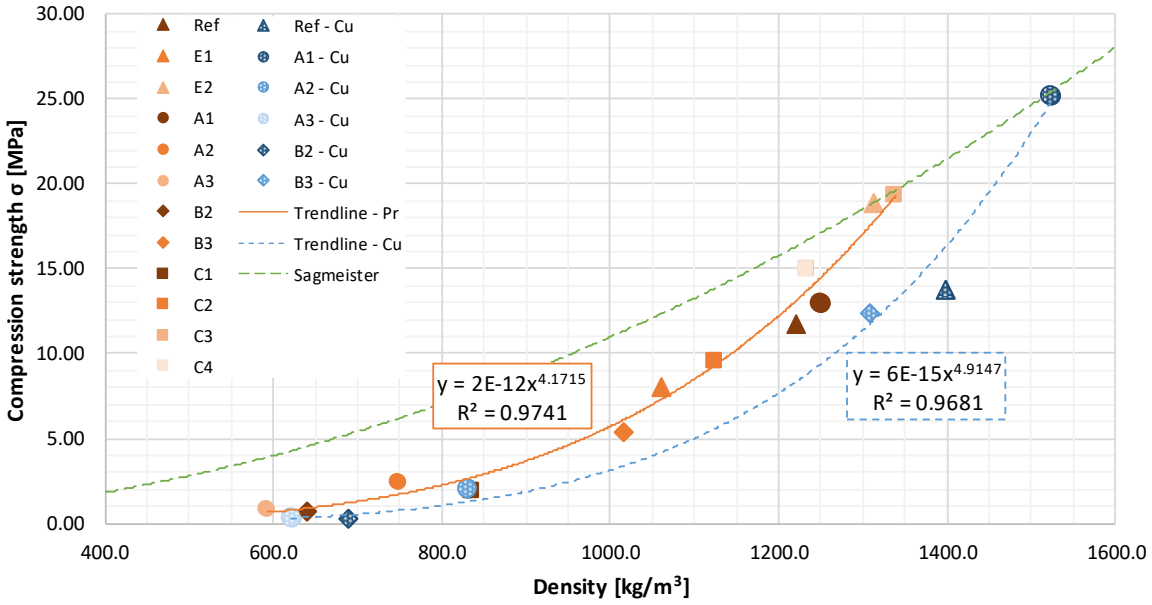

Fig. 4-10: Compressive strength in function of the density for prisms compared to the results given by Sagmeister [173] for a lightweight concrete without fines

4.4.2.5 Pre-treatment variation

Moreover, the impact of the pre-treatment of the Miscanthus fibres on the compressive strength is analysed. Therefore, the density and compressive strength (mean values of three tests per mixture) of the mixture Ref are compared to the mixture D1 and D2. Both mixtures achieved a higher compressive strength than the mixture Ref (+60.5 % for D1 and +23.4 % for D2). D1 reached the highest compressive strength and density. However, the mixture D1 has a higher density than the mixture Ref. Due to the close link between compressive strength and density, the mixture D1 has to be compared to mixture E2. As previously mentioned, the mixtures E1 and E2 have the same components as the mixture Ref (**Table 4-3** and section 4.4.2.4). The only difference is given by distinct densities. Consequently, a comparison of the compressive strength of D1 to E2 is possible and shows similar results for the density and the compressive strength. Nonetheless, comparing the mixture D2 to Ref the densities are similar, but the mixture that uses Mxg fibres without pre-treatment (D2) reaches a higher compressive strength (14.5 MPa) than the mixture Ref (11.7 MPa).

A microscopic analysis shows a clear difference between the non-treated and the treated Mxg fibres (**Fig. 4-11**). A non-treated fibre presents an explicitly visible epidermis, outer ring and parenchyma ring (**Fig. 4-11** (a)). This is not the case for a fibre treated with a silicate sealant. In this case, the outer ring, as well as the parenchyma of the fibre, is mostly filled (**Fig. 4-11** (b)). This fact avoids a high absorption of water from the Miscanthus fibre, which induces that more water is available for the cement hydration. The Miscanthus fibre treated with the CQCH treatment shows an almost complete layered cross-section (**Fig. 4-11** (c)). The analysed fibre was not fully covered by the pre-treatment product during the application procedure and a small part of the epidermis, as well as the outer ring, are still visible. The layer over the fibres can be considered as a cement hydration product. The consequence of completely covered Miscanthus fibres is that less water can be absorbed during the mixing procedure. However, the disadvantage of the covered fibres is also that the binder cannot enter the fibres and therefore, the bond between the binder and the Mxg is reduced.

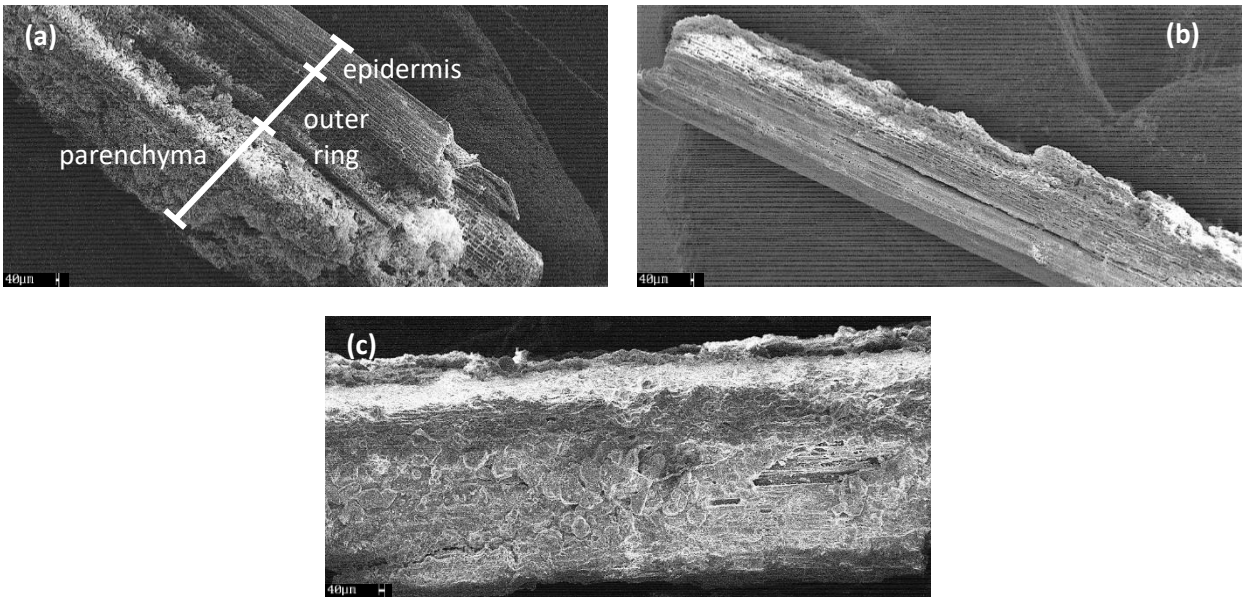

Fig. 4-11: SEM of Mxg fibres (a) non-treated (b) treatment based on silicate sealant (c) treatment based on CQCH

4.4.3 Analysis of the Young's Modulus

In **Fig. 4-12**, the compressive strength of the mixtures presented in **Table 4-4** (results of the prisms) are illustrated in function of the Young's Modulus. The Young's Modulus is calculated according to EN1992-1-1:2004-11.3.2 [169] using the density and the achieved compressive strength by the prisms at the age of 28 days as presented in eq. 4-1.

$$E_{lcm}[MPa] = 22 \cdot \left(\frac{compressive\ strength}{10}\right)^{0.3} \cdot \left(\frac{density}{2200}\right)^{2} \qquad \text{(eq. 4-1)}$$

Thus, a parabolic regression with a determination coefficient of R^2=0.9984 can be observed relating all the prismatic shapes of the mixtures. Besides, the Young's Modulus is calculated for the measurements of Sagmeister and represented in the same figure. As expected, a positive correlation between the compressive strength and the Young's Modulus is visible. On one hand, the mixtures with a Mxg to water ratio between 0.51:1 (mix C1) and 0.82:1 (mix A3) reach a Young's Modulus below 2.0 GPa. On the other hand, a Young's Modulus above 9.0 GPa is reached by the mixtures E2 and C3, which show to have a higher stiffness leading to a smaller deformation of the shape due to loading. At this point, the relation between the Mxg and the water amount is not taken into consideration since they are all below 0.5:1. Furthermore, an increasing Young's Modulus converges to the curves provided by Sagmeister. Therefore, it can be concluded that the Young's Modulus reached by the mixtures based on Miscanthus can be compared to the Young's Modulus of the lightweight concrete studied by Sagmeister.[173]

In addition, three cylinders are produced using the same components as mixture C2. However, compared to the studied mixture C2 on the prisms, the three cylinders presented a considerably lower density. The results of the achieved density, compressive strength and Young's Modulus are reported on **Table 4-6**. These two last are added to **Fig. 4-12** (red crosses) and it is visible that they are situated between the trendline based on the presented mixtures and the trendline studied by Sagmeister. [173]

Specimen	Mix	Density [kg/m³]	Compressive strength [MPa]	Young's Modulus [GPa]
Cylinder 1	C2	830.2	1.59	0.67
Cylinder 2		897.2	1.74	0.73
Cylinder 3		978.7	1.96	0.97

Table 4-6: Results of the density, compressive strength and Young's Modulus of the three cylinders

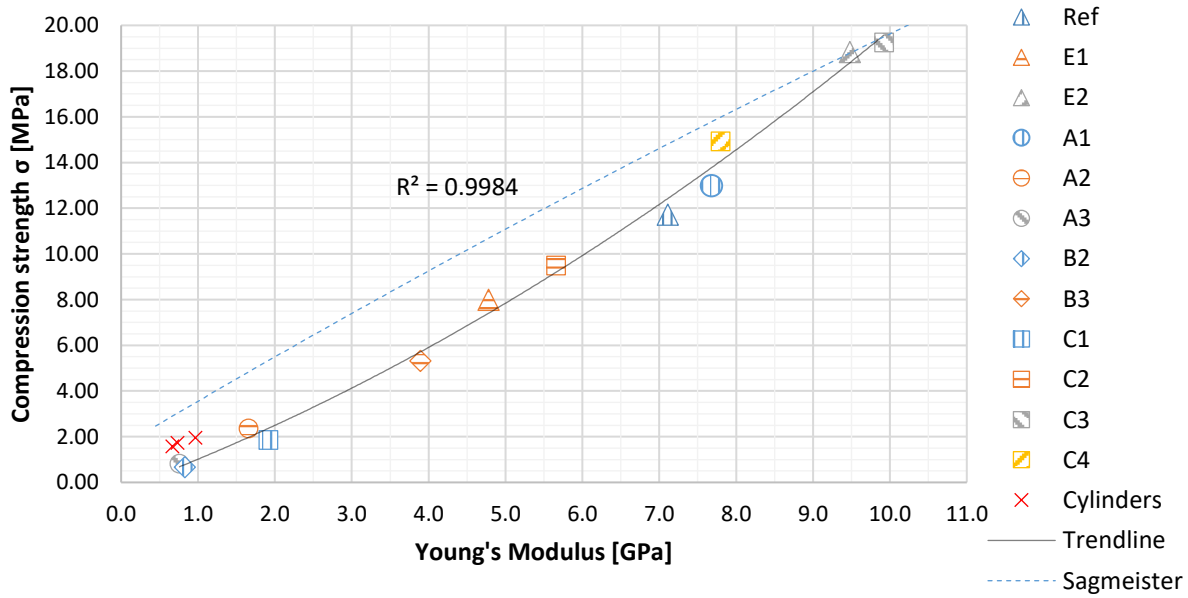

Fig. 4-12: Young's Modulus of the tested prisms in relation to their compressive strength

4.4.4 ANALYSIS OF THE HYGRIC PROPERTIES OF MISCANTHUS LIGHTWEIGHT CONCRETE

The hygric properties of the reference mixture Ref are measured on shrinkage drains (**Fig. 4-13**) for 609 days (**Fig. 4-14**), as well as the relative humidity and the room temperature. These are presented on the lower and middle graph of **Fig. 4-14**. The upper graph presents the shrinkage development in $\mu m/m$ of three drains (Drain-1_S, Drain-2_S and Drain-3_S) based on the mixture Ref (**Table 4-3**) in function of time. The drains were wrapped with cellophane for 90 days to analyse the swelling behaviour of the specimens. The cellophane prevented direct contact to the outer ambient. After casting, first a swelling of the mixture can be observed. This expansion occurring after casting is the result of the Miscanthus fibers absorbing moisture from the matrix and presenting thus swelling. This process reached a value of 500 $\mu m/m$. The cellophane was discarded, and the shrinkage procedure of the mixtures started. With the reduction of the internal relative humidity over time due to the hardnening process, the mixture starts desorbing which results in a global increase of the shrinkage values over time.

Fig. 4-13: Shrinkage drain with the mixture before applying the transducer

During the measurement period, the registered relative humidity fluctuated, which was related to the ambient temperature and humidity changes in the room the drains have been stored. Therfore, in addition to the main global increase of shrinkage variations due to the fluctuation of the external temperature and humidity could be observed. In general, an increase in temperature lead to a decrease in the shrinkage as could be observed at a curing time of 275 - 285 days: the increase of the temperature from 9°C to 16°C at a relative humidity above 70 % lead to a swelling of the mixture. However, this only happened during the periods where a high relative humidity was present (the period from 400-420 days). This statement was confirmed at the age of 320 days. Here, the increase in temperature with a ΔT= 7°C (from 10°C to 17°C) and a relative humidity of 50 % does not induce any swelling. Furthermore, after a curing time of 480 days the drains showed a horizontal tendency. Therefore, it can be assumed that the degree of shrinkage is achieved and reached an average deformation of 2244 $\mu m/m$.

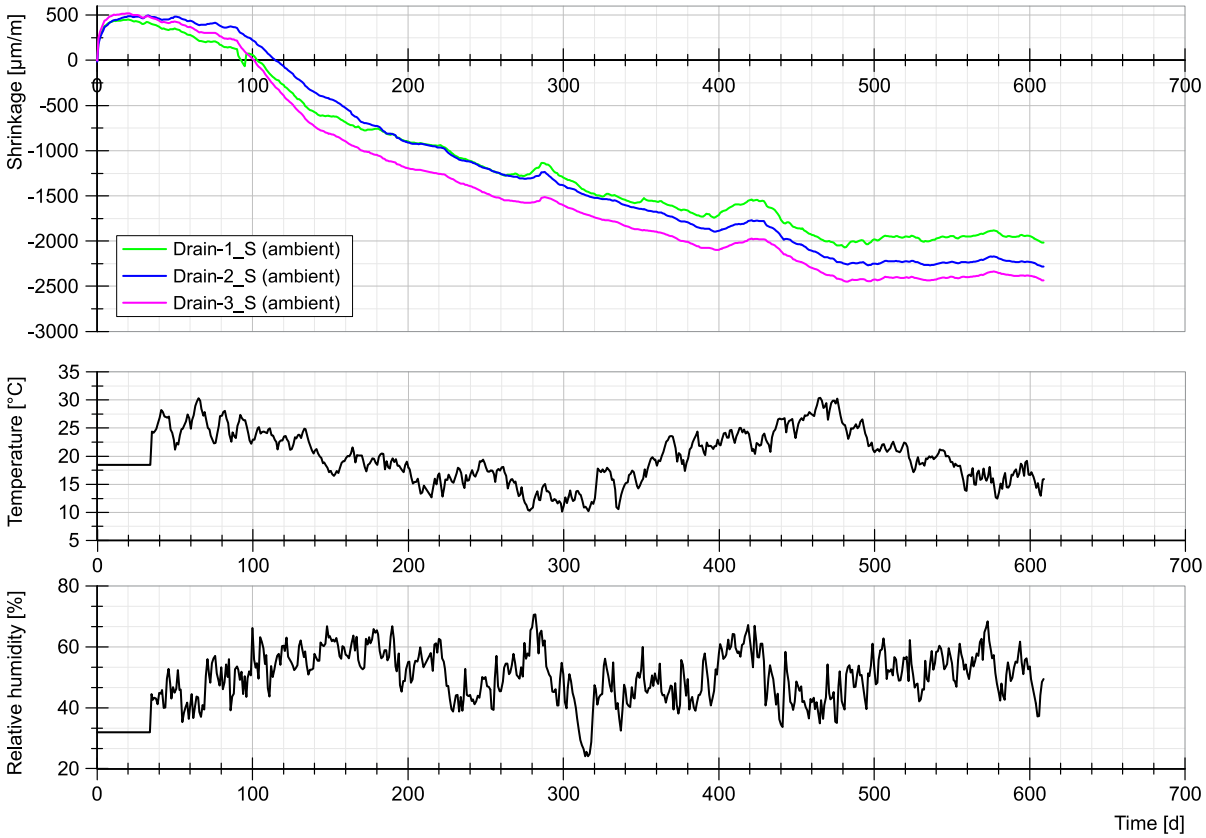

Fig. 4-14: Shrinkage drains of the mixture Ref

In order to compare the recorded shrinkage deformation, the shrinkage development of several conventional LC according to the standard EN1992-1-1:2011-01 are presented in **Fig. 4-15**. These results are not pretended to predict or model the shrinkage behaviour of Miscanthus lightweight concrete but aim to add to add a comparison between the experimental data and aconventional LC according to the standard EN1992-1-1:2011-01. The shrinkage course of the latter is calculated analytically according to EN1992-1-1:2011-01 by using the specific environmental conditions from **Fig. 4-14**. These analytical calculations of the LC show a swelling lower than 50 $\mu m/m$ for the first days. According to the calculations, LC reach a value between 500 and 1 000 $\mu m/m$ already after 70 days. The deformation is dependent on the type of the LC. However, the highest shrinkage deformation of 1 000 – 1 200 $\mu m/m$ is achieved by the LC12/13, which is less than half of the degree of shrinkage of the mixture Ref. Furthermore, the high value of shrinkage (2244 $\mu m/m$) could induce more warping and cracking, which makes the Mxg concrete mixture based on a silicate pre-treatment (section 4.3.2 - **Table 4-3**) not ideal considering long-time deformations.

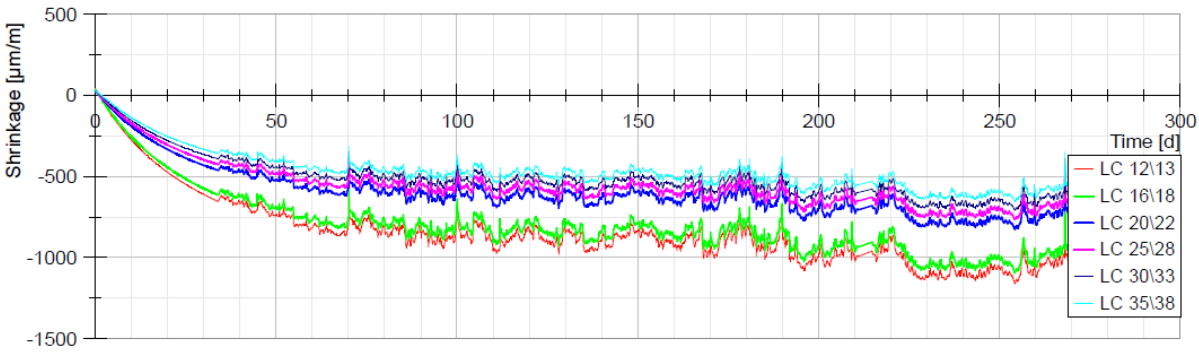

Fig. 4-15: Shrinkage drain of lightweight concrete calculated analytically using the environmental conditions from **Fig. 4-14**

Furthermore, the impact of the pre-treatment on the shrinkage deformation is analysed. Therefore, the degree of shrinkage is also measured for the mixture D1 on three drains (Drain-1_CQCH, Drain-2_CQCH and Drain-3_CQCH) (**Fig. 4-16**). The deformation, as well as the temperature and the relative humidity, were recorded for 574 days. As before, the drains were wrapped with cellophane but only for 56 days. The early start of shrinkage of Drain-1_CQCH was due to a leakage in the cellophane that allowed an exchange with the environment. After a period of 240 days, the drains were moistened, and the velocity of shrinkage increased until reaching the previous path of the shrinkage deformation. The final deformation with an average of 2 473$\mu m/m$ was achieved after a curing time of 440 days.

It can be concluded that comparing the pre-treatment based on a silicate sealant and the pre-treatment based on CQCH; a higher shrinkage deformation is generated by the mixture D1 (2 473$\mu m/m$). However, the differences remain smaller than 10% but are 2.2-2.4 times higher than the deformations achieved by a LC12/13 (**Fig. 4-17**). Furthermore, the presented mixtures based on Miscanthus aggregates showed to achieve lower shrinkage deformations than a Hemp-concrete ($4500 - 8500\ \mu m/m$) or a Flax-Hemp-concrete ($4000 - 7500\ \mu m/m$) [161].

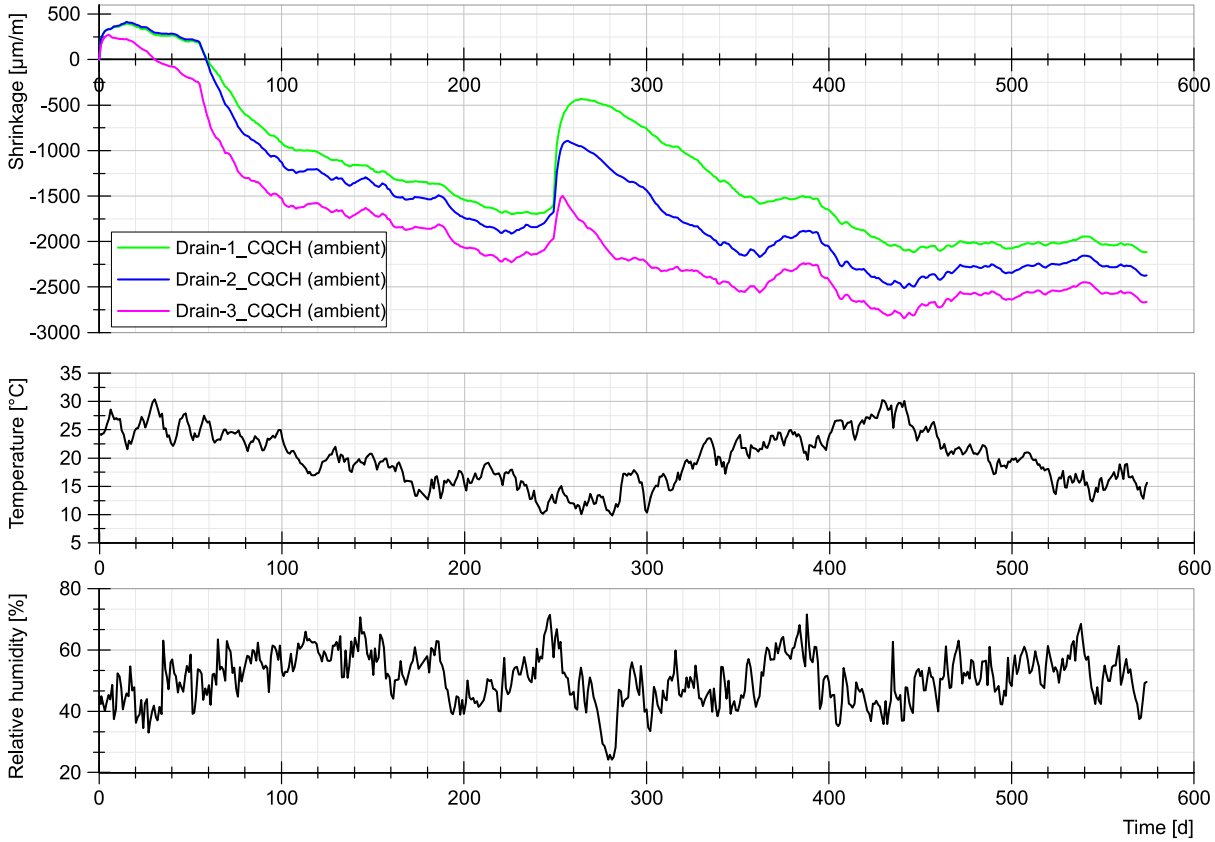

Fig. 4-16: Shrinkage drains of the mixture D1

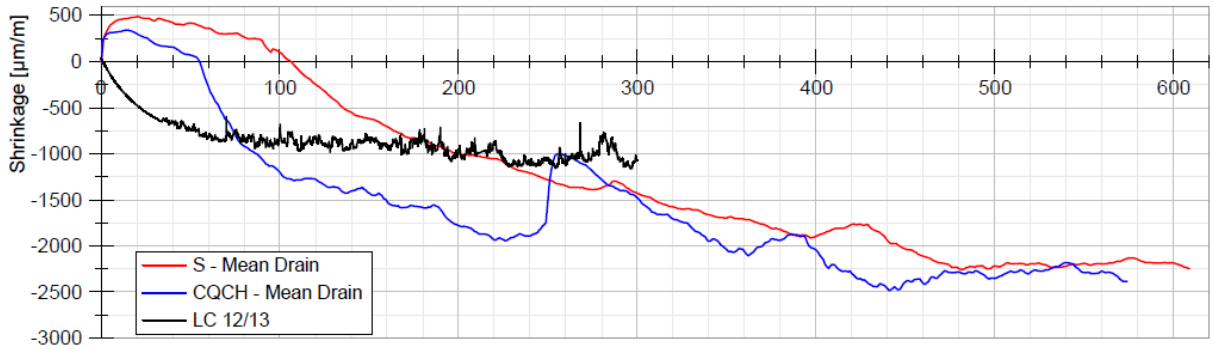

Fig. 4-17: Comparison of the shrinkage deformations between the mean drains of the mixture Ref, D1 and the calculated LC12/13

4.5 CONCLUSIONS

This study reached to develop an LC based on Mxg fibres that can be used as a bearing material. The identification of a mixture of the Mxg lightweight concrete with a bearing capacity is achieved by varying the components of the mixture. The conclusions taken from this paper are summarised in the following:

- The reference mixture Ref using 150 kg/m^3 of Mxg fibres, which were pre-treated with a silicate sealant, allows achieving a compressive strength of 11.7 MPa (for prisms, and 13.8 MPa for cubes) with a density over 1000 kg/m^3. However, increasing the ratio between Mxg and cement from 0.25:1 (mix Ref) to 0.40:1 (mix A2) reduces the compressive strength by -79.8 % for the prismatic specimens and by -85.1 % for the cubic specimens.
- Any variation of the amount of cement resulted in a decrease in the compressive strength. Since the W/C ratio remained unchanged, an increase of the cement amount induced a proportional increase of the water volume and lead therefore finally to air voids in the hardened matrix, which disrupt the bond between the Mxg and the binder.
- A W/C ratio of 0.8 (mix C3) leads to a compressive strength of 19.3 MPa, which is higher (+64.1 %) than the reference mix. A change of this ratio to 0.9 (mix C4), 0.6 (mix C2) or 0.5 (mix C1) induces a loss in the compressive strength of at least -19.1 % compared to the reference mix.
- An increase in the density of the mixtures leads to a parabolic increase of the compressive strength independent from the shape. For the prismatic specimens, a density below 900 kg/m^3 presents a compressive strength below 4 MPa and a density above 1300 kg/m^3 leads to a compressive strength above 18 MPa.
- A mixture with a CQCH pre-treatment (D1) achieved a similar density and compressive strength as the mixture E2 using a silicate sealant as a pre-treatment. Hence, both pre-treatments have the same impact on the compressive strength.
- A mixture without any pre-treatment of the fibres (D2) conducts to a compressive strength of 14.5 MPa, which is higher than the mixture Ref (11.7 MPa), whose fibres were pre-treated using a silicate sealant.
- A compressive strength of 18.8 MPa leads to a Young's Modulus of 9.5 GPa (mix E2). A mixture with a Young's Modulus of 3.9 GPa (mix B3) presents a compressive strength reduced by 72 % compared to mix E2. Furthermore, if the relation between the used Mxg and water is above 0.50:1, a Young's modulus below 2 GPa is expected.
- A pre-treatment of the fibres using a silicate sealant presents a 10 % lower shrinkage degree than a mixture using CQCH pre-treated fibres, which signifies that the pre-treatment has an influence on the shrinkage degree. Therefore, it can be concluded that a pre-treatment based on a silicate sealant shows to be more beneficial considering the long-term deformation than a CQCH pre-treatment.

Finally, it can be concluded that according to the results presented in this paper, the theoretical best mixture considering the compressive strength, not taking into account a study of the combination of the materials, would constitute of $150\ kg/m^3$ of Miscanthus, $592\ kg/m^3$ of cement and a W/C ratio of 0.8.

Furthermore, considering the long-term deformation a pre-treatment based on a silicate sealant would be more beneficial than a CQCH pre-treatment.

This field of sustainable construction materials needs further investigations to enlarge the experimental database and evaluate the crack propagation due to shrinkage or tension as well as the deformation behaviour due to creeping. Also, cost-effective analysis of the lightweight concrete based on Miscanthus fibres needs to be performed.

4.6 ACKNOWLEDGEMENTS

The authors of this paper would like to thank Contern S.A. for the financial support of the research project. Moreover, they would like to express their gratitude to the staff of the University of Luxembourg as well as to Mrs Fabienne Leclerc, Mr Cristiano Garcia Monteiro and Mr Michael Gonçalves Dantas for their practical and competent help.

Chapter 5 MACHINE LEARNING IN MIX DESIGN OF MISCANTHUS LIGHTWEIGHT CONCRETE (MANUSCRIPT ON MACHINE LEARNING)

5.1 ABSTRACT

This research is carried out to investigate the Gaussian process regression (GPR) based on a machine learning model to predict the compressive strength of Miscanthus lightweight concrete (MLWC). A database of 414 experimental data, which includes ten input variables such as six mix constituents of concrete, water/cement ratio, form of specimen, curing time and pre-treatment condition and an output variable of compressive strength of MLWC, is constructed from the data collected by a series of experimental tests on MLWC. Two kernel functions, namely, the squared exponential and rational quadratic are used in the GPR model. It is found from experiments that the GPR model with rational quadratic kernel gives minimum errors for predicting compressive strength of MLWC. In addition, a user-friendly graphical user interface is created using MATLAB software to deploy the GPR model which can be used at an early stage of designing the Miscanthus concrete members instead of using costly experimental investigation.

Keywords – Miscanthus; Lightweight concrete; Machine learning; Gaussian process regression; Mix design

5.2 INTRODUCTION

Concrete, a mixture of cement, water, fine aggregates (sand) and coarse aggregates, is the most common material used in the construction industry due to its various advantages over other materials such as durability, integrity and economy. However, the process of producing concrete causes several impacts on the environment, not only the large amount of CO_2 emissions, but natural resources such as sand and gravel also become depleted. The extraction of natural aggregates, often from environmentally sensitive areas such as river valleys, can lead to a destruction of an ecosystem. Using Miscanthus in concrete formulations is a possible solution to lower the use of natural aggregates in concrete [174]. In addition, if the Miscanthus can replace the use of aggregates in concrete, benefits can be gained through reducing energy consumption and carbon emission [85].

Many efforts have been made in the last decade to achieve improved Miscanthus fibre-binder bond characteristics in the concrete mix as well as to replace the conventional building materials with Miscanthus [86, 175-179]. Pude et al. [157] stated that Miscanthus could be used as basic material for structures because it contains considerably strong fibre compounds made of silicon, cellulose and lignin. They investigated the suitability of four genotypes of Miscanthus stems as lightweight concrete aggregates. Acikel [83] showed that using the grinded Miscanthus with a diameter 4-8 mm and a length of 60-80 mm as lightweight aggregates in a concrete mixture, the strength of concrete in compression, tension and bending is increased by 4 to 28%, 9 to 25% and 4 to 9%, respectively. The pore structure of Miscanthus contributes to reduce the thermal conductivity of the Miscanthus concrete [46, 180]. Chen et al. [162] analysed the thermal and acoustic performance of Miscanthus lightweight concrete (MLWC). The test results showed that MLWC has better thermal and sound insulation characteristics compared to normal-weight concrete, which is due to the high porosity of MLWC. It was also concluded that the sound absorption coefficient increases from 0.28 to 0.63 with the increase of the volume of Miscanthus from 0 to 30%.

The use of Miscanthus as a lightweight aggregate in concrete is limited due to several reasons such as inconsistent properties of the porous composite and lack of research on the characteristics and performance of Miscanthus as lightweight aggregate in concrete. This research was designed to address the above issues by conducting laboratory experiments on MLWC to investigate the effects of different constituents and moisture content on the strength and performance characteristics of MLWC. It is also needed to know which mix proportions should be used to achieve the specific properties of concrete, especially the desired compressive strength. If the strength of concrete could be predicted beforehand, it could save a lot of time and cost. However, such a topic has never been studied on MLWC. Thus, as the first step of such a detailed investigation of MLWC, this paper focuses on developing an accurate

and reliable prediction model to quantify accurately the volumes of the different constituents for an optimisation of the mixture regarding the compressive strength of MLWC.

Recently, machine learning (ML) techniques have been utilised increasingly for mixture design and optimisation due to their excellent pattern recognition, auto-association and self-learning. The ML models can be used for predicting output data, based on a defined input dataset [131]. Various researchers used different ML techniques such as regression analysis [137-139], artificial neural networks (ANN) [132-134], fuzzy logic [135, 136] for the prediction of compressive strength of concrete.

Linear regression (LR) is a basic and relatively simple supervised-ML algorithm that can be implemented very easily compared to other ML techniques. Due to its lower computational time when compared to other ML algorithms, it has been widely used to define the relationship between a dependent variable and one or more independent predictors [150]. Chopra et al. [137] used it for the prediction of compressive strength of concrete with and without fly ash. Huang et al. [151] used multiple linear regression (MLR) to estimate the bond strength of fibre reinforced polymer concrete.

In the last years, ANN structures are being used to solve many complex problems in civil engineering applications due to its capability of performing multiple tasks in parallel without affecting the system performance. Yeh [141] developed a model with eight input variables (i.e. cement, fly ash, blast furnace slag, water, superplasticizer, coarse aggregate, fine aggregate and age of testing) to optimise the high-performance concrete mix for given workability and strength using ANN. Alshihri et al. [142] predicted the compressive strength of structural lightweight concrete using ANN. They used laboratory test results to train and to validate the neural networks. Ni and Wang [132] showed that the single-layer ANN model could accurately predict the 28-day compressive strength of concrete. Bingol et al. [143] predicted the compressive strength of lightweight concrete with pumice aggregate subjected to high temperatures using ANN. Das et al. [144] developed an ANN model with seven inputs to predict the mix proportions of concrete. The hidden-layer neurons were adjusted by trial and error method to achieve optimal value. Topcu and Saridemir [135] gathered 52 different mixes with 180 specimens to develop a model to accurately predict the compressive strength of concrete containing fly ash using ANN and fuzzy logic.

Kewalramani and Gupta [181] developed MLR and ANN models to predict the long-term compressive strength of concrete. They concluded that ANN is more efficient in producing reliable strength compared to MLR. Similarly, Khademi et al. [182] developed three different models based on MLR, ANN and adaptive neuro-fuzzy inference system (ANFIS) to predict the 28-day compressive strength of concrete. They concluded that ANN and ANFIS models produced reliable results, while MLR model was not capable enough due to the nonlinear relationship between mix parameters. Omran et al. [152] compared the accuracy of different ML techniques for predicting the compressive strength of environmentally

friendly concrete. They found that ensemble models such as additive regression and bootstrap aggregating was able to achieve good prediction performance. Their results have shown that the Gaussian process regression (GPR) model had the best prediction accuracy as an individual data-mining model. Pal and Deswal [154] also found that GPR model could provide a reliability response to an input data. Another advantage of the GPR model was the prior fitted function could be shaped by the choice of kernel function.

Accordingly, this paper utilises state-of-the-art achievements in machine learning techniques for Miscanthus concrete mix design. The objective of this paper is to illustrate that the ML model that employs the GPR can be used to accurately predict the compressive strength of MLWC. The subsequent part of the paper is organised as follows. Section 5.3 discusses the materials and the experimental procedure used to produce required dataset. Section 5.4 then describes the ML technique and the evaluation method, followed by the discussion of the results. The conclusion of this study is presented in the final section.

5.3 EXPERIMENTAL PROCEDURE

The experimental tests have been conducted at the laboratory of Solid Structures of the University of Luxembourg. The main characteristics of materials and procedures used for the purpose of this study are presented in this section.

5.3.1 MATERIALS

The Miscanthus concrete mixtures consisted of six components such as Miscanthus, cement, water, lime, a superplasticizer and a mineraliser. Miscanthus x giganteus (Mxg), the giant Miscanthus, which was produced by Luxembourgish farmers, was chosen because of its wide availability. In this study, dried Miscanthus with average density of 120 kg/m^3 was used. The length of the used Mxg fibres ranged from 15 to 60 mm with a cross-section of 1 to 6 mm. As Mxg has high water absorption capacity, pre-treatment condition of the Mxg will also have an impact on the compressive strength. Therefore, a silicate sealant was applied on the Mxg fibres before their application in some mixtures in order to investigate the effect a pre-treatment.

CEM I Portland cement of class 42.5R (CEM I 42.5R) as per EN 197-1:2011 [183] and natural hydraulic lime strength class 3.5 (NHL 3.5) as per EN 459-1 [184] were used as the binder materials. It is well known that the lime improves the workability and permeability of the lime-cement mortar, while increase of cement in the binder improves the mechanical strengths of the mortar [185, 186]. Calcium Chloride ($CaCl_2$) was added as mineraliser to avoid the Miscanthus fibres to absorb the water needed

for the hydration process. It leads to an increase of the compressive strength without increasing the amount of cement [33, 165]. Since the Miscanthus fibres have a high water absorption, cement hydration process has to be increased before the Miscanthus fibres can absorb the water. On this purpose, MasterGlenium ACE 456 superplasticiser was introduced with the mortar due to its advantages of improving the rheology of the mixture and accelerating the cement hydration [174]. Normal tap water was used as mixing water. **Table 5-1** summarises the properties of the materials used in the Miscanthus concrete mixture. More details on the materials and their preparation can be found in ref. [174].

Material	Properties
Miscanthus x giganteus	Density: 120 kg/m^3 15-60 mm with a cross section of 1-6 mm fibres
Cement (CEM I 42.5R)	Density: 3100 kg/m^3
Natural hydraulic lime (NHL 3.5)	Density: 740 kg/m^3
$CaCl_2$	Density: 710 kg/m^3 Particle size: 2-5 mm
Superplasticizer ACE 456	Density: 1060 kg/m^3
Water	Density: 1000 kg/m^3 PH: 6.9

Table 5-1: Properties of the materials used in the Miscanthus concrete mixture

5.3.2 TEST DETAILS

Since this study focused to study the effect of mix proportions on the compressive strength of MLWC, 73 different kind of mixtures were used to prepare the test specimens. The amounts of Mxg and cement were varied from 67.8 to 300 kg/m^3 and 75 to 750 kg/m^3, respectively. Initially, a water/cement (W/C) ratio of 0.7 was used to prepare the mixtures. However, additional mixtures were prepared using different W/C ratios (between 0.5 and 1.8) to study their effect on the strength of MLWC. The amounts of NHL3.5, superplasticizer and $CaCl_2$ used in this study were between 0 and 483.15 kg/m^3, 0 and 8.7, and 6 and 19.65 in kg/m^3, respectively. The details of first 20 mix proportions used in this study are given in **Table 5-2**.

Weight proportions of the mixture						W/C ratio
Mxg	**Cement**	**NHL 3.5**	**ACE 456**	**$CaCl_2$**	**Water**	
1	3.96	2.17	0.04	0.09	2.78	0.7
1	3.96	2.17	0.04	0.09	2.08	0.53
1	2.97	2.17	0.04	0.06	2.78	0.94
1	3.96	0	0.04	0.09	2.78	0.7
1	8.33	4.56	0.08	0.19	5.84	0.7
1	2.48	1.36	0.02	0.06	1.74	0.7
1	1.75	0.96	0.02	0.04	1.23	0.7
1	2.02	2.17	0.04	0.09	1.42	0.7
1	11.06	2.17	0.04	0.09	7.76	0.7
1	3.96	2.17	0.04	0.09	1.98	0.5
1	3.96	2.17	0.04	0.09	2.37	0.6
1	3.96	2.17	0.04	0.09	3.16	0.8
1	3.96	2.17	0.04	0.09	3.56	0.9
1	3.44	1.38	0.04	0.09	2.78	0.81
1	3.77	1.89	0.04	0.09	2.78	0.74
1	4.17	2.5	0.04	0.09	2.78	0.66
1	4.68	3.27	0.04	0.09	2.78	0.59
1	3.96	2.17	0.04	0.09	2.78	0.7
1	3.97	2.19	0.04	0.09	2.02	0.51
1	3.97	2.19	0	0.09	5.26	1.32

Table 5-2: Various mix proportions used in the study

The mixing procedure to get the MLWC test specimens was as follows. First, the dry Mxg and the lime were mixed without water. Then, the water volume was subdivided into two equal parts, and the first half of the water volume was mixed with the superplasticizer (ACE 456) and the mineraliser ($CaCl_2$). Next, it was poured into the dry mixture of Mxg and the lime, followed by the cement. After that, the remaining water volume was added on the ongoing mixture and it was mixed for about 7.5 minutes until a homogenous mixture was obtained. Finally, mixture was casted in 40 mm x 40 mm x 160 mm prism moulds and 150 mm x 150 mm x 150 mm cubical moulds in two successive stages with a needle vibration according to EN 196-1:2005 [187]. From the mixtures, test prisms and test cubes were prepared for the compression tests.

The specimens were stored in their moulds for 1 day at room temperature (around 20 – 22 ˚C). After 1 day, they were demoulded and wrapped in cellophane to avoid the loss of water. After the curing time reached 13 days, the cellophane was removed and the specimens cured for the remaining time at room temperature. The specimens were tested in compression according to EN 12390-7:2019 [188]. More details on the test details can be found in the ref. [174].

5.4 METHODOLOGY

5.4.1 GAUSSIAN PROCESS REGRESSION (GPR)

ML models have been widely used in many fields to simulate material behaviour. In this study, GPR is used to predict the compressive strength of MLWC. GPR is an efficient, probabilistic and nonparametric supervised ML approach for modelling nonlinear and complex functional mappings [153]. GPR implements Gaussian process (GP) for regression purposes.

GP is used to describe a distribution over functions. Theoretically, set of function values in a finite dimensional space can be sampled from a probability distribution of functions determined by a mean function and a covariance function. In GP, the covariance function is determined by a chosen kernel function that describes how much influence one point has on another, and hence, it is very efficient to handle nonlinear data [153].

Mathematically, a Gaussian variable X can be defined in a normal distribution with its mean μ and covariance ∑ as,

$$X \sim N(\mu, \sum) \qquad \text{(eq. 5-1)}$$

GP is more rigorously defined as: f is a Gaussian process if for any vector of inputs $x = [x_1, \dots \dots, x_n]^T$, the vector of output $f(x) = [f(x_1), \dots \dots, f(x_n)]^T$ is Gaussian distributed.

$$f(x) \sim N(m(x), k(x, x')) \qquad \text{(eq. 5-2)}$$

where x ∈ $\mathbb{R}$D , $m(x)$ and $k(x, x')$ are the mean function and covariance function, respectively.

The mean function can be any function maps index points x onto real values. In GP, the mean function is often set to be zero to make notation easier as well as to compare different models together. In the modelling context, the kernel function, which is the covariance function, is the more important. It maps

the input space onto a real value. The most commonly used kernel function in ML is the squared exponential function defined as,

$$k(x, x') = \sigma^2 \exp\left(-\frac{(x - x')^2}{2l^2}\right) \quad \text{(eq. 5-3)}$$

where σ^2 and l are two hyper parameters. The length scale, l, defines the influence of the function value in length, while the variance, σ^2, specifies the height of the kernel.

It is common to many applications of regression that there is noise in the observations. Therefore, in GPR with noise, for a given training data set $D = \{(x_i, y_i \mid i = 1, \ldots \ldots, n)\}$, where $x \in \mathbb{R}^{D\,x\,n}$ is the input data matrix and $y \in \mathbb{R}^D$ is the vector of output, the output y differs from the function values $f(x)$ by the additive noise as [189],

$$y = f(x) + \varepsilon, \qquad \varepsilon \sim N(0, \sigma_n^2) \quad \text{(eq. 5-4)}$$

where ε is the Gaussian noise with variance σ_n^2. Then, the new covariance function can be written as,

$$k(x, x') = \sigma^2 \exp\left(-\frac{(x - x')^2}{2l^2}\right) + \sigma_n^2 \delta(x, x') \quad \text{(eq. 5-5)}$$

where $\delta(x, x')$ represents the Kronecker delta function: i.e. $\delta_{ij} = 1$ if $i = j$ and $\delta_{ij} = 0$ if $i \neq j$.

For a given training data x ($x \in \mathbb{R}^{D\,x\,n}$), corresponding observations y ($y \in \mathbb{R}^D$), and test data points x_* ($x \in \mathbb{R}^{D\,x\,n_*}$) which is needed to predict y_*, a joint distribution can be expressed as,

$$\begin{bmatrix} y \\ y_* \end{bmatrix} \sim N\left(\begin{bmatrix} \mu \\ \mu_* \end{bmatrix}, \begin{bmatrix} K & K_*^T \\ K_* & K_{**} \end{bmatrix}\right) \quad \text{(eq. 5-6)}$$

where μ and μ_* are the means of training sets and test sets, respectively. K, K_* and K_{**} are the training set covariances, training-test set covariances and test set covariances, respectively.

$$\mu = m(x) \quad \text{and} \quad \mu_* = m(x_*) \quad \text{(eq. 5-7)}$$

$$K = K(x, x) = \begin{bmatrix} k(x_1, x_1) & \cdots & k(x_1, x_n) \\ \vdots & \ddots & \vdots \\ k(x_n, x_1) & \cdots & k(x_n, x_n) \end{bmatrix} \quad \text{(eq. 5-8)}$$

$$K_* = K_*(x_*, x) = [k(x_*, x_1) \quad k(x_*, x_2) \quad \ldots \quad \ldots \quad k(x_*, x_n)] \quad \text{(eq. 5-9)}$$

$$K_{**} = k(x_*, x_*) \quad \text{(eq. 5-10)}$$

Since the values for the training set y are known, the conditional distribution of y_* given y can be expressed as,

$$p(y_*|y) = N(\mu_{2|1}, K_{2|1}) \quad \text{(eq. 5-11)}$$

where

$$\mu_{2|1} = \mu_* + K_* K^{-1}(y - \mu) \quad \text{(eq. 5-12)}$$

$$K_{2|1} = K_{**} + K_* K^{-1} K_*{}^T \quad \text{(eq. 5-13)}$$

If we assume the mean prior $\mu = 0$, then eq. 5-12 can be rewritten as,

$$\mu_{2|1} = K_* K^{-1} y \quad \text{(eq. 5-14)}$$

By using the mean $\mu_{2|1}$ of the resulting distribution as a prediction, it is then possible to predict y_* corresponding to the test sets x_*.

5.4.2 DATASET

In this study, the ML model was trained and evaluated using the experimental dataset of compressive strength of MLWC, described in section 5.3.2. The compressive strengths of test specimens were evaluated at 7, 14 and 28 days after casting. The experimental dataset consisted of 414 specimens having different concrete mixture compositions. Some samples of the dataset are presented in **Table 5-3**.

Mix proportions (kg/m^3)						W/C ratio	Form	Curing time (days)	Pre-treatment of Mxg	Compressive strength (MPa)
Mxg	Cement	NHL3.5	ACE 456	$CaCl_2$	Water					
130.92	518.23	284.09	5.21	11.60	363.64	0.7	Prism	7	Yes	6.364
144.04	569.97	312.56	5.65	12.78	299.91	0.53	Prism	14	Yes	15.187
144.04	427.44	312.57	5.60	8.00	399.96	0.94	Prism	14	Yes	5.037
144.04	570.03	0.00	5.66	12.68	399.95	0.7	Prism	14	Yes	8.260
75.00	624.45	342.30	6.15	13.95	438.15	0.7	Prism	28	No	10.509
225.00	558.75	306.30	5.55	12.45	391.95	0.7	Prism	28	No	2.474
300.00	525.75	288.30	5.25	11.70	369.00	0.7	Cube	14	No	0.416
222.75	450.00	483.15	8.70	19.65	315.75	0.7	Cube	28	No	0.262
67.80	750.00	147.30	2.70	6.00	526.20	0.7	Cube	28	No	13.371
162.45	642.90	352.50	6.30	14.40	321.45	0.5	Prism	14	No	2.798
155.85	616.50	337.80	6.15	13.80	369.90	0.6	Cube	14	Yes	3.556
144.00	569.70	312.15	5.70	12.75	455.70	0.8	Prism	28	No	19.388
138.75	548.85	300.75	5.40	12.30	493.95	0.9	Prism	28	No	15.642
172.05	591.75	236.70	6.75	15.15	477.60	0.81	Prism	7	Yes	9.552
156.87	591.75	295.88	6.14	13.85	435.52	0.74	Prism	7	Yes	6.625
141.75	591.75	355.05	5.55	12.45	393.45	0.66	Prism	28	Yes	13.367
126.55	591.75	414.23	4.95	11.17	351.35	0.59	Prism	14	Yes	13.198
144.06	570.01	312.53	5.64	12.72	399.95	0.7	Prism	14	Yes	13.984
113.00	449.00	247.00	4.49	10.00	228.00	0.51	Prism	28	Yes	5.648
113.00	449.00	247.00	0.00	10.00	594.00	1.32	Prism	28	Yes	4.560

Table 5-3: Some samples in the dataset of compressive strength of MLWC

5.4.3 CROSS-VALIDATION AND PERFORMANCE EVALUATION

In the present study, the 10-fold cross-validation algorithm was used to improve the model prediction in the ML model by using a MATLAB program [190]. This was achieved by using the inbuilt MATLAB function “Crossval” with scalar 10 [190]. In the 10-fold cross-validation, the dataset is randomly divided into ten non-overlapping groups (folds), as shown in **Fig. 5-1**. Each fold will have an equal number of data samples. In each of the ten validation rounds, nine of ten folds are used to train the ML model and the remaining fold is used to test the ML model.

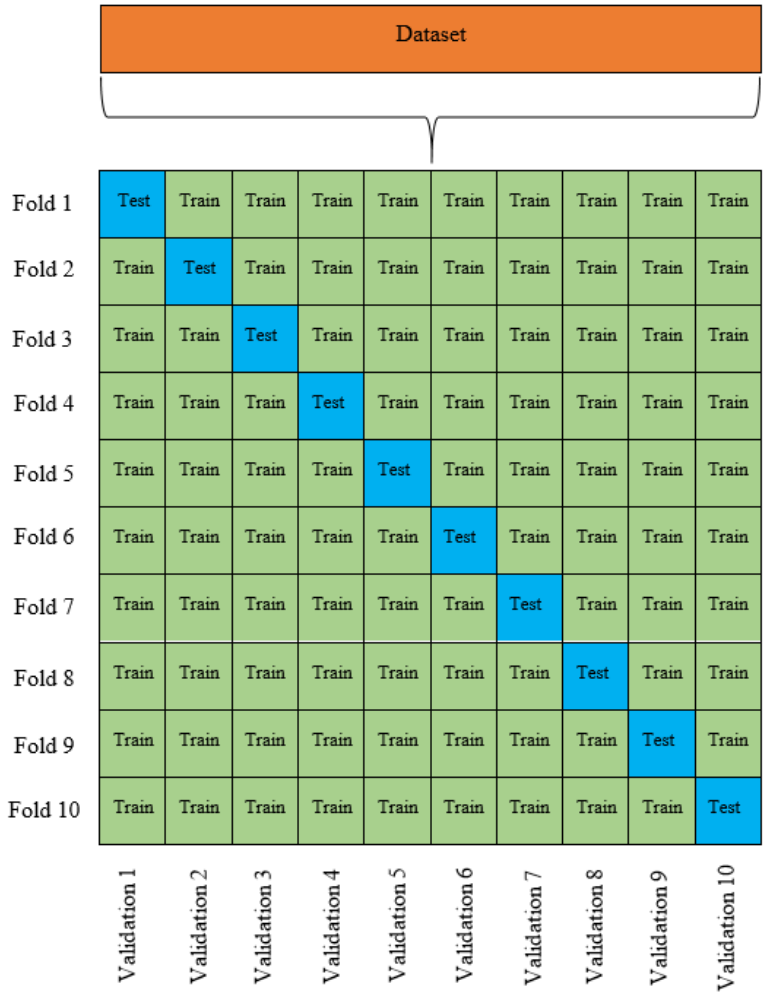

Fig. 5-1: 10-fold cross-validation algorithm

The predictive accuracy of each validation round was evaluated in terms of errors in regression. Four of such common indicators such as the Mean Absolute Error (MAE), the Mean Squared Error (MSE), the Root Mean Squared Error (RMSE) and this R-Squared (R^2) were used for this purpose.

MAE is the average of the absolute value of the error, which is very commonly used to measure the accuracy of predicted values. It is defined as,

$$MAE = \frac{1}{n}\sum_{i=1}^{n}|y_i - y_i'| \qquad \text{(eq. 5-15)}$$

where y_i' is the predicted value, y_i is the actual value and n is the number of observations.

MSE is the average of the squared value of the error. It is used as a default metric for the evaluation of the performance of most regression algorithms in MATLAB, and it is defined as,

$$MSE = \frac{1}{n}\sum_{i=1}^{n}(y_i - y_i')^2 \quad \text{(eq. 5-16)}$$

RMSE is the square root of the mean of the square of all of the error. It is defined as,

$$RMSE = \sqrt{\frac{1}{n}\sum_{i=1}^{n}(y_i - y_i')^2} \quad \text{(eq. 5-17)}$$

R^2 represents the proportion of the variance in the dependent variable from the independent variables. It is defined as,

$$R^2 = 1 - \frac{\sum_{i=1}^{n}(y_i - y_i')^2}{\sum_{i=1}^{n}(y_i - \bar{y})^2} \quad \text{(eq. 5-18)}$$

where $\bar{y}$ is the averaged actual value.

5.5 RESULTS AND DISCUSSION

The basic concept of this ML model is to establish a reliable nonlinear functional mapping between the compressive strength MLWC and its own mix proportions. The variables used in the model as predictors to relate with compressive strength of MLWC were: 1) six mix proportions (i.e. Miscanthus, cement, lime, superplasticizer, $CaCl_2$ and water), 2) water/cement ratio, 3) form of specimen, 4) curing time, and 4) pre-treatment condition.

As described in section 5.4.1, the predictive performance of GPR on a given data is highly dependent on the choice of the kernel function. The inbuilt MATLAB function "fitrgp" was used to fit a GP to the given data x and y [190]. There are a number of inbuilt kernel functions available in MATLAB. In this study, two kernel functions, namely, ARD squared exponential (ARD-SE) kernel and ARD rational quadratic (ARD-RQ) kernel were used by comparing the fit that can be achieved to determine which one best suits with the given data. Since more than one input (predictor) were used in the model, different length-scale parameters for each predictor are used in these two kernel functions. Here, ARD stands for automatic relevance determination and it implies that the estimation of the length scale parameters implicitly determines the relevance of each predictor.

ARD-SE kernel has the form [190]:

$$k(x,x') = \sigma^2 \exp\left(-\frac{1}{2}\sum_{i=1}^{D}\frac{(x_i - x_i')^2}{l_i^2}\right) \quad \text{(eq. 5-19)}$$

where l_i is the length-scale parameter for predictor i and D is the number of predictor variables.

ARD-RQ kernel has the form [190]:

$$k(x,x') = \sigma^2\left(1 + \frac{1}{2\alpha}\sum_{i=1}^{D}\frac{(x_i - x_i')^2}{l_i^2}\right)^{-\alpha} \quad \text{(eq. 5-20)}$$

where α is a positive-valued scale-mixture parameter.

Fig. 5-2 shows the scatter plot of measured and predicted values of compressive strength of MLWC obtained from ML models for the dataset of 414 records. It reveals that both ML models have a good agreement between measured and predicted compressive strength of MLWC.

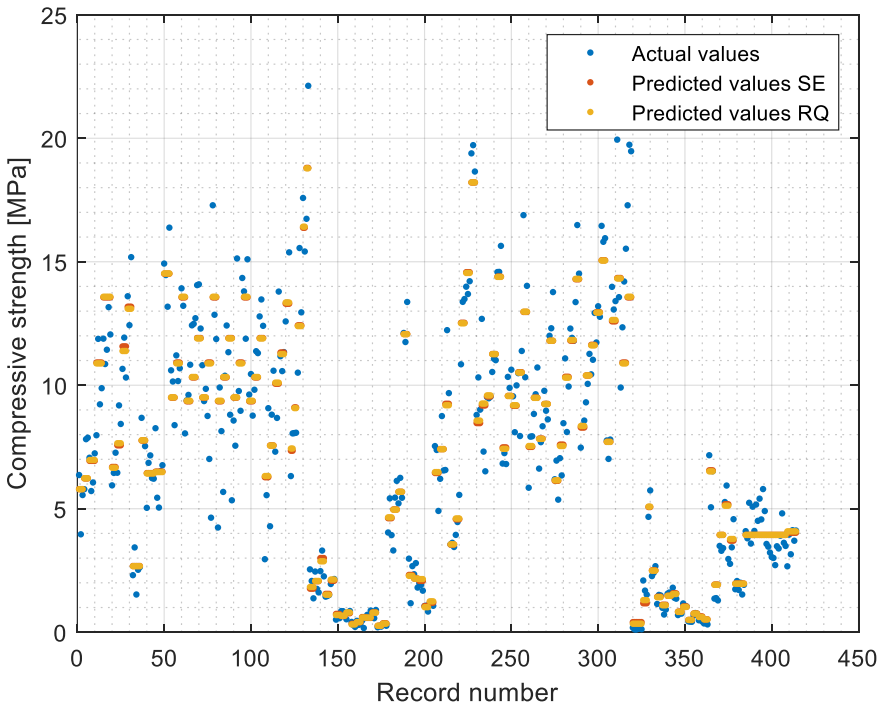

Fig. 5-2: Actual and predicted values of compressive strength of MLWC by using GPR

Fig. 5-3 shows the prediction outcome of the GPR between two kernel functions and actual values of the compressive strength of MLWC on the input dataset. **Fig. 5-4** compares the predicted results from

two developed models. These results emphasize that the prediction performances of the GPR rational quadratic and the GPR squared exponential models were almost similar. However, the validity of the proposed model for prediction of compressive strength of MLWC for any set of data was checked in terms of MAE, MSE, RMSE and R^2. The comparison of accuracy of the model is reported in **Table 5-4**. It can be seen that the GPR rational quadratic model has achieved a considerably good prediction result in all of the indicators compared to the other model.

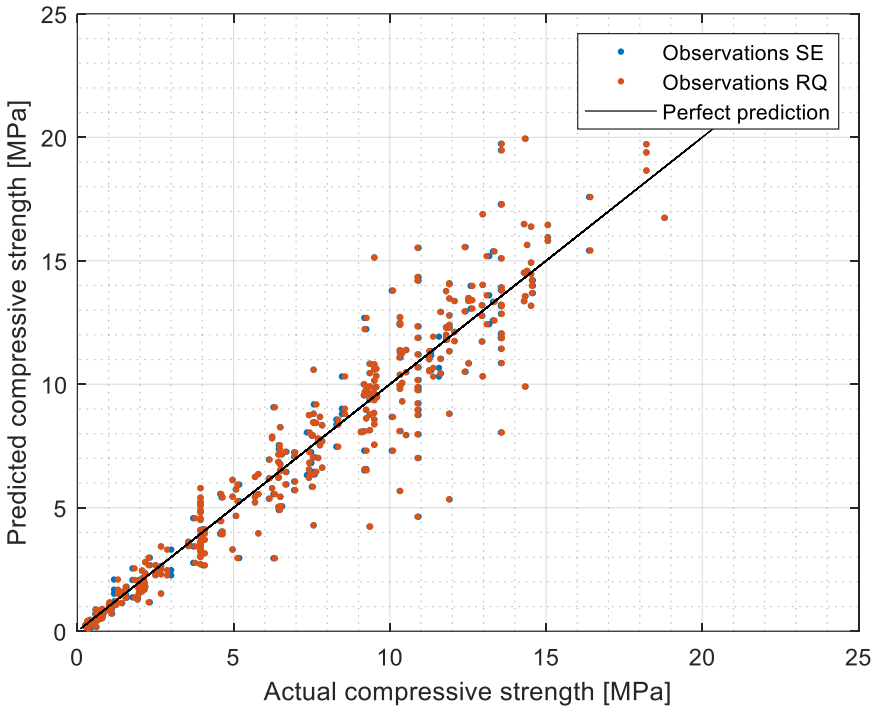

Fig. 5-3: Prediction results for the dataset by using GPR

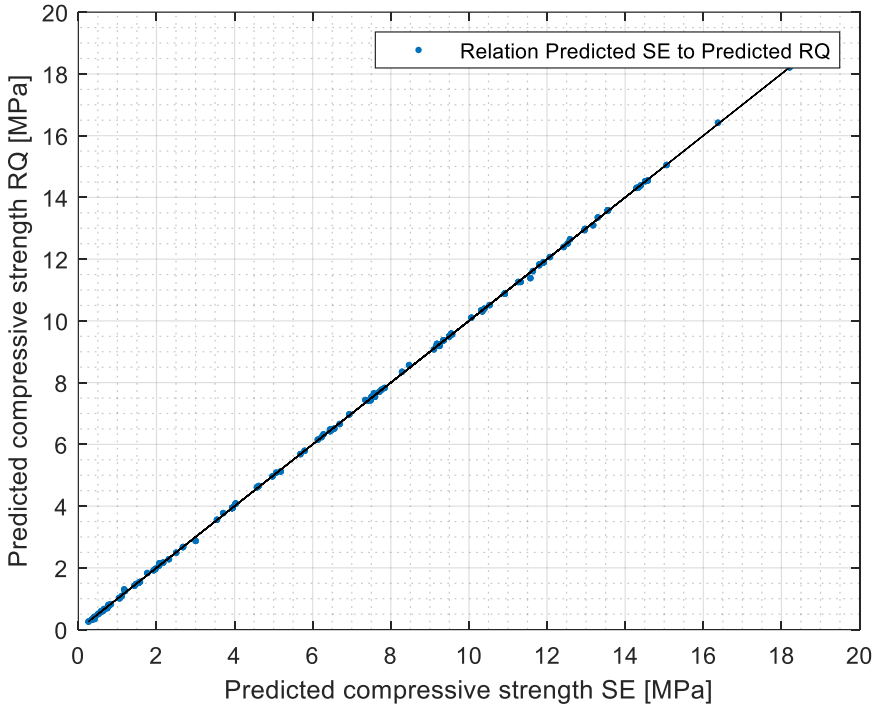

Fig. 5-4: Prediction results for the dataset by using GPR

Indicator	GPR squared exponential	GPR rational quadratic
MAE	0.905	0.900
MSE	2.061	2.054
RMSE	1.436	1.433
R^2	0.917	0.918

Table 5-4: Comparison of the accuracy of the model

The effect of each constituents of Miscanthus concrete mixture on the compressive strength of MLWC are illustrated in **Fig. 5-5**. These results emphasize that for both models the relationship between input variables of constituents of MLWC and the output of compressive strength of MLWC can be successfully mapped. In general, it can be seen that the compressive strength increases as the amount of each constituent increases. For example, compressive strength increases as the amount of cement increases. However, this is not true always but can be up to an extent, as if the W/C ratio keep unchanged, an increase of the cement induces also a proportional increase of the water volume. As a result, air voids in the hardened matrix are increased, which disrupt the bond between the Mxg and binder, and hence the compressive strength is decreased [174].

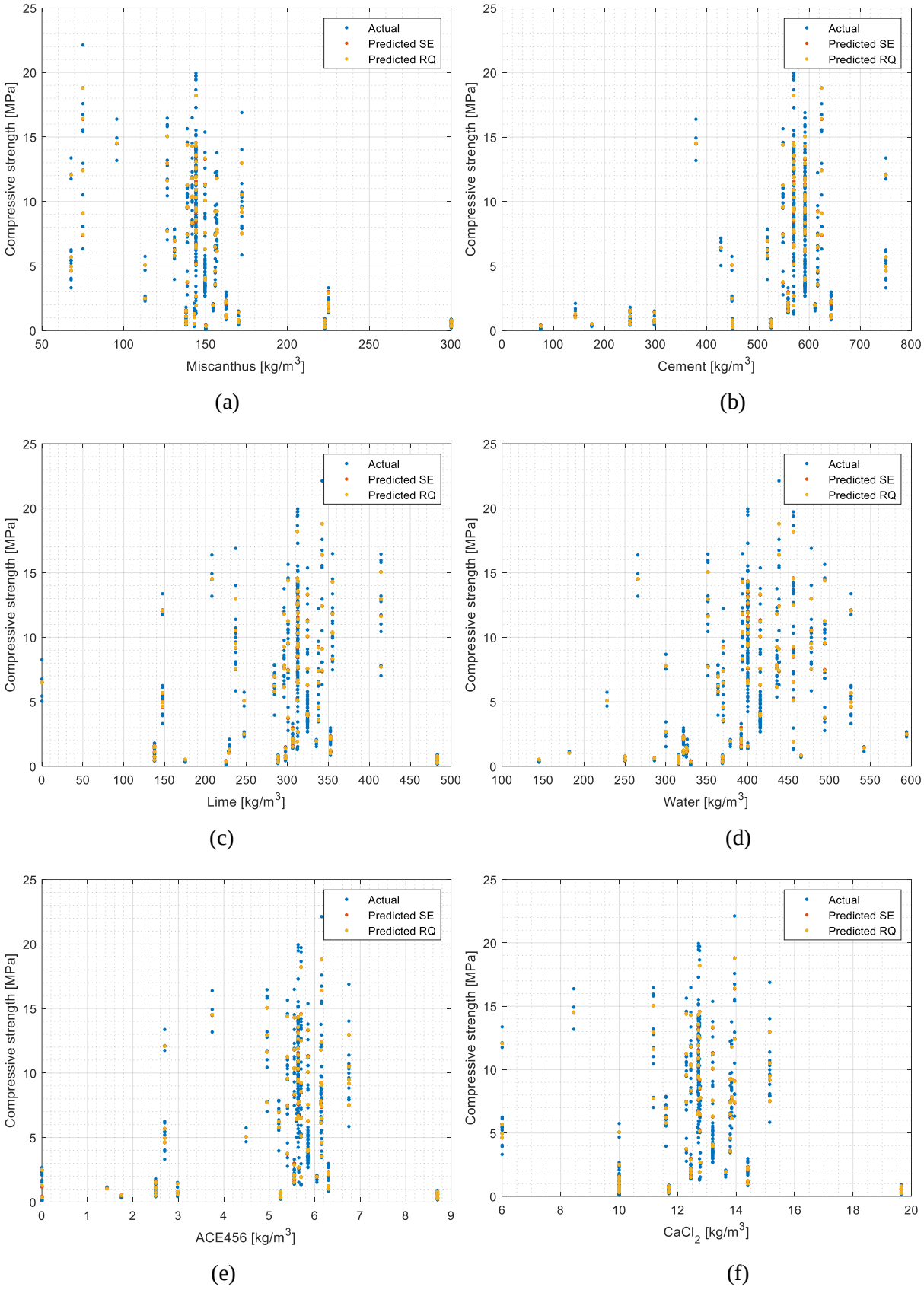

Fig. 5-5: The scatter plots of compressive strength of MLWC versus the input variables of (a) Miscanthus (b) cement (c) lime (d) ACE456 (e) $CaCl_2$ and (f) water

Since the GPR model can be successfully used to predict the compressive strength of the MLWC for different mix constituents of MLWC, a tool was developed using MATLAB [190] to deploy the model. This tool was developed to study the sensitivity of each variable on the compressive strength. It was developed with a simple user interface so that everyone can use it without knowledge in programming. The interface was divided into two sections as an input section to enter the mix proportions as required data and output section to display results for the entered data. The user interface of the developed tool for predicting the compressive strength of MLWC is shown in **Fig. 5-6**.

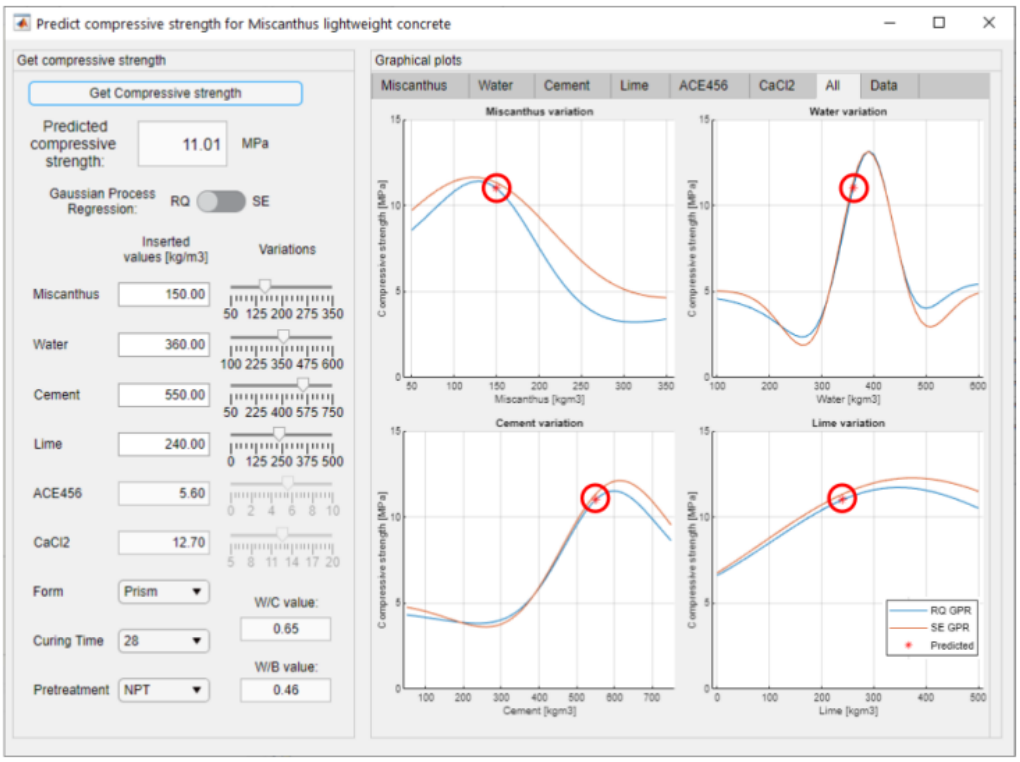

Fig. 5-6: The user interface of the tool

The main inputs of the tool are: the amount of Miscanthus, water, cement, lime, ACE456 (superplasticizer) and $CaCl_2$ in kg/m^3 as well as the form of the specimen, the curing time and the pre-treatment condition of Miscanthus. The users have the choice between two options for the form of the specimen, mainly prism or cube. The curing time can be picked to be 7, 14 or 28 days. The user can select pre-treated or not treated as pre-treatment condition. Moreover, the user may decide to use the RQ or SE kernel function for the GPR.

The developed tool can be used to check the different mixture combinations which will indicate the compressive strength for the given parameter combination. The influence of sensitivity of each input variable on the final prediction of the compressive strength can also be analysed using the graphs in the developed tool. It is achieved by randomly changing the values of the selected variable while keeping the remaining ingredients unchanged. The difference of the predictions when changing the value of the

selected ingredient makes a sense to define the importance of each ingredient. If the difference in the predictions is high, that ingredient has a significant influence on the compressive strength. It was found that the cement content has the most significant influence on final compressive strength of MLWC. On the other hand, the amount of $CaCl_2$ is the least critical factor affecting the compressive strength of MLWC. Also, a given mixture can be optimised using the graphs in the developed tool. Thus, this tool can be used as a design tool in the construction industry as well as a support tool in research institutions.

5.6 CONCLUSION

This study proposed a ML model for predicting compressive strength of MLWC. For that, 414 sets of compressive test results were collected. Test variables were divided into ten inputs as mix constituents of concrete (cement, Miscanthus, lime, water, $CaCl_2$ and superplasticizer), water/cement ratio, form of specimen, curing time and pre-treatment condition and one output variable (compressive strength of MLWC). In this paper, two GPR models with ARD-SE and ARD-RQ were used for the purpose of predicting the compressive strength of different MLWC mix designs. Four indicators such as MAE, MSE, RMSE and R^2 were used to express the model accuracy. The overall performance of GPR model with ARD-RQ kernel function was more accurate to be applied to predict the compressive strength of MLWC.

A tool was developed to deploy the GPR model, which can be used to check the sensitivity of each constituents in the MLWC mixture on the compressive strength. It was revealed that cement, W/C ratio and Miscanthus are the most significant parameters on the final predictions of compressive strength of MLWC.

The results of this study provide helpful information on engineers to select the optimal mix proportions of the Miscanthus concrete, and the developed tool can be used at an early stage of designing the Miscanthus concrete members instead of using costly experimental investigation.

Chapter 6 ANALYSIS OF THE GEOMETRICAL IMPERFECTIONS OF A DRY-STACKED MASONRY BLOCK BASED ON MISCANTHUS (MANUSCRIPT ON MISCANTHUS MASONRY BLOCKS)

6.1 ABSTRACT

This paper aims to verify the suitability of masonry blocks based on Miscanthus concrete to be used in dry-stacked walls. Therefore, masonry blocks based on different mixture composition and procedure were analysed and the highest ultimate load was 5.42 MPa. A gradual loading on a masonry block allowed concluding an exponential relation between the contact area and the load. Next, the load-bearing capacity is experimentally measured on small wallets for which an ultimate load of 4.84 MPa was measured. In addition, a numerical model of the wallet was validated based on the experimental data, which allowed performing a sensitivity analysis on the material properties and studying the impact of height and roughness imperfections. The latter reduced the load-bearing capacity by a maximum of only 31 %, whereas the height differences reduced it in average by only 2.5 % The authors concluded that the low Young's Modulus of the Miscanthus concrete causes this kind of material to be suitable to be used as a masonry block for dry-stacked walls.

Keywords – Miscanthus x giganteus; dry-stacked masonry; load-bearing capacity; roughness; contact surface; height differences

6.2 INTRODUCTION

The need for a sustainable building is rising more and more to reduce the enormous energy consumption rates and CO_2 emission provoked by the construction sector. According to the Global Alliance for Buildings and Construction, 36% of the energy use and 39% of the CO_2 emissions in the world are attributable to the construction sector [191-194]. Numerous measures are studied to reduce these rates and simultaneously reduce the usage of non-renewable resources such as natural sand and gravel, which are consecutively decreasing due to their substantial exploitation [37]. The latter can be attained by replacing the filling with a sustainable plant-based filler with good thermal and acoustic properties [51, 195, 196]. Furthermore, an asset of a filler such as Miscanthus grass, which can grow on industrially contaminated grounds [197-199], has also a favourable CO_2 balance. Applying these materials on a dry-stacked masonry system would reduce the usage of mortar, which implies reduced energy consumption [108].

The C_4-plant Miscanthus has a wide range of genotypes, and its origins are from East Asia [6, 155]. Due to its capacity to grow under a vast range of climatic conditions [200] Aksel Olsen introduced the Miscanthus x giganteus (MxG) grass from Japan to Europe in the 1930s [6]. The advantages of achieving a height of up to 4 m and a high yield with a low input on fertilisers and pesticides cause this plant to be very interesting economically and ecologically [7, 14, 18]. Besides, MxG can grow on contaminated soil and simultaneously improving it by reducing its contamination, which increases its fertility [16, 17]. Furthermore, the water use of MxG results in a surface stabilisation of the soil, which impedes soil erosion, metal transportation due to wind and water movement [16].

MxG plant is, due to its high yield potential, mostly used for bioenergy production for direct combustion, gasification or as chopped material [15, 26]. MxG is also applied as an oil binding material, in agriculture, e.g. as mulch or bedding for animals, mulch for pathways and in the construction sector [25]. R. Pude et al. [22] analysed the suitability of the fibres of MxG and three other Miscanthus genotypes (Miscanthus sacchariflorus, Miscanthus sinensis and Miscanthus Robustus) used as a filler for lightweight concrete and investigated the achieved compressive strength. According to R. Pude et al. [22], the highest compressive strength was performed by the genotype MxG due to its high cellulose content and its high binding capacities of water in the concrete matrix. Furthermore, according to Godard et al. and Wang et al. [35, 36], the cost competitiveness of the usage of MxG as a filler could be increased by diminishing the transport distances of this material. This decrease could be achieved by encouraging local farming, which implies a reduction in CO_2 emissions and benefits the local economy.

An economical way of building a wall is to use a dry-stacked system instead of a conventional system. The difference between these two systems is the omitted mortar in the horizontal joints on the dry-stacked system. This absence has the advantage of increasing the labour speed since there is no need to

lay the mortar or wait for it to dry, so the next layer of masonry blocks can be applied [100, 101]. These benefits favoured the adoption of different interlocking systems. The latter can be classified in a geometric and non-geometric mechanism [100]. The first holds due to its geometry, which can be a dovetail connection between the blocks or a tongue and groove arrangement or a post-tensioned technique [102]. The second one holds due to a post-treatment on a wall, which can be due to grout inward the masonry blocks to bond the surfaces of the prism, or to insert synthetic strips between the blocks.

Anand and Ramamurthy [100] analysed two geometric interlocking systems using different ways of the dovetail connection and two different normal concretes with the proportions 1:2:4:0.55 and 1:3:5:0.6 (cement:sand:coarse aggregate:w/c). The first concept was based on blocks with a part coming out as a dovetail (I-shape). The second concept was a channel shape that can also be considered as the negative of the first one. On the next step, wallets were created and evaluated on their axial and eccentric load-bearing capacity as well as on their bending resistance. The latter was subdivided in tension parallel to bed joint and a tension normal to bed joint (**Fig. 6-1**). Both systems resulted in a high-efficiency factor for the compressive strength (0.62-0.77) as well as for the eccentric-to-axial capacity ratio compared to the conventional masonry. Furthermore, the I-shaped and the channel-shaped concept reached a bending resistance normal to the bed joint comparable to a mortar-bedded prism.

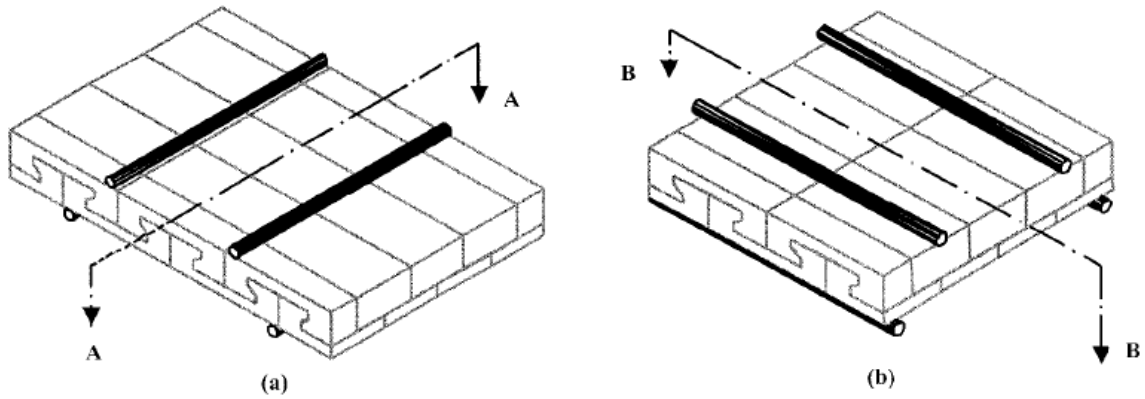

Fig. 6-1: Bending loading (a) tension parallel to bed joint; (b) tension normal to bed joint (adapted from [100])

Kohail et al. [102] analysed and compared the behaviour of a conventional wall (conventional block, **Fig. 6-2**) to two dry-stacked interlocking masonry blocks (Sparlock system and Azar system, **Fig. 6-2**). The conventional block used had the highest compressive strength of 12.10 MPa (Sparlock: 6.9 MPa and Azar: 8.40 MPa). Two approaches were explored on the stacked system, grouted and un-grouted blocks. The conventional system reached the highest compressive strength for both systems (8.9 and 10,2 MPa).

The un-grouted system showed to be beneficial considering the compressive strength (3-15 % higher) independent from the masonry blocks. Besides Kohail et al. [102] evaluated nine full-scale shear walls under lateral cyclic loading for the three masonry blocks under different conditions, grouted, un-grouted and partially grouted, positioning of reinforcement and the use or non-use of post-tension bars on the masonry panel. They concluded that the load-bearing capacity of the un-grouted and post-tensioned conventional and Azar system was 62% higher than the one of the traditional reinforced and fully grouted masonry panel. They stated that the utilisation of post-tension bars without grout benefits the effective stiffness, the energy dissipation and the lateral load-bearing capacity.

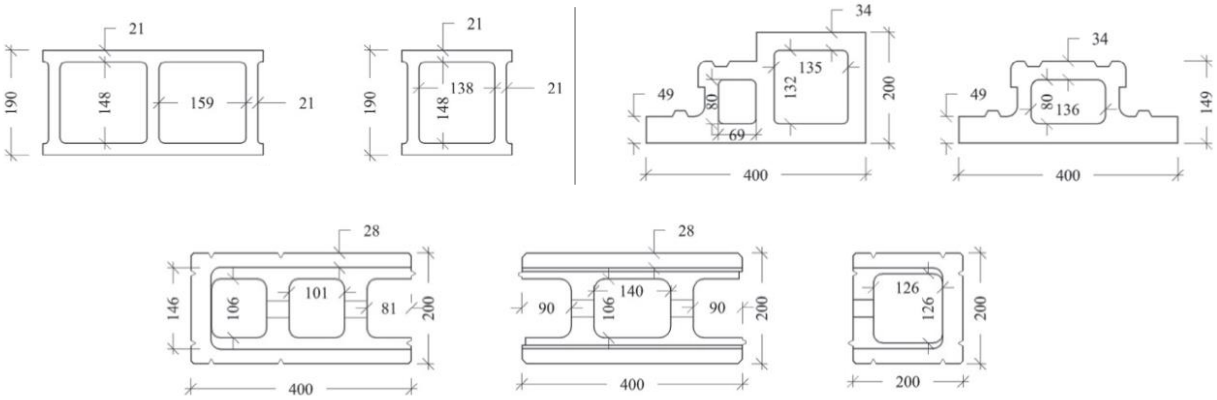

Fig. 6-2: Geometry and dimensions of the three analysed blocks, conventional block (left, top), Sparlock system (right, top) and Azar system (middle, bottom) (unit: mm), adapted from Kohail et al. [22]

Chewe et al. [107] analysed the impact of the geometrical imperfections on the load-bearing capacity of a dry-stacked wall, more precisely the height differences and the surface roughness, using numerical and analytical approaches and comparing them to the experimental tests performed by Agaajani [108]. The analysis was performed on single masonry blocks and masonry panels of different heights. The height distribution of the masonry blocks followed a Gaussian law of +/- 2 mm. Chewe et al. [107] claimed that the height imperfections impact the load-bearing capacity of the wall and distinguished 5 cases of the load percolation on a single masonry block (**Fig. 6-3**). This statement was based on the random distribution of blocks with different heights in the wall. This last induced a random load percolation system leading to five possible individual loading cases of a masonry block. On each case on top of the masonry block acts a load on the full or the half-length of the block and the percolation of the load is distributed differently for each case on the lower part of the block. Furthermore, they analysed the useful section of a masonry block on a wall. They concluded that the section is statistically reduced related to an increase in the wall height and length. In this paper, a similar occurrence is expected on the wallet based on Miscanthus concrete masonry blocks.

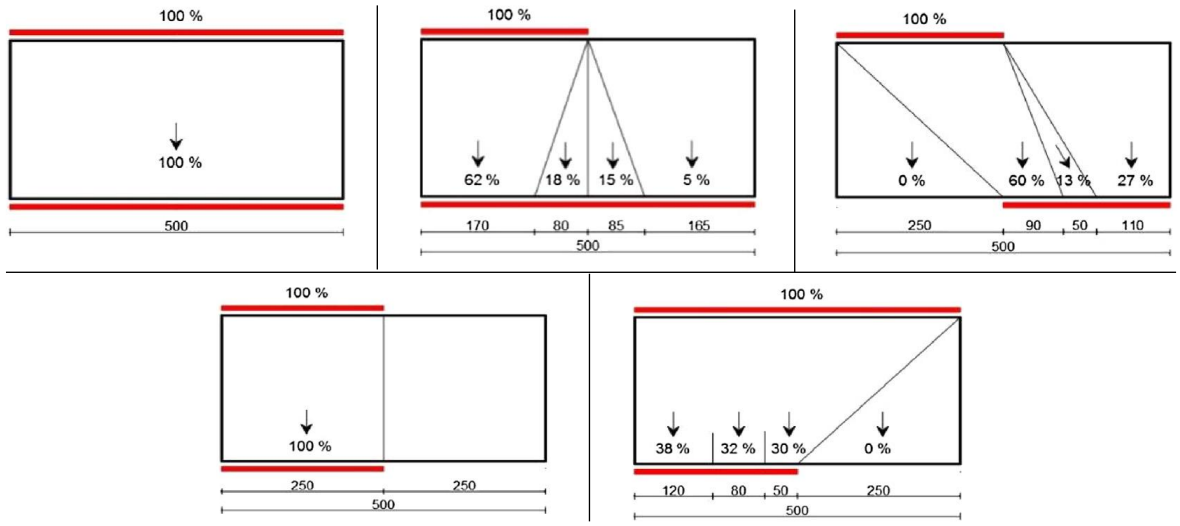

Fig. 6-3: 5 cases of the load percolation, adapted from Chewe et al. [107]

An increase of the useful section, and so an improvement of the load-bearing capacity, was analysed by Chewe and Waldmann [109] by introducing a contact layer on top of each masonry block. This latter was composed of two face-shells connected by two web faces. The contact layer should lift the height and the roughness imperfections of a block due to its low stiffness [110]. Four contact layers were considered using four distinguished materials with a compressive strength of 5.2-38 MPa and a Young's Modulus of 3-11.5 GPa. A low Young's Modulus has the advantage of alleviating a higher amount of stress peaks but with the detriment of generating significant lateral deformations. Chewe and Waldmann [109] evaluated the load-bearing capacity of these masonry blocks with their respective contact layers on dry-stacked walls of 1000 x 830 mm and compared them to a dry-stacked wall with the same dimension and using masonry blocks without any contact layer. During the experimental tests, three damage paths were observed. The first was a crack on the outer face-shell, followed by another one on the face-shell connection to the web face and pursued by a spalling around the bed-joint interfaces. Chewe and Waldmann [109] observed a load-bearing capacity of 4.83 MPa on the wallet using the masonry blocks with a contact layer, which was 32 % higher than the load-bearing capacity of the dry-stacked wall using masonry blocks without contact layer. The authors of this paper will analyse the use of masonry blocks based on Miscanthus concrete for the wallets and expect to reduce the impact of the roughness and the height differences due to the low Young's Modulus of this material [174].

For a conventional wall with mortared joints, the load-bearing capacity can be determined according to the standard EN 1996-1-1 [111] using different constants, the compressive strength of the mortar and the masonry unit. Chewe and Waldmann [109] expanded the proposed equation from the EN 1996-1-1 to be used on dry-stacked masonry walls by implementing the imperfections of a masonry unit, more precisely the roughness and the height variation. The height was determined by measuring over 100 masonry blocks, and as for Agaajani [108], a Gaussian distribution was established with a mean

elevation of 200.2 mm and a standard deviation of 1.0. The asperity height of the roughness of the masonry blocks was evaluated by the rate of the actual area in contact. Therefore, Prescale FUJIFILM strips were set on the joints of three stacked masonry blocks and after the test digitalised to calculate the contact area. Chewe and Waldmann [109] determined that a masonry block without contact layer showed a net contact area of 23 %. In contrast, a contact layer on top of the masonry unit increased the contact area. The gain of contact area depends on the material of the contact layer [109, 114] and induces an increase of the load-bearing capacity of a dry-stacked masonry wall [112, 113]. In this paper, the contact area will be determined using a similar technique with the Prescale FUJIFILM.

This publication aims to analyse the suitability of Miscanthus masonry blocks on dry-stacked walls. Therefore, the mixture composition and the mixture procedure are first studied on a single masonry block and then these findings are applied on wallets. Furthermore, since Chewe and Waldmann [109] stated the impact of the roughness and the height differences of the masonry blocks on the load-bearing capacity of a wallet, the impact of these imperfections are also analysed for a dry-stacked masonry wallet based on a much more ductile Miscanthus concrete. In addition, using the generated experimental data, a numerical model is validated, based on which the impact of the roughness and the height imperfections are analysed as well as a relation of the achieved load-bearing capacity and the ratio (H/L).

6.3 MATERIALS AND EXPERIMENTAL AND NUMERICAL APPROACH

6.3.1 MATERIALS AND MIXTURES

The Miscanthus concrete mixtures were based on the study performed by Pereira Dias and Waldmann [174]. The used materials were pre-treated Miscanthus x giganteus fibres, cement (CEM I, 42.5 R), tap water, hydraulic lime (NHL 3.5), calcium chloride ($CaCl_2$) and a superplasticiser (MasterGlenium® ACE 456). In this study, the fibres were not priory pre-treated due to their low benefit [174]. Besides the physical and mechanical advantages, it also has the convenience of reducing the whole procedure by one-step and discards the need for a second repository for the treated fibres. The composition of the mixtures (Mix 1, Mix 2, Mix 3 and Mix 4) used in this study are reported in **Table 6-1**. The main difference between the mixes 1-4 is the water/cement ratio, respectively, the water/binder ratio. The amount of the superplasticiser and the $CaCl_2$ were $5.8 - 5.9\ kg/m^3$ resp. $13.2 - 13.3\ kg/m^3$.

Sample ID	Miscanthus [kg/m^3]	Cement [kg/m^3]	W/C ratio	L/C ratio	W/B ratio
Mix 1	150	593	**0.62**	0.55	**0.40**
Mix 2			**0.70**		**0.45**
Mix 3			**0.80**		**0.52**
Mix 4			**0.90**		**0.58**

Table 6-1: Composition of the mixtures

These materials were used to create three mixture procedures (A, B and C in **Table 6-2**). The first step of the proceeding is to perform a dry mix between two components (Comp.), Miscanthus and lime for mix A, cement and lime for mix B and C. After blending for one minute, the water including the dissolved superplasticiser and the $CaCl_2$ is poured. Depending on the mix, half of the total amount of water was run at this step. The following step after blending for 2-2.5min subsists in inserting the last component, the cement for mix A and Miscanthus for mix B and C. The mixture (A and C) is then blended for 1min and the remaining water is poured in the blender. Finally, the mixtures are blended for 3-3.5min, and after a total blending time of 7-7.5min, the mixture can be used for moulding the specimens.

Name	Comp.	Mix. time	Comp.	Mix. time	Comp.	Mix. time	Comp.	Mix. time	Total time
A	Miscanthus + Lime	1min	Half of the water amount*	2min	Cement	1min	Remaining water	3.5min	7.5 min
B	Cement + Lime	1min	Complete water amount*	2.5min	Miscanthus	3.5min	-	-	7 min
C	Cement + Lime	1min	Half of the water amount*	2min	Miscanthus	1min	Remaining water	3min	7 min
*: including ACE 456 and $CaCl_2$									

Table 6-2: Mixing procedure

Two kinds of specimens were created, prisms of 16x4x4cm and masonry blocks of 40x20x10cm. The prisms were conceived in a precision three-gang mould (left in **Fig. 6-4**) according to the EN 196. The masonry blocks were constituted in self-made wooden formworks (middle and right in **Fig. 6-4**). Dependent on the analysis, one mix was performed to fill prisms and masonry blocks. In this case, the

masonry blocks were always produced before the prisms due to their higher volume and to avoid a more substantial settlement of the fresh concrete, which would induce bleeding of the Miscanthus concrete. Independent from the shape of the specimen, the moulding procedure was the same. The mould was first half-filled, hand-compacted and vibrated for 5 seconds. Next, the remaining part of the mould was filled until the top, and as on the previous step; it was hand-compacted and shook for 5 seconds. Finally, if needed, more material was poured inside, and the mould was covered with a wooden plate to enclose the surface in contact with the ambient.

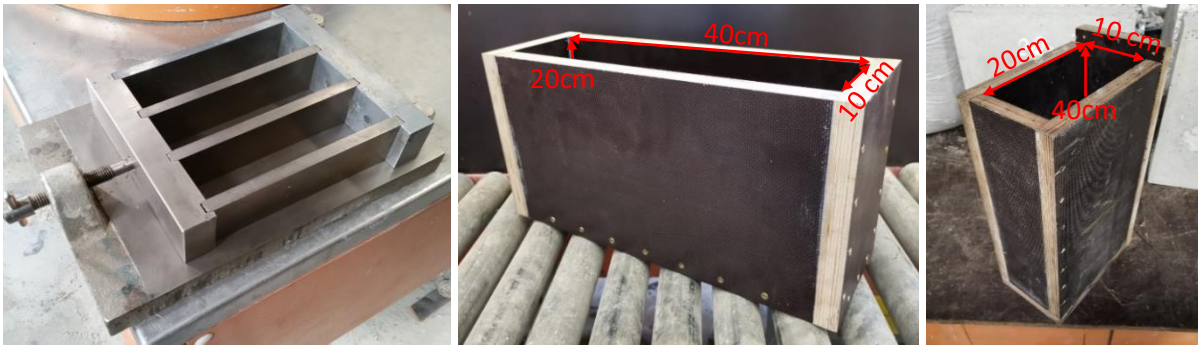

Fig. 6-4: Mould and dimensions of the samples: (left) prisms, (middle and right) masonry blocks

After one day of curing in laboratory conditions, the specimens were removed from the moulds, weighed and wrapped with cellophane to avoid an excess of water evaporation. After 13 days of curing, the translucent was removed, and the specimens were stored under ambient conditions for 1 respectively 15 days depending on the analysis performed.

6.3.2 Experimental Approach

The suitability of Miscanthus concrete on masonry blocks and wallets was analysed in 5 steps (Trial 1-5 in **Table 6-3**). According to Pereira Dias and Waldmann [174], the W/C ratio has a high impact on the achieved load-bearing capacity of prisms and cubes. Therefore, the first study (Trial 1) consisted of analysing the impact of the W/C ratio (varying the water amount) on the compressive strength using the mixing procedure A (**Table 6-2**) on the mixtures Mix 2, Mix 3 and Mix 4(**Table 6-1**), for which 6 prisms and 2 masonry blocks were produced per mixture. The presented compressive strength of the prisms was averaged out of 3 prisms per variation according to the standard DIN EN 197-1 [201]. Each masonry block of Trial 1 was produced by filling the mould from the top surface (middle **Fig. 6-4**). Due to the cement settlement during casting, the filling procedure for the masonry blocks from the following trials was adapted and the mould in **Fig. 6-4** (left) was used.

A critical factor in achieving a homogenous masonry block is a uniform distribution of the mix components. Therefore, Trial 2 analysed the mixing procedure's impact (A, B and C in **Table 6-2**) on the compressive strength using Mix 2 and generating 6 prisms per mix. It is assumed that a combination

of Trial 1 and 2 would affect the achieved load-bearing capacity. Accordingly, the subsequent analysis (Trial 3) comprised a variation of the water amount (similar to Trial 1) but using the mixing procedure B on Mix 1 and 2 to set up 6 prisms and 6 masonry blocks per mix. Furthermore, it is known that the rheological properties of ordinary concrete are impacted by vibration [202]. Therefore, in addition to the stated analysis of Trial 1, 2 and 3, the impact of vibration on the compressive strength is evaluated according to the surface in contact. Trial 4 was divided into two parts; both were based on Mix 2 and the mixing procedure B. It is expected that the curing time affects the load-bearing capacity. Thus, the first part analyses the compressive strength of masonry blocks and prisms after a curing time of 28 days. Besides, the contact surface of the masonry blocks is simultaneously evaluated. The peaks of the roughness are crushed with an increasing load. Therefore, the second part consisted of putting a stepwise load (loading and unloading) on a masonry block cured for 14 days, and analysing the contact surface at each load-step of 1MPa as well as the final load-bearing capacity. Finally, to analyse the suitability of the masonry blocks for the use on a dry-stacked wallet, 18 masonry blocks were created in Trial 5, which were used at the age of more than 90 days to create 3 dry-stacked wallets (Wallet 1-3).

Trial	Used Mixes	Mixing procedure	Vibration analysis	Contact analysis	Curing Time [d]	Created specimens per mix
Trial 1	Mix 2 Mix 3 Mix 4	A	Yes	Yes	14	6 Prisms 2 Masonry blocks
Trial 2	Mix 2	A B C	Yes	-	14	6 Prisms
Trial 3	Mix 1 Mix 2	B	Yes	Yes	14	6 Prisms 6 Masonry blocks
Trial 4	Mix 2	B	-	Yes	28	3 Prisms 3 Masonry blocks
				Stepwise	14	3 Masonry blocks
Trial 5	Mix 2	B	-	-	90	18 Masonry blocks

Table 6-3: Experimental trials

Each wallet had a height of 3 and a length of 2 masonry blocks (60*80cm) (**Fig. 6-5**). The lower and the upper row (R1 + R3) consisted of two full masonry blocks, and the middle row (R2) is composed of one entire block and two half-blocks. The masonry blocks were staggered above each other without any mortar in the bed joints (J1 + J2). For a better analysis of the experiment, the vertical deformation of the

bed joints and each masonry block was measured. The sensors on the front (front in **Fig. 6-5**), measured the deformation between the rows. The transducers positioned on R1, R2 are averaged as D_R1 and the captors measuring the vertical deformation from R2 and R3 are averaged as D_R2. Furthermore, the deformation in the third row (D_R3) is calculated deducting D_R1 and D_R2 from the total deformation of the wallet. The sensors on the back measured the vertical deformation in the bed joints (D_J1 and D_J2).

To apply a uniform compressive loading on the masonry blocks 4 and 5 (**Fig. 6-5**) a steel beam (HEA180 – S235) has been used and fixed to the cylindrical hydraulic press with a max. loading capacity of 1 MN. The vertical displacement of the steel beam was measured using two transducers on top of this steel beam (D-Tot-L and D-Tot-R in **Fig. 6-5**).

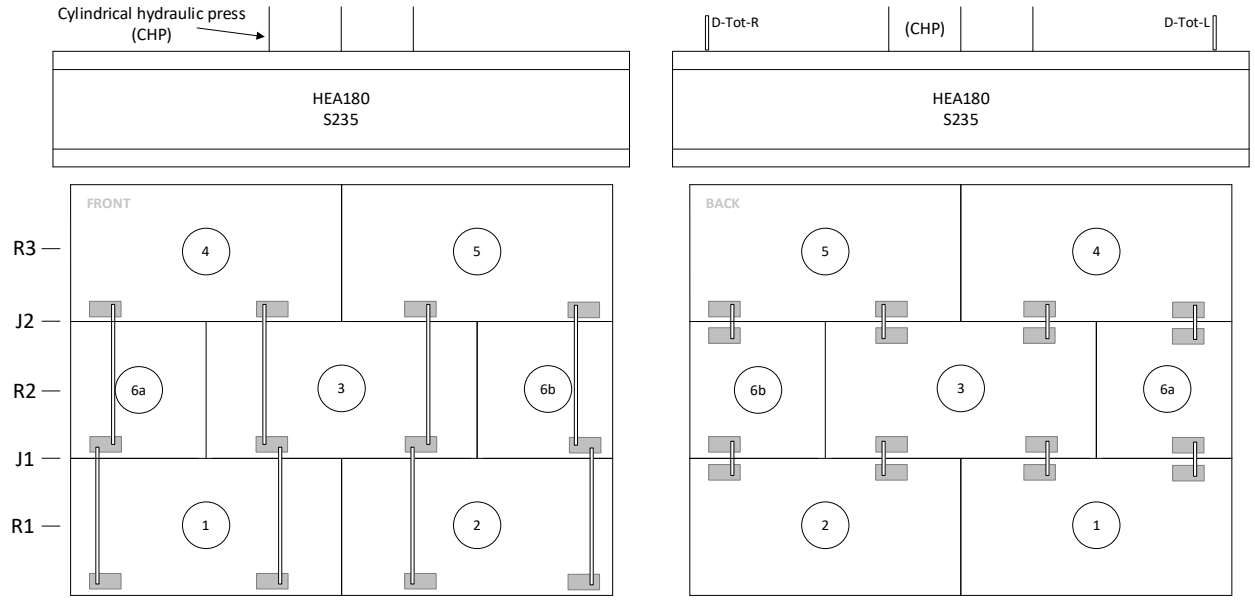

Fig. 6-5: Position of the masonry blocks and the transducers

The aim of Wallet 1 was to measure the load-bearing capacity of the masonry blocks based on Miscanthus concrete. Therefore, no contact analysis was performed on Wallet 1 and no transducers were applied on the back part of the wallet and on top of the steel beam. The load was continuously applied (at a rate of 2mm/min), contrarily to Wallet 2 and 3, where the application of the pressure was controlled to form a hysteresis curve. In addition, a contact analysis was performed on J1 and J2 of Wallet 2 and 3.

All the contact analysis previously mentioned were performed using strips of a two-sheet type of Prescale FUJIFILM (left in **Fig. 6-6**), which is composed of two films (A + C) put above each other with the colour layers together. Film A has on one side a red-colour-forming layer with microcapsules and Film C has a layer, which develops a colour using the absorbed microcapsules that break due to a pressure application. The breakage depends on the measurable pressure range. Since in this work, the contact on a masonry block is analysed at different loads, the used pressure range is 0.5-2.5 MPa

(Prescale Super Low Pressure (LLW)). Afterwards, depending on the density of the red colour (right in **Fig. 6-6**), the pressure can be measured using different techniques. Here, the FUJIFILM strips were scanned using a conventional scanner and the colour of the resulting images were converted to grayscale.

Finally, a script is created using MATLAB to analyse each pixel's colour and extracts the grayscaled colour number. This last is compared to a range based on the colour-density (right in **Fig. 6-6**), which was also grayscaled before. Each field can be associated with the applied pressure using the diagram in the instruction manual of the Prescale LLW [203], which associates the force to the colour density.

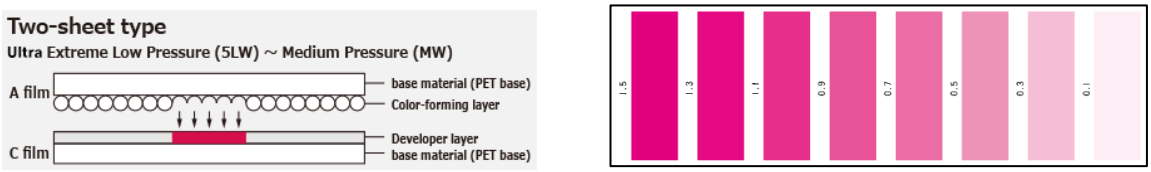

Fig. 6-6: Features of the used Prescale FUJIFILM (left) and the densities of the red colour (right) [203]

6.3.3 Analysis of the height imperfections of masonry blocks

During the production process of conventional masonry blocks the height of the masonry blocks is not constant and follows a Gaussian distribution [108]. This occurrence is also expected on the masonry blocks based on Miscanthus concrete. Therefore, the masonry blocks are dimensioned and categorised according to their production mould (middle and right **Fig. 6-4**) before being tested.

6.3.4 Numerical Approach

The aim of the numerical calculation is to predict the behaviour of a wallet with diverse variations without having to create an experimental test, which is very time and resource consuming. Therefore, a model with material properties based on literature is established in ANSYS and validated with the experimental data. Additionally, a parametric study is performed on the numerical model of one masonry block by varying the material properties (stress, strain and Young's Modulus), the roughness and the smeared reinforcement. After this parameter study, the validated properties are transferred into the numerical masonry wallet and the impact of the dimensions of the wallet are analysed. Furthermore, as the height differences in the wallet have an important impact on the load-bearing capacity of the wall [107], the height of the masonry blocks are varied and related to the load-bearing capacity.

6.3.4.1 Composition of the numerical masonry block

The dimensions of the numerical masonry block are identical to the experiment (40x20x10 cm = LxHxT). It was observed that in the upper and lower extremities of a casted masonry block the embedment of Miscanthus fibres is not homogeneous and much weaker as in central area of the bloc. This fact has been considered by modelling the masonry block with two different material laws: the

upper and the lower part of the model referenced as rough part (RP) and the central core part (**Fig. 6-7**). For the central core, a material strength of 11 MPa has been chosen. These values are based on the density of one masonry block after a curing time of 28 days (1082 kg/m^3) and on the relation between density and compressive strength presented by Sagmeister [173]. Since the material of the rough part is weaker, an assumption has been made that the material strength would be reduced by 20-25 %, which results in a compressive strength for the rough part of in average 9 MPa. The Young's Modulus of the core part is evaluated with 2 GPa based on the relation between the compressive strength and the Young's Modulus established by Sagmeister for lightweight concrete mixtures [173]. The Young's Modulus of the weaker part is lower because the Miscanthus fibres are in the upper and lower area of the masonry block not completely enveloped by the cement paste. According to the standard EN 1992-1-1 [204], the Young's Modulus of a concrete mixture is based on the Modulus of its components. Sandstone aggregates have a Young's Modulus of 11.3-40 GPa [205]. Therefore, according to the standard EN 1992-1-1 [204], the Young's Modulus of the mixture can be reduced by 30 %. Since in this paper Miscanthus fibres were used, which have a Young's Modulus of only 2-8 GPa [43], a reduction of 60 % compared to the Young's Modulus of the core part was assumed for the rough part which led to a value of 0.8 GPa.

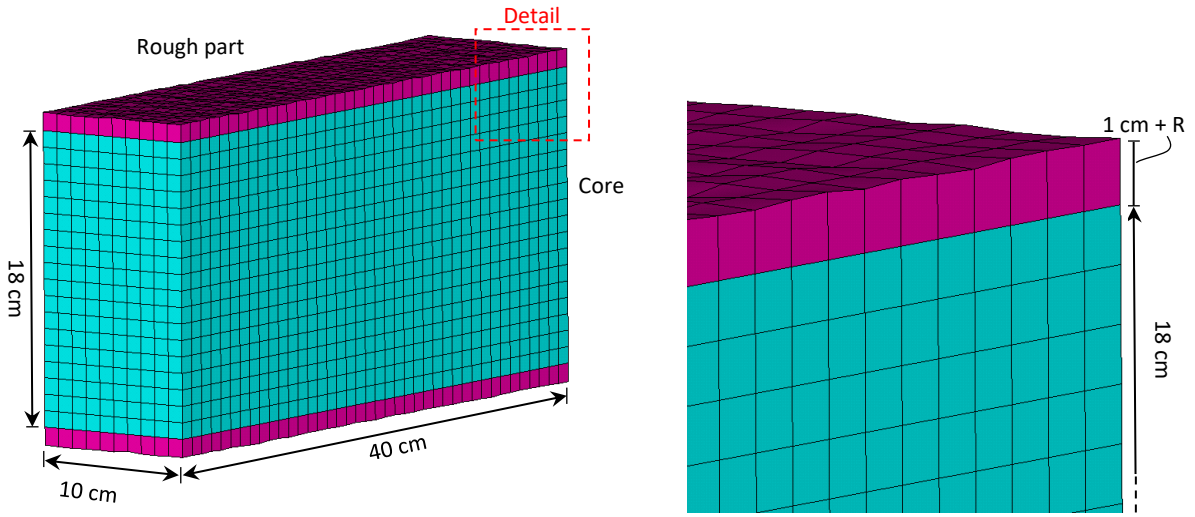

Fig. 6-7: Concept of the numerical masonry block and detailed top roughness part

The imperfections of masonry blocks, which affect mostly the load-bearing capacity of a dry-stacked wall, are the roughness and the height differences of the masonry blocks [114]. A roughness is added on the top and the bottom of the rough part of the masonry block. The height of the block consists of 18 cm of the core and 1 cm of the rough part on the upper and 1 cm on the lower part of the masonry block. The thickness of the rough part is based on half of the maximum length of the Miscanthus fibres, which are 1.5-2.0 cm. The diameter of the fibres corresponds to 0.10-0.30 cm and half of this dimension is used as reference for the roughness to define the difference between peak and valleys of the roughness R to

0.15-0.20 cm. According to Passaribu and Shipper [118], the roughness of a surface follows a Gaussian distribution. As stated in the theory of a Gaussian distribution, 99.7 % of the values are between minus and plus 3 times the standard deviation (σ) [206]. Therefore, 6 times the standard deviation corresponds to the difference between the highest peak and valley, which is 0.15-0.20 cm. From the latter the standard deviation is extracted by dividing 0.15-0.20 cm by 6, which results in a standard deviation of 0.03 cm. The mean value μ of the Gaussian distribution is set to 0 cm, which represents a reduction of the height of the masonry block for the valleys and an increase of the height for the peaks.

First, the possibilities of roughness (in mm) are calculated using the cumulative distribution function (eq. 6-1) [206] for all possible probabilities going from]0 %-100 %[. Next, the Gaussian distribution is created using the density function (eq. 6-2) and a course is created as shown in **Fig. 6-8**. Finally, a roughness value is extracted from the presented course, by picking a randomly chosen probability and extracting the corresponding roughness, as shown in **Fig. 6-8** with the position of the dashed line, e.g. a probability of 84.1 % corresponds to a roughness of +0.3 mm.

$$F(R) = \frac{1}{\sqrt{2\pi}} \int_{-\infty}^{(R-\mu)/\sigma} e^{-u^2/2}\, du \qquad \text{(eq. 6-1)}$$

$$f(R) = \frac{1}{\sigma\sqrt{2\pi}} \cdot e^{-\left(\frac{(R-\mu)^2}{2\sigma^2}\right)} \qquad \text{(eq. 6-2)}$$

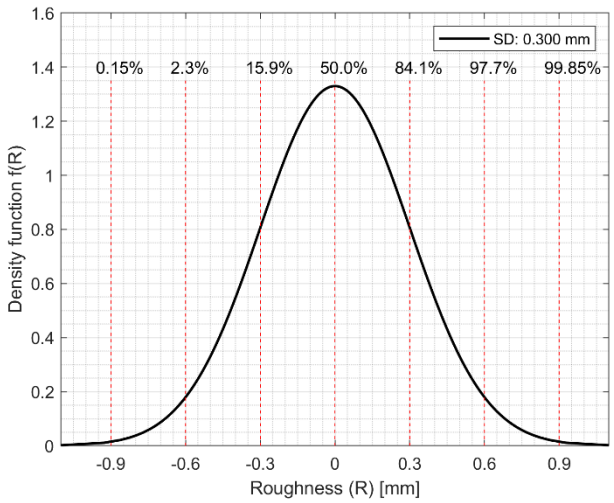

Fig. 6-8: Gaussian distribution of the roughness using a mean of 0 mm and a standard deviation (SD) of 0.30 mm and the probabilities at the different roughness R

The material properties and the roughness are introduced into the numerical masonry block **Fig. 6-7**. The element used to define the material in the masonry block is SOLID65, which uses the Willam-Warnke failure criterion [207] and includes an internal smeared reinforcement. The Miscanthus fibres were considered acting similar to a reinforcement in the Miscanthus concrete. Therefore, a smeared

reinforcement is implemented in the model with a volume ratio of 30 %. This value is reduced from the effective volume of fibres present in mixture Mix 2 as shown in section 6.3.1 (50 %), since the fibres are distributed randomly in the specimen and only one part is working in the needed direction. Therefore, an assumption was made and the volume ratio of 50 % was reduced by 1/3. The density and the Young's Modulus of the smeared reinforcement were set to 120 kg/m^3, resp. 5 GPa [43, 174].

As in the experimental test, two steel plates are used in the model, one below and another above the masonry block (**Fig. 6-9**). The upper steel plate is used as a pressure plate, where a load is vertically applied on the top surface. During the calculation process to avoid a body motion of the masonry block, horizontal supports are set on two points in the edges (red dots in **Fig. 6-9**).

Then, the connection between the steel plates and the masonry block is modelled by using contact-target elements: the upper and the lower layer of the masonry block are defined as the contact surface using the element model CONTA174 and the opposite surface, which is on the plates, is defined as the target surface using the element model TARGE170.

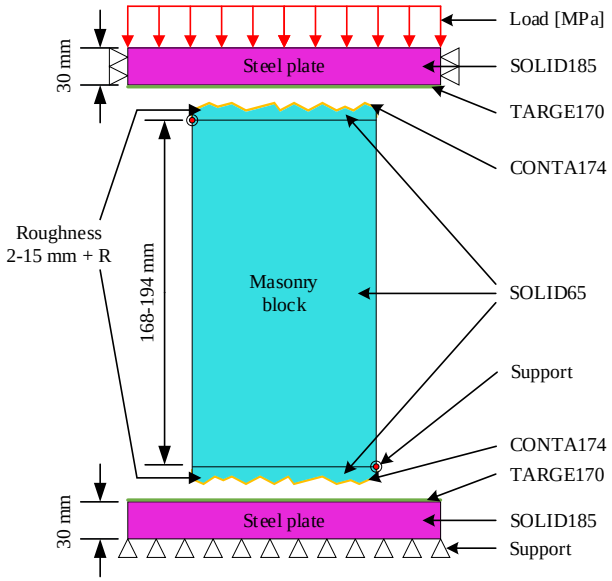

Fig. 6-9: Composition of the numerical model including dimensions, element types and boundary conditions

6.3.4.2 PARAMETRICAL STUDY

The parametrical study of the numerical model was performed by varying the material properties (strength and Young's Modulus), the standard deviation of the roughness, the height of the roughness part and the volume of the smeared reinforcement.

The variation of the material properties (stress and Young's Modulus) were based on the experimental data performed by Pereira Dias and Waldmann [174]. The peak strength of the material strength from

the analysed materials for the masonry block varied from 10-17 MPa. The boundaries of the Young's Modulus are set to 0.6-10 GPa are based on the extremes measured by Pereira Dias and Waldmann in [174].

In this paper, 9 roughness are analysed based on a peak to valley distance varying from 0.45 – 2.4 mm, which corresponds approximatively to the diameter of the used Miscanthus fibres (1-3 mm). The standard deviation of each roughness is calculated by dividing the distance between a peak and a valley by 6: e.g. if the distance between peak and valley is of 2.4 mm, the standard deviation will be of σ = 0.40 mm, which equals to 2.4 mm/6. The range of the peaks and valleys of each roughness is limited by -3 and +3 times the corresponding standard deviation; e.g. a σ = 0.40 mm results in a boundary from -1.2 to +1.2 mm with a mean of μ = 0 mm. The standard deviation of the 9 roughness is in the range of σ= 0.075 - 0.40 mm and μ=0 mm (**Fig. 6-10**). As presented in section 6.3.4.1, the mean value μ, the standard deviation of each roughness and a by the randomly chosen probability are used to extract the roughness value in mm from **Fig. 6-10.**

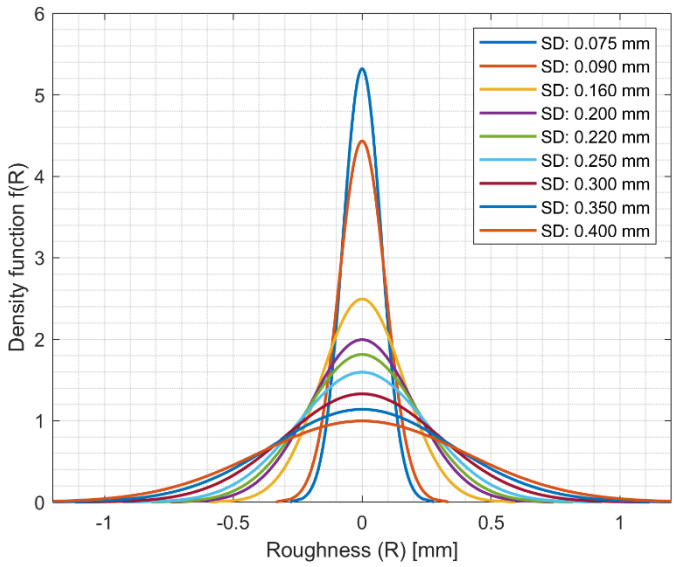

Fig. 6-10: Normal distributions with a mean of μ of 0 mm and different standard deviations (SD)

In addition, the height of the roughness part is varied from 2-15 mm to analyse the impact of the weaker part on the load-bearing capacity. The lower boundary is chosen according to the mean diameter of the Miscanthus fibres (1-3 mm) and the upper boundary is related to the length of the fibres (15-20 mm). Furthermore, the volume of smeared reinforcement is analysed from 0-50 %, basing the maximum on the volume of fibres present in Mix 2 whereas 0% would not consider this effect at all.

The parametrical study is performed on 7 parameters, composed of the limits previously defined (**Table 6-4**). The first parameter being varied is the material strength (MS). First, an identical material is used for the core and the rough part (MS 1) to analyse the impact of one material strength on the load-bearing

capacity of the masonry block. MS 2 analyses the impact of the material strength on the core and the rough part. The third variation consists of varying the material strength of the core and the rough part and the Young's Modulus (MS 3 & YM 1). However, in this case the Young's Modulus of the core and the rough part are identical. Next, a focus on the Young's Modulus is performed by varying it for one material strength of 13 MPa (YM 2). As previously, an identical material is used for the core and the rough part of this variation, which is not the case for variation YM 3. Here, two distinct material strengths are used for the core and the rough part and the Young's Modulus of both parts are varied. Next, the roughness is analysed (Std. dev. R) by varying only the standard deviation of the applied roughness. The roughness height is diversified on the variation (RH) and finally the volume of the smeared reinforcement is analysed in the variation VR SR from **Table 6-4**.

Variation	Material strength [MPa]		Young's Modulus [GPa]		Std. dev. roughness [mm]	RH [mm]	Volume ratio of SR [%]
	Core	Rough part	Core	Rough part			
MS 1	10 - 17	*	2.4	*	0.30	2	0
MS 2	10 - 12	8 - 10	2.4	0.6	0.30	10	30
MS 3 & YM 1	11 & 12	10 & 11	1.2 & 2.4	*	0.30	2	0
YM 2	13	*	1.2-10	*	0.30	2	0
YM 3	12	10	1.2 - 6.7	0.6 & 1.2	0.30	2	0
Std. dev. R	13	*	2.4	*	0.075-0.40	2	0
RH	12	10	2.4	0.6	0.30	2 - 15	0
VR SR	12	10	2.4	0.6	0.30	2	0 - 50

Abbreviations:
MS : Material strength
YM : Young's Modulus
Std. dev. R : Standard deviation of the roughness
RH : Roughness height
VR SR : Volume ratio of smeared reinforcement

Table 6-4: Parametric study of the numerical model (* = identical to the core property)

6.3.4.3 CREATION OF A FEM OF A DRY-STACKED WALLET

The load-bearing capacity of a masonry wallet with a height of 3 rows (60 cm) and a length of 2 masonry blocks (80 cm) is analysed using the numerical masonry block previously presented with the validated properties. The first and the third row of the dry-stacked wallet consists of two full masonry blocks and the second of one full and two half blocks (**Fig. 6-11**). As previously, two steel plates were generated below and above the wallet. The load is applied on the upper surface of the top steel plate. An identical

contact-target (CONTA174 and TARGE170) technique, as for the model with a single masonry block, is used between the rows of the wallet and among the steel plates and the masonry blocks.

Furthermore, the impact of the height differences (ΔH) of the masonry blocks on the load-bearing capacity is analysed. Therefore, four cases of height differences are implemented in the masonry blocks (**Table 6-5**). The nomenclature of each case identifies the number of the masonry block on which an increase in height was performed. The "+" resp. "-" in **Table 6-5** represents an increase resp. a decrease of 3 times the standard deviation of the height differences analysed in section 6.3.3, which makes these 4 instances the worst possible cases. Furthermore, to deduct a real case scenario and identify the most relevant cases an analysis is performed on all possible load percolation systems in the numerical masonry wallets, where the height differences are attributed randomly based on a Gaussian distribution (**Fig. 6-23**). Finally, a relation between the height (0.6, 1.2, 1.8 and 2.4 m) and the length (0.8, 1.6 and 2.4 m) of the wall is investigated to assess the use of this masonry block on a dry-stacked wall. To analyse the maximum bearing capacity of the walls with different dimensions, no height differences were implemented in the masonry blocks.

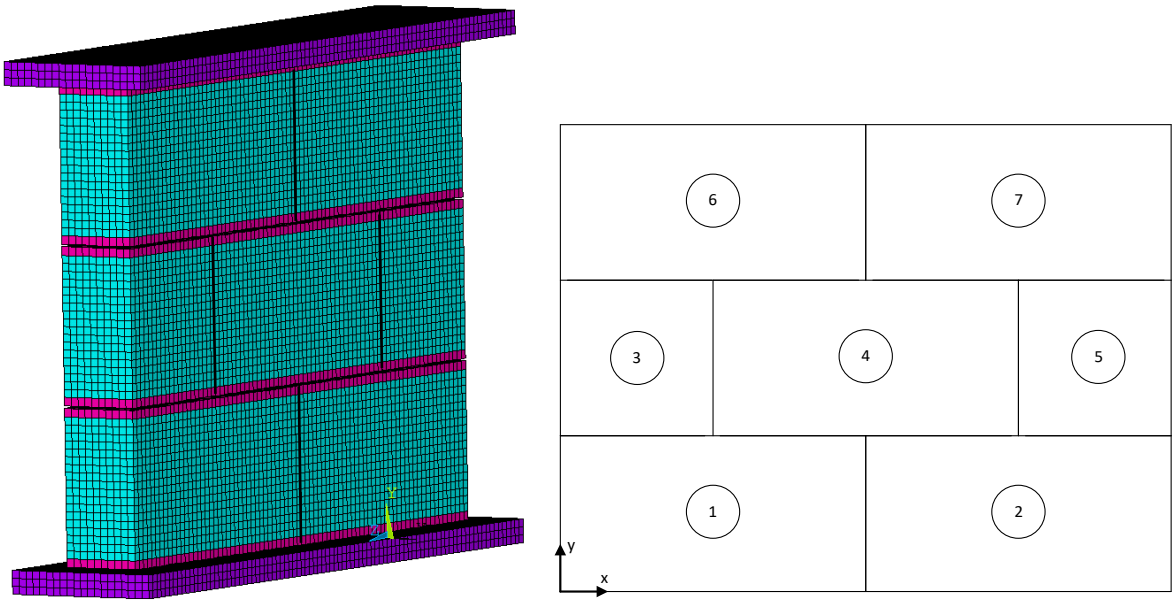

Fig. 6-11: (left) Numerical wallet of three blocks height and two blocks length; (right) illustration of the wallet

Cases		Position of the masonry block based on Fig. 6-11 (right)						
		①	②	③	④	⑤	⑥	⑦
1.	BL 3-5	/	/	+3σ	/	+3σ	/	/
2.	BL 1-3-5	+3σ	/	+3σ	/	+3σ	/	/
3.	BL 1-4-6	+3σ	-3σ	-3σ	+3σ	-3σ	+3σ	-3σ
4.	BL 2-4-6	-3σ	+3σ	-3σ	+3σ	-3σ	+3σ	-3σ

Table 6-5: Height differences (ΔH) implemented in the numerical model (σ = standard deviation; / = no change of the height, which corresponds to ΔH=0)

6.4 RESULTS AND DISCUSSION

In the following sections, the load-bearing capacity and the roughness are analysed for each trial presented in **Table 6-3**. In addition, the height imperfections are studied by measuring the height of the masonry blocks and creating a normal distribution according to the data. A numerical parameter study is performed on a validated model for one masonry block. Then, a numerical wall is modelled using the validated parameters from the single masonry block and the impact of the height differences as well as the impact of the dimensions of the wall on the load-bearing capacity are analysed.

6.4.1 LOAD-BEARING CAPACITY

6.4.1.1 PARAMETRIC STUDY: W/C RATIO VARIATION

The achieved load-bearing capacity of the prisms, and masonry blocks from Trial 1 are presented in **Table 6-6**. The vibrated mixtures developed a denser structure due to reduced free water in the mix, which compromises the bond fibre matrix [208-210]. As the vibration ends up expelling the voids from the sample, the matrix is better compacted and consequently, presents a higher density [211]. Vibrating the prisms relates to an increase of 2-21% of the density compared to the non-vibrated ones. It is noticeable that the higher the water-cement (W/C) ratio, the less the vibration action has an impact on the final density.

A similar observation is done for the achieved compressive strength, where the practice of not vibrating the prisms reduced the strength by 6-60%. If these results are compared to literature, it becomes evident that due to the lower water/binder ratio a higher compressive strength could be achieved. In [45, 46] e.g. a W/B ratio between 1.16 and 1.59 led to densities between 291-500 kg/m^3 and compressive strengths from 0.18-0.85 MPa. The highest compressive strength was achieved by Arnaud et al. [45] with a W/B of 1.30 and a density of 500 kg/m^3. However, in this trial, similar to the study performed by Pereira Dias

and Waldmann [174], the prisms with a W/C ratio of 0.8 (Mix 3, W/B = 0.52) and 0.9 (Mix 4, W/B = 0.58) reached a higher compressive strength than Mix 2 (W/C = 0.7 and W/B = 0.45).

The shape of samples	Mixture	Density [kg/m³]			Load-bearing capacity [MPa]		
		vibrated	Not vibrated	Rel. difference [%]	vibrated	Not vibrated	Rel. difference [%]
Prisms	Mix 2	884.1	705.8	- 20.2	3.30	1.32	- 60.1
	Mix 3	1025.5	1008.4	- 1.7	4.64	2.59	- 44.2
	Mix 4	1008.4	949.0	- 5.9	3.44	3.23	- 6.0
Masonry blocks	Mix 2	1063.5	934.1	- 12.2	1.46	0.63	- 57.3
	Mix 3	914.6	1096.8	+ 19.9	1.15	0.99	- 13.9
	Mix 4	1096.8	1144.2	+ 4.3	1.60	1.79	+ 11.9

Table 6-6: Results for Trial 1 of the density, compressive strength and the relative difference between the vibrated and the non-vibrated mixture

The prisms with a higher W/C-ratio (Mix 4) are less homogeneous in their structure, forming a hardened material at their base due to the high water amount. The latter induces a division of the specimen. Due to the seeping of water and cement, the lower part is denser. It becomes more resistant and rigid than the upper part, where a more considerable amount of Miscanthus is visible. At the time of compaction, the latter is more deformable and fragile due to a grouping of grains.

Fig. 6-12: Mix 2 vibrated (left) and not vibrated (right)

The stress-strain distribution achieved by the prisms from Trial 1 are shown in **Fig. 6-13** (left). Each test is averaged from 3 specimens with a standard deviation varying from 0.08-1.27 MPa (**Fig. 6-13** right). The behaviour of the prisms from Mix 2 (**Fig. 6-12)** can be defined as ductile elastoplastic, as large deformations are developed before maximum strength is reached (**Fig. 6-13** (left)). This behaviour is not

the case for Mix 4 and the vibrated Mix 3, which comes to its full capacity more quickly by the less ductile material formed at the base of the prism.

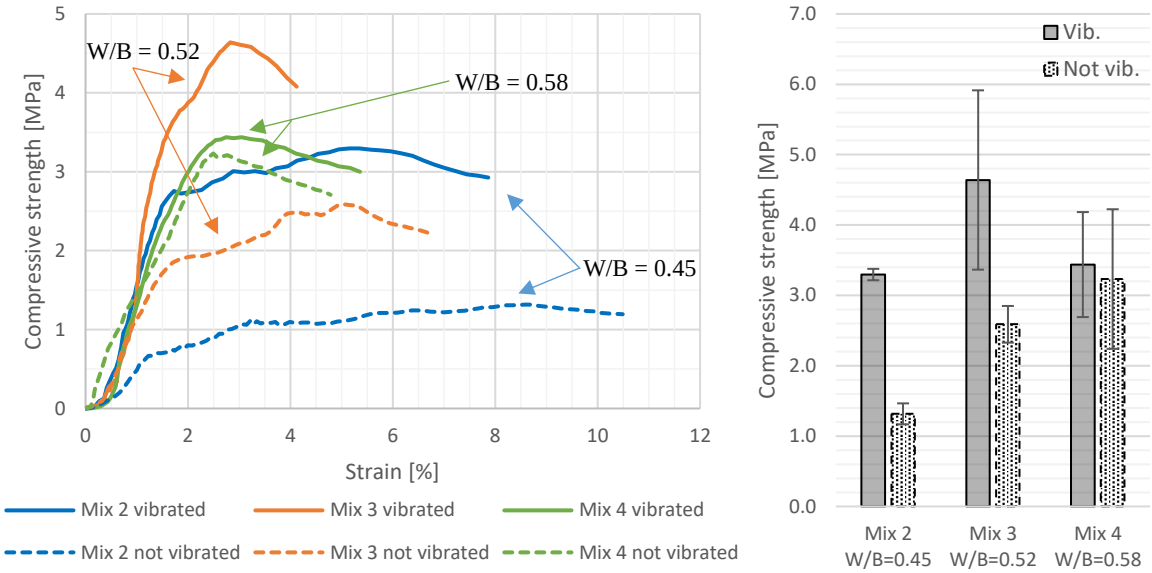

Fig. 6-13: (Left) Stress-strain curves of the prims at 14 days from Trial 1 and (right) achieved compressive strength in [MPa] and standard deviation of 3 specimens per test

The Miscanthus-to-binder ratio tends to exhibit a higher degree of ductility, as reported in literature [50, 85, 212], where fibres are characterised by a high degree of porosity, resulting in a high deformation capacity. As can be seen in **Fig. 6-13**, the water to binder ratio has a strong influence on the deformation capacity and prism resistance, which is clearly visible on the not vibrated mixtures. As the water-to-binder ratio increases, the deformability rate decreases. This statement can be well observed for the mixtures where the vibration during the filling procedure was omitted.

The masonry blocks (**Fig. 6-14**) based on the same mixture composition as the prisms delivered a different behaviour, which indicates a shape dependency of each mixture for the load-bearing capacity, as claimed by Pereira Dias and Waldmann [174] and Pavía [213]. The ultimate load showed to be lower for all the masonry blocks compared to the prisms, even if in most cases the density of the block was higher than the one of the prisms. As for the prisms, the impact of a vibration during casting on the load-bearing capacity was reduced with an increase of the W/C ratio (**Table 6-6**). Except for the masonry blocks based on the mixture with a W/C ratio of 0.9 (Mix 4), which achieved a load-bearing capacity of 11.9 % higher by omitting the vibration.

Fig. 6-14: Vibrated and non-vibrated masonry blocks based on Mix 2

6.4.1.2 PARAMETRIC STUDY: ANALYSIS OF THE MIXING PROCEDURE

Next, the impact of the mixing procedure is analysed (Trial 2). The achieved load-bearing capacity and density by the prisms are presented in **Table 6-7**. It is noticeable that the prisms based on the mixing procedure C achieved the lowest density. In addition, these same prisms showed to have the highest reduction in density (13.6 %) due to an absence of vibration. This same procedure also led to the smallest compressive strength in both categories, vibrated 3.17 MPa and not vibrated 1.54 MPa.

The prisms based on the mixing procedure A achieved the highest density (1118.2 kg/m^3) and reached a compressive strength of 4.32 MPa. These results were higher than the ones from Trial 1 (884 kg/m^3 and 3.40 MPa), despite using the same components and conditions. The occurrence is due to a difference during the manual filling procedure of the mould, where more material had to be squeezed to fill the mould up to the top, which resulted in a higher density.

The vibrated prisms based on the mixing procedure B achieved the highest load-bearing capacity (5.06 MPa). This method also reached the lowest relative difference of the density (5.3 %) between the vibrated and the non-vibrated mixture. The main reason for this procedure being the most promising was the fact that cement and lime were first mixed with the full amount of water to generate a liquid paste and the Miscanthus was poured after 3.5min of blending. This technique provides to the binders the possibility to use the water needed for their chemical reactions before the Miscanthus fibres start to absorb the water. After blending the binders with water, Miscanthus is poured and is enveloped with the liquid paste. Then, it only starts to absorb the excess of water of this paste due to its porous structure and high absorption capability. For this reason, the Miscanthus fibres, which only had access to the remaining water and which was not used by the binder, made the samples develop a better mechanical behaviour.

Prisms	Density [kg/m³]			Load-bearing capacity [MPa]		
Mix Procedure	**vibrated**	**Not vibrated**	**Rel. difference [%]**	**vibrated**	**Not vibrated**	**Rel. difference [%]**
A	1118.2	998.4	- 10.7	4.32	3.11	- 28.0
B	1089.2	1031.5	- 5.3	5.06	3.65	- 27.8
C	973.0	841.0	- 13.6	3.17	1.54	- 51.5

Table 6-7: Results for Trial 2 of the density, compressive strength and the relative difference between the vibrated and the non-vibrated mixture

6.4.1.3 Parametric study: combination of mixing procedure and W/C ratio

Trial 3 consisted of using the mixing procedure, which previously gave the highest compressive strength on Mix 2 and compare it to Mix 1, which has a lower water-cement ratio. The density and the compressive strength of Mix 1 (**Table 6-8**) showed to be lower than Mix 2 independent from the shape of the analysed specimen. It has been possible to verify for prisms and blocks that if the volume of water in the mixture decreases the fibres lose cohesion to the binder. In addition, the reduction of the W/C ratio from 0.7 to 0.62 causes a reduction of the density of the prisms by 15 % and their compressive strength is reduced by 49-51 %.

A similar behaviour could be observed on the masonry blocks, a reduction of the W/C ratio induced a decrease of the density by 7-13 %. The compressive resistance was diminished by 46 % for the vibrated specimens and by 73 % for the non-vibrated ones. Furthermore, the impact of the vibration on Mix 1 was 1.7 times higher on the masonry blocks than on the prisms. Therefore, at this stage, two aspects could be deduced.

The first observation, a decrease of the W/C ratio induces a lack of water in the mixture and consequently achieves a lower resistance and the second point is regarding the vibration. Independent from the mixing procedures, analysing the impact of the vibration on the mixes from Trial 1 and Trial 3 it can be stated that if the W/C ratio decreases, the fact of vibrating during moulding affects more the compressive strength of the Miscanthus concrete than with an increasing W/C ratio. A reason for this is that an increased W/C ratio, as Mix 4 in Trial 1, in combination with a vibration can cause a segregation of Miscanthus from the binders.

The shape of samples	Mix.	Density [kg/m^3]			Load-bearing capacity [MPa]		
		vibrated	Not vibrated	Rel. difference [%]	vibrated	Not vibrated	Rel. difference [%]
Prisms	Mix 1	880.6	770.0	- 12.6	1.83	1.14	- 37.5
	Mix 2	1040.7	902.4	- 13.3	3.78	2.24	- 40.8
Masonry Blocks	Mix 1	1078.3	875.1	- 18.9	1.84	0.64	- 65.1
	Mix 2	1154.3	1006.0	- 12.9	3.44	2.35	- 31.7

Table 6-8: Results for Trial 3 of the density, compressive strength and the relative difference between the vibrated and the non-vibrated mixture

6.4.1.4 Parametric study: curing time of 28d and stepwise analysis

The analysis of the specimens cured for 28-days is essential to verify the development of the material properties, helping to characterise the mechanical behaviour of Miscanthus-based blocks. Therefore, Mix 2 with the mixing procedure B was used, as it showed the most favourable results considering the compressive strength (**Table 6-6**, **Table 6-7** and **Table 6-8**). In this section, the prisms cured during 28 days are analysed, followed by a similar analysis on the masonry blocks and finalising with a discussion about the achieved load-bearing capacity by loading and unloading a masonry block cured for 14 days.

6.4.1.4.1 Analysis of the specimens cured for 28 days

The prisms showed a difference in the compressive strength of 3 % between a curing time of 14 and 28d (**Table 6-9**). This modest difference can be explained by the low density of the prisms at 28d (922.1 kg/m^3), which is a reduction of 11.4 % related to the density at 14d (1040.1 kg/m^3). The reduction of the density can be explained by the higher curing time, which implies a higher amount of evaporated water in the matrix.

The masonry blocks reached after a curing time of 28d a compressive strength of 5.42 MPa (**Table 6-9**), which is an increase of 57.5 % compared to a curing time of 14d (3.44 MPa from Trial 3). The density decreased by 6.3 % over a time of 14d. This huge difference in the compressive strength is due to the water evaporation in the specimen that takes longer for a masonry block (40x20x10 cm) than for a prism (16x4x4 cm). Due to the high volume of the masonry block, it increases the time to achieve its final compressive strength. Hence, it can be concluded that a specimen with a high volume based on

Miscanthus concrete is more sensitive to the curing time than one with a lower volume. So, the mechanical behaviour is affected by the shape and size of the samples [213].

The shape of samples	Curing time [d]	Density [kg/m^3]	Load-bearing capacity [MPa]
Prisms	14	1040.7	3.63
	28	922.1	3.73
Masonry Blocks	14	1154.0	3.44
	28	1082.1	5.42
Masonry Blocks*	14	1191.6	4.75

Table 6-9: Results for Trial 4 of the density and the compressive strength for 14 and 28 days (*stepwise load)

6.4.1.4.2 IMPACT OF A GRADUAL LOADING

The second part of Trial 4 consisted of analysing the behaviour of masonry blocks that were gradual loaded. This procedure was performed by loading and unloading the masonry blocks in steps of 40 kN. On average, the masonry blocks with a density of 1191.6 kg/m^3 achieved a compressive strength of 4.75 MPa after a curing time of 14d (**Table 6-9**). The masonry blocks, which were subjected to a gradual loading achieved in average a 38 % higher compressive strength compared to masonry blocks that were continuous loaded (3.44 MPa). This can be explained by the known effect, represented by the coefficient α_{cc} from normal concrete, which reduces the characteristic strength by 0-20 % [204]. This reduction factor is, among other reasons, applied due to effects resulting from the duration the load is applied. Since a continuous load implies a shorter time test, the load bearing capacity of a short time test is always reduced compared to a long time test due to creeping effects. The coefficient α_{cc} is between 0.8-1.0 for a normal concrete [204]. The behaviour of a concrete based on Miscanthus aggregates is different in several aspects and therefore, a lower reduction factor of $\alpha_{cc} = 0.62$ has been measured. This value is lower than the minimum value imposed by the standard because the masonry blocks had only a curing time of 14 d.

6.4.1.5 ANALYSIS ON WALLETS

The experimental wallets (**Fig. 6-15**) created with the Miscanthus-based masonry blocks served to analyse the mechanical behaviour of the material by applying a compressive strength until reaching the load-bearing capacity of the system (Trial 5). Even after the structure reached its ultimate load (**Table 6-10**), the masonry showed almost no visual cracks, loss of stability or inclination (**Fig. 6-16, a**). Furthermore, the structure remained stable and functional at load-bearing capacity.

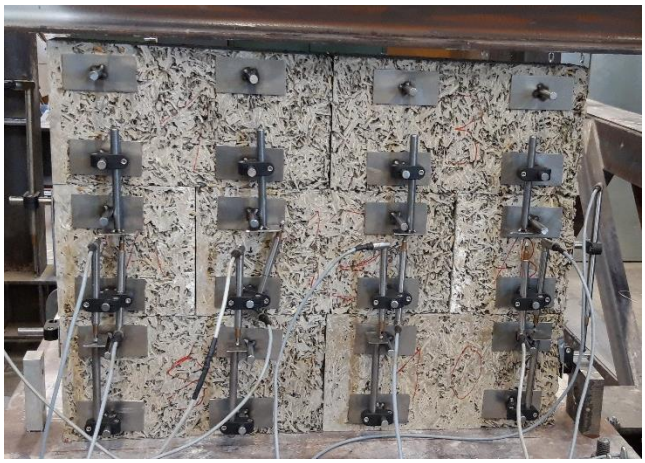

Fig. 6-15: Test setup in the front part of Wallet 1

The shape of samples	Density	Load-bearing capacity (LBC)	Strain at LBC	Plastic strain
	[kg/m^3]	[MPa]	[%]	[%]
Wallet 1	1121.6	4.84	1.21	0.50
Wallet 2	1146.1	5.65	1.19	0.49
Wallet 3	1125.6	5.56	1.16	0.46

Table 6-10: Results for Trial 5 of the density, the load-bearing capacity, the deformation at and the plastic deformation after reaching the load-bearing capacity

Wallet 1 generated at its load-bearing capacity of 4.84 MPa a strain of 1.21 % (**Fig. 6-17**) and after unloading the wallet, a plastic strain of 0.50 % could be measured. Only three places with cracks could visually be investigated on the wallet after reaching its load-bearing capacity and being unloaded (**Fig. 6-16, a**)). The distribution of these cracks are a consequence of the impact of imperfections such as the roughness of the block surface and height differences between the masonry blocks. The observed cracks had two major causes. Next, the masonry was fully reloaded (post-load) to analyse a compromised failure. At a strain of 4.78 % (**Fig. 6-17**), the masonry lost its stability and the crack pattern, as well as the damage, was visible (**Fig. 6-16, b**). Nevertheless, due to the fibrous Miscanthus concrete, the wallet behaved ductile during the whole loading and post-loading process.

Fig. 6-16: a) Cracks in Wallet 1 at maximum load capacity; b) Cracks in Wallet 1 after application of the load beyond its maximum capacity (post-load)

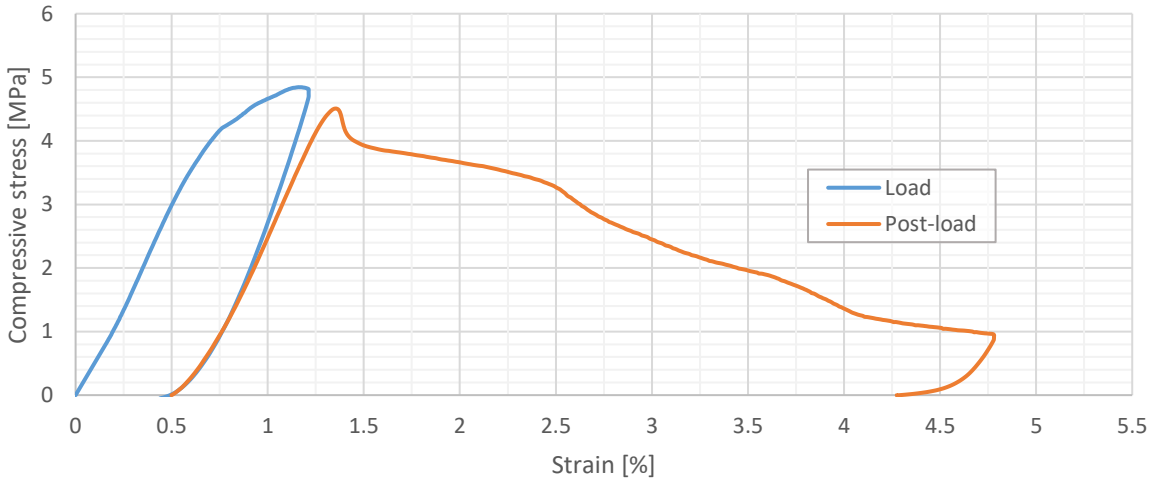

Fig. 6-17: Stress-strain curve in the load phase and post-load phase of Wallet 1

The stress-strain distribution presented in **Fig. 6-17** shows that no sudden failure occurs on the wallet based on Miscanthus concrete even after reaching its load-bearing capacity and overloading (post-load) the system. The masonry showed a very ductile behaviour and proved to be a safe material in overload collapse situations, with a strain at the load-bearing capacity of 1.16 % to 1.21 %, which is at least 3.6 times higher than a dry-stacked masonry using conventional masonry blocks without any additional contact layer [114].

A hysteresis load was applied on wallets 2 and 3 until they reached their load-bearing capacity. The pressure was with every loading step increased by 1 MPa (±80 kN). **Fig. 6-18** shows the hysteris loading that occurred on wallet 2 and a detailed view of the stress-strain distribution of wallet 2 until reaching its load-bearing capacity. A clear elastic behaviour is visible after unloading of each load-step showing the ductile behaviour of this material. However, when the pressure is removed, the masonry keeps a

plastic deformation, which is increased at each loading step (**Table 6-11**). Determined by the phase difference in a given cycle, the applied force tension curve and the displacement curve scheme a hysteresis loop [214].

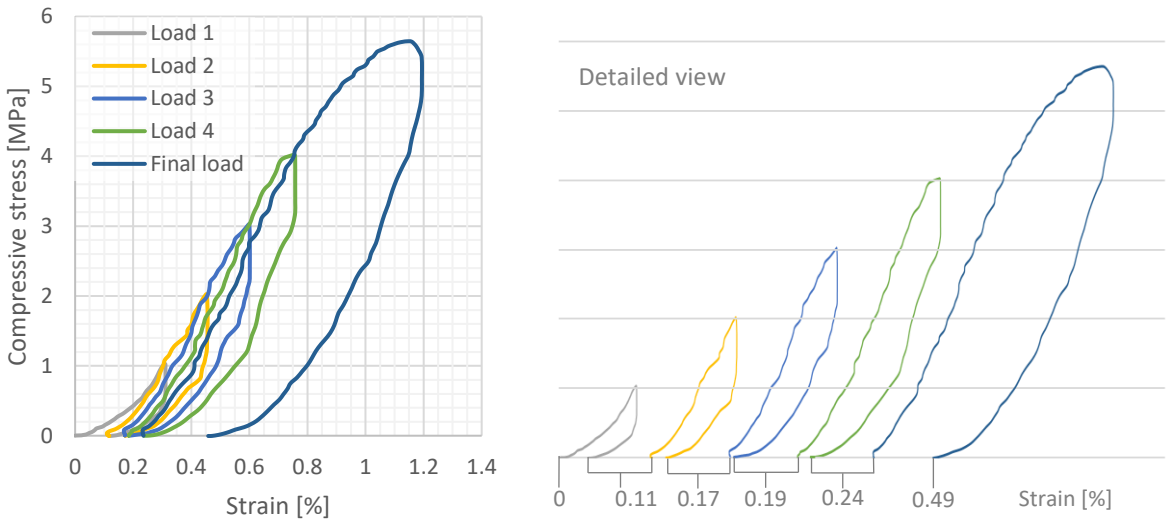

Fig. 6-18: Stress-strain curve during the load phase for Wallet 2 as well as a detailed view of the 5 loading steps

According to the results presented in **Table 6-10**, the wallets submitted to a hysteris loading, achieved a 15-17 % higher load-bearing capacity than Wallet 1, which was continuously loaded. The reason for this occurrence is similar to the one presented on the test of a single masonry block (section 6.4.1.4.2), where an α_{cc} value of 0.62 was discussed. In this case, the α_{cc} value of 0.83-0.85 is higher than previously, because the masonry blocks had a longer curing time (90 days). Furthermore, the value for this wall is in the range presented in the standard (0.8-1.0), which validates the presented relation.

Plastic strain (at the end of each load step) [%]	**Load 1 (1 MPa)**	**Load 2 (2 MPa)**	**Load 3 (3 MPa)**	**Load 4 (4 MPa)**	**Final Load (at LBC)**
Wallet 2	0.11	0.17	0.19	0.24	0.49
Wallet 3	0.06	0.09	0.17	0.24	0.46

Table 6-11: Plastic strain [%] after each load-step

The behaviour of all three tests followed the same initial pattern. Even when the sample reached their load-bearing capacity, almost no cracks were visible on the masonry. The fracture lines on the wallet could only be visualised during post-failure loading where a very ductile behaviour of the wallet can be observed, which is advantageous concerning safety aspects. This ductile behaviour is not the case for a

dry-stacked wall using conventional masonry blocks based on normal concrete, which are usually less flexible and more rigid [114].

Next, the deformation of each row at ultimate load (D_R1, D_R2 and D_R3), which includes a small part of the deformation of the adjacent blocks, as well as the deformation of the horizontal bed joints (D_J1 and D_J2) are analysed to determine in which row the highest deformation of the masonry blocks occurs (**Fig. 6-19**). Except for Wallet 1, the deformation was the highest on the top row (D_R3) and the lowest on the bottom row (D_R1). In a dry-stacked masonry wall the height differences have a high impact on the behaviour and the load-bearing capacity of the wall [107]. The reason for the deformation of D_R1 being the highest for Wallet 1 is due to the height differences in one masonry block of the bottom row.

The height of the masonry blocks casted with the formwork from **Fig. 6-4** (right) followed a normal Gaussian distribution (**Fig. 6-23**) with a standard deviation of μ=0.285 mm. On Wallet 2 and 3, which were loaded differently from Wallet 1, the load-bearing behaviour was less impacted by the roughness and the height differences of the masonry blocks.

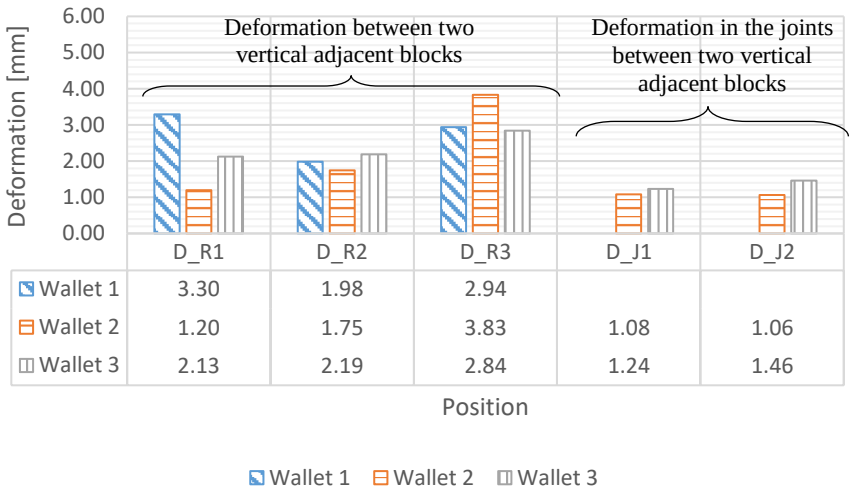

Fig. 6-19: Deformation [mm] of the masonry blocks in each row measured on the three wallets

6.4.2 Analysis of the roughness

During the compressive strength test, the contact area of the top and the bottom surface of the masonry blocks was recorded using FUJIFILM strips. In the following sections, the contact area achieved by each trial will be analysed.

6.4.2.1 *Parametric study: W/C ratio variation*

The FUJIFILM layers were withdrawn from the upper and the lower surface of the masonry blocks after reaching their load-bearing capacity. The averaged results, based on the top and the bottom surface, showed clearly that the mixtures with a higher W/C ratio (Mix 4) induced a higher contact surface (**Fig. 6-20**). This increment is larger if the vibration of the mixture is omitted during casting. Mix 2 showed to be more dependent on the vibration to reach a higher contact area than the other varieties.

Independent from the analysed specimen, the top surface showed to be more even than the bottom surface. This last fact is due to the filling procedure (middle **Fig. 6-4**).

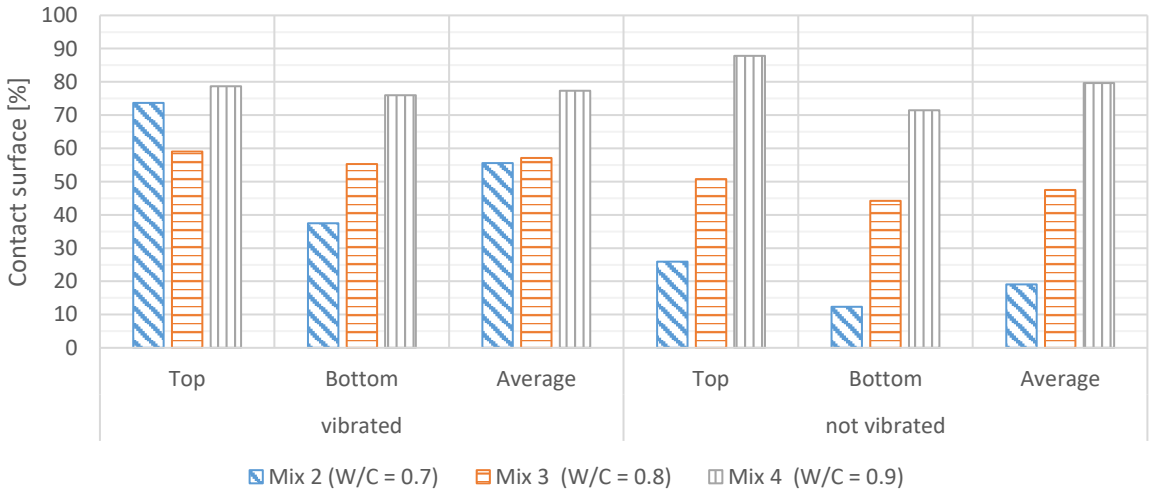

Fig. 6-20: Contact surface of the top and bottom at ultimate load of the masonry blocks from Trial 1 and their respective average

6.4.2.2 *Parametric study: combination of mixing procedure and W/C ratio*

The masonry blocks from Trial 3 were established using the second filling technique and so the loaded surfaces are casted against the framework (right **Fig. 6-4**). Due to this alteration, the contact area of Mix 2 from Trial 3 (**Table 6-12**) is higher than the contact area from the mixture Ref in Trial 1 (**Fig. 6-20**). Furthermore, a vibration of the specimens from Trial 3 showed to be beneficial considering the performed contact surface at ultimate load. Considering the W/C ratio, a reduction of the W/C-ratio to 0.62 (Mix 1) reduces the contact surface at ultimate load by 20.8 % for the vibrated specimens and by 43.8 % for the non-vibrated ones (**Table 6-12**). These results were coherent to the analysis on the compressive strength in section 6.4.1.3.

	vibrated			Not vibrated		
	Top	**Bottom**	**Avg.**	**Top**	**Bottom**	**Avg.**
Mix 1	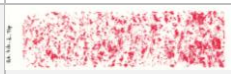 54.1	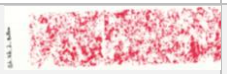 60.2	57.2	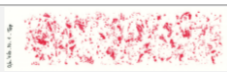 32.4	 36.1	34.2
Mix 2	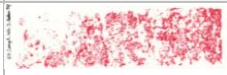 67.6	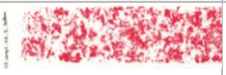 76.8	72.2	 59.6	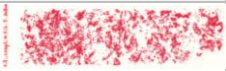 62.2	60.9

Table 6-12: FUJIFILM strips showing the contact surface of one out of three masonry blocks for each vibrated and not vibrated mixture from Trial 3 as well as their contact surface in [%] and average in [%]

6.4.2.3 Parametric study: curing time of 28 days and stepwise analysis

As previously stated and generally known, a curing time of 28d induces a higher compressive strength than a curing time of 14d for the masonry blocks. The same observation can be done for the contact surfaces, which increased in average for the three tested masonry blocks (MB 1_28-MB 3_28) from 72.2 % to 83.2 % (**Fig. 6-21**). These specimens showed identical contact surfaces on top and on bottom of the masonry blocks, which implies that the filling technique is validated for both sides.

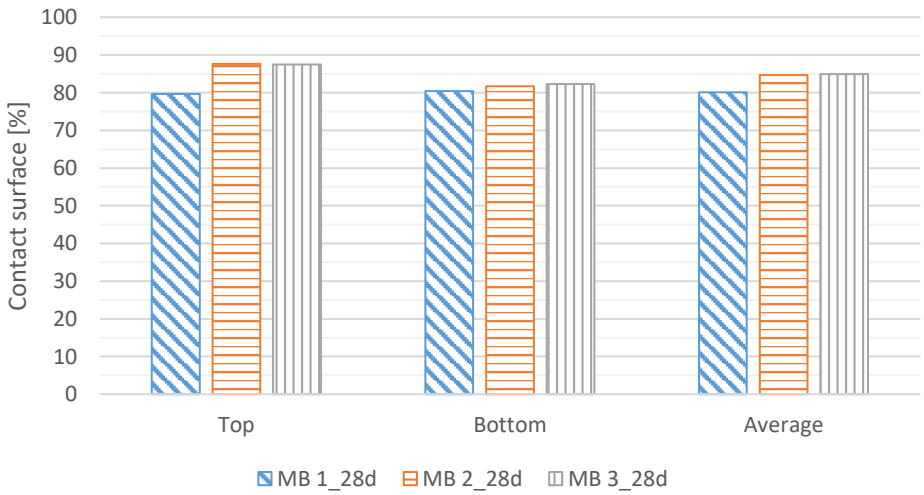

Fig. 6-21: Contact surface and average of the masonry blocks after a curing time of 28d (Trial 4)

By applying a gradual load on top of the three masonry blocks (MB1_14d_g – MB3_14d_g), it is possible to study the relation between the contact area and the compressive strength (**Fig. 6-22**). By loading and unloading the contact area was in average 80.6 % for the three masonry blocks and thus, 1.3 times higher than the contact surface achieved with a continuous loading (Trial 3 **Table 6-12**). The reason for a gradual load implying a higher contact surface at ultimate load is due to the movement of the fibres in the matrix, which indicates also a compacter matrix.

The relationship between the stress and the contact area that the block presents with the gradual load could be demonstrated through an exponential equation (**Fig. 6-22**) with a coefficient of determination (R^2) of 0.99. According to the analysis, the higher the applied compressive strength, the higher the percentage of contact between the surfaces. By inserting the load-bearing capacity achieved in Trial 3 (3.44 MPa in **Table 6-8**) into the exponential equation from **Fig. 6-22**, a theoretical contact of 67.9 % can be calculated, which is 6 % lower than the measured value (72.2 % from **Table 6-12**). Since a gradual loading implies a higher load-bearing capacity of the masonry block, the difference of 6 % originates from the duration of the loading test.

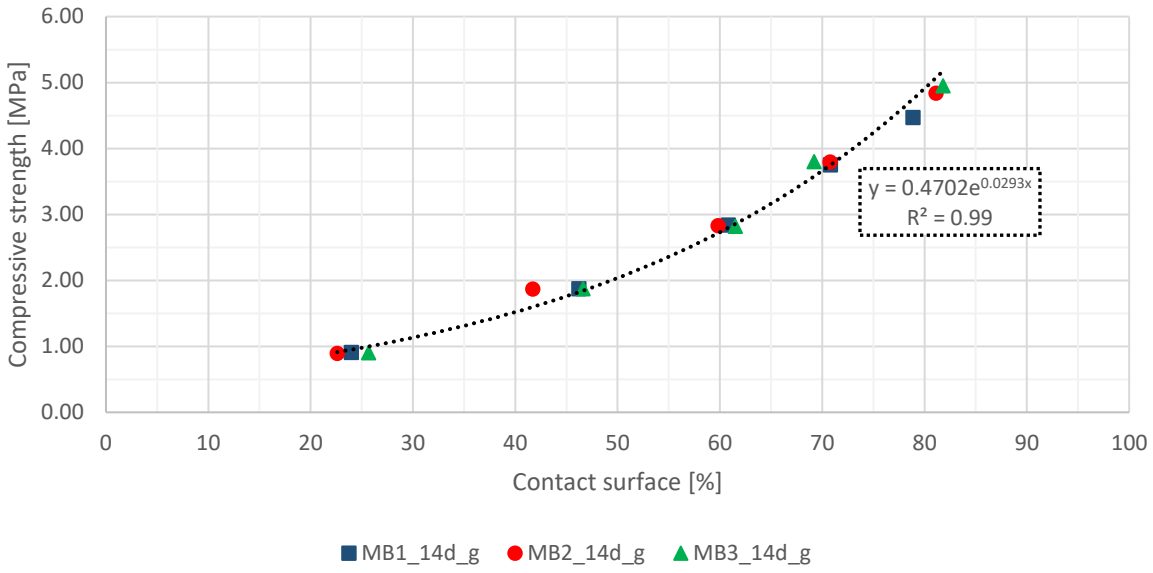

Fig. 6-22: Compressive strength in function of the contact surface from the three masonry blocks based on Mix 2 (Trial 4) at a curing time of 14d

6.4.2.4 ANALYSIS ON WALLETS

The contact surface of both Wallet 2 and 3 was similar, and for both joints (J1 and J2) between 55-59 % (**Table 6-13**). The vertical joints between each neighbouring masonry block are visible because no mortar was used between the blocks, so the roughness and height imperfections could not be rectified, and this is visible in the contact strips. Furthermore, on both wallets, the pressure was distributed entirely over the whole area without any specific point concentration. It is also visible in **Table 6-13** that the highest peak stresses (black dots at 3.0 MPa) were mostly in the middle part of the contact area.

Position	Wallet 2 Contact surface [%]	Wallet 3 Contact surface [%]
J1	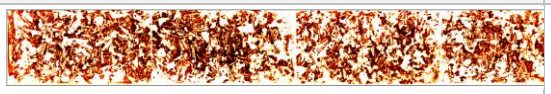 55.8	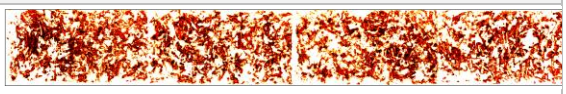 55.7
J2	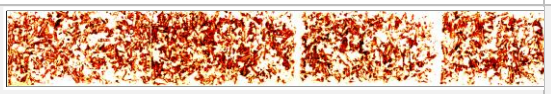 58.5	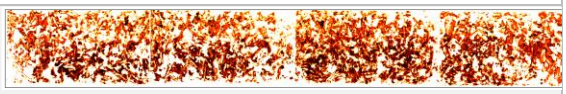 58.6

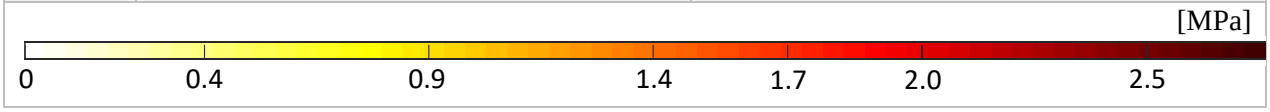

Table 6-13: Analysed strips showing the contact surface [%] for both horizontal joints of Wallet 2 and 3 at their respective load-bearing capacity and the point pressure in a scale from 0 - 3.0 MPa

In conclusion, the roughness of all models was constant for all masonry blocks created using the second moulding procedure and the height differences had a low standard deviation of μ=0.285 mm (**Fig. 6-23**). Furthermore, the low Young's Modulus from the mixtures (0.5 – 4.0 GPa) [174] reduces the impact of the roughness and the height differences on the contact surface, accordingly also on the load-bearing capacity. So, the low Young's Modulus is the reason for a coherent and constant contact between the masonry blocks of the wallets.

6.4.3 HEIGHT DIFFERENCES OF THE MASONRY BLOCKS

The height of the masonry blocks were measured and categorised according to the mould in which they were produced. The mould presented in **Fig. 6-4** (middle) was filled from the upper side of the block, which is also the surface on which the loading is later applied. By filling the mould from the side (**Fig. 6-4** right), the height of the masonry block is limited by the surface of the mould and is therefore more even. The masonry blocks based filled from the upper side generated a mean height of 202.78 mm and a standard deviation of 1.581 mm. Meanwhile the masonry blocks established with a filling from the side surface achieved a mean height of 201.52 mm and a standard deviation of 0.285 mm. According to this data a normal Gaussian distribution could be settled and both models could be compared by converting both mean heights to μ = 0 mm (**Fig. 6-23**). Hence, it can be concluded that filling the masonry block from the side (right **Fig. 6-4**) implies a reduction of the standard deviation of the heights of the masonry block by 82 %.

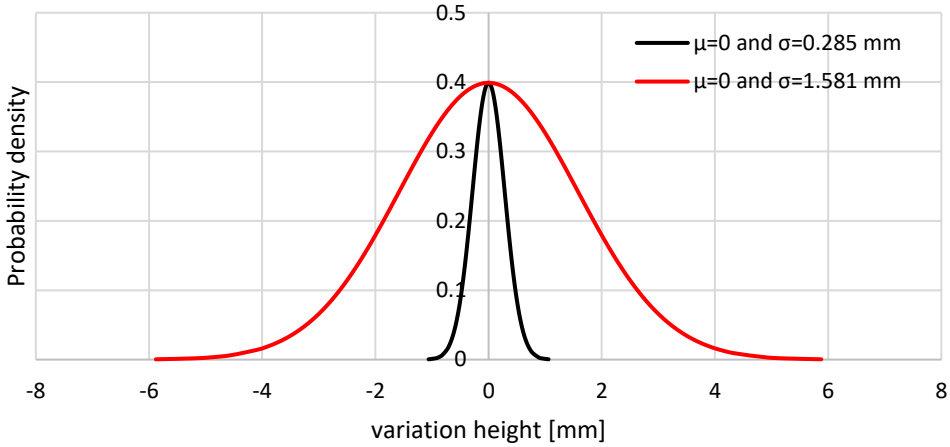

Fig. 6-23: Gaussian normal distribution of the height of the masonry blocks

6.4.4 NUMERICAL ANALYSIS

In the following section, the developed numerical model of one masonry block is analysed using the predetermined properties and calibrated with regards to the experimental results of a single masonry block. Next, a parametric study is performed as a sensitivity analysis on one masonry block by varying the material properties. The imperfections of the masonry blocks are analysed in two steps. The roughness of the surface of the masonry block is performed on a single masonry block. The impact of the height differences are analysed on a wall by investigating a worst case and a real case scenario. The real case scenario is based on a large number of calculations, for which the load percolation system was varied. Furthermore, the dimensions of the wall were varied to analyse their impact on the load-bearing capacity.

6.4.4.1 SINGLE MASONRY BLOCK

Calibration of the numerical model

The numerical model of the masonry block was established using the previously (section 6.3.4.1) properties (**6-14**) and compared to the experimental results of the masonry blocks cured for 28 d (Trial 4 in section 6.4.1.4.1), which achieved a compressive strength of 5.42 MPa (**Table 6-9**). The numerical model achieved a load-bearing capacity of 5.70 MPa (**Fig. 6-24**), which was 5 % higher than the experimental test. Furthermore, the stress-strain distribution is similar to the course from the experimental masonry block cured for 28 days (**Fig. 6-14)**. These results led to the conclusion that the numerical model is validated using the calibrated properties presented in **Table 6-14**.

Variation	Material strength [MPa]		Young's Modulus [GPa]		Std. dev. roughness [mm]	RH [mm]	Volume ratio of SR [%]
	Core	Rough part	Core	Rough part			
Calibrated properties	11	9	2	0.8	0.3	10	30

Abbreviations:
Std. dev. : Standard deviation; RH : Roughness height; SR : Smeared reinforcement

Table 6-14: Imposed and calibrated properties of the numerical model

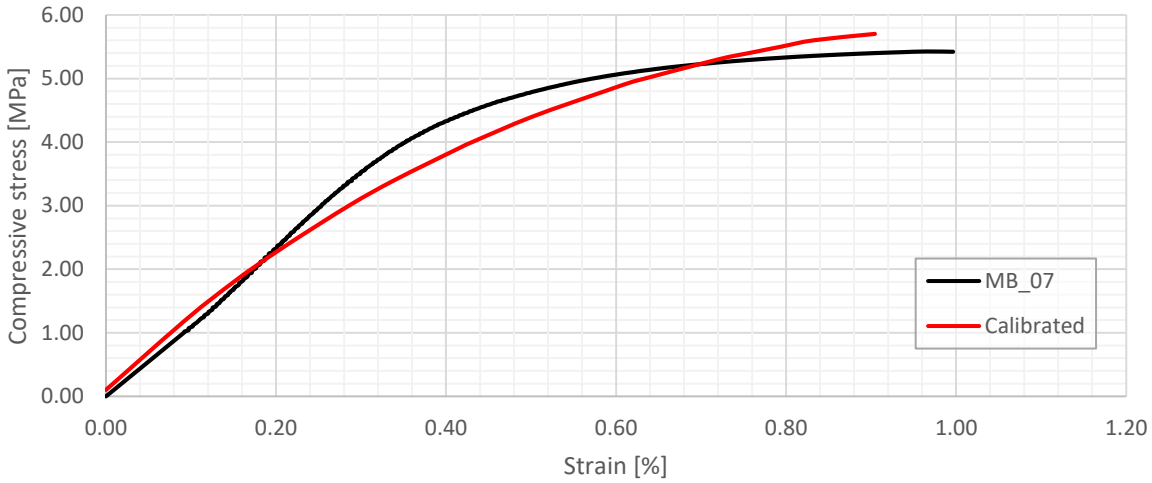

Fig. 6-24: Stress-strain distribution of the experimental masonry block compared to the designed and calibrated numerical model

Parametrical study

The parametrical study is performed as sensitivity study by varying only one property at a time to analyse essentially its impact on the load-bearing capacity. An analysis is first performed on the impact of the material properties, consisting of studying the impact of the material strength and the Young's Modulus variation on the load-bearing capacity (MS 1, MS 2, YM 2, YM 3 and MS 3 & YM 1). Then, this is completed by two studies on the impact of the roughness on the load-bearing capacity. Finally, the volume ratio of the assumed smeared reinforcement is varied (VR SR).

An increase of the material strength (10 - 17 MPa in MS 1) showed as expected to increase the load-bearing capacity (**Fig. 6-25**). Since the Young's Modulus was constant in MS 1, the stiffness of the different variations was similar for all the analysed materials. The next variation MS 2 consisted of varying the material strength of the core (10 – 12 MPa) and the rough part (8 - 10 MPa) and using apart from the material strength identical properties as used for the calibrated model. The first number after "Mat" in the legend in **Fig. 6-25** (MS 2) corresponds to the material strength of the core and the second

number to the material strength of the rough part. The material strength of the core part of the numerical block affects the load-bearing capacity by increasing it in average 11.7 % per MPa, whereas the material strength of the rough part influences the achieved strain at load-bearing capacity.

In the next variation (MS 3 & YM 1), the impact of the Young's Modulus (1.2 and 2.4 GPa) combined to different material strengths (core: 11 and 12 MPa, rough part: 10 and 11 MPa) is analysed. The low difference in the material strength had an insignificant impact on the load-bearing capacity. However, the Young's Modulus of the materials had not only an impact on the stiffness but also on the achieved load-bearing capacity. Dividing the Young's Modulus by 2 increases the load-bearing capacity by 34 %. This occurrence can be explained by the more ductile behaviour of the material the lower the number of punctual load concentrations in the roughness.

The impact of the Young's Modulus on the load-bearing capacity is analysed in variation YM 2 from 1.2-10 GPa. The higher the Young's Modulus the stiffer the model and the lower the load-bearing capacity due to a less ductile material. Next, the effect of a different Young's Modulus on the core (1.2 - 6.7 GPa) and the rough part (0.6 and 1.2 GPa) on the load-bearing capacity is analysed (YM 3). The first number of the nomenclature used in **Fig. 6-25** (YM3) designates the Young's Modulus of the core and the second the one of the rough part. It can be observed that independent from the core, reducing the Young's Modulus of the rough part by 2 increases the load-bearing capacity up to 13 %. The stress-strain course of both models is similar until achieving a minimum of 71 % of the load-bearing capacity, which designates the starting point of the effect of a ductile material on the rough part.

Moreover, the imperfections due to roughness are analysed by implementing a roughness, which follows different Gaussian distributions (0.075-0.40 mm) (Std. dev. R). The lowest standard deviation (SD: 0.075 mm) of the roughness made the numerical model achieve the highest load-bearing capacity. This occurs because the higher the difference between peak and valleys, the higher the punctual stress concentration, which induces more cracks into the numerical masonry block and reduces the load-bearing capacity. Increasing the standard deviation of the roughness from 0.075 mm to 0.40 mm reduces the load-bearing capacity by 31 %. As previously stated, the material strength of the rough part affected the load-bearing capacity of the numerical model (YM 3). This impact is increased if the height of the rough part (RH) is increased (2-15 mm). A higher rough part induces a decrease of the stiffness of the model due to the low Young's Modulus of the rough part compared to the one of the core. As expected, the higher the roughness height, the higher is the impact of the rough part on the stiffness of the model.

Lastly, the impact of the volume ratio (VR SR) (0-50 %) of the smeared reinforcement on the load-bearing capacity is analysed in VR SR of **Fig. 6-25**. It can be noticed that an increase of the volume ratio implies a reduction of the stiffness of the model due to the material properties of the smeared reinforcement that represents the Miscanthus fibres. Furthermore, a volume ratio of 20 % achieved the

highest load-bearing capacity, which shows the significance of smeared reinforcement in the numerical model. However, increasing this value up to 50 % results in reducing the load-bearing capacity of the model by 36 %. In general, a reinforcement should strengthen the structure; nevertheless, a high volume of smeared reinforcement reduces the strength of the structure due to its low Young's Modulus of 5 GPa.

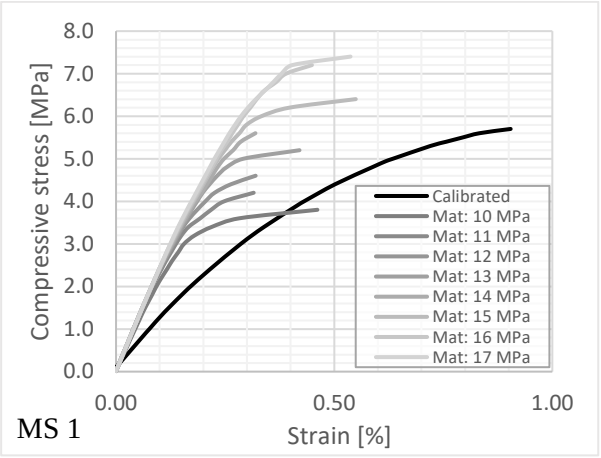

MS 1

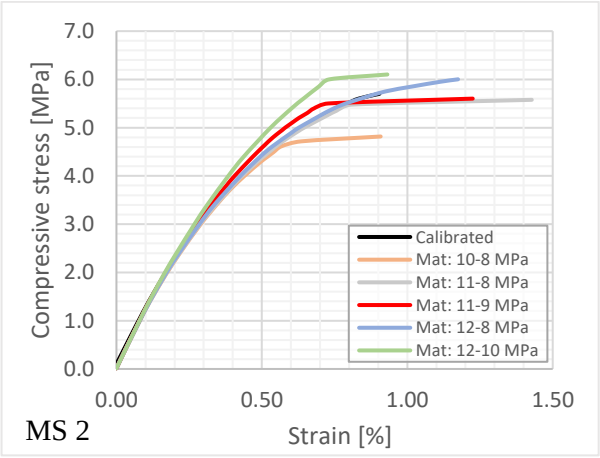

MS 2

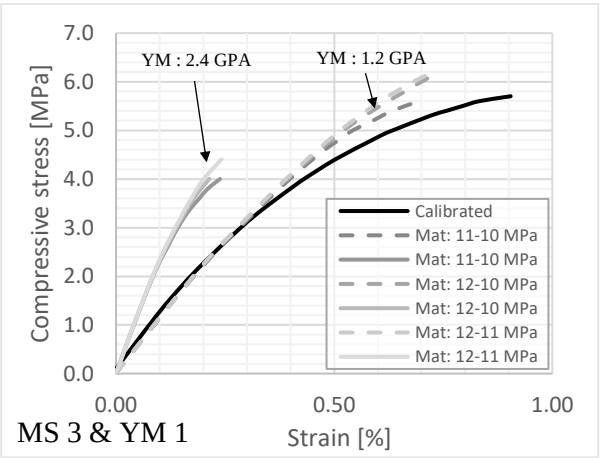

MS 3 & YM 1

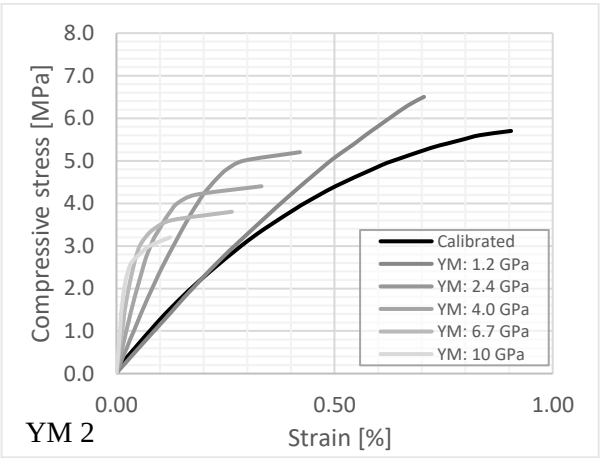

YM 2

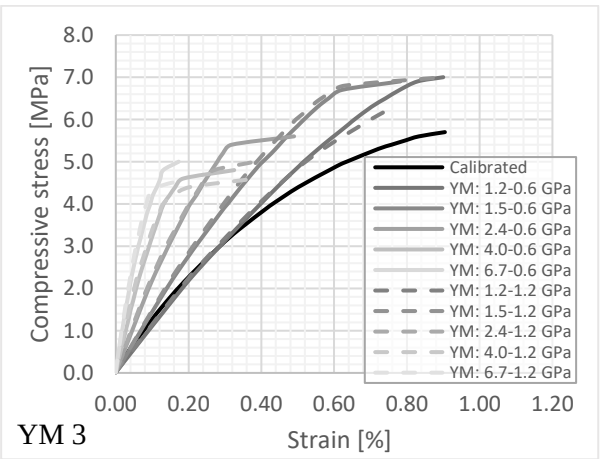

YM 3

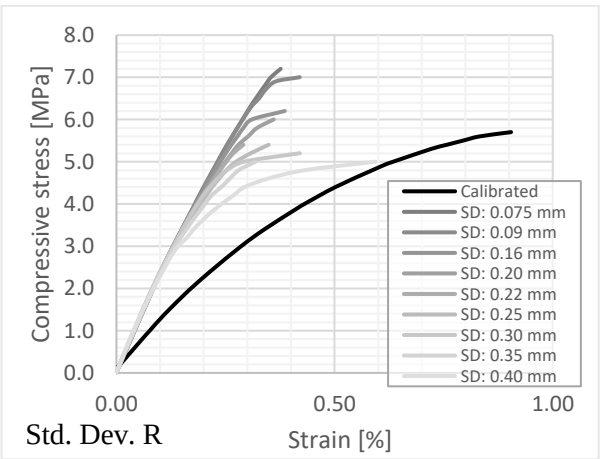

Std. Dev. R

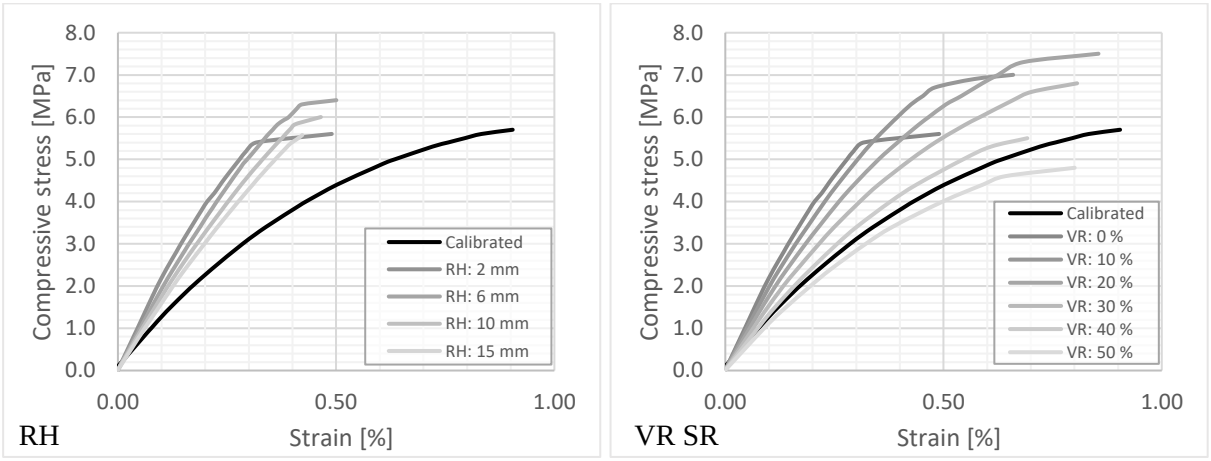

Fig. 6-25: Stress-strain distribution of each variation presented in **Table 6-4** in relation to the calibrated numerical model

6.4.4.2 WALLET

The following section is divided in two parts. First, the wallet using the calibrated material properties from the previous section is analysed by integrating height differences on the masonry blocks in order to analyse their impact on the load-bearing capacity and on the stiffness of the model. Secondly, the impact of the dimensions of the wall on the load-bearing capacity are analysed by representing the ultimate load in function of a ratio of the height to the length (H/L) of the wall.

6.4.4.2.1 ANALYSIS OF THE MATERIAL PROPERTIES AND THE IMPACT OF THE HEIGHT DIFFERENCES

The experimental results of Wallet 1 were used to validate the numerical model using the calibrated properties based on the experimental masonry block. The numerical model of the wallet achieved a similar load-bearing capacity (4.93 MPa) as the experimental test (**Fig. 6-28**). The stress-strain course of the model correlates with the experimental model. The strain difference of 20% between the two models can be related to two major reasons. The first reason is the smeared reinforcement of the numerical model, which could not represent the exact behaviour of the Miscanthus fibres in the masonry blocks of the experimental wallet. The second motive is that no height differences were implemented in the calibrated model. Therefore, an analysis of a model which included height differences on the masonry blocks of the wallet is performed: Firstly, a worst-case scenario is created to analyse the impact of the height differences on the stress-stain distribution by implementing the heights of the masonry blocks, as presented in **Table 6-5**. Due to the height differences, the load percolation was concentrated on one single or one half block per row, which reduces the load-bearing capacity and the stiffness of a dry-stacked wall as also observed by Chewe and Waldmann [107]. Secondly, a real case scenario is

created, where the height differences are applied randomly based on the normal Gaussian distribution with a standard deviation of σ = 0.285 mm, as presented in **Fig. 6-23**.

The worst-case scenario consists of 4 models presented in **Table 6-5** (BL 3-5, BL 1-3-5, BL 1-4-6 and BL 2-4-6). In the first two models (BL 3-5 and BL 1-3-5) no height differences (ΔH) were implemented on the top row (row 3) of the dry-stacked wall (**Fig. 6-26**). The difference between BL 3-5 and BL 1-3-5 is the amount of masonry blocks increased by 0.86 mm (=+3σ=3x0.285 mm). In the model BL 3-5 the height of two masonry blocks (③ and ⑤) were increased by 0.86 mm, whereas on the model BL 1-3-5 three masonry blocks (①, ③ and ⑤) were increased by 0.86 mm. The two models showed a similar stress-strain behaviour as the calibrated model until a compressive strength of 3.3 MPa (**Fig. 6-28**), which was in parallel also to the load-bearing capacity of BL 1-3-5 (**Fig. 6-26** right). The higher load-bearing capacity of BL 3-5 (4.4 MPa) is due to the low difference in height, which implies a load distribution in two phases (**Fig. 6-26** left). The first phase corresponds to the beginning of load-application on the wall, where the load distribution is concentrated on edge blocks (③ and ⑤). The second phase starts soon after the load application due to the low height differences between the masonry blocks (0.86 mm), which implies that the whole wall is loaded. The load of the wall BL 1-3-5 is due to the low height differences also divided in two phases (**Fig. 6-26** right). However, the load percolation creates load concentration on masonry block 1 and induces therefore a 25 % lower load-bearing capacity compared to BL 3-5.

The mean height of the masonry blocks of the models BL 1-4-6 and BL 2-4-6 from the worst-case scenario are all varied by +/- 0.86 mm, which corresponds to +/-3 times the standard deviation σ of 0.285 mm (**Fig. 6-27**). The difference between the models BL 1-4-6 and BL 2-4-6 are the predicted load percolation due to the position of the imposed height differences. The masonry blocks ①, ④ and ⑥ of the model BL 1-4-6 are increased by 0.86 mm (ΔH=+3σ) and the remaining blocks of this wall (②, ③, ⑤ and ⑦) are reduced by 0.86 mm (ΔH=-3σ). These changes represented a difference between two adjacent blocks of 1.72 mm (2*0.86 mm). Therefore, the load-percolation of this model (BL 1-4-6) was concentrated on the higher masonry blocks as shown in red in **Fig. 6-27** (left). This occurrence implied that the load is almost not carried by the right side of the wall and therefore, the load-bearing capacity was 32% lower than the load-bearing capacity of the calibrated model.

The model BL 2-4-6 on which the masonry blocks ②, ④ and ⑥ were increased by 0.86 mm and the remaining ones reduced by 0.86 mm (**Fig. 6-27** right) achieved a load-bearing capacity of 3,93 MPa, which is an increase of 18 % compared to BL 1-4-6. This higher capacity is due to the deformation of the masonry blocks, which avoids a single diagonal load percolation but distributes the load also on the masonry block ① of the lower row (row 1).

Due to the ductility of the material these models achieved a load-bearing capacity, only reduced by 20-32 % compared to the calibrated model with no height differences. These two models (BL 1-4-6 and BL 2-4-6) had also a lower stiffness than the two models (BL 3-5 and BL 1-3-5) on which no height differences were implemented on the upper row. Therefore, it can be stated that the models BL 1-4-6 and BL 2-4-6 are the worst-case scenario. These results are very promising compared to a dry-stacked wall using conventional masonry blocks, where an average reduction of the load-bearing capacity of 50 % could be measured on experimental tests performed by Chewe and Waldmann [114].

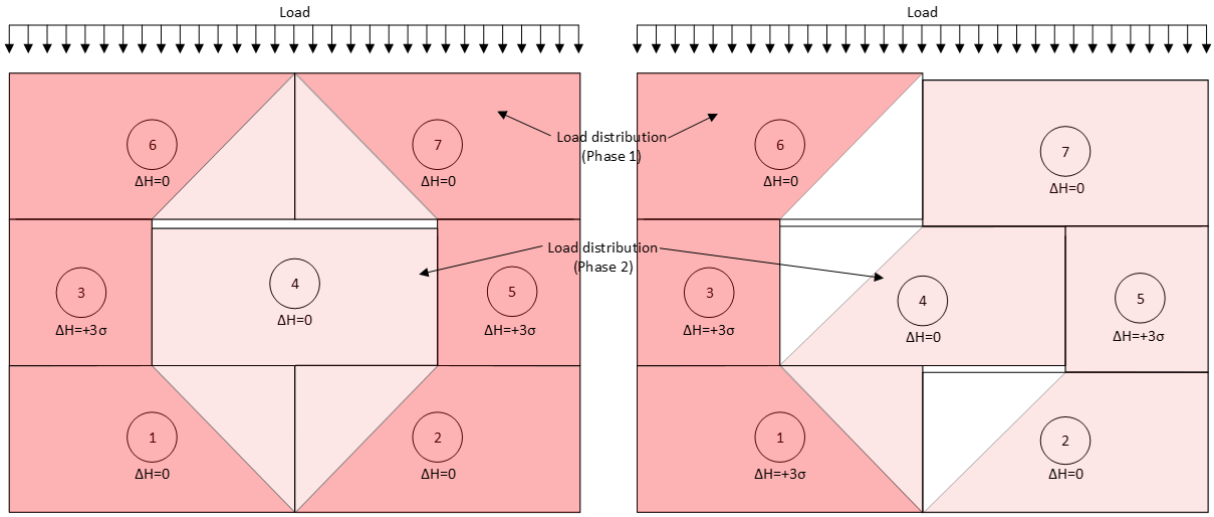

Fig. 6-26: Load percolation system for the two worst cases (left: BL 3-5 and right: BL 1-3-5), ΔH: the height difference of each block, +3σ: height increased by 0.86 mm (dark red: phase 1 of load distribution with the very beginning loading; light red: phase 2 of load distribution)

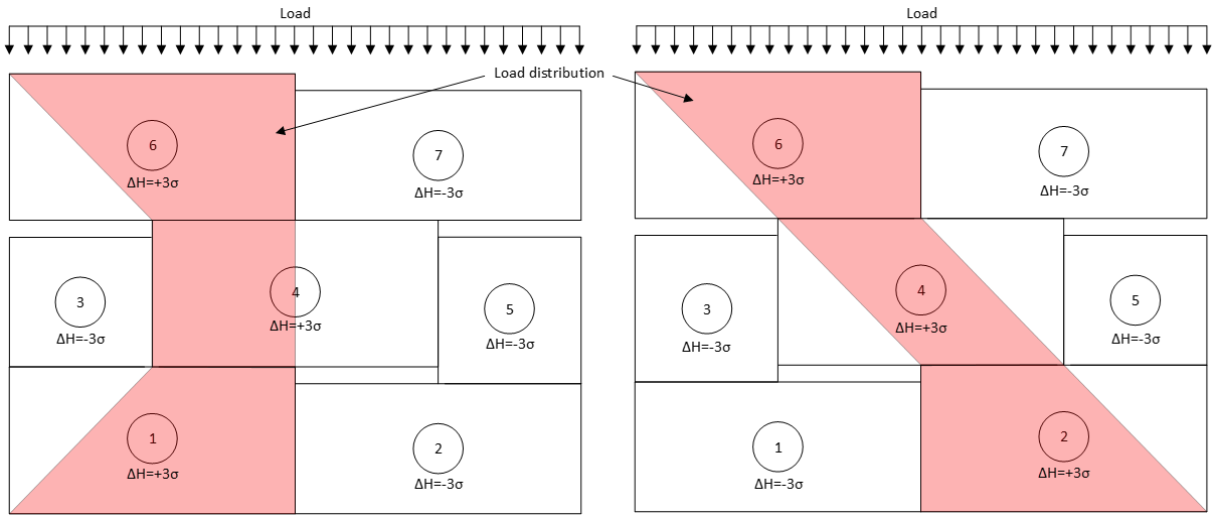

Fig. 6-27: Load percolation system for the two worst cases (left: BL 1-4-6 and right: BL 2-4-6), ΔH: the height difference of each block, +3σ/-3 σ: height increased/reduced by 0.86 mm

To approach a real-case scenario, all possible load percolation systems were analysed to identify the most relevant ones. In average, the models achieved a slightly lower stress-strain distribution than the calibrated model (**Fig. 6-28**). In general, their stiffness is lower due to the height differences implemented on the masonry blocks. The models achieved an average load-bearing capacity of 4.74 MPa. These results compared to the calibrated model represent a reduction of 2.1 % of the load-bearing capacity, which is more than 20 times less as the impact of the height differences presented by Chewe and Waldmann. Furthermore, it becomes apparent that the distribution of the implemented height differences lead to a better correlation of the numerical model to the experimental model.

Hence, it can be concluded that a masonry block based on Miscanthus concrete is suitable for a dry-stacked wall, due to its ability to adapt itself to the height differences between the blocks, which is linked to the low Young's Modulus of this material [174] and its ductility.

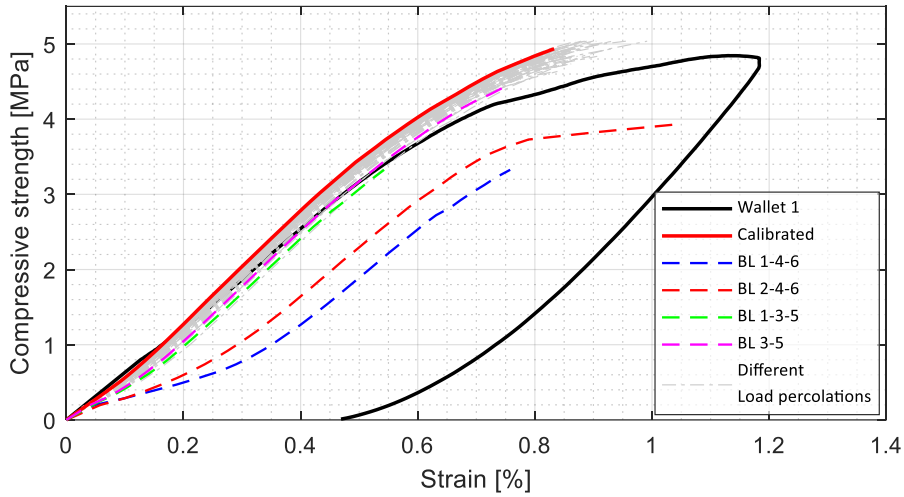

Fig. 6-28: Stress-strain distribution of the experimental Wallet 1 compared to the numerical analysis, the four worst-case scenarios and the models with different load percolations using height differences randomly chosen

6.4.4.2.2 Impact of the ratio H/L on the load-bearing capacity

To assess the use of a masonry block based on Miscanthus concrete for walls with increased heights compared to the studied wallets, an analysis is performed on the impact of the ratio H/L (height/length) on the load-bearing capacity. For these investigations, no height differences between the masonry blocks have been considered in order to compare the impact of ratio H/L on the load-bearing capacity without being affected by the impact of the height imperfections. The ratio H/L and the load-bearing capacity showed to have a decreasing linear relation (**Fig. 6-29**). For comparison, Agaajani [108] stated that an increase of the height of a dry-stacked wall based on conventional masonry blocks reduced the compressive strength exponentially. A wall with a lower height achieved generally a higher ultimate

load. However, if H/L is bigger than 1 an effect of lateral bending occurs and induces horizontal cracks which reduces the load-bearing capacity of the wall and stability issues.

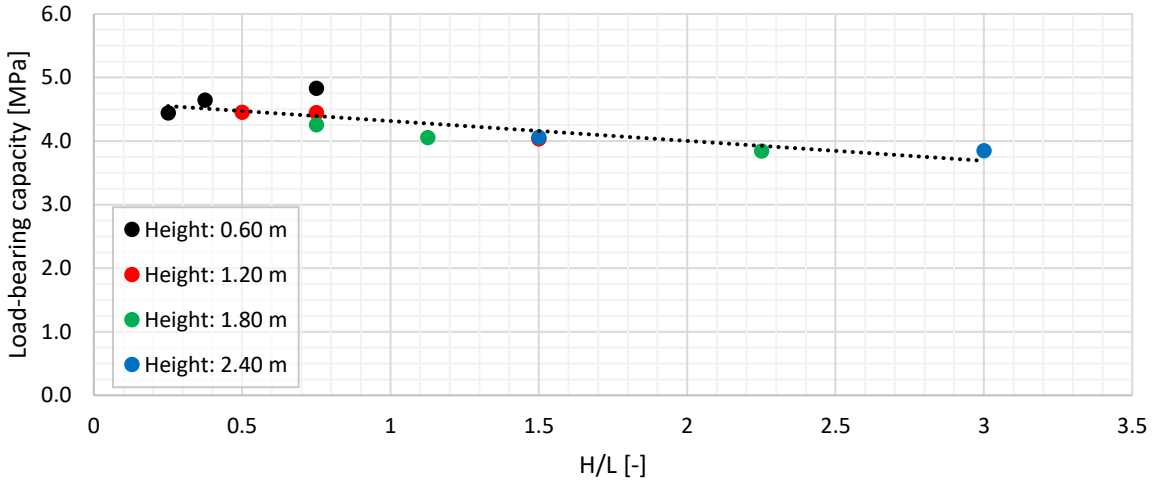

Fig. 6-29: Relation between the load-bearing capacity and the H/L ratio of walls based on Miscanthus concrete masonry blocks

6.5 CONCLUSIONS

This study reached to develop and analyse a Miscanthus concrete mixture experimentally and numerically for masonry blocks and walls. The height differences of the masonry blocks followed a Gaussian distribution with a standard deviation of σ=0.285 mm. Furthermore, the roughness was analysed by interpreting the contact surface at different tests. The conclusions of the treated points are summarised as follows:

- The impact of the vibration on the load-bearing capacity (LBC) of Miscanthus concrete was reduced with an increasing W/C-ratio. Mix 4 (W/C =0.9) showed a reduction of 7 % in the LBC for the prisms but an increase of 12 % for the masonry blocks by omitting the vibration during the creation process.
- The mixing procedure of first creating a cement paste with the full amount of water and introduce the Miscanthus fibres as last showed to be the most suitable considering the LBC. Independent from the vibration state the specimens based on the mixing procedure B showed the highest LBC.
- The prisms from Mix 2 increased their LBC by 6 % with an increasing curing time from 14 to 28 d. A more important observation was performed on the masonry blocks, where a 57.5 % development could be experienced by increasing the curing time from 14 to 28 days.

- An exponential relation between the compressive strength and the contact surface could be established and be used to forecast the contact area of a masonry block. Nevertheless, a reduction of 6-12 % needs to be taken into consideration for a non-gradual loading.
- A hysteresis load on a single masonry block showed to increase its LBC by 25 %. The same procedure of loading showed to increase the LBC on the wallets by 15 %. These occurrences can be explained by the coefficient α_{cc} from a normal concrete, which includes the effects of the loading duration.
- The contact area in a wallet between two rows of masonry blocks showed to be between 55 and 59 %.
- Filling a masonry block from the side instead from the top reduces the standard deviation of the height differences by 82%.
- A numerical model of the wallet was validated using the experimental data and the impact of the height imperfections showed to reduce in average only by 2.1 % the load-bearing capacity compared to a model without any height imperfections.

Finally, deducing from the results presented in this paper, the highest LBC was achieved using Mix 2 (W/C=0.7) and the mixing procedure B. The contact surface of a single masonry block presented an exponential relation to the compressive strength. The joints of the dry-stacked wallets showed to achieve a contact surface of almost 60 % without any additional external layer between the blocks.

The results of a Miscanthus lightweight concrete are promising and could be used to produce masonry blocks for the use in dry-stacked walls and subsequently expand the sustainable construction.

6.6 ACKNOWLEDGEMENTS

The authors of this paper would like to thank Contern S.A. for the financial support of the research project. Moreover, they would like to express their gratitude to the staff of the University of Luxembourg as well as to Mr Michael Gonçalves Dantas for his practical and competent help.

Chapter 7 INVESTIGATION OF MYCELIUM-MISCANTHUS COMPOSITES AS BUILDING INSULATION MATERIAL (PUBLICATION ON MYCELIUM-MISCANTHUS)

7.1 ABSTRACT

Good insulation materials have low thermal conductivity which is mainly related with the density of the material. Bio-composite insulation materials contribute to reduce the environmental footprint of buildings. The main goal of this study is to study the effectiveness of a self-growing, bio-composite building insulation material made of Miscanthus x giganteus and the mushroom Mycelium. Different mix proportions of Miscanthus and Mycelium were considered to identify the most suitable mixture to produce a porous composite which has a lower density. Scanning electron microscopy images were used to evaluate the microstructural geometry of the composite material. Thermal conductivity test was conducted on eight composite plates, and the results showed that the thermal conductivity of this new material is between 0.0882 and 0.104 Wm-1K-1. Moreover, other experiments were carried out to characterize the density, compressive strength and water absorption. In addition, fire resistant tests on composite plates with and without render were conducted, and it was found that the composite plates belong to the category EI15 according to the EN13501-2:2003. The initial results were found to be satisfactory to make a sustainable insulation material out of Miscanthus and Mycelium.

Keywords – Miscanthus; Mycelium; Thermal insulation; Bio-composite

7.2 INTRODUCTION

Depletion of natural resources, such as sand and gravel, is occurring at an alarming rate because the current pace of consumption in the construction industry is not sustainable [174]. Besides, the extraction, processing, manufacturing and transportation of building materials have the highest contributions in carbon emissions related to the construction industry. In order to protect the environment and reduce the overall environmental footprint of buildings, natural resources have to be used more efficiently, reducing the carbon emissions related to construction activities. As a result, several action plans have been issued in Europe, such as the European Green Deal, a fundamental roadmap to make the EU economy sustainable resulting in zero net carbon emissions in 2050 [215].

Traditional insulation materials come from different sources like animal products (such as sheep wool and feathers), plant-based products (such as cotton and wood fibre) and synthetic compounds (such as polystyrene and polyurethane). Nowadays, synthetic compounds, which are based on plastic-based fibres and foams, are more likely to be used in the building insulations. The creation and development of these materials takes a lot of time and is often very complicated and costly. On the other hand, these materials exhibit high-embodied energy, have high carbon footprint and produce toxic substances. Generally speaking, current insulation materials are not sustainable and environmentally friendly. As of today, new environmental-friendly bio-based insulation materials are introduced which often require less energy to be produced than traditional materials. As a result, this paper focus on the possibility of introducing a self-growing insulation material based on a Mycelium-Miscanthus composite that could replace traditional insulation materials.

With the increasing demands on grappling with the concepts of low-carbon economies by bringing in photosynthesis as the driver, researchers have given their focus on new environmental-friendly, energy efficiency and sustainable alternatives over the last few years. In this respect, it has been found that bioenergy crops have all the right characteristics to substitute many building materials [83-85].

Miscanthus, which is a C4 grass that originated in Eastern Asia, is one of those crops, and it is very efficient and economical to grow in most states in European climate [86]. Higher water use efficiency, low use of fertilizers and the capability to absorb large amounts of CO_2 from the environment compared to other C4 grass lead Miscanthus to high yield [87-89]. Due to its versatility and favourable properties, a large amount of Miscanthus plants have been planted for various purposes as well as to make value-added products from it all over Europe in the recent [157].

Miscanthus has already been used in a variety of different ways whereas Miscanthus lightweight concrete is one of these interesting products based on Miscanthus. Investigations on Miscanthus showed that it can be used in passive noise protection and fire protection [38]. It has already been proven that

Miscanthus fibres have relatively high insulation capacity with respect to temperature [86, 90, 91]. Eschenhagen et al. [86] developed low-cost insulation particleboard panels by using Miscanthus and Sunflower stalk in France and showed that they have great potentials because they have low density and good thermal conductivity. El Hage et al. [90] carried out an investigation about new insulating bio-composite made of Miscanthus and recycled textile fibres bunded with chitosan and found that its thermal conductivity varies between 0.069 and 0.09 WmK^{-1}. Miscanthus fibres have thermal conductivity of 0.04 WmK^{-1} which is equivalent to the thermal conductivity of conventional insulation materials available on the market [91].

Used as lightweight aggregates in a concrete mixture, Miscanthus fibres increased the compressive strength of concrete by 4 to 28% [83]. Pereira Dias and Waldmann [174] concluded that the best theoretical mixture considering the compressive strength of the Miscanthus concrete would constitute of 150 kg/m^3 of Miscanthus and 592 kg/m^3 of cement with 0.8 of water/cement ratio. Moreover, pore structure of Miscanthus contribute to reduce the thermal conductivity of the Miscanthus concrete [46, 180]. Miscanthus fibres significantly enhanced the acoustic absorption properties of bio-based lightweight concrete containing Miscanthus [162].

Mycelium is the vegetative part of the mushroom and is considered as one of the largest living organisms on earth [216]. It is formaldehyde free and non-toxic. Recently, the use of mycelium has been investigated to replace the already used resin by a fully natural one. Mycelium is a fungus which spreads its branches and acts like a binder within the fibres. It comes from biological and agricultural waste and is therefore very inexpensive on a large scale. In other words producing more of these, prices will decrease because it allows optimized growing procedures. Over the last decade, Mycelium based bio-composites have appeared to be used as a green alternative to several building materials such as building insulation [92, 93]. Elsacker et al. [94] mentioned that these composites have thermal conductivity of 0.08 WmK^{-1} and density of 57-99 kg/m^3. Yang et al. [95] showed that a Mycelium bio-form has higher characteristics than the conventional expanded polystyrene foam except density.

From the above perspectives, it implies that there is a huge potential to develop a Mycelium-Miscanthus bio-composite as a new building insulation material. Therefore, this research offers a novel way of combining Miscanthus and Mycelium for the production of a new bio-based building insulation material. This study investigated the optimal mix proportions of Mycelium and Miscanthus to produce a lightweight bio-composite. Furthermore, the properties of the composite including density, strength, water absorption and thermal conductivity were investigated.

This paper is structured in four sections including an introduction. Section 7.3 presents the experimental procedure. In section 7.4, the results are presented with a discussion, followed by the conclusion of study.

7.3 EXPERIMENTAL STUDY

This section reports the experimental tests carried out by the authors at the laboratory of Solid Structures of the University of Luxembourg. Firstly, the different materials used in this study are discussed. Then, the preparation procedure of the samples are presented. Weight and volume changes of each sample were measured to identify the optimal mix proportion of the materials. Then, on the selected samples, compressive test, water absorption test and thermal test were conducted. The results obtained from the experiments are presented and discussed in section 7.4.

7.3.1 MATERIALS

The two main materials used in this study are Miscanthus and Mycelium. In this study, Miscanthus x giganteus (**Fig. 7-1** (a)), the giant Miscanthus, which was produced by Luxembourgish farmers, was chosen due to its wide availability on the European market because of its high potential, good environmental profile and minimal risk of invasiveness [15]. It is a renewable raw material, that grows up to 4 m, on basically any type of hydromorphic grounds. Miscanthus x giganteus is able to filter up to 30 metric tons of CO_2 per hectare over one year. It has high rigidity with low density due to a high content of parenchyma surrounded by a tough fibrous structure [217]. In this study, dried Miscanthus with average density of 120 kg/m^3 was used. **Fig. 7-1** (b) shows the dried and chopped Miscanthus fibres used in this study.

(a) (b)

Fig. 7-1: (a) Miscanthus x giganteus plant [92] (b) Dried Miscanthus

As mentioned above, Mycelium is the vegetative part of mushroom. In this study, Mycelium was obtained from Ganoderma resinaceum mushroom. The Mycelium from the Ganoderma family develops better than other mushrooms. Only the grains of the Mycelium were used to envelop the Miscanthus

(**Fig. 7-2**). The Mycelium penetrates its nutrients by physical pressure and not enzymic secretion to break the host's polymers in order to transform them into more easily transportable nutrients such as sugars. In this study, the selected nutrient substrates are pure cellulose biopolymers and cellulose-potato dextrose both are composed of potato Infusion solids and Dextrose (sugar). This choice was made because of the abundance and availability of this natural polymer for cellulose and for the latter, it is because this medium is the most common used for the development of mushrooms thanks to its composition based on sugar easily digestible by the Mycelium. Because of their similar chemical form as well as by their surface homogeneity it is expected that these two nutritive bases allow a hydrolysis without gene with the Mycelium to guarantee a growth which will not depend on the nutritive base to provide a homogeneity of the material [92]. It does not need additional energy input to propagate. It only needs the usual fungus propagation conditions to grow (high humidity, the sample should stay in a dark place and stay under room temperature). Sterilization is important for the growing process of mycelium, because other spores could affect it or worse kill it. Thus, the development environment should be sealed to protect it from contamination [92].

Fig. 7-2: Mycelium Ganoderma resinaceum grains

In addition to these two main materials, as mentioned above, potato starch extracted from potatoes (**Fig. 7-3**) were used as substratum of Mycelium, which is the base material used by the mycelium to grow. Here starch was used for the Mycelium to grow as a web. The potato starch itself contains large oval spherical granules, which size is between 5 and 100 μm.

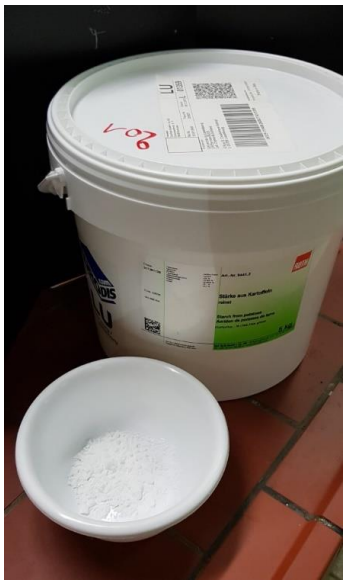

Fig. 7-3: Potato starch

7.3.2 PREPARATION OF SAMPLES

Twelve different weight percentages of Miscanthus fibres, Ganoderma resinaceum mushroom and potato starch were used to manufacture the test samples. The mix proportions used are given in **Table 7-1**. Samples ID are labelled to easily identify the mix proportions of three materials. The letters G, M and P in the sample IDs represent the materials Ganoderma resinaceum mushroom, Miscanthus fibres and Potato starch, respectively. The number associated to each letter defines the ratio of corresponding material to the amount of Miscanthus. In the last four mix proportions, NS stands for non-sterile. In other words, in these samples not constantly disinfected materials were used.

Sample ID	**Mix proportion (Ganoderma resinaceum mushroom : Miscanthus fibres: Potato starch)**		
G0.2_M1_P0.1	0.2	1	0.1
G0.2_M1_P0.2	0.2	1	0.2
G0.2_M1_P0.5	0.2	1	0.5
G0.3_M1_P0.1	0.3	1	0.1
G0.5_M1_P0.1	0.5	1	0.1
G0.7_M1_P0.1	0.7	1	0.1
G0.7_M1_P0.2	0.7	1	0.2
G0.7_M1_P0.5	0.7	1	0.5
G0.2_M1_P0.2_NS	0.2	1	0.2

G0.5_M1_P0.1_NS	0.5	1	0.1
G0.7_M1_P0.1_NS	0.7	1	0.1
G0.7_M1_P0.2_NS	0.7	1	0.2

Table 7-1: Mix proportions used for manufacturing of test samples

Three test samples were carefully manufactured from each mix proportions for the testing. The manufacturing procedure of the test samples involves mixing of potato starch and water, adding mixture to the dried Miscanthus, boiling the mixture, cooling down the mixture, mixing the mushroom to the Miscanthus-potato starch mixture and manufacturing of samples using the prism moulds, as shown in **Fig. 7-4**.

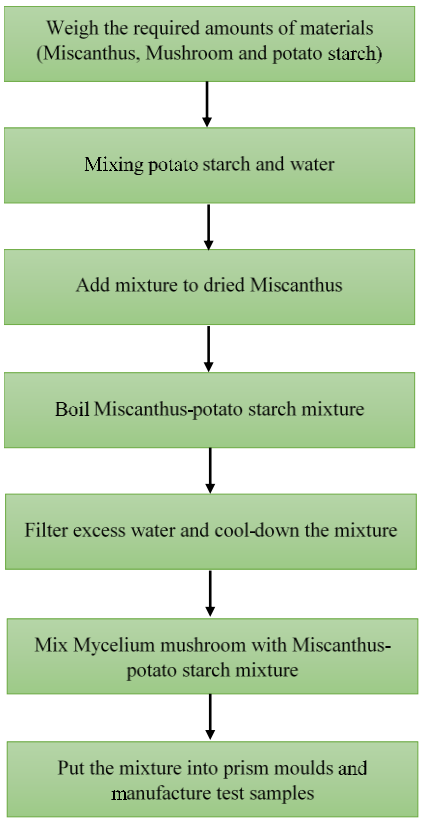

Fig. 7-4: Manufacturing procedure of test samples

The mixing procedure was done as follows: weighted potato starch was mixed with 15l of water, and then the mixture was added into 150g of dried Miscanthus. The mixture was boiled for 30 minutes to kill most of the bacteria on the Miscanthus fibres. After that, the excess water was filtered away by using a sterilized strainer, and the wet Miscanthus-potato starch mixture was then put on a sterilized bowl to cool down itself until 30 to 35 ˚C. This was done to avoid a high difference as this would have killed the Mycelium before its growth. It has to be noted that the Mycelium was kept at 4 ˚C before being mixed to the rest in order to prevent the mushroom from growing already before its application in these

specimens. Once the desired temperature was reached, the Miscanthus was mixed with the mushroom Mycelium until a homogeneous mixture was obtained. Finally, the mixture is put inside three prism moulds with the dimensions of 40 mm x 40 mm x 160 mm and covered with a sterilized plastic wrap, as shown in **Fig. 7-5** (a).

Since a dark environment is helpful to the growth of the mushroom, the samples were kept in a closed cabinet for 7 days at room temperature (around 20 – 22 ˚C). The given condition is ideal for Mycelium to grow in the prisms, so that a good binding between the Mycelium grains and Miscanthus fibres can be achieved. After 7 days, the samples were taken out from the cabinet and demoulded. **Fig. 7-5** (b) and (c) show the samples after the first growing phase. Mycelium is a fast growing fungus. Thus, in the first growth phase it develops and bind surrounding material, i.e. Miscanthus. In this phase, Mycelium grows the most due to higher amount of starch available. Thus, it can be assumed that the samples will have firm shape after the first growing phase.

The dimensions and weights of the demoulded test samples were measured, and the samples were then put separately in sterilized bags and sealed in order to begin the second growing phase. Although the samples had a stable shape at the end of the first growing phase, it was observed that the part of the sample which was against the mould was not enveloped by the Mycelium ligaments. Thus, the second growth phase is aimed to reinforce the structure of Mycelium which leads to stiffer and stronger final product. Therefore, the samples were put in the same cabinet again as in the first phase to stimulate Mycelium growth towards a denser network and to obtain a better homogeneity on the surfaces. The Mycelium continued to grow in this environment although the growth in this second phase is slower. The second growing phases was limited to 10 days to prevent the initiation of the growing of fruiting bodies as well as the deterioration of the fungus in the mixture. The samples were measured and weighed again at the end of the second growth phase. Then, the samples were put in an oven and continuously dried at 80 ˚C to stop the Mycelium from growing. The samples were measured and weighted repeatedly every 1 hour. The drying process was stopped after 24h or when the samples reached at least 35% of the initial weight. **Fig. 7-5** (d) shows all the final test samples after the drying process.

(a) (b)

(c) (d)

Fig. 7-5: Test samples (a) Miscanthus mixture in the prism moulds covered with plastic wrap (b) Test samples after first growing phase (c) Demoulded test samples after first growing phase (d) Test samples after the drying process

7.4 RESULTS AND DISCUSSION

The prism test samples were completed in a total time of 18 days. Based on visual analysis, a difference in growth of Mycelium on the test samples was observed. The varied amount of white visible on the samples might be a result of various factors such as a lack of mycelium, the availability of the substrate for Mycelium to grow or the differences in airflow. It was observed that the prism test samples of G0.7_M1_P0.1 was completely white at the end of first growing phase and had enough growth of Mycelium to hold the composite together. The prism test samples of G0.2_M1_P0.1 had built some yellow-brownish liquid after the first growth phase compared to other test samples. The composition of the liquid was not analysed in this study. However, it was assumed that the brownish colour would come

from the Miscanthus and the yellow watery part represent the initiation of the growing phase of fruiting bodies or the deterioration of the fungus in the mixture.

The measured average density of all the mixtures after each phase was compared and are presented in **Fig. 7-6**. It is observed that the weight of the all the samples except G0.2_M1_P0.5, G0.5_M1_P0.1, G0.7_M1_P0.1_NS and G0.7_M1_P0.2_NS has changed at the end of the second growing phase. At this phase, the weight changes depend on how the Mycelium grew and on the humidity lost. In the first hours of the drying process, the weight decreased considerably every hour. This is due to the evaporation of the humidity present in the samples. After 24h the decrease of the weight slowed down.

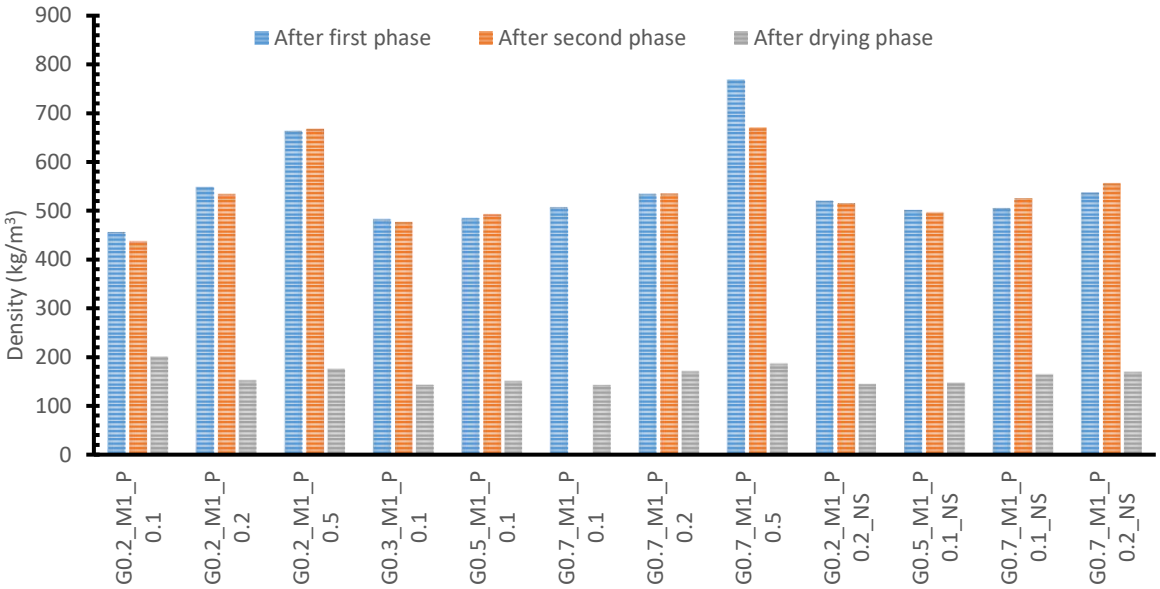

Fig. 7-6: Average density of all the mixtures after each phase

As the mixtures G0.3_M1_P0.1 and G0.7_M1_P0.1 present a low-density, for these mixtures an excellent thermal insulation capacity could be expected. However, since for mixture G0.3_M1_P0.1 sample less Mushroom, that is 45g, is used, it was identified as well-balanced mix proportion for being applied in a lightweight Mycelium-Miscanthus thermal insulation board.

7.4.1 FEASIBILITY OF USE COFFEE AS STARCH

As described in section 7.3.1, Mycelium needs a base material to start natural growth. In this subsection, further experiments were carried out by substituting the potato starch by coffee to check the usefulness of the coffee as ecological, renewable and biodegradable material. A mixture of G0.3_M1_C0.1 with a ratio of 0.3 times the weight of Miscanthus for Mycelium and a ratio of 0.1 times for coffee was produced.

Fig. 7-7 compares the observed results on average density of these two test mixtures. It can be seen that the average density was obtained for both samples is almost the same after the first growth phase. In general, the samples made of used ground coffee has slightly lower density than samples made with potato starch, after the drying phase. It was also observed that there is no visible difference between prisms made with potato starch and prisms made with used ground coffee. Apart from the fact that during the development of the mushroom, a strong smell of coffee emanates from the samples.

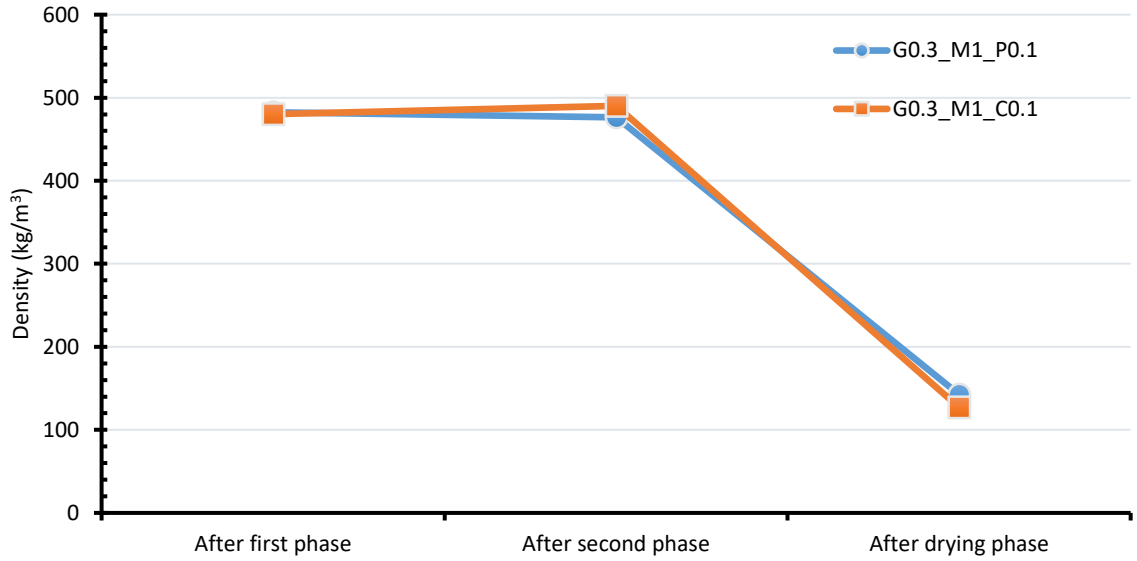

Fig. 7-7: Comparison of average density for the mixtures of G0.3_M1_P0.1 and G0.3_M1_C0.1

7.4.2 SCANNING ELECTRON MICROSCOPY (SEM) ANALYSIS

SEM analysis was carried out to evaluate the microstructural formation of the Mycelium in the composites, using a JSM-6010LA scanning electron microscope. The SEM images of the formation of Mycelium around the Miscanthus fibres were analysed on the test samples of G0.7_M1_P0.5. **Fig. 7-8** (a) and (b) show the fibrous network of Miscanthus and Mycelium matrix from Ganoderma resinaceum mushroom, respectively. These images indicate that the microstructure of Miscanthus is not isotropic and it is formed by numerous hollow tubes that all points oriented in the same direction. Moreover, the Mycelium in the mushroom exhibits an interconnected network like microstructure, formed from randomly arranged filaments.

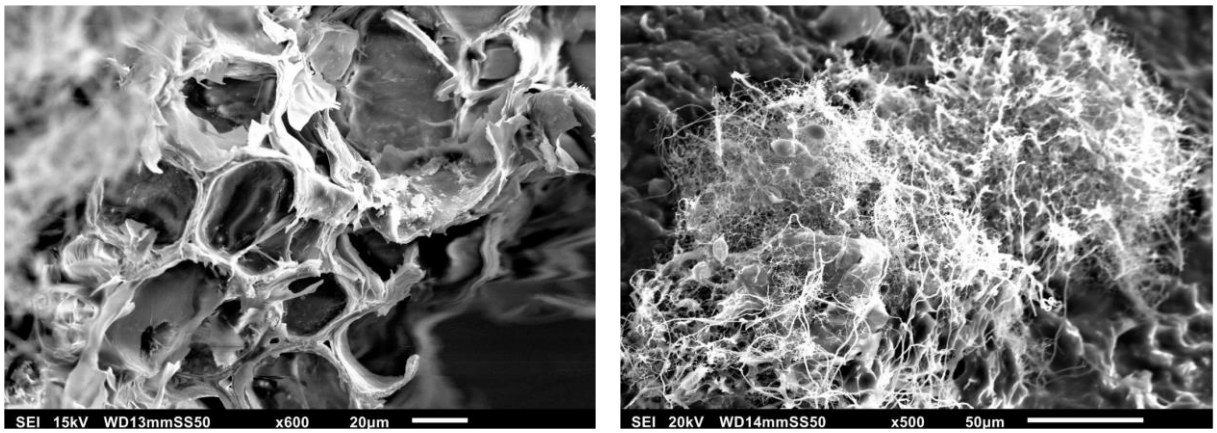

(a) (b)

Fig. 7-8: SEM image of (a) Miscanthus fibre structure (b) Mycelium matrix in Ganoderma resinaceum mushroom

The morphology of the Mycelium-Miscanthus composite is shown in **Fig. 7-9** (a). It shows that there is Mycelium growth between and around the Miscanthus fibres, successfully embedding the Miscanthus into the composite. **Fig. 7-9** (b) depicts a closer view of the Mycelium growing into the Miscanthus fibres. Although it is not clear how deep the Mycelium hypha penetrates into the fibres, it is clear that the Mycelium grew within the composite and bonded with the Miscanthus fibres. The abundance of the Mycelium in the center of the composite may be due to the insufficient airflow through the materials. The presence of voids in the center of the composite is expected to affect the mechanical and thermal properties of the composite.

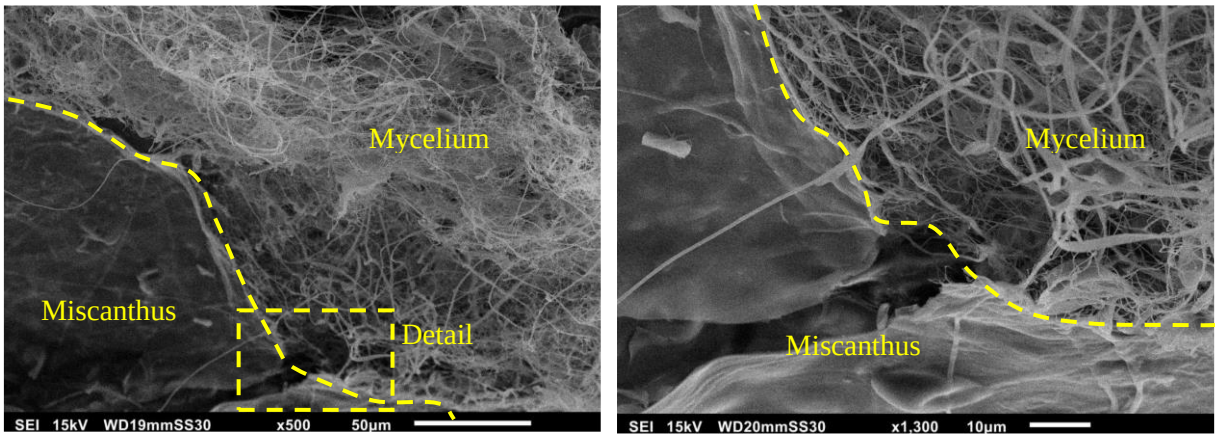

(a) (b)

Fig. 7-9: SEM image of (a) Mycelium bonded with Miscanthus (b) closer view of the Mycelium growth within the composite

7.4.3 COMPRESSIVE TEST

The experimental study was further extended in order to analyse the mechanical characteristics of Mycelium-Miscanthus samples. Compressive tests on prisms were carried out to determine their compressive strength. Compressive strength of a prism depends on its porosity, pore size and material characteristics including the bonding of the Miscanthus fibres to the Mycelium used. **Fig. 7-10** shows a test prism made of G0.3_M1_P0.1 after subjected to compression test. The load on the compression tip was applied at a constant rate and the load vs displacement data were recorded. The compression test was continued until the specimen reaches 10% relative displacement, and the compressive strength was defined according to [218] as the stress at 10% relative deformation displayed if the test specimen does not yield or rupture before it reaches the required deformation. The results for strain versus stress through the compression test are represented in **Fig. 7-11**. It can be seen that the compressive strength of the prisms varies between 1.2 N/mm2 to 1.8 N/mm2. It was also observed that the composite stick together even after it reached to the non-reversible deformation.

Fig. 7-10: The compressed test sample G0.3_M1_P0.1

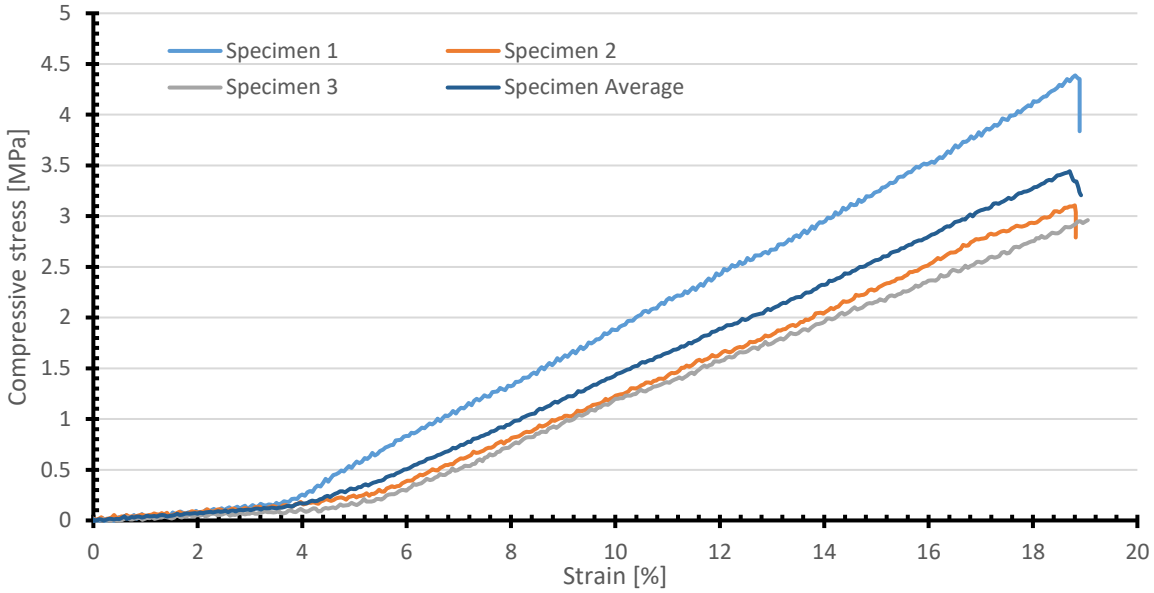

Fig. 7-11: Stress-strain relationship

7.4.4 WATER ABSORPTION

Since the composites are hydrophilic, the durability of the material could be affected when the studied Mycelium-Miscanthus composites is used as insulation material. Therefore, the water absorption was measured by immersing the selected test sample made of G0.3_M1_P0.1 in water until the increase in water absorption is negligible. The water absorption capability in percentage was calculated as eq. 7-1, where M1 is the initial dry mass and M2 is the water-soaked mass.

$$Water\ absorption = \frac{M_2 - M_1}{M_1}\ x\ 100\% \qquad \text{(eq. 7-1)}$$

The initial dry mass of the sample was 0.0555 kg. **Fig. 7-12** shows the observed results on the water absorption of test sample. It is reported that the water absorption of Mycelium-based materials is very fast and it increases in weight by 40-580 wt% in contact with water for 48-192 hours [219]. The rate of absorption is dependent on the characteristic of the pores with their size, distribution and continuity. It was found that the sample absorbs more water around the first 30 seconds and it has then been reduced with time. This is due to Mycelium-Miscanthus composite, which has a high porosity and a complicated internal structure. Since the thermal insulations are usually used in internally dry conditions, the weight increase occurred within first few seconds is not a significant problem [220], as for other insulation materials too, a render will protect the composite from environmental impacts.

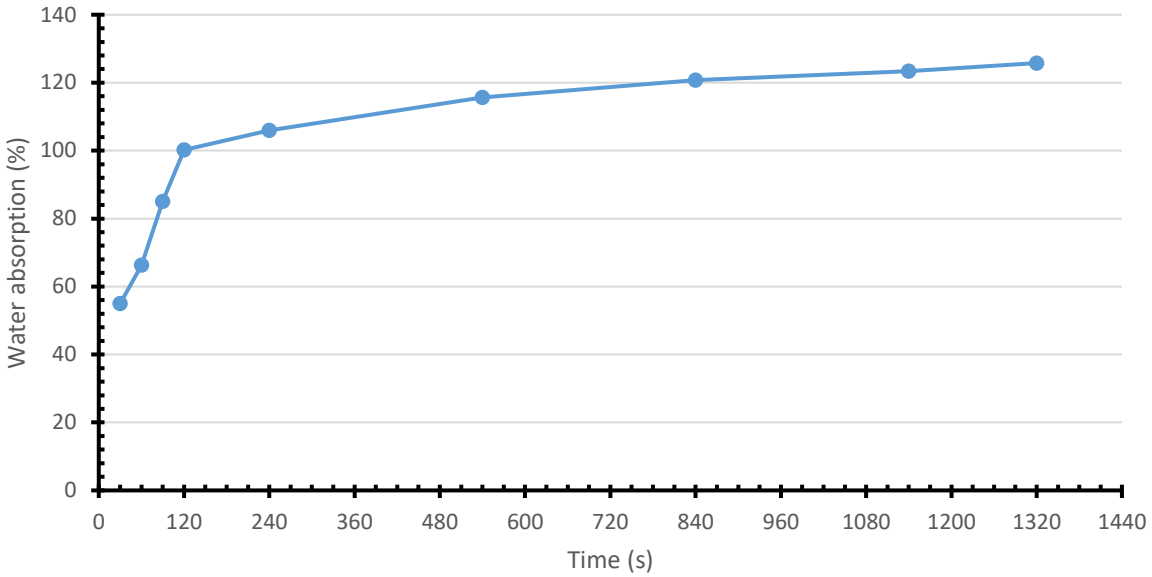

Fig. 7-12: Water absorption in relation of time

Once the absorption test was completed, the test sample was kept in the water for a certain period to observe the possible changes and developments on the sample. Although the composite was observed during 1 month, no development of Ganoderma was observed. After 1 month, a sample was cut in half to inspect inside, and it was observed that Ganoderma had not developed inside the composite as well, as shown in **Fig. 7-13**. It is apparent that despite the water is partially raised in the sample, the development of the mould stops at the outer space (**Fig. 7-13**). This, it can be concluded that drying the mixture at 80 ˚C effectively kills the fungus.

Fig. 7-13: Test sample G0.3_M1_P0.1 after 28 days (cut in half); Red circle has drawn around the developed mould on the sample

7.4.5 THERMAL INSULATION TEST

After having studied the mixture properties with prism samples, Mycelium-Miscanthus plates were produced using the same procedure and the same ratios as for the prisms, described in section 7.3.2. The

only differences were related to the volumes and the formworks used. The plate dimensions were 500 mm x 500 mm x 70 mm. G0.3_M1_P0.1 mixture was used to manufacture the bio-composite plates. The aim of this experiment was to study the insulation capacity of the Miscanthus and Mycelium composite, and its interaction with plaster. The final plates are shown in **Fig. 7-14**.

Fig. 7-14: Test sample of Mycelium-Miscanthus plate used to assess the thermal performance

In total, six plates were manufactured. Plates 1 to 4 were made produced without a render, while Plates 5 and 6 were covered with a render. Two layers of render were applied on those two plates according to ETAG-004 [221]. A 15 mm thick layer of Weber DUR 137 was used as a base coat layer and 10 mm thick of Weber TOP 200 was put on the first render layer as a finishing coat. After the application of base layer, a 5mm x 5mm grid was placed on the top of the base layer as reinforcement. Before application of Weber TOP 200, it was ensured that the first layer is completely dry and dust free. **Fig. 7-15** shows the manufactured plates with two layers of render.

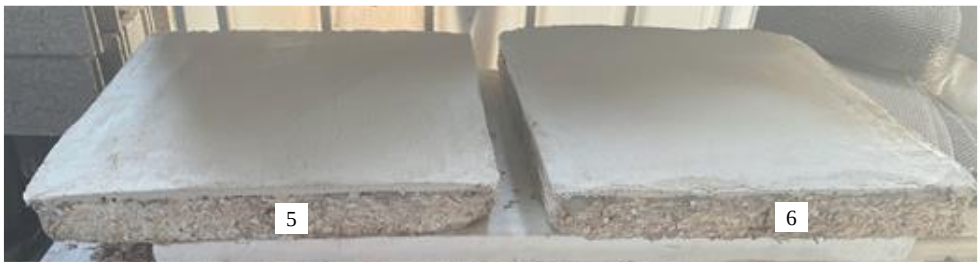

Fig. 7-15: Plates 5 and 6 with two layers of render

Fig. 7-16 compares the final density of each plate. The first four plates are very light having a density between 122.5 and 167.3 kg/m^3. Low density of the composite is desirable for reducing the packaging and transportation costs as well as thermal properties of the composite. The larger thermal conductivity can be attributed to the higher density of the material [94, 222, 223]. Yang et al. [95] showed that Mycelium-based bio-composite has a thermal conductivity between 0.05 and 0.07 Wm-1K-1 with a density between 160 and 280 kg/m^3. Giovanna Cadena and Bula Silvera [224] developed bio-composite

insulation boards based on rice husks and yucca starch which has a thermal conductivity of 0.065 Wm-1K-1 and density of 195 kg/m^3.

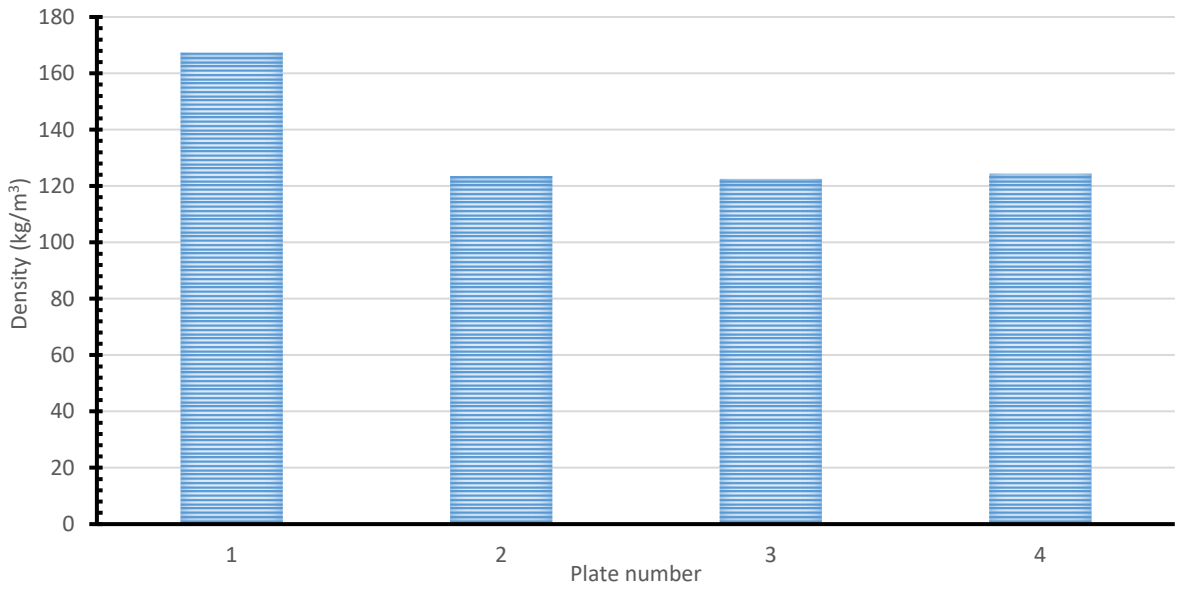

Fig. 7-16: Comparison of density of plates

They were first left for 76 days outdoor in order to study the impact of humidity and temperature changes as well as and UV radiation on them. It was observed that the renders on the plates were unaltered. There were neither cracks nor curvatures visible. However, after six weeks, a bump appeared on the Plate 6. **Fig. 7-17** shows the variation of weight of the Plates 5 and 6 during the experiment. In general, it was observed that the plates did not change a lot, which shows that the Mycelium-Miscanthus plates are resistant on the environmental conditions.

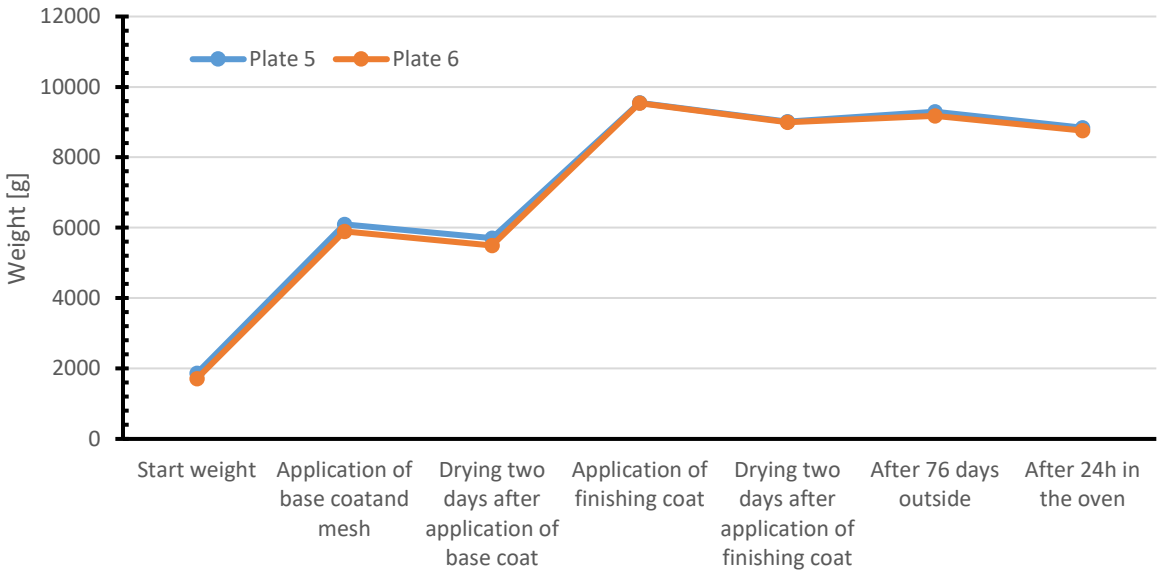

Fig. 7-17: Weight of the plates during the experiment

In the next step, the insulation capabilities of composite plates were studied by measuring their thermal conductivity. The device Taurus TLP800/900 was used to determine the thermal conductivity of Mycelium-Miscanthus composite plates. **Fig. 7-18** (a) shows the thermal conductivity test carried out by the Taurus TLP800/900 device on the composite plate according to ISO 8302/EN 1946-3. In total, three tests were carried out. For the first test, two composite plates (Plates 2 and 4) were used at the same time, as illustrated in **Fig. 7-18** (b), while the second test was carried out for a single composite plate (Plate 1), as illustrated in **Fig. 7-18** (c). The third test was carried out using the two composite plates with render (i.e. Plates 5 and 6) after their exposition to outside environmental conditions for 2 months. In **Fig. 7-18** (b), the test setup for the measurement of the heat conductivity using two composite plates is illustrated. The bottom of the measuring device consists a cooling plate following by a levelling mat and thermocouples. At the middle of the machine, a heating plate is positioned. On the top of the machine, another cooling plate is positioned. During the thermal insulation test, each composite plate (test sample) was put between a cooling and a heating plate in order to install a temperature difference of 10 K within each composite plate. This is needed to calculate the thermal conductivity (i.e. λ-value). In addition, a thin layer of temperature sensors was introduced between each heating/cooling plate and these sensors measure the temperature at 5 points on the composite plate (test sample), as shown in **Fig. 7-18** (d). Moreover, the composite plates were insulated on the four sides so that they are positioned in the middle by use of Styrofoam are placed around the composite plate, as shown in **Fig. 7-18** (d).

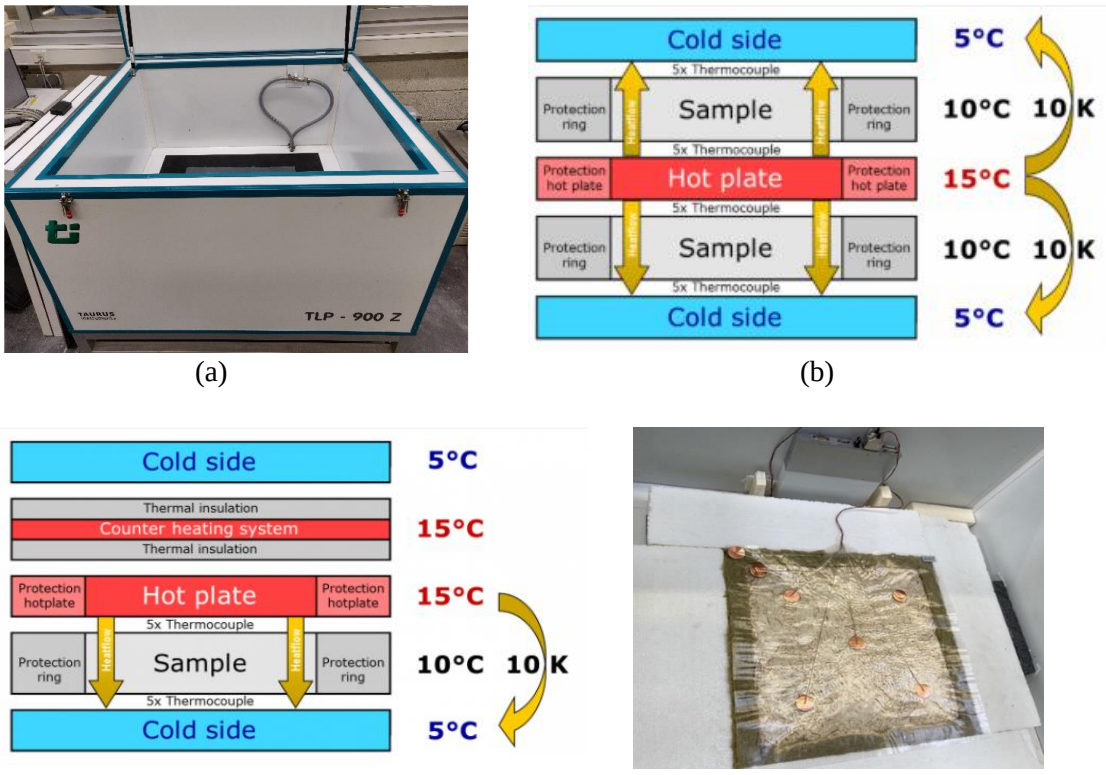

(a) (b)

(c) (d)

Fig. 7-18: Thermal conductivity test (a) Taurus TLP800/900 (b) Principle illustration of measuring with two plate method [225] (c) Principle illustration of measuring with single plate method [225] (d) Thermocouples attached on the test sample

The thermal conductivity of each plate was measured at three different mean temperatures because of the temperature difference between the heating plate and the cooling plate. The λ-value is calculated from the power which is put into the heating plate, the thickness of the sample and the temperature difference. It gives the thermal conductivity of a material in the unit of Wm-1K-1. The obtained results are plotted in **Fig. 7-19**. From these results, it can be seen that the λ-values for plates 2&4, 1, and 5&6 are 0.0882, 0.104 and 0.121 Wm-1K-1, respectively. Thus, it is clear that the associated λ-value of new insulation material of Mycelium-Miscanthus composite is between 0.0882 and 0.104 Wm-1K-1. These result can be compared to λ-values of straw, hemp concrete, softwoods and gypsum about 0.08 [226], 0.10 [227], 0.12 [228] and 0.17 Wm-1K-1 [228], respectively. However, when comparing production costs and environmental impacts, the new Mycelium-Miscanthus composite is cheaper to manufacture and has a significantly lower carbon footprint.

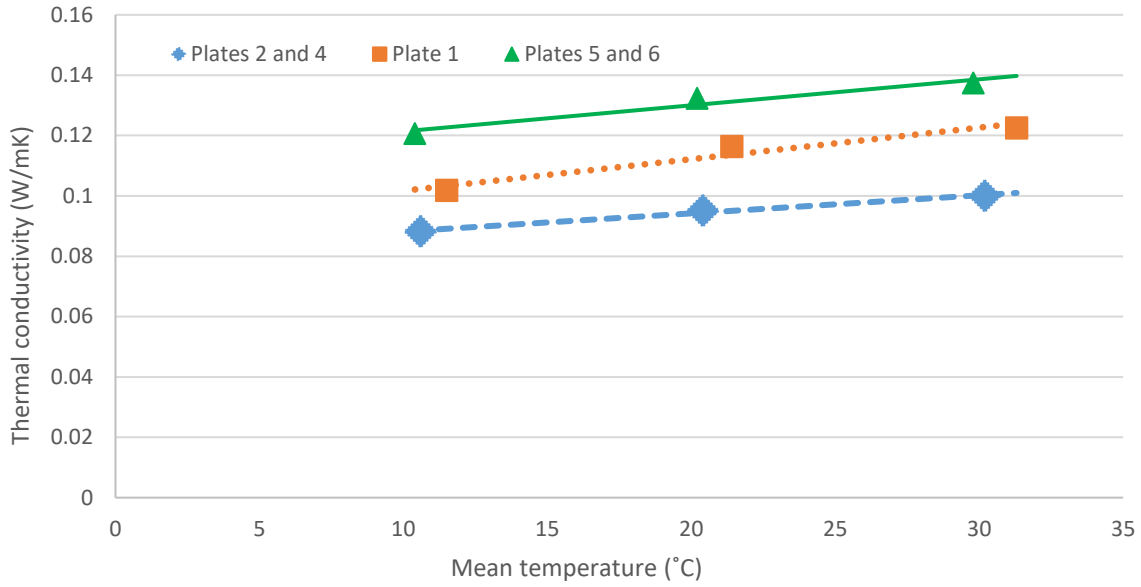

Fig. 7-19: Average results for thermal conductivity

7.4.6 FIRE RESISTANCE TEST

Even though Mycelium and Miscanthus have no notable fire-resistant properties, fire resistance tests focused primarily on the Mycelium-Miscanthus composite in order to analyse the fire resistance so that it can be classified according to the standard EN 13501-2:2003 [229]. The test samples (plates with and without render) were manufactured in a similar way as described above. The fire resistance test involved placing a sample approximately 5 cm above a Bunsen burner, which was attached to the gas consisting of 60% Methane, 34.5% CO2 and 0.5% Oxygen. The experiment was captured with a thermal camera to determine the temperature evolution.

First, a plate without render was tested. According to the standard EN 13501-2:2003 [229], a piece of cotton wool was put on the top of the plate, and the test has to be considered to be over when the cotton begins to burn, a gap or opening is visible or the presence of a persistent flame on the side facing away from the fire is appearing. It was observed that a gap was visible and the cotton wool started to burn after 40 minutes. **Fig. 7-20** shows the plate before and after it was burned for 40 minutes.

(a) (b) (c)

Fig. 7-20: Plate without render subjected to fire test (a) before start to burn (b) after 40 minutes (c) bottom of the plate after 40 minutes

Fig. 7-21 shows the captured temperature progression by the thermal camera during the fire test. It can be seen that the heat from the flame took about 7 minutes to get to the top of the plate and another 33 minutes to burn the cotton wool and create an opening on the top of the plate. Moreover, **Fig. 7-22** depicts the variation of temperature at two points, one is on the cotton wool (P1) and another is on top of the plate just close to the cotton wool (P2), during the fire test. It was observed that the temperature at point P1 slightly decreased until 22 minutes. This is due to the high amount of fume, which was created during the test.

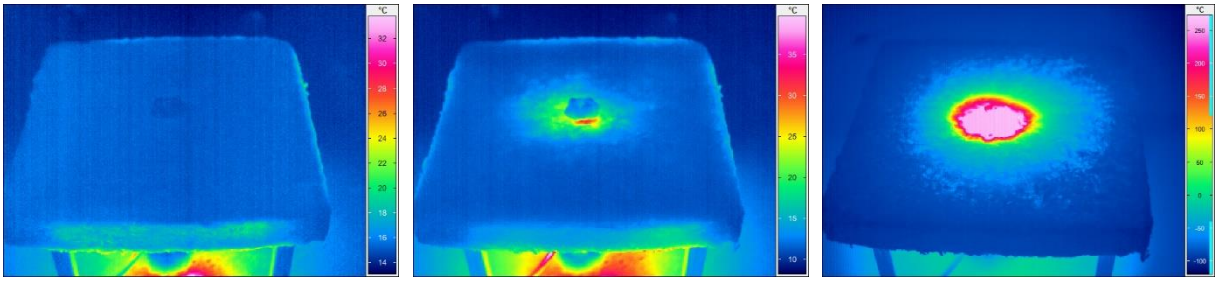

(a) (b) (c)

Fig. 7-21: Temperature progression during the fire test (a) before start to burn (b) after 7 minutes (c) after 40 minutes

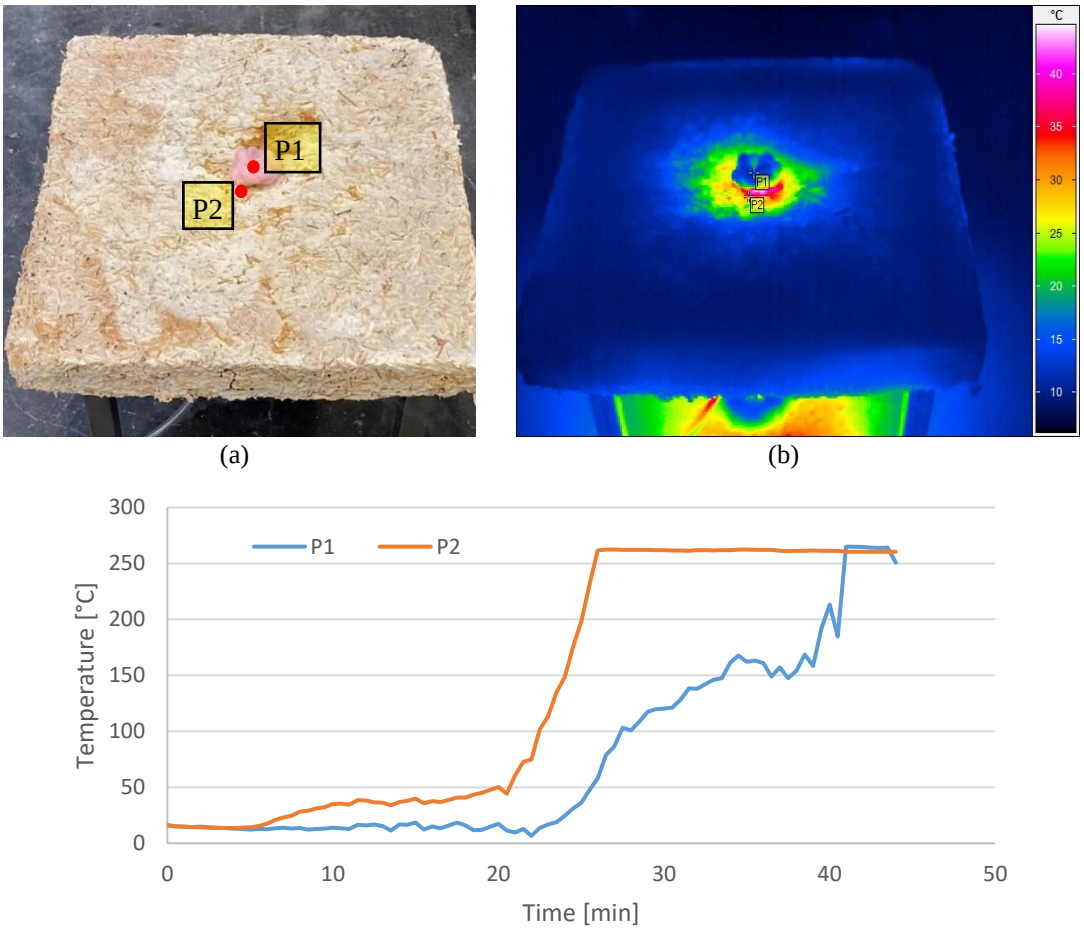

Fig. 7-22: (a) Measurement points P1 and P2 (b) Captured temperature at P1 and P2 (c) Variation of temperature at P1 and P2

Then, the same procedure was conducted on a plate with render. The side which has no render was placed over the flame, as shown in **Fig. 7-23** (a). It was burned for 1 hour and 10 minutes. Since the sample did not show any combustion over this period, the test was then stopped. It was observed that the cotton wool did not burn like in the first test, as shown in **Fig. 7-23** (b), because the fire did not go through the plate. However, it can be seen that the bottom of the plate has burned, as shown in **Fig. 7-23** (c).

(a) (b) (c)

Fig. 7-23: Plate with render subjected to fire test (a) before start to burn (b) after 1 hour and 10 minutes (c) bottom of the plate after 1 hour and 10 minutes

Based on the results from fire test and according to the EN13501-2:2003 [229], it can be concluded that the fire resistance of the Mycelium-Miscanthus composite is EI15. The classification of EI was chosen because of the consideration both parameters E and I. E is attributed if the integrity of the component is maintained and no breakthrough of flames is generated, while I is attributed if the temperature of the non-exposed side of the element does not rise over 140 ˚C [229].

7.5 CONCLUSION

Research on bioenergy crops based products are one of the key strategies to reduce the use of non-renewable resources. The current market is established for mainly non-bio based building insulation materials. However, developing and promoting bio-based building insulation materials have great benefits on the environment. This paper focused on the Mycelium-Miscanthus composites as an economical and sustainable alternative material to traditional building insulation materials. Since the thermal conductivity depends on the density, different proportions of Mycelium to Miscanthus were considered to produce lightweight porous composite. The best mix proportion was identified as G0.3_M1_P0.1 which has the mix proportions of 0.3:1:0.1 of Ganoderma resinaceum mushroom, Miscanthus x giganteus fibres and potato starch. Compressive strength and water absorption of the composite were also investigated. The microstructural geometry of the composite was evaluated using the SEM images, and it was observed that the Mycelium grew around the Miscanthus fibres. Insulation capability of the composite was measured by measuring their thermal conductivity. The thermal conductivity between 0.0882 and 0.104 Wm-1K-1 observed for new insulation material Mycelium-Miscanthus composite with average density of 122 kg/m^3. Furthermore, fire tests on composite plates were proving that they have considerable fire resistance and belong to the category EI15 according to the EN13501-2:2003. It was found that the prepared new composite has comparatively better properties than the conventional insulation materials and meet most of required for the indoor building applications.

7.6 ACKNOWLEDGEMENTS

The authors of this paper would like to thank Contern S.A. for the supply of the Miscanthus. Moreover, they would like to express their gratitude to the staff of the University of Luxembourg as well as to Mr. Mike Paulus, Mr. Yannick Zimmer and Ms. Elma Arifi for the supports given on the experimental works presented in this paper.

Chapter 8 ANALYSIS OF A WALL BASED ON MASONRY BLOCKS WITH A BEARING AND INSULATION PART BASED ON MISCANTHUS

In this section, a masonry block based on the findings of the previous chapters is analysed. First, the concept of the masonry block using a bearing and insulation part, which are connected by a dovetail connection, will be presented. The material laws are based on the results presented in Chapter 6 and Chapter 7 of this dissertation. Next, the load-bearing capacity of a wall will be analysed and a sensitivity analysis on the geometry of the masonry block will be performed by varying different geometrical parameters. Furthermore, an analytical calculation will be performed on the masonry block to investigate its thermal transmittance value and to identify the needed thickness of the insulation part considering the insulation regulations imposing a U value of 0.13 W/m^2K.

8.1 CREATION OF THE MODEL

The objective is to develop a numerical model, which includes the bearing as well as the insulation part. The dimensions of the block are based on existing masonry blocks manufactured by the company Contern S.A. for bearing and structural purposes [103]. The length of the formats presented by this company vary from 24 – 50 cm (**Table 8-1**). Since in this work, space was needed for the dovetail connection, a length of 46 cm was adopted for the numerical masonry block. Whereas, the width of the commercialised masonry blocks varied between 11.5 and 36.5 cm, the width of the numerical model was fixed to 30 cm. As the height of the manufactured masonry blocks is in average 20 cm, the imposed height of the masonry block is chosen to be 20 cm whereas a tongue of 3 cm height is added, which results in a total height of the masonry block of 23 cm.

	Luxembourgish format	DIN format	Belgian format	French format
Length [cm]	36.5 – 49	24 – 49	39	50
Width [cm]	11.5 – 36.5	11.5 – 36.5	9 – 29	5 – 30
Height [cm]	17.5	23.8	19	20
Weight [kg]	15 – 33	19 – 31	11.5 – 30	8.1 – 36.9

Table 8-1: Dimensions of the masonry blocks manufactured by Contern S.A. [103]

The material laws used in the numerical model were based on the results obtained in the previous chapters (Chapter 6 and Chapter 7). The density of the bearing and the insulation part corresponds to a Miscanthus concrete of 1082 kg/m^3, resp. 125 kg/m^3. The bearing and the insulation part have a thickness of 15.5 and 14.5 cm, which corresponds to a weight of 15.4 and 7.4 kg. These results correspond to a total weight of the numerical masonry block of 22.8 kg, which is in the range of the masonry blocks manufactured by Contern S.A. (**Table 8-1**) and is below the recommendation of 25 kg stated by the Luxembourgish accident insurance association "Association d'assurance accident" [230].

The geometry of the masonry blocks consists of a bearing and insulation part connected by a dovetail connection and two tongue groove systems, one on the vertical and one on the horizontal direction to guarantee the modular principle (**Fig. 8-1**). In the horizontal direction, the tongue-groove system with a length of HMP = 3 cm (left **Fig. 8-1**) is inserted in both parts. The tongue-groove system is also adopted vertically in the middle of the masonry block. The dimensions of the remaining parameters in the geometry are listed in annex A (Chapter 13). Furthermore, a prototype of the masonry block (**Fig. 8-2**) was performed to investigate the suitability of merging the two Miscanthus materials with a dovetail connection.

As in Chapter 6, two materials were used to design the bearing part. One for the core of the bearing part with a compressive strength and a Young's Modulus of 11 MPa, resp. 2 GPa (blue part in **Fig. 8-3**) and one for the top and bottom roughness of the bearing part with a compressive strength and a Young's Modulus of 9 MPa, resp. 0.8 GPa (pink part in **Fig. 8-3**). The distribution of the asperities of the roughness are based on **Fig. 6-8** from Chapter 6. The insulation part of the numerical masonry block (green part in **Fig. 8-3**) is principally based on the results investigated in Chapter 7. The compressive strength of this part is set to 1.4 MPa and the Young's Modulus was based on the stress strain distribution (**Fig. 7-11**) and is set to 0.11 GPa [94].

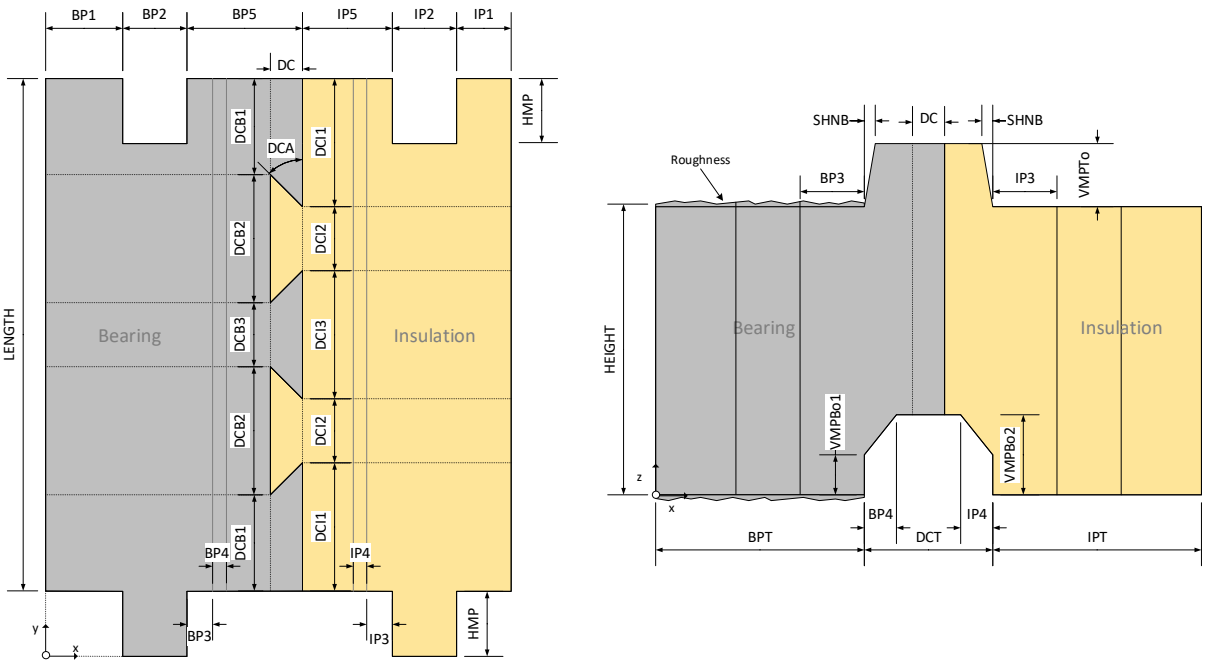

Fig. 8-1: Geometry of the numerical masonry block with a bearing and an insulation part, top (left) and front view (right)

Fig. 8-2: Prototype of the masonry block, (left) top view; (right) Bottom view

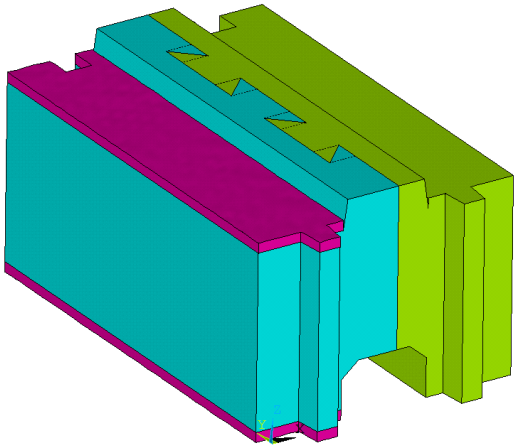

Fig. 8-3: Three materials of the numerical masonry block

Finally, a dry-stacked wall of two blocks in the length and three blocks in the height is generated using the presented masonry blocks. The contact-target method is applied on the upper and bottom surface of each masonry block, as performed in Chapter 6. In addition, the contact-target technique is also applied in the horizontal tongue-groove system. The wall is placed on a fixed steel plate (purple plate on bottom **Fig. 8-4**). The load-application is performed on the upper steel plate, which transfers the load to the bearing part on a thickness of BPT = 10 cm (right **Fig. 8-1**). Furthermore, the upper steel plate is fixed on both horizontal directions (x and y-direction), so that it can only move in the negative z-direction.

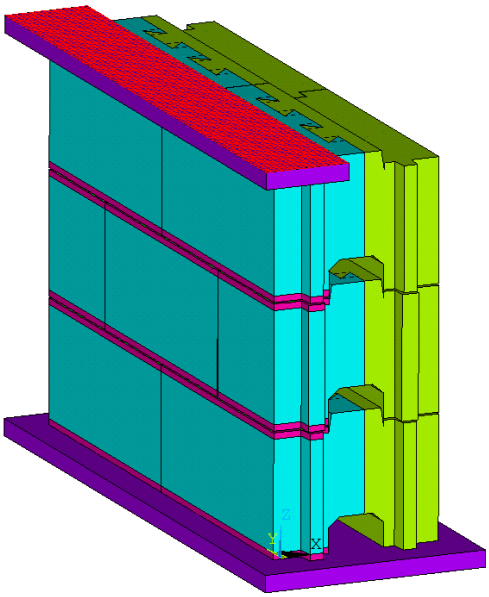

Fig. 8-4: Numerical dry-stacked wall using the masonry blocks with a bearing and an insulation part (red = load-application)

8.2 INTRODUCTION TO THE SENSITIVITY ANALYSIS OF THE GEOMETRY

The sensitivity analysis of the geometry on the load-bearing capacity of the dry-stacked masonry wall (**Fig. 8-4**) is categorised in six parts (A-F from **Table 8-2**). The variation of each category is related to the reference model previously presented. The first part (A), consists of varying the standard deviation of the roughness of the masonry blocks from 0.10 – 0.40 as performed in Chapter 6 in **Fig. 6-10**. Next, the variation B consists of implementing the geometrical height imperfections into each masonry block. Therefore, 10 calculations were performed using different height imperfections following the Gaussian distribution presented in **Fig. 6-23** (μ=0 and σ=0.285 mm). The third variation (C) consists of first varying the thickness of the bearing part, more precisely (BPT in **Fig. 8-1**) and in a next instance the thickness of the insulation part (IPT in **Fig. 8-1**).

In the fourth variation (D) two variations were investigated, the total thickness of the block and the height of the dry-stacked wall. The total thickness was varied between 25 – 35 cm by reducing or increasing simultaneously BP1 and IP1. Furthermore, the load-bearing capacity of the different heights of the wall (60, 120, 180 and 240 cm) were analysed. The next variation (E), consists of alternating the angle of the dovetail (DCA in **Fig. 8-1**) connection between 30 and 75 °. The last variation (F) consists of analysing the impact of the position of the horizontal tongue of the masonry block. Therefore, the thickness of BP1 and IP1 (**Fig. 8-1**) are reduced to 1 and 3 cm. Simultaneously, the thickness of BP3 and IP3 are increased to keep the thickness of the bearing and insulation part constant.

	Std. dev. roughness [mm]	**Height differences [-]**	**Thickness of masonry block [cm]**	**Height of wall [cm]**	**Angle of dovetail connection [°]**	**Position of tongue* [cm]**
Ref	0.30	No	30	60	45	5
A	0.10 – 0.40	No	30	60	45	5
B	0.30	Yes	30	60	45	5
C	0.30	No	27 – 40	60	45	5
D	0.30	No	25 – 35	60 – 240	45	5
E	0.30	No	30	60	30 – 70	5
F	0.30	No	30	60	45	1 – 3
Additional information: The position of the tongue is based on the variable BP1 and IP1 (**Fig. 8-1**)						

Table 8-2: Sensitivity analysis of the numerical dry-stacked wall

8.3 ANALYTICAL CALCULATION OF THE THERMAL TRANSMITTANCE VALUE

The thermal transmittance value (U) of building designs its ability to transfer heat through a structure. A low U-value of wall indicates that the object has a low capability of transmitting the heat from the inside to the outside. The U-value of a wall of a building is calculated using the sum of the thermal resistance of each material (R) and the inner (R_{si}) and exterior thermal resistance (R_{se}) as shown in eq. 8-1. The inner and the outer horizontal thermal resistance values are based on the heat flow rate imposed by the national regulation ($\alpha_{si} = 8\frac{W}{m^2K}$ and $\alpha_{se} = 25\frac{W}{m^2K}$). The thermal resistance value of the masonry block is based on the thermal conductivity λ and the thickness d of each material.

$$U = \left(R_{si} + \sum_j R_j + R_{se} \right)^{-1} \quad \text{(eq. 8-2)}$$

In the case of the numerical masonry block, the thermal resistance value is based on the materials of the bearing and the insulation part. Therefore, the thermal conductivity of each material has to be defined according to experimental tests. The thermal conductivity of the bearing part λ_{BP} is calculated using its density (1082 kg/m^3) and the equation proposed by Waldmann et al. [33], which results in $\lambda_{BP} = 0.2164\ W/mK$. The thermal conductivity of the insulation part is based on the experimental results presented in Chapter 7 and is set to $\lambda_{IP} = 0.09\ W/mK$.

8.4 NUMERICAL ANALYSIS

In this section, the numerical dry-stacked wall based on the two-part masonry blocks is used as reference and is compared to the numerical wall from Chapter 6. Next, the different variations stated in section 8.2 are compared to the reference wall.

8.4.1 COMPARISON TO THE WALL USING RECTANGULAR MASONRY BLOCKS FROM CHAPTER 6

The numerical wall based on the two-part masonry block achieved a load-bearing capacity (LBC) of 4.94 MPa (**Fig. 8-5**). This model was compared to the wall based on the rectangular masonry blocks from Chapter 6 and a similar stress-strain distribution could be observed. The two part-masonry blocks showed a more ductile behaviour due to its higher amount of bearing material compared to the rectangular blocks. However, the LBC of both models was identical, which proves that the change in the geometry of the model had a low impact on the achieved compressive strength of the wall. However, due to the different shape of the masonry blocks used in the walls, a comparison on the crack distribution between both models is performed at 25, 50, 75 and 100 % of the LBC (**Fig. 8-6** and **Fig. 8-7**). First, an

analysis is performed on the numerical wall based on the two-part masonry block and then it is compared to the numerical wall from Chapter 6.

Due to the roughness on the top and bottom surface of the masonry block, the contact faces are filled with micro cracks at 25 % of the LBC. A continuous load up to 50 % of the LBC induces cracks in the tongues of the masonry blocks. Furthermore, since the load is only applied on one side of the masonry block a rotation in y-axis occurs, which induces first horizontal cracks in the dovetail connection of the upper row. Then these cracks are increased with a continuous increase of loading and similar cracks occur in the middle row of the wall. Finally, the LBC is achieved and no total failure could be observed. The crack distribution that occurred in the numerical wall from Chapter 6 is similar to the one from the wall based on the two-part masonry blocks. First, the upper and lower rough surfaces crack due to load-application and next, the outer left side of the bearing part of the masonry blocks (**Fig. 8-4**) start to crack. It is important to mention that due to a central loading, the core of the masonry blocks does not crack, even at LBC.

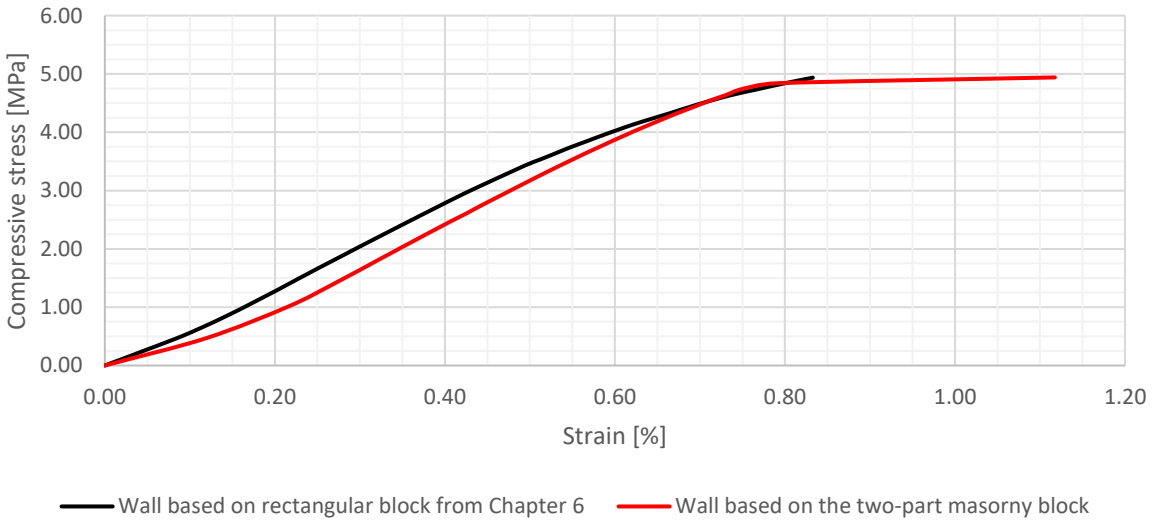

Fig. 8-5: Stress-strain distribution of the numerical wall from Chapter 6 compared to the numerical wall based on the two-part masonry block

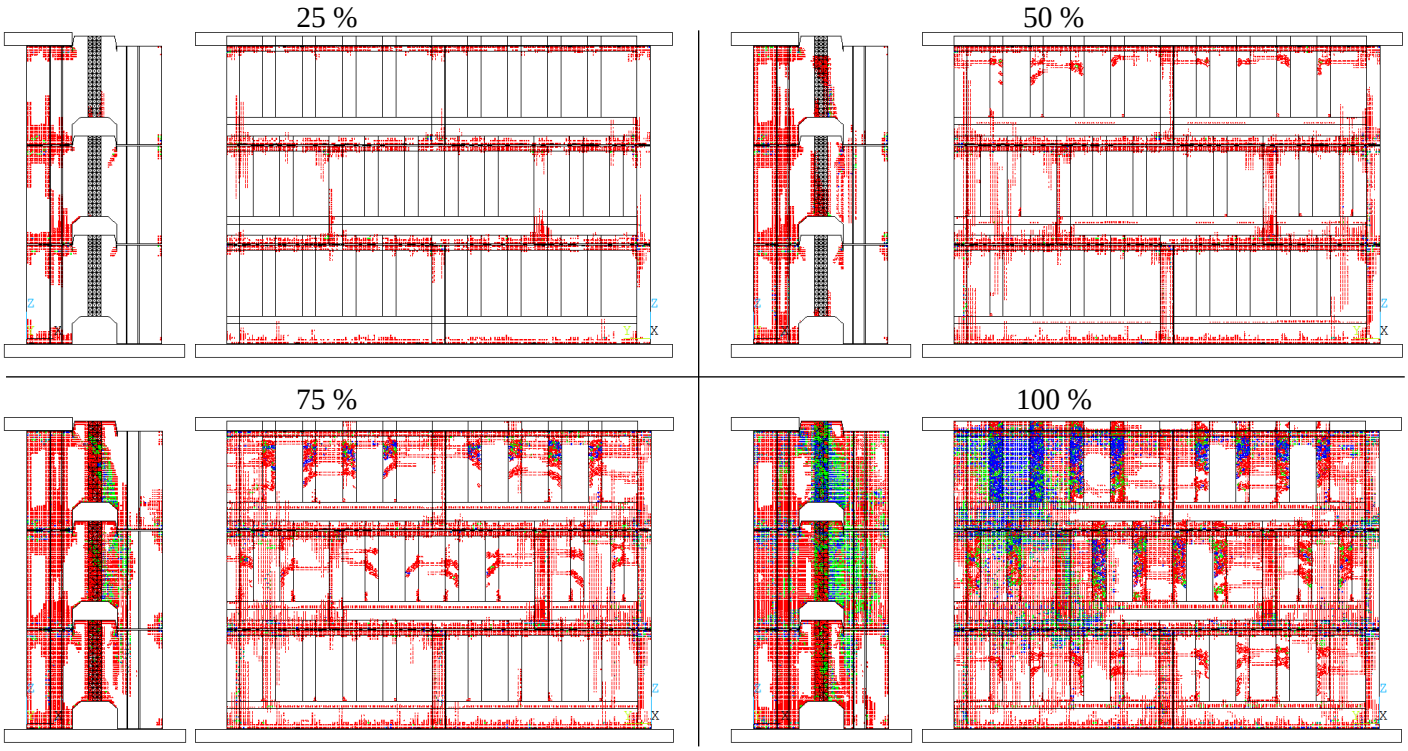

Fig. 8-6: Front and side view of the crack distribution of the numerical wall based on the two-part masonry block for a load of 25, 50, 75 and 100% of the load-bearing capacity (insulation part not included in the side view)

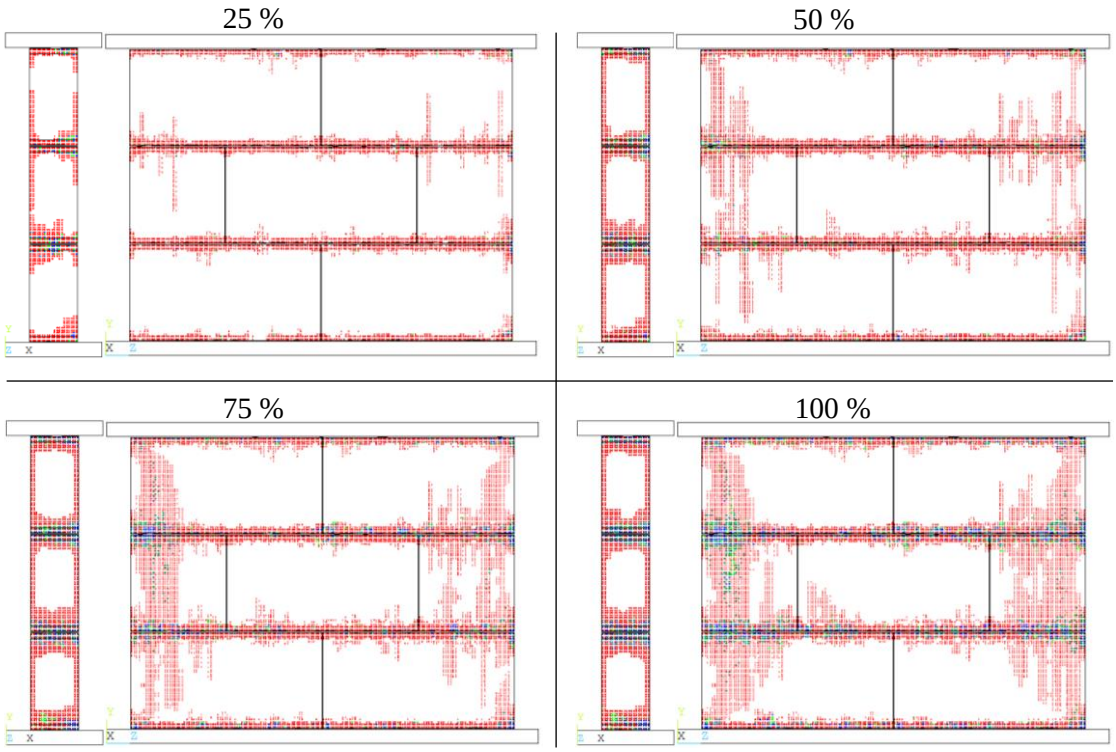

Fig. 8-7: Front and side view of the crack distribution of the numerical reference wall from Chapter 6 for load of 25, 50, 75 and 100% of the load-bearing capacity

8.4.2 SENSITIVITY ANALYSIS ON THE DRY-STACKED WALL

This section comprises the sensitivity analysis introduced in section 8.2, which compares the different variations to the reference model explained previously. One or more of the following factors will be compared to assess the most suitable model. The first element is the stress-strain distribution, followed by the contact ratio in function of the loading and finally the relation between the height of the wall and the thickness of the masonry block.

The first variation consists of varying the standard deviation of the roughness of the masonry blocks according to **Fig. 6-10** in the numerical wall. A roughness with a standard deviation of 0.10 mm (R: 0.10) resulted in the highest load-bearing capacity of 5.53 MPa (left **Fig. 8-8**), which is an increase of 12 % compared to the achieved compressive strength of the reference model. An increase of the standard deviation of the roughness induces a reduction in the load-bearing capacity and stiffness of the model. The model with the lowest standard deviation of the roughness achieved the highest compressive strength due to a higher contact at very low strength (right **Fig. 8-8**). In average, 52 % of the surfaces are in contact at a compressive strength of 1 MPa for the model R: 0.10. The other three numerical models in this graph have a contact surface between 22 and 35 % for the same compressive strength, which engenders a higher amount of punctual load on the surfaces and results in a lower compressive strength.

Next, the impact of the height imperfections is analysed on the load-bearing capacity. The elevation of the height imperfection is based on **Fig. 6-23** (μ=0 and σ=0.285 mm). Ten numerical calculations of the wall were performed inserting the height variations presented in **Fig. 8-9** for each masonry block (MB 1 – MB 7), whose nomenclature is identical with the one presented in Chapter 6 on **Fig. 6-11** (right). The height imperfections had a very low impact on the stress-strain distribution (**Fig. 8-10**) and followed a similar path as the reference model with no height differences. The load-bearing capacity of the models with height imperfections was +/- 7 % compared to the reference model. It can be concluded that due to the ductile behaviour of the Miscanthus concrete, the impact due to height differences is very low.

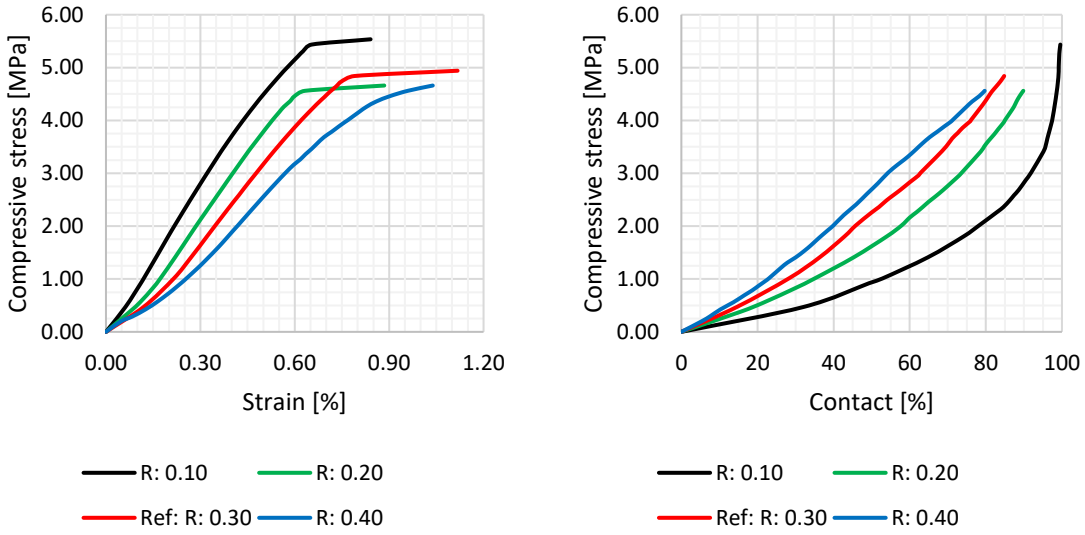

Fig. 8-8: Left: stress-strain distribution of the numerical walls with different roughness on the masonry blocks; Right: stress in function of the actual contact between the masonry blocks

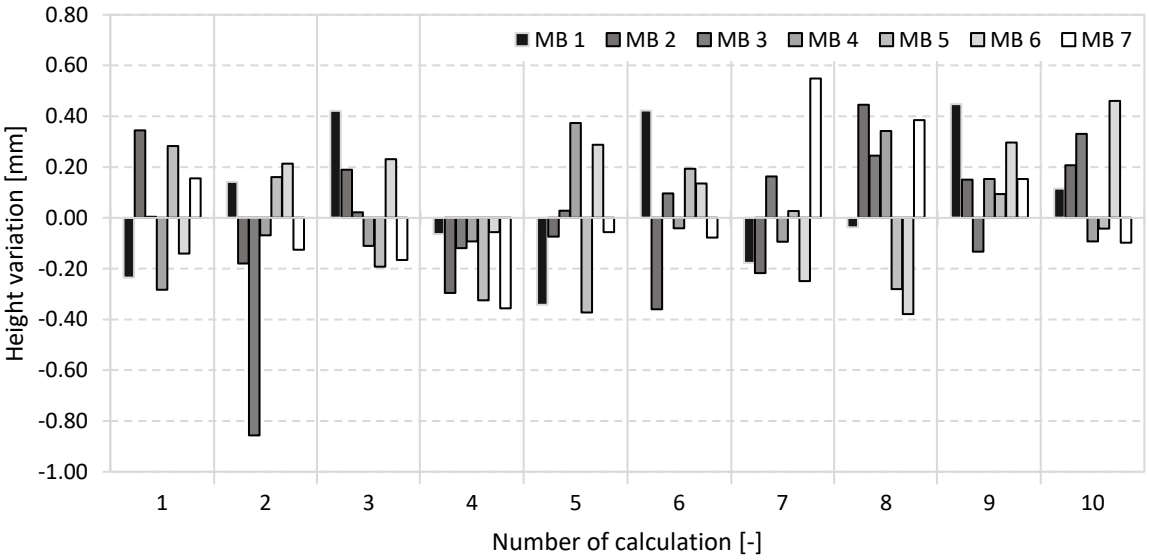

Fig. 8-9: Height variations of each masonry block for each numerical calculation in this set

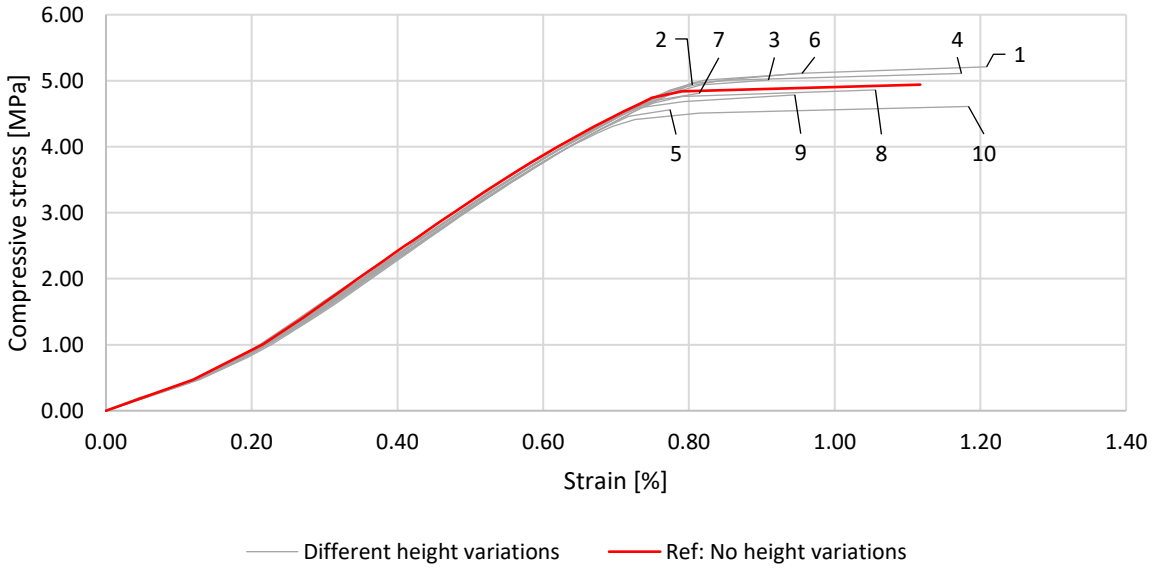

Fig. 8-10: Stress-strain distribution of 10 numerical walls (numbers in graph) with height variations based on **Fig. 8-9**

The impact of the thickness on the load-bearing capacity is analysed in three steps. The first step consists of varying the width of the bearing part (BPT) (left **Fig. 8-11**) and the second phase consists of varying the width of the insulation part (IPT) (right **Fig. 8-11**). The third and last stage consists of varying the thickness of the masonry blocks by alternating identically the thickness of the bearing and insulation part (**Fig. 8-12**).

A numerical wall based on masonry blocks with a bearing part of 20 cm (T-40; BPT-20) induces a load-bearing capacity of 9.52 MPa (left **Fig. 8-11**). A reduction of the width of the bearing part induces a reduction in the achieved compressive strength. Furthermore, reducing the thickness from 20 cm (T-40; BPT-20) by 25, 50 and 65 % induces a reduction in the load-bearing capacity of 29.7, 48.1 and 67.5 %. Therefore, it can be concluded that a linear relation can be established between the thickness of the bearing part of masonry block and the load-bearing capacity.

The variation of the thickness of the insulation part showed to have no impact on the stress-strain distribution or the achieved load-bearing capacity (right **Fig. 8-11**). This occurrence is a consequence of the eccentric load application, which leads to a buckling of the wall and reduces the load application on the insulation side. However, a too long insulation part could induce cracks in the dovetail connection due to the distance between the centre of gravity of the insulation and the bearing part. Furthermore, a long insulation part would increase the self-weight of the insulation. This circumstance could lead to a high load on the insulation side of the masonry block and provoke a failure of that side of the masonry block.

Finally, a relation between the thickness of the masonry block and the height of the wall is investigated (**Fig. 8-12**). The analysed thicknesses of the block are 25, 30 and 35 cm (t) and the height of the wall varies from 0.60 to 2.40 m (H). The highest load-bearing capacity of 5.472 MPa was achieved by the 0.60 m height wall and the masonry blocks consisting of a width of 35 cm. Independent from the thickness of the masonry blocks it can be observed that an increase of the height of the numerical wall induces a decrease in the load-bearing capacity of the masonry block. The reason for this decrease is based on the eccentric load-application, which induces an always more intensive buckling of the wall. Besides, the impact of the slenderness of the wall on the load-bearing capacity can also be related to stability aspects, which increases with increasing slenderness of the wall. Furthermore, comparing the results from **Fig. 8-12** to the achieved compressive strength of the rectangular masonry block from Chapter 6 (**Fig. 6-29**), it can be noticed that the fact of using a different geometry of the masonry block induces an exponential relation between the factor H/t and the load-bearing capacity.

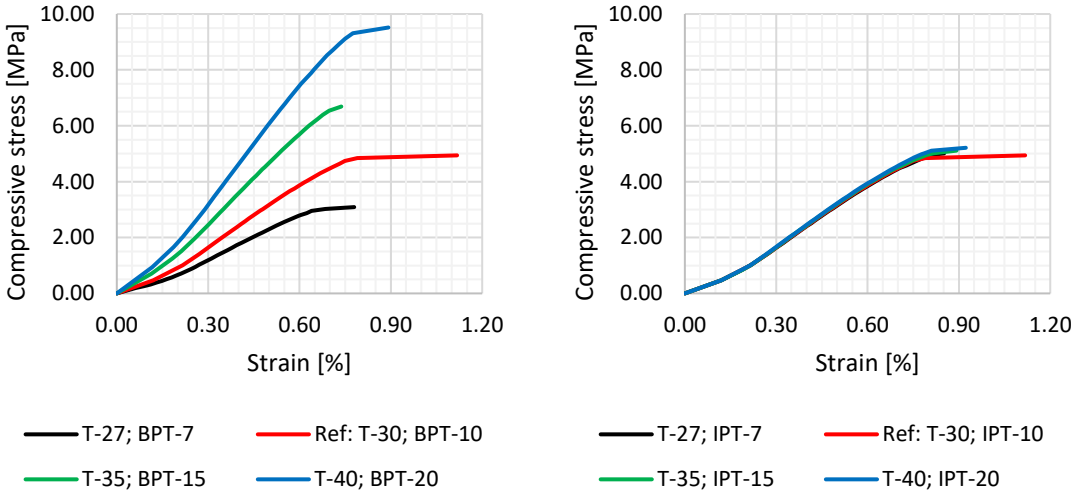

Fig. 8-11: Stress-strain distribution of the numerical walls by: (left) varying the thickness of the bearing part (BPT), (right) varying the thickness of the insulation part (IPT) (legend: T = total thickness of the masonry block and presented values are in cm)

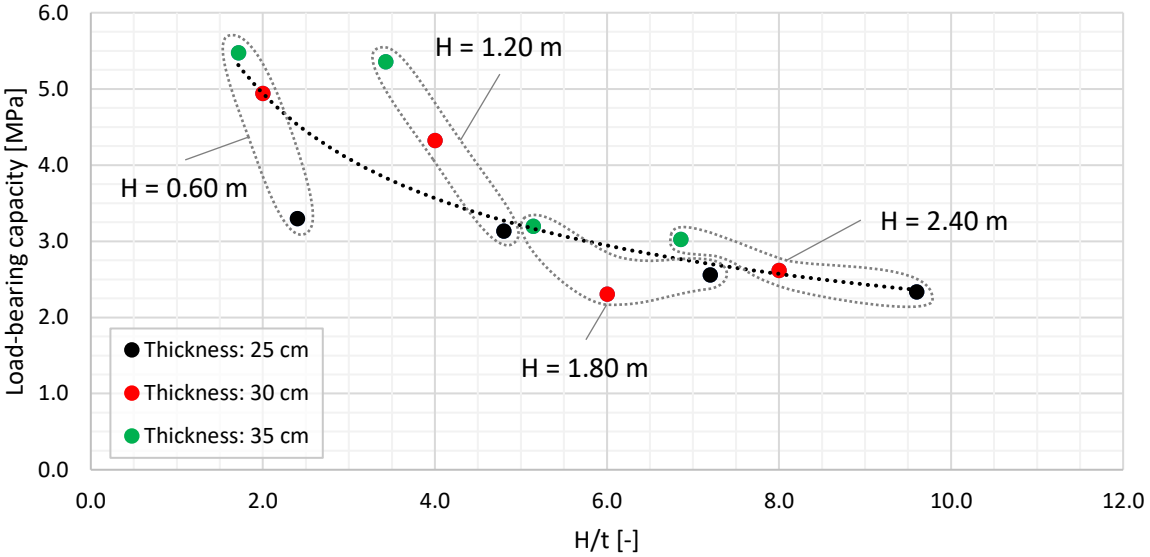

Fig. 8-12: Load-bearing capacity in function of height of the numerical wall and the thickness of the masonry block (H/t)

Next, the angle of the dovetail connection is varied. The bearing and the insulation part of the reference model are connected by a dovetail connection with an angle of 45°. The stress-strain distribution was not affected by the variation of the angle of connection. Therefore, only the achieved load-bearing capacity is presented **Fig. 8-13** (left) in function of the angle of the dovetail connection. It can be observed that varying the angle from 45° reduces the load-bearing capacity up to 6 %. Therefore, it can be concluded that considering the achieved compressive strength an angle of 45° is the most suitable. An alternative angle of the dovetail connection would worsen the bond between both parts of the masonry block and reduce the load-bearing capacity. However, if for any reason a different angle would ease the manufacture process of the masonry blocks in the industry, this loss of strength has to be taken into consideration.

According to the results presented in **Fig. 8-13** (right), a similar observation can be performed in the position of the tongue. Putting the tongue at 3 cm from the border of the masonry block has a positive impact of 5 % on the load-bearing capacity of the numerical wall. This length of 3 cm shows to be the most suitable and optimal, because it allows the tongue to be the farthest away from the outer and the inner face of the masonry block (BP1=3 cm and BP3=4 cm). However, as for the angle of the dovetail connection, if for any reason a different position of the tongue would ease the manufacture process, its impact has to be taken into consideration.

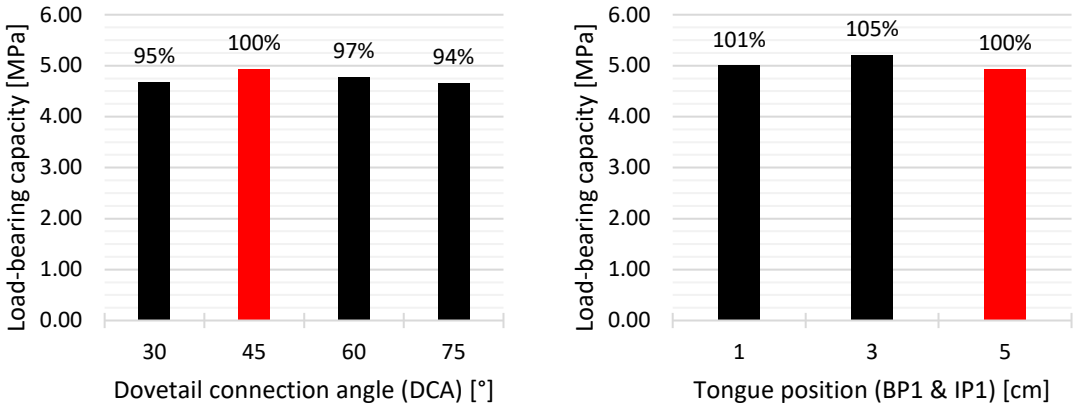

Fig. 8-13: (Left) – load-bearing capacity in function of the dovetail connection, (right) – load-bearing capacity in function of the position of the tongue of the masonry block

8.5 THERMAL TRANSMITTANCE VALUE OF THE MASONRY BLOCK

The thermal transmittance value (U) of the masonry block is calculated based on eq. 8.1. Therefore, a thermal conductivity of 0.2164 W/mK and 0.09 W/mK is set for the bearing and insulation part. In **Fig. 8-14**, the thermal transmittance value is presented in function of the thickness of the masonry block. The latter is based on a bearing part with a width of 0.155 m and a varying thickness for the insulation part. Furthermore, the limit imposed by the regulations is set in black to U=0.13 W/m^{2}K in **Fig. 8-14**. Currently, the masonry block used previously in the numerical calculation with an insulation thickness of 0.145 m possesses a thermal transmittance value of U=0.40 W/m^{2}K. It is obvious that with an increase of the thickness a decreasing U-value is expected. Therefore, the aim of this diagram is to figure out the needed thickness of the insulation to achieve the imposed limit using only one masonry block. The intersection point between the U-value of the masonry block and the imposed limit is achieved if at least a total thickness of the masonry block of 0.77 m is used. The latter value consists of 0.155 m of the bearing part and 0.615 m of the insulation part. A masonry block with these dimensions would weigh 22.5 kg which is below the recommendation of 25 kg [230]. However, it is clear that the production and transport of such a masonry block to a construction site would induces several difficulties. Therefore, a possible solution would be to transport both parts separately to a construction site and slide them together while constructing a wall.

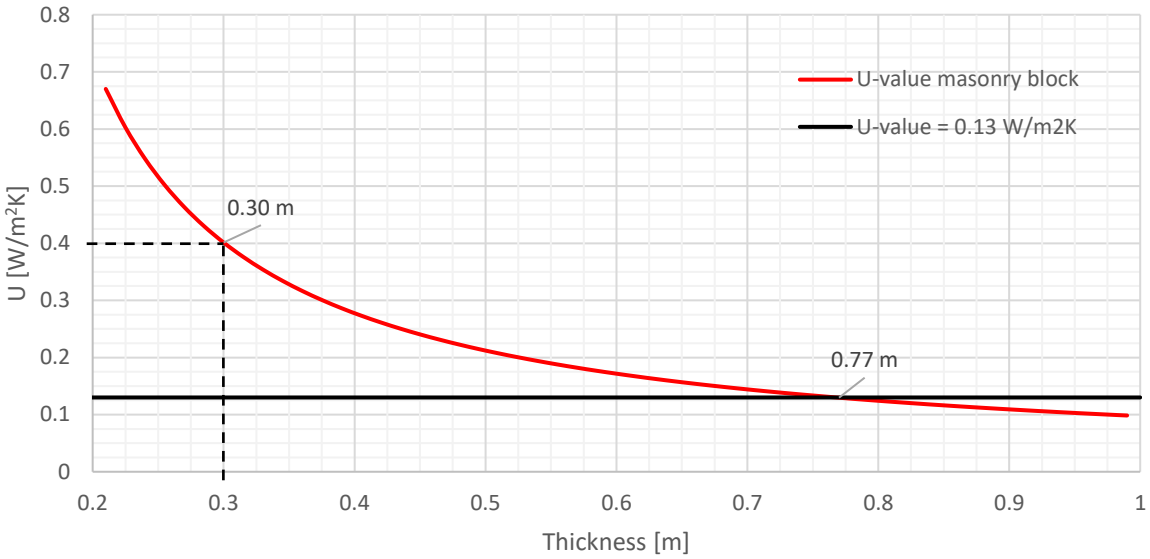

Fig. 8-14: Thermal transmittance value of the masonry block in function of its thickness

8.6 CONCLUSION

In the present study, the use of a masonry block based on a bearing and an insulation part is analysed on its application in a wall by numerical calculations and its thermal transmittance value by analytical calculations. The conclusions drawn from the performed analysis can be summarised as follows:

- The numerical wall based on masonry blocks with a bearing and an insulation part achieve the same load-bearing capacity (4.94 MPa) as the wall based on the rectangular masonry blocks. The biggest difference between both models is the crack distribution. Conversely, to the wall based on the rectangular masonry blocks, the core of the blocks also cracks.
- The sensitivity analysis showed that a lower roughness induces a higher contact at a low load-application, which results in a higher load-bearing capacity.
- The geometrical imperfections in height had a low impact on the load-bearing capacity of the numerical wall (+/- 7 %), as it was the case for the numerical wall based on rectangular masonry blocks.
- An increase in thickness of the bearing part (BPT) resulted in an increment of the achieved load-bearing capacity. This statement drove to deduce that the thickness BPT and the load-bearing capacity have a linear relation.
- A variation of the thickness of the insulation part had no impact on the achieved compressive strength.
- An increase in the height of the wall has a negative exponential impact on the load-bearing capacity, due to lateral bending and thus stability aspects. This occurrence appears independent from the thickness of the masonry block. However, the impact of the wall's slenderness can also not be neglected.

- The ideal angle for the dovetail connection is 45° and the position of the tongue (BP1) is 3 cm. However, since these two variations have a low impact on the load-bearing capacity (-6 % and +5 %), the value which is the most suitable to ease the manufacture process should be adopted.

Finally, it can be concluded that the possibility to create a masonry block based on Miscanthus with a bearing and insulation part exists and that it can be applied on a wall. Furthermore, the masonry block could also respect the thermal transmittance value of U=0.13 W/m^{2}K if a thickness of 61.5 cm is used for the insulation side, which would result in a total thickness of 77 cm of the masonry block. This high width of insulation could lead to difficulties e.g. in transportation. Therefore, a possible solution to overcome this problem would be to join the bearing and the insulation part on a construction site. The disadvantage of one additional working step is recovered by the advantage that both materials can be joined together due to the dovetail connection and no additional material is needed.

Chapter 9 SUMMARY

The principal aim of this research is to analyse an insulation masonry block based on Miscanthus concrete. Therefore, a masonry block based on two parts, a bearing and an insulation part, is developed. The structural and insulation properties of each material are investigated in this thesis. Furthermore, the use of a dry-stacked shape of a masonry block in a wall is numerically analysed to determine its behaviour.

In this summary the principal findings and conclusions of this cumulative dissertation entitled “Dry-stacked insulation masonry blocks based on Miscanthus concrete” are presented. The principal aim is to increase the sustainability in the construction sector by using a sustainable material such as Miscanthus as concrete mixture in a masonry block. Therefore, the highest possible amount of Miscanthus aggregates should be used without using sand or any coarse aggregates to reduce depletion due to the extraction of these. These goals were the basis to reach the conclusions presented in the following paragraphs.

The study of a Miscanthus lightweight concrete allowed concluding that doubling the amount of Miscanthus aggregates in a mixture would lead to a reduction of at least 80 % of the load-bearing capacity. Furthermore, a pre-treatment of the Miscanthus fibres was not beneficial considering the compressive strength. However, the pre-treatment on the fibres was important considering the shrinkage behaviour. The mixtures based on Miscanthus fibres pre-treated with a silicate sealant achieved in average 10 % less long-term deformations than the mixtures based on Miscanthus fibres pre-treated with a cement-based treatment (CQCH). Finally, the most promising mixture experimentally investigated consisted of 150 kg/m^3 of Miscanthus, 592 kg/m^3 of cement and a W/C ratio between 0.7 and 0.8.

414 sets, consisting of ten predictors and one response, were analysed using a machine-learning tool to predict the achieved compressive strength of prisms or cubes cured for 7, 14 or 28 days. The Gaussian

process regression was used to determine the load-bearing capacity. Furthermore, two kernel functions, squared exponential and rational quadratic, were investigated to analyse their impact on the result. The determination of the most accurate kernel function was performed using four indicators MAE, MSE, RMSE and R^2. According to these factors, the Gaussian process regression based on the rational quadratic function was the most accurate to predict the compressive strength of the specimens. In addition, a user interface was developed to analyse the sensitivity of each component on the load-bearing capacity and optimise the mixture accordingly.

In the following, the application of a Miscanthus concrete mixture on masonry blocks is analysed experimentally and numerically on single masonry blocks and on dry-stacked walls. The experimental part consists also of investigating the most suitable mixture and mixture procedure to be used for the production of a masonry block. The most convenient mixture procedure considering the load-bearing capacity consists of introducing the Miscanthus fibres to a first created cement paste. This procedure allows the cement to use the needed water and let the excess of water be absorbed by the fibres.

Furthermore, the impact of the geometrical height and roughness imperfections on the load-bearing capacity are investigated. The latter was performed by measuring the top and bottom contact surfaces of the masonry blocks, which allowed extracting an exponential relation between the compressive strength and the contact surface. The latter was also measured on the walls and a contact in the joints between two interlocking blocks of 59 % was measured. The geometrical height imperfections could be reduced by 82 % by adapting the filling procedure of the masonry blocks. Finally, a numerical model of the masonry block and the wall was established and it could be concluded that the geometrical height imperfections of the masonry blocks affected the load-bearing capacity by only 2.1 %.

The current building insulation materials are mostly based on non-renewable resources. In this work, an insulation based on Miscanthus was established using Mycelium and starch, which signifies that only organic components were used. Furthermore, this bio-based insulation is a very interesting, economical and sustainable material for the construction sector. As analysed using an SEM analysis, the bond between the biomaterials consists of the Mycelium webs growing around the Miscanthus. This composite achieved a thermal conductivity of 0.09 W/mK with a density of 122 kg/m^3. Furthermore, the fire resistance of this composite achieved the category of EI15 according to the standard EN13501-2:2003.

In the last part of this dissertation, the defined material properties of the bearing and the insulation material are used to develop a numerical masonry block with bearing and insulation properties and apply it on a numerical dry-stacked wall. The latter achieved a load-bearing capacity of 4.94 MPa. Furthermore, the sensitivity analysis of the model showed that the geometrical height imperfections of the masonry block had a low impact on the load-bearing capacity of the dry-stacked wall. Furthermore,

a linear relation was established between the thickness of the bearing part BPT and the achieved load-bearing capacity. Conversely, the thickness of the insulation part had no impact on the achieved compressive strength. An increase in the height of the numerical wall resulted in an exponential decrease in the load-bearing capacity, due to lateral bending. Finally, the analysis on the needed thickness of the masonry block to achieve the imposed thermal transmittance value of $U=0.13\ W/m^2K$ resulted in a needed insulation part of 61.5 cm, which would induce a total thickness of the masonry block of 77 cm. This width could lead to difficulties in different domains. Therefore, one possible solution suggested by the author to reduce the difficulties would be to join the bearing and the insulation part only on the construction site. This disadvantage would be retrieved by the usage of the dovetail connection to join the materials, which avoids the use of additional material and skilled labour people.

Finally, it can be concluded that the aim of this research was achieved and a masonry block based on Miscanthus with bearing and insulation properties could be presented. The properties of both materials as well as their use as a masonry block in a dry-stacked wall were investigated in this thesis. The results provided in this work can be used to expand the sustainable construction. The use of lightweight concrete based on Miscanthus can be extended by using the optimal mixture based on the Machine-learning tool. Furthermore, the masonry block based on Miscanthus is optimal for a dry-stacked system due to its low Young's Modulus, which prevents the use of mortar or any additional material between the joints.

Lastly, it can be concluded that the presented work has a significant scientific impact on the current research about the use of Miscanthus in the construction sector. The research in this field is not completed, but can be seen as an endless improvement of actual complications. Numerous improvements could be performed in the frame of this thesis. However, as it is a time-limited project, the researcher could not tackle the presented subjects more in detail. Therefore, different additional open questions and future potential projects based on this research project are highlighted in the following chapter.

Chapter 10 OUTLOOK

The findings and the techniques used in this thesis could be used to further investigate the application of Miscanthus in the construction sector. Although, the results presented have a stable foundation, different aspects in this dissertation could be further developed and analysed. They could not be treated yet, as it would have extended the length of this dissertation. Therefore, a short recapitulation of a possible outlook is presented in the following paragraphs.

Assessment of the precise fibre orientation in a specimen

The assessment as well as the prediction of the precise fibre orientation in a specimen would increase the comprehension in the stress distribution at a macro scale. The determination could be performed on a large-scale specimen, by cutting it at constant small intervals of 1 or 2 cm and analysing the positioning of the fibres at each cut surface using e.g. photogrammetry and object reconstruction. This technique would allow developing a 3D numerical model using the 2D images. Moreover, the application of a machine-learning tool could be chosen to learn the positioning of the fibres and predicting the stress distribution inside of the specimen, which could allow a prediction of the cracks in the specimen. This knowledge could be used to fortify the weaker positions in different ways.

Replace the non-sustainable materials in the bearing mixture

A high amount of the bearing mixture presented in this dissertation is cement. It is known that the CO_2 footprint of cement is very high, principally due to the calcination process during production. Therefore, one possible solution would be to investigate the partial or complete replacement of cement by a waste product like gravel wash mud. However, such a change would interfere in the bond between the Miscanthus and the binder. Therefore, a complete analysis should be performed to analyse the impact of this change on the load-bearing capacity of the specimens. The use of this kind of material could reduce

the CO_2 emission considering the life cycle of manufacturing a masonry block based on Miscanthus concrete. Another solution would be to reduce the ratio Miscanthus/binder by reducing the amount of cement in the mixture, which would also reduce the environmental impact of this Miscanthus bearing mixture.

Experimentally investigate the masonry block with two parts and development

Even if one part of the presented masonry block was created (**Fig. 10-1**), during the framework of this thesis, it could not be investigated experimentally. Therefore, an additional study to assess the numerical model could be performed. Furthermore, different tests could be further evaluated, like a measurement of thermal transmittance value of a wall. This could be performed in addition to the already performed thermal conductivity tests on the used materials. The aim of the proposed test would be to investigate the impact of the tongue and groove system on the thermal transmittance value. Moreover, a very crucial point would be to develop the masonry block based on a bearing and insulation part for an edge or header. These pieces should then be investigated numerically to develop a sensitivity analysis on them to optimise their shape according to the conditions of use.

Fig. 10-1: Masonry block with dovetail connection and tongue-groove system horizontally and vertically

Improve the thermal conductivity of the insulation material based on Miscanthus

The thickness of the presented numerically masonry block could be a burden for his evolution and application. Therefore, it is crucial to reduce the size of the insulation part to achieve a masonry block with a thickness below 50 cm. This could be performed by reducing the thermal conductivity of the Miscanthus-Mycelium composite by at least 45 %. Different approaches to achieve this goal could be

performed. One suggestion could be opting for less and better-distributed Miscanthus fibres over the specimen. Another suggestion would be to implement a supplementary sustainable material to improve the thermal conductivity and keep the sustainability of the presented insulation. However, if changes are performed on the presented Mycelium-Miscanthus composite, the presented results cannot be used and new experimental analysis have to be performed.

The function of a Mycelium-Miscanthus composite as insulation Material has still to be validated, as there are still a lot of open questions regarding this construction material. One of them is the long-time behaviour of the Mycelium. It could deteriorate after exposure to the environmental conditions of the outside due to temperature variations of exposure to UV radiation. Furthermore, an analysis on the possibility of the Mycelium starting to grow again should be performed, as it is exposed to any microbe from the outside. In addition, the risk that other fungus will settle on the surface of the Mycelium-Miscanthus must still be analysed. These aspects as well as different production aspects of the Mycelium should be considered before using a complete sustainable insulation based on Mycelium-Miscanthus.

Progression from laboratory to automatic industrial process

A complicated and demanding challenge is the transition from the production under laboratory conditions to the automatic industrial process. This transition has to be analysed in detail and accurately for every processing step, such as component preparation, mixture composition and manufacture of masonry block. Furthermore, in addition to the cost intensive investment a meticulous analysis should be performed on the method of producing the masonry block, which is very complex due to the dovetail connection and the tongue-groove systems to adopt the dry-stacked system.

Chapter 11 LIST OF FIGURES

Chapter 1

Chapter 3

Chapter 4

Chapter 5

Chapter 6

Chapter 7

Chapter 8

Chapter 10

Chapter 13

Chapter 12 LIST OF TABLES

Chapter 3

Chapter 4

Chapter 5

Chapter 6

Chapter 13 ANNEX A

This annex provides the detail measurements of the numerical masonry block used in Chapter 8.

MB_Length	:	0.46	m	IP4	:	0.02	m
MB_Height	:	0.20	m	IP5	:	0.055	m
TotHeight_MB	:	0.23	m	SHNB	:	0.005	m
DCT	:	0.10	m	DC	:	0.03	m
BPT	:	0.10	m	DCI1	:	0.11	m
IPT	:	0.10	m	DCI2	:	0.06	m
BP1	:	0.05	m	DCI3	:	0.12	m
BP2	:	0.03	m	DCB1	:	0.08	m
BP3	:	0.02	m	DCB2	:	0.12	m
BP4	:	0.02	m	DCB3	:	0.06	m
BP5	:	0.085	m	HMP	:	0.03	m
IP1	:	0.05	m	VMPTo	:	0.033	m
IP2	:	0.03	m	VMPBo1	:	0.033	m
IP3	:	0.02	m	VMPBo2	:	0.05	m

Table 13-1: Dimensions of the numerical masonry block

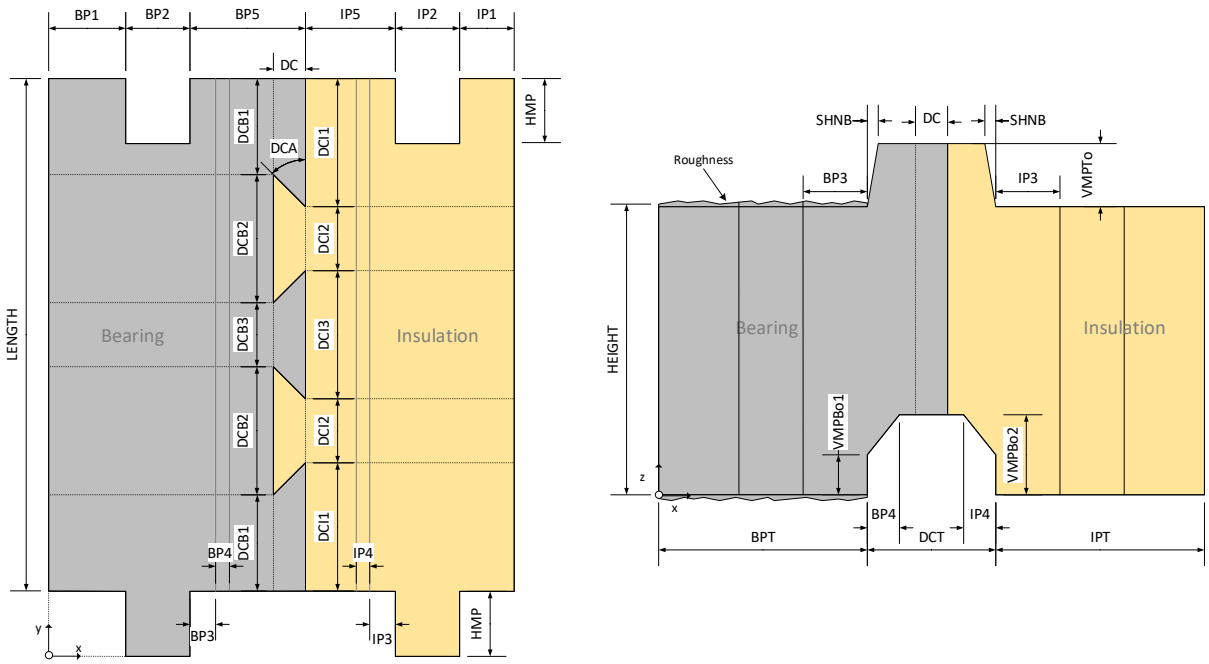

Fig. 13-1: Geometry of the numerical masonry block with a bearing and an insulation part

Chapter 14 REFERENCES

[1] J. M. Greef and M. Deuter, *Syntaxonomy of Miscanthus x giganteus GREEF et DEU.* ANGEWANDTE BOTANIK, 1993, vol. 67, no. 3/4, p. 87-90.

[2] P. Ralf, *Bedeutung morphologischer, chemischer und physikalischer Parameter sowie ihre Interaktionen zur Beurteilung der Baustoffeignung unterschiedlicher Miscanthus-Herkünfte*. Beiträge zu Agrarwissenschaften. Vol. 30. 2005, Bad Neuenahr: Wehle.

[3] R. Mayr, *Lagerungs- und Heiztechnik bei Miscanthus in Österreich*, in *Beiträge zu Agrarwissenschaften*. 2000, Wehle: Bad Neuenahr. p. 80-83

[4] A. Lischka, *Miscanthus als Energiequelle: Der neue Miscanthus-Heizkessel der Firma*, in *Beiträge zu Agrarwissenschaften*. 2004, Wehle: Bad Neuenahr. p. 80

[5] P. Carver, *Commercial crops of Miscanthus in UK*, in *Beiträge zu Agrarwissenschaften*. 2002, Wehle: Bad Neuenahr. p. 60-64

[6] I. Lewandowski, J. Clifton-Brown, A. Kiesel, A. Hastings, et al., *2 - Miscanthus*, in *Perennial Grasses for Bioenergy and Bioproducts*, E. Alexopoulou, Editor. 2018, Academic Press. p. 35-59 DOI: https://doi.org/10.1016/B978-0-12-812900-5.00002-3.

[7] K. Głowacka, *A review of the genetic study of the energy crop Miscanthus.* Biomass and Bioenergy, 2011, vol. 35, no. 7, p. 2445-2454, DOI: https://doi.org/10.1016/j.biombioe.2011.01.041.

[8] F. H. Farms, *Fox Hollow Farms*, [cited 2021]; Available from: https://heritagemiscanthus.com/.

[9] E. A. Heaton, F. G. Dohleman, A. F. Miguez, J. A. Juvik, et al., *Chapter 3 - Miscanthus: A Promising Biomass Crop*, in *Advances in Botanical Research*, J.-C. Kader and Delseny, M., Editors. 2010, Academic Press. p. 75-137 DOI: https://doi.org/10.1016/B978-0-12-381518-7.00003-0.

[10] T. Le Ngoc Huyen, C. Rémond, R. M. Dheilly, and B. Chabbert, *Effect of harvesting date on the composition and saccharification of Miscanthus x giganteus.* Bioresource Technology, 2010, vol. 101, no. 21, p. 8224-8231, DOI: https://doi.org/10.1016/j.biortech.2010.05.087.

[11] P. Ralf, *Die Winterfestigkeit von Miscanthus in der Etablierungsphase.* Beiträge zu Agrarwissenschaften. Vol. 14. 1997, Witterschlick/Bonn: Wehle.

[12] K. U. Schwarz, D. P. L. Murphy, and E. Schnug, *Studies of the growth and yield of Miscanthus X giganteus in Germany.* Aspects of Applied Biology, 1994, no. 40ii, p. 533-540.

[13] E. Anderson, R. Arundale, M. Maughan, A. Oladeinde, et al., *Growth and agronomy of Miscanthus x giganteus for biomass production.* Biofuels, 2011, vol. 2, no. 1, p. 71-87, DOI: https://doi.org/10.4155/bfs.10.80.

[14] D. G. Christian, A. B. Riche, and N. E. Yates, *Growth, yield and mineral content of Miscanthus×giganteus grown as a biofuel for 14 successive harvests.* Industrial Crops and Products, 2008, vol. 28, no. 3, p. 320-327, DOI: https://doi.org/10.1016/j.indcrop.2008.02.009.

[15] U. Jørgensen, *Benefits versus risks of growing biofuel crops: the case of Miscanthus.* Current Opinion in Environmental Sustainability, 2011, vol. 3, no. 1, p. 24-30, DOI: https://doi.org/10.1016/j.cosust.2010.12.003.

[16] V. Pidlisnyuk, T. Stefanovska, E. E. Lewis, L. E. Erickson, et al., *Miscanthus as a Productive Biofuel Crop for Phytoremediation.* Critical Reviews in Plant Sciences, 2014, vol. 33, no. 1, p. 1-19, DOI: https://doi.org/10.1080/07352689.2014.847616.

[17] N. Bilandžija. *Perspective and potential use of Miscanthus x Giganteus Culture in Croatia*. in *13th international waste management symposium*. 2014. Zagreb.

[18] B. Barbosa, S. Boléo, S. Sidella, J. Costa, et al., *Phytoremediation of Heavy Metal-Contaminated Soils Using the Perennial Energy Crops Miscanthus spp. and Arundo donax L.* BioEnergy Research, 2015, vol. 8, p. 1500-1511, DOI: https://doi.org/10.1007/s12155-015-9688-9.

[19] M. N. Zealand, *Miscanthus x giganteus (MxG) Research,* [cited 2021]; Available from: https://www.miscanthus.co.nz/miscanthus-x-giganteus-mxg-research/.

[20] B. Chabbert, A. Habrant, M. Herbaut, L. Foulon, et al., *Action of lytic polysaccharide monooxygenase on plant tissue is governed by cellular type.* Sci Rep, 2017, vol. 7, no. 1, p. 17792, DOI: https://doi.org/10.1038/s41598-017-17938-2.

[21] P. Klímek, R. Wimmer, P. Meinlschmidt, and J. Kúdela, *Utilizing Miscanthus stalks as raw material for particleboards.* Industrial Crops and Products, 2018, vol. 111, p. 270-276, DOI: https://doi.org/10.1016/j.indcrop.2017.10.032.

[22] R. Pude, C. H. Treseler, R. Trettin, and G. Noga, *Suitability of Miscanthus Genotypes for Lightweight Concrete.* Die Bodenkultur - Journal for Land Management, Food and Environment, 2005, vol. 56, no. 1/4, p. 61-69.

[23] D. P. L. Murphy, J.-G. Krentler, and H. Georg, *Einsatz von schnellwachsenden Rohstoffen im Bauwesen.* Landtechnik, 1995, vol. 50, no. 6, p. 342-355.

[24] B. Görtz, R. TRETTIN, T. Kowald, and R. Pude. *Nutzung nachwachsender Rohstoffe in Bindebaustoffen – Hydratationsverlauf, Mikrogefüge und Eigenschaften*. in *GDCh-Tagung Bauchemie*. 2004. Erlangen.

[25] Miscanthus.de and R. Pude, *Verwertungsvielfalt von Miscanthus* 2012 [cited 2020]; Available from: http://miscanthus.de/verwertung.html.

[26] T. B. Voigt, *Are the environmental benefits of Miscanthus × giganteus suggested by early studies of this crop supported by the broader and longer-term contemporary studies?* GCB Bioenergy, 2015, vol. 7, no. 4, p. 567-569, DOI: https://doi.org/10.1111/gcbb.12150.

[27] J. Dauber, C. Brown, A. L. Fernando, J. Finnan, et al., *Bioenergy from "surplus" land: environmental and socio-economic implications.* BioRisk, 2012, vol. 7, p. 5-50.

[28] R. Hesch, *Bau- und Dämmplatten sowie Schüttdämmung aus Miscanthus x giganteus*, in *Beiträge zu Agrarwissenschaften*. 2000, Wehle. p. 63-67

[29] K. Kaack, K.-U. Schwarz, and P. E. Brander, *Variation in morphology, anatomy and chemistry of stems of Miscanthus genotypes differing in mechanical properties.* Industrial Crops and Products, 2003, vol. 17, no. 2, p. 131-142, DOI: https://doi.org/10.1016/S0926-6690(02)00093-6.

[30] B. Ruxanda, C. Teacă, and I. Spiridon, *Chemical modification of beech wood: Effect on thermal stability*. BioResources, 2008, vol. 3, p. 789-800.

[31] V. Richins Myers and B. Gilette, *Five Common Varieties of Beech Trees*, the Spruce 2020 [cited 2021]; Available from: https://www.thespruce.com/five-kinds-of-beech-trees-3269706.

[32] M. Suwak, *Conifer Confusion: An Identification Guide for Pine, Spruce, and Fir Trees*, Gardener's path 2017 [cited 2021]; Available from: https://gardenerspath.com/plants/landscape-trees/identifying-conifers/.

[33] D. Waldmann, V. Thapa, F. Dahm, and C. Faltz, *Masonry Blocks from Lightweight Concrete on the Basis of Miscanthus as Aggregates*, in *Perennial Biomass Crops for a Resource-Constrained World*. 2016. p. 273-295 DOI: https://doi.org/10.1007/978-3-319-44530-4_23.

[34] H. Açikel, *Mechanical properties of miscanthus reinforced concrete.* International Journal of Development Research, 2018, vol. 8, p. 23789-23793.

[35] C. Godard, J. Boissy, and B. Gabrielle, *Life-cycle assessment of local feedstock supply scenarios to compare candidate biomass sources.* GCB Bioenergy, 2013, vol. 5, no. 1, p. 16-29, DOI: https://doi.org/10.1111/j.1757-1707.2012.01187.x.

[36] S. Wang, S. Wang, A. Hastings, M. Pogson, et al., *Economic and greenhouse gas costs of Miscanthus supply chains in the United Kingdom.* GCB Bioenergy, 2012, vol. 4, no. 3, p. 358-363, DOI: https://doi.org/10.1111/j.1757-1707.2011.01125.x.

[37] OECD, *Global Material Resources Outlook to 2060: Economic Drivers and Environmental*. 2019, Paris: OECD Publishing, no.°p. 212, DOI: https://doi.org/10.1787/9789264307452-en.

[38] L. T. T. Vo and P. Navard, *Treatments of plant biomass for cementitious building materials – A review.* Construction and Building Materials, 2016, vol. 121, p. 161-176, DOI: https://doi.org/10.1016/j.conbuildmat.2016.05.125.

[39] L. Long-Jiao, W. Yue-Ping, W. Ge, C. Hai-Tao, et al., *Evaluation of Properties of Natural Bamboo Fiber for Application in Summer Textiles* Journal of Fiber Bioengineering and Informatics 2010, vol. 3, no. 2, p. 94-99, DOI: https://doi.org/10.3993/jfbi09201006.

[40] A. M. Mullen, C. Álvarez, M. Pojić, T. D. Hadnadev, et al., *Chapter 2 - Classification and target compounds*, in *Food Waste Recovery*, C.M. Galanakis, Editor. 2015, Academic Press: San Diego. p. 25-57 DOI: https://doi.org/10.1016/B978-0-12-800351-0.00002-X.

[41] O. Faruk, A. K. Bledzki, H.-P. Fink, and M. Sain, *Biocomposites reinforced with natural fibers: 2000–2010.* Progress in Polymer Science, 2012, vol. 37, no. 11, p. 1552-1596, DOI: https://doi.org/10.1016/j.progpolymsci.2012.04.003.

[42] S. S. Munawar, K. Umemura, and S. Kawai, *Characterization of the morphological, physical, and mechanical properties of seven nonwood plant fiber bundles.* Journal of Wood Science, 2007, vol. 53, no. 2, p. 108-113, DOI: https://doi.org/10.1007/s10086-006-0836-x.

[43] K. Kaack and K.-U. Schwarz, *Morphological and mechanical properties of Miscanthus in relation to harvesting, lodging, and growth conditions.* Industrial Crops and Products, 2001, vol. 14, no. 2, p. 145-154, DOI: https://doi.org/10.1016/S0926-6690(01)00078-4.

[44] H. S. Ramaswamy, B. M. Ahuja, and S. Krishnamoorthy, *Behaviour of concrete reinforced with jute, coir and bamboo fibres.* International Journal of Cement Composites and Lightweight Concrete, 1983, vol. 5, no. 1, p. 3-13, DOI: https://doi.org/10.1016/0262-5075(83)90044-1.

[45] L. Arnaud and E. Gourlay, *Experimental study of parameters influencing mechanical properties of hemp concretes.* Construction and Building Materials, 2012, vol. 28, no. 1, p. 50-56, DOI: https://doi.org/10.1016/j.conbuildmat.2011.07.052.

[46] S. Elfordy, F. Lucas, F. Tancret, Y. Scudeller, et al., *Mechanical and thermal properties of lime and hemp concrete ("hempcrete") manufactured by a projection process.* Construction and Building Materials, 2008, vol. 22, no. 10, p. 2116-2123, DOI: https://doi.org/10.1016/j.conbuildmat.2007.07.016.

[47] E. P. Aigbomian and M. Fan, *Development of Wood-Crete building materials from sawdust and waste paper*. Construction and Building Materials, 2013, vol. 40, p. 361-366, DOI: https://doi.org/10.1016/j.conbuildmat.2012.11.018.

[48] P. B. De Bruijn, K.-H. Jeppsson, K. Sandin, and C. Nilsson, *Mechanical properties of lime–hemp concrete containing shives and fibres.* Biosystems Engineering, 2009, vol. 103, no. 4, p. 474-479, DOI: https://doi.org/10.1016/j.biosystemseng.2009.02.005.

[49] V. Dubois, E. Wirquin, C. Flament, and P. Sloma, *Fresh and hardened state properties of hemp concrete made up of a large proportion of quarry fines for the production of blocks.* Construction and Building Materials, 2016, vol. 102, p. 84-93, DOI: https://doi.org/10.1016/j.conbuildmat.2015.10.196.

[50] I. Merta and E. K. Tschegg, *Fracture energy of natural fibre reinforced concrete.* Construction and Building Materials, 2013, vol. 40, p. 991-997, DOI: https://doi.org/10.1016/j.conbuildmat.2012.11.060.

[51] C. Niyigena, S. Amziane, and A. Chateauneuf. *Investigating Hemp Concrete Mechanical Properties Variability Due to Hemp Particles*. in *Mechanics of Composite and Multi-functional Materials, Volume 7*. 2017. Cham: Springer International Publishing DOI: https://doi.org/10.1007/978-3-319-41766-0_2.

[52] C. Niyigena, S. Amziane, and A. Chateauneuf, *Multicriteria analysis demonstrating the impact of shiv on the properties of hemp concrete.* Construction and Building Materials, 2018, vol. 160, p. 211-222, DOI: https://doi.org/10.1016/j.conbuildmat.2017.11.026.

[53] M. Ildikó, K. Katalin, and K. T. Elmar, *Durability of Hemp Fibres in the alkaline environment of cement matrix*, in *8th RILEM International Symposium on Fiber*

Reinforced Concrete: challenges and opportunities (BEFIB 2012), J.A.O. Barros, Editor. 2012, RILEM Publications SARL. p. 671 - 679.

[54] E. Awwad, M. Mabsout, B. Hamad, M. T. Farran, et al., *Studies on fiber-reinforced concrete using industrial hemp fibers.* Construction and Building Materials, 2012, vol. 35, p. 710-717, DOI: https://doi.org/10.1016/j.conbuildmat.2012.04.119.

[55] E. Awwad, B. Hamad, M. Mabsout, and H. Khatib, *Sustainable concrete using hemp fibers.* Proceedings of the ICE - Construction Materials, 2012, vol. 166, p. 45-53, DOI: https://doi.org/10.1680/coma.11.00006.

[56] M. E. Alves Fidelis, R. Dias Toledo Filho, F. de Andrade Silva, V. Mechtcherine, et al., *The effect of accelerated aging on the interface of jute textile reinforced concrete.* Cement and Concrete Composites, 2016, vol. 74, p. 7-15, DOI: https://doi.org/10.1016/j.cemconcomp.2016.09.002.

[57] Y. Li, Y.-W. Mai, and L. Ye, *Sisal fibre and its composites: a review of recent developments.* Composites Science and Technology, 2000, vol. 60, no. 11, p. 2037-2055, DOI: https://doi.org/10.1016/S0266-3538(00)00101-9.

[58] S. Liu, L. Ge, S. Gao, L. Zhuang, et al., *Activated carbon derived from bio-waste hemp hurd and retted hemp hurd for CO2 adsorption.* Composites Communications, 2017, vol. 5, p. 27-30, DOI: https://doi.org/10.1016/j.coco.2017.06.002.

[59] K. Ip and A. Miller, *Life cycle greenhouse gas emissions of hemp–lime wall constructions in the UK.* Resources, Conservation and Recycling, 2012, vol. 69, p. 1-9, DOI: https://doi.org/10.1016/j.resconrec.2012.09.001.

[60] A. L. Fernando, N. Rettenmaier, P. Soldatos, and C. Panoutsou, *8 - Sustainability of Perennial Crops Production for Bioenergy and Bioproducts*, in *Perennial Grasses for Bioenergy and Bioproducts*, E. Alexopoulou, Editor. 2018, Academic Press. p. 245-283 DOI: https://doi.org/10.1016/B978-0-12-812900-5.00008-4.

[61] M. Perić, M. Komatina, D. Antonijević, B. Bugarski, et al., *Life Cycle Impact Assessment of Miscanthus Crop for Sustainable Household Heating in Serbia.* Forests, 2018, vol. 9, no. 10, DOI: https://doi.org/10.3390/f9100654.

[62] M. Freudiger, *Construction material on a plant basis and method for the producing of this construction material*. 2002: Switzerland. Patent. EP 1 554 228 B1.

[63] H. Höhn, *Building material with a plant filler*. 2004: Luxembourg. Patent. EP 1 765 742 B1.

[64] H. Höhn, *Building material with plant filler*. 2007: Luxembourg. Patent. EP 2 069 255 B1.

[65] J. Peters, *Material or dry blend with vegetable aggregate*. 2008: Luxembourg / Germany. Patent. EP 2 154 117 A1.

[66] I. Höhn and H. Höhn, *Construction material with filler or vegetable origin*. 2008: Luxembourg. Patent. EP 2 177 489 B1.

[67] F. Jacquemot and P. Rougeau, *Agro-sourced lightweight concrete and use thereof*. 2013: France. Patent. EP 2 724 996 A2.

[68] J. Michels, *Bearing capacity of steel fibre reinforced concrete flat slabs*. Doctoral Dissertation, 2009, University of Luxembourg: Luxembourg.

[69] K. Holschemacher, T. Mueller, and Y. Ribakov, *Effect of steel fibres on mechanical properties of high-strength concrete.* Materials & Design (1980-2015), 2010, vol. 31, no. 5, p. 2604-2615, DOI: https://doi.org/10.1016/j.matdes.2009.11.025.

[70] A. F. David and E. N. Antoine, *Stress-Strain Properties of Fiber Reinforced Mortar in Compression.* ACI Journal Proceedings, vol. 82, no. 4, DOI: https://doi.org/10.14359/10359.

[71] H. A. Homayoun and M. Denis, *Influence of Steel Fibers on Tension Stiffening.* ACI Structural Journal, vol. 94, no. 6, DOI: https://doi.org/10.14359/9736.

[72] R. V. Balendran, F. P. Zhou, A. Nadeem, and A. Y. T. Leung, *Influence of steel fibres on strength and ductility of normal and lightweight high strength concrete.* Building and Environment, 2002, vol. 37, no. 12, p. 1361-1367, DOI: https://doi.org/10.1016/S0360-1323(01)00109-3.

[73] J. Bothma. *Literature Review on Macro Synthetic Fibres in Concrete*. 2013.

[74] M. Rezania, H. Moradnezhad, M. Panahandeh, M. Kami, et al., *Effects of Diethanolamine (DEA) and Glass Fibre Reinforced polymer (GFRP) on setting time and mechanical properties of shotcrete.* Journal of Building Engineering, 2020, vol. 31, p. 101343, DOI: https://doi.org/10.1016/j.jobe.2020.101343.

[75] H. Su, J. Xu, and W. Ren, *Mechanical properties of ceramic fiber-reinforced concrete under quasi-static and dynamic compression.* Materials & Design, 2014, vol. 57, p. 426-434, DOI: https://doi.org/10.1016/j.matdes.2013.12.061.

[76] S. Akihama, T. Suenaga, and T. Banno, *The behaviour of carbon fibre reinforced cement composites in direct tension.* International Journal of Cement Composites and Lightweight Concrete, 1984, vol. 6, no. 3, p. 159-168, DOI: https://doi.org/10.1016/0262-5075(84)90004-6.

[77] Y. G. Barabanshchikov, A. Turkebayev, A. Dalabayev, and D. Tleukhanov, *Influence of Synthetic Fibers Dispersed Reinforced Concrete.* Applied Mechanics and Materials, 2015, vol. 725-726, p. 543-558, DOI: https://doi.org/10.4028/www.scientific.net/AMM.725-726.543.

[78] B. Schultheis, *Mam Lëtzebuerger Pilzkenner hu mer iwwer d'Champignonen zu Lëtzebuerg geschwat*, in *Am Gespréich*, C. Ludowicy, Editor. 01.10.2018, RTL.LU: RTL.LU.

[79] J. Houbraken, R. P. de Vries, and R. A. Samson, *Chapter Four - Modern Taxonomy of Biotechnologically Important Aspergillus and Penicillium Species*, in *Advances in Applied Microbiology*, S. Sariaslani and Gadd, G.M., Editors. 2014, Academic Press. p. 199-249 DOI: https://doi.org/10.1016/B978-0-12-800262-9.00004-4.

[80] D. Nigam, M. Asthana, and A. Kumar, *Chapter 10 - Penicillium: A Fungus in the Wine and Beer Industries*, in *New and Future Developments in Microbial Biotechnology and Bioengineering*, V.K. Gupta and Rodriguez-Couto, S., Editors. 2018, Elsevier: Amsterdam. p. 187-200 DOI: https://doi.org/10.1016/B978-0-444-63501-3.00010-7.

[81] S. Blanc, *Vector Transmission of Plant Viruses*, in *Encyclopedia of Virology (Third Edition)*, B.W.J. Mahy and Van Regenmortel, M.H.V., Editors. 2008, Academic Press: Oxford. p. 274-282 DOI: https://doi.org/10.1016/B978-012374410-4.00433-7.

[82] B. Chen, B. Ke, L. Ye, S. Jin, et al., *Isolation and varietal characterization of Ganoderma resinaceum from areas of Ganoderma lucidum production in China.* Scientia Horticulturae, 2017, vol. 224, p. 109-114, DOI: https://doi.org/10.1016/j.scienta.2017.06.002.

[83] H. Acikel, *The use of miscanthus (Giganteus) as a plant fiber in concrete production.* Scientific Research and Essays, 2011, vol. 6, no. 13, p. 2660-2667.

[84] O. Onuaguluchi and N. Banthia, *Plant-based natural fibre reinforced cement composites: A review.* Cement and Concrete Composites, 2016, vol. 68, p. 96-108, DOI: https://doi.org/10.1016/j.cemconcomp.2016.02.014.

[85] L. Courard and V. Parmentier, *Carbonated Miscanthus mineralized aggregates for reducing environmental impact of lightweight concrete blocks.* Sust. Build., 2017, vol. 2, p. 9, DOI: https://doi.org/10.1051/sbuild/2017004.

[86] A. Eschenhagen, M. Raj, N. Rodrigo, A. Zamora, et al., *Investigation of Miscanthus and Sunflower Stalk Fiber-Reinforced Composites for Insulation Applications.* Advances in Civil Engineering, 2019, vol. 2019, p. 9328087, DOI: https://doi.org/10.1155/2019/9328087.

[87] J. C. Clifton-Brown and I. Lewandowski, *Water Use Efficiency and Biomass Partitioning of Three Different Miscanthus Genotypes with Limited and Unlimited Water Supply.* Annals of Botany, 2000, vol. 86, no. 1, p. 191-200, DOI: https://doi.org/10.1006/anbo.2000.1183.

[88] A. VanLoocke, T. E. Twine, M. Zeri, and C. J. Bernacchi, *A regional comparison of water use efficiency for miscanthus, switchgrass and maize.* Agricultural and Forest Meteorology, 2012, vol. 164, p. 82-95, DOI: https://doi.org/10.1016/j.agrformet.2012.05.016.

[89] J. Yan, C. Zhu, W. Liu, F. Luo, et al., *High photosynthetic rate and water use efficiency of Miscanthus lutarioriparius characterize an energy crop in the semiarid temperate region.* GCB Bioenergy, 2015, vol. 7, no. 2, p. 207-218, DOI: https://doi.org/10.1111/gcbb.12118.

[90] R. El Hage, Y. Khalaf, C. Lacoste, M. Nakhl, et al., *A flame retarded chitosan binder for insulating miscanthus/recycled textile fibers reinforced biocomposites.* Journal of Applied Polymer Science, 2019, vol. 136, no. 13, p. 47306, DOI: https://doi.org/10.1002/app.47306.

[91] T. Schnabel, H. Huber, A. Petutschnigg, and A. Jäger, *Analysis of plant materials pre-treated by steam explosion technology for their usability as insulating materials.* Agronomy Research, 2019, vol. 17, p. 1191-1198, DOI: https://doi.org/10.15159/AR.19.061.

[92] R. Abhijith, A. Ashok, and C. R. Rejeesh, *Sustainable packaging applications from mycelium to substitute polystyrene: a review.* Materials Today: Proceedings, 2018, vol. 5, no. 1, Part 2, p. 2139-2145, DOI: https://doi.org/10.1016/j.matpr.2017.09.211.

[93] L. Jiang, D. Walczyk, G. McIntyre, and W. K. Chan, *Cost modeling and optimization of a manufacturing system for mycelium-based biocomposite parts.* Journal of Manufacturing Systems, 2016, vol. 41, p. 8-20, DOI: https://doi.org/10.1016/j.jmsy.2016.07.004.

[94] E. Elsacker, S. Vandelook, J. Brancart, E. Peeters, et al., *Mechanical, physical and chemical characterisation of mycelium-based composites with different types of lignocellulosic substrates.* PLOS ONE, 2019, vol. 14, no. 7, p. e0213954, DOI: https://doi.org/10.1371/journal.pone.0213954.

[95] Z. Yang, F. Zhang, B. Still, M. White, et al., *Physical and Mechanical Properties of Fungal Mycelium-Based Biofoam.* Journal of Materials in Civil Engineering, 2017, vol. 29, no. 7, p. 04017030, DOI: https://doi.org/10.1061/(ASCE)MT.1943-5533.0001866.

[96] C. Cavette, *Concrete Block,* How Products Are Made 2021; Available from: https://www.encyclopedia.com/manufacturing/news-wires-white-papers-and-books/concrete-block.

[97] I. Soto Izquierdo, O. Soto Izquierdo, M. A. Ramalho, and A. Taliercio, *Sisal fiber reinforced hollow concrete blocks for structural applications: Testing and modeling.* Construction and Building Materials, 2017, vol. 151, p. 98-112, DOI: https://doi.org/10.1016/j.conbuildmat.2017.06.072.

[98] E. Awwad, Choueiter, and H. Khatib. *Concrete Masonry Blocks Reinforced with Local Industrial Hemp Fibers and Hurds*. in *Proceedings of the 3rd International Conference on Sustainable Construction Materials and Technologies (SCMT3)*. 2013. Kyoto Research Park, Kyoto, Japan.

[99] M. Gunther, *Prehistoric Temples of Malta,* Art-and-archeaology.com 1998; Available from: http://www.art-and-archaeology.com/malta/malta.html.

[100] K. B. Anand and K. Ramamurthy, *Development and Performance Evaluation of Interlocking-Block Masonry.* Journal of Architectural Engineering, 2000, vol. 6, no. 2, p. 45-51, DOI: https://doi.org/10.1061/(ASCE)1076-0431(2000)6:2(45).

[101] M. Martínez and S. Atamturktur, *Experimental and numerical evaluation of reinforced dry-stacked concrete masonry walls.* Journal of Building Engineering, 2019, vol. 22, p. 181-191, DOI: https://doi.org/10.1016/j.jobe.2018.12.007.

[102] M. Kohail, H. Elshafie, A. Rashad, and H. Okail, *Behavior of post-tensioned dry-stack interlocking masonry shear walls under cyclic in-plane loading.* Construction and Building Materials, 2019, vol. 196, p. 539-554, DOI: https://doi.org/10.1016/j.conbuildmat.2018.11.149.

[103] Contern S.A., *Catalogue produits (Gros oeuvre),* 2021.

[104] M. Ali, R. J. Gultom, and N. Chouw, *Capacity of innovative interlocking blocks under monotonic loading.* Construction and Building Materials, 2012, vol. 37, p. 812-821, DOI: https://doi.org/10.1016/j.conbuildmat.2012.08.002.

[105] H. Ben Ayed, O. Limam, M. Aidi, and A. Jelidi, *Experimental and numerical study of Interlocking Stabilized Earth Blocks mechanical behavior.* Journal of Building Engineering, 2016, vol. 7, p. 207-216, DOI: https://doi.org/10.1016/j.jobe.2016.06.012.

[106] M. S. Jaafar, A. H. Alwathaf, W. A. Thanoon, J. Noorzaei, et al., *Behaviour of interlocking mortarless block masonry.* Proceedings of the Institution of Civil Engineers - Construction Materials, 2006, vol. 159, no. 3, p. 111-117, DOI: https://doi.org/10.1680/coma.2006.159.3.111.

[107] G. G. Chewe Ngapeya, D. Waldmann, and F. Scholzen, *Impact of the height imperfections of masonry blocks on the load bearing capacity of dry-stack masonry walls.* Construction and Building Materials, 2018, vol. 165, p. 898-913, DOI: https://doi.org/10.1016/j.conbuildmat.2017.12.183.

[108] S. Agaajani, *Development and investigation of a new dry-stacked wall system*. Doctoral Dissertation, 2015, University of Luxembourg: Luxembourg. Available from: http://hdl.handle.net/10993/21575.

[109] G. G. Chewe Ngapeya and D. Waldmann, *Experimental and analytical analysis of the load-bearing capacity Pu of improved dry-stacked masonry.* Journal of Building Engineering, 2020, vol. 27, DOI: https://doi.org/10.1016/j.jobe.2019.100927.

[110] G. Vasconcelos and P. B. Lourenço, *Experimental characterization of stone masonry in shear and compression.* Construction and Building Materials, 2009, vol. 23, no. 11, p. 3337-3345, DOI: https://doi.org/10.1016/j.conbuildmat.2009.06.045.

[111] C. members, *EN1996-1-1:2005, Eurocode 6 - Design of masonry structures - Part 1-1: General rules for reinforced and unreinforced masonry structures*. 2005.

[112] J. A. Greenwood and J. B. P. Williamson, *Contact of nominally flat surfaces.* Proceedings of the Royal Society A: Mathematical, Physical and Engineering Sciences, 1966, DOI: https://doi.org/10.1098/rspa.1966.0242.

[113] Y. Yin and Y. Fan, *Influence of Roughness on Shear Bonding Performance of CFRP-Concrete Interface.* Materials, 2018, vol. 11, no. 10, DOI: https://doi.org/10.3390/ma11101875.

[114] G. G. Chewe Ngapeya and D. Waldmann, *Overcome of bed-joint imperfections and improvement of actual contact in dry-stacked masonry.* Construction and Building Materials, 2020, vol. 233, DOI: https://doi.org/10.1016/j.conbuildmat.2019.117173.

[115] T. Zahra and M. Dhanasekar, *Characterisation and strategies for mitigation of the contact surface unevenness in dry-stack masonry.* Construction and Building Materials, 2018, vol. 169, p. 612-628, DOI: https://doi.org/10.1016/j.conbuildmat.2018.03.002.

[116] A. Pogačnik and M. Kalin, *How to determine the number of asperity peaks, their radii and their heights for engineering surfaces: A critical appraisal.* Wear, 2013, vol. 300, no. 1, p. 143-154, DOI: https://doi.org/10.1016/j.wear.2013.01.105.

[117] Y. Zhao, D. M. Maietta, and L. Chang, *An Asperity Microcontact Model Incorporating the Transition From Elastic Deformation to Fully Plastic Flow.* Journal of Tribology, 1999, vol. 122, no. 1, p. 86-93, DOI: https://doi.org/10.1115/1.555332.

[118] H. R. Pasaribu and D. J. Schipper, *Application of a Deterministic Contact Model to Analyze the Contact of a Rough Surface Against a Flat Layered Surface.* Journal of Tribology, 2005, vol. 127, no. 2, p. 451-455, DOI: https://doi.org/10.1115/1.1866163.

[119] A. G. Quarrell, *The Hardness of Metals.* Nature, 1952, vol. 170, no. 4333, p. 818-818, DOI: https://doi.org/10.1038/170818b0.

[120] M. A. Sherbiney and J. Halling, *Friction and wear of ion-plated soft metallic films.* Wear, 1977, vol. 45, no. 2, p. 211-220, DOI: https://doi.org/10.1016/0043-1648(77)90075-8.

[121] K. C. Tang and R. D. Arnell, *Determination of coating mechanical properties using spherical indenters.* Thin Solid Films, 1999, vol. 355-356, p. 263-269, DOI: https://doi.org/10.1016/S0040-6090(99)00444-7.

[122] J. A. Greenwood, *A Unified Theory of Surface Roughness.* Proceedings of the Royal Society A: Mathematical, Physical and Engineering Sciences, 1984, vol. 393, no. 1804, p. 133-157, DOI: https://doi.org/10.1098/rspa.1984.0050.

[123] Service Central de Législation, boulevard F.-D. Roosevelt, L-2450 Luxembourg, *Mémorial A – N° 146 du 1er août 2016*, in *Règlement grand-ducal du 23 juillet 2016 modifiant le Règlement grand-ducal du 30.11.2007 concernant la performance énergétique des bâtiments d'habitations*. Association momentanée Imprimerie Centrale / Victor Buck: Luxembourg, 2016.

[124] J. Pierzchlewicz, *Modern concrete wall-units with improved thermal resistance for housing in hot climate.* Sci. Technol., 1996, vol. 1, p. 69-80.

[125] N. Leufgens, *Mechanische und thermische Untersuchungen zur Entwicklung eines Wärmedämmsteines aus Leichtbeton*, in *FSTC*. Doctoral thesis, 2010, University of Luxembourg: Luxembourg.

[126] M. Zukowski and G. Haese, *Experimental and numerical investigation of a hollow brick filled with perlite insulation.* Energy and Buildings, 2010, vol. 42, no. 9, p. 1402-1408, DOI: https://doi.org/10.1016/j.enbuild.2010.03.009.

[127] K. S. Al-Jabri, A. W. Hago, A. S. Al-Nuaimi, and A. H. Al-Saidy, *Concrete blocks for thermal insulation in hot climate.* Cement and Concrete Research, 2005, vol. 35, no. 8, p. 1472-1479, DOI: https://doi.org/10.1016/j.cemconres.2004.08.018.

[128] Liapor, *LiaTop50*, 2021 [cited 11-02-2021]; Available from: https://www.liapor.com/at/anwendungen/hochbau/steine/liatop-50.html.

[129] ISOTEX, *BLOCS DE COFFRAGE STANDARD - HDIII Graphite*, 2021 [cited 11-02-2021]; Available from: https://www.isotexfrance.com/les-blocs-de-coffrage-isotex/.

[130] Al Manaratain, *Insulated Blocks and Sanwich Block*, 2021 [cited 11-02-2021]; Available from: https://almanaratain.com/product/insulated-blocks/.

[131] M. Kurpinska and L. Kułak, *Predicting Performance of Lightweight Concrete with Granulated Expanded Glass and Ash Aggregate by Means of Using Artificial Neural Networks.* Materials, 2019, vol. 12, no. 12, DOI: https://doi.org/10.3390/ma12122002.

[132] H.-G. Ni and J.-Z. Wang, *Prediction of compressive strength of concrete by neural networks.* Cement and Concrete Research, 2000, vol. 30, no. 8, p. 1245-1250, DOI: https://doi.org/10.1016/S0008-8846(00)00345-8.

[133] F. Altun, Ö. Kişi, and K. Aydin, *Predicting the compressive strength of steel fiber added lightweight concrete using neural network.* Computational Materials Science, 2008, vol. 42, no. 2, p. 259-265, DOI: https://doi.org/10.1016/j.commatsci.2007.07.011.

[134] I. C. Yeh, *Modeling of strength of high-performance concrete using artificial neural networks.* Cement and Concrete Research, 1998, vol. 28, no. 12, p. 1797-1808, DOI: https://doi.org/10.1016/S0008-8846(98)00165-3.

[135] İ. B. Topçu and M. Saridemir, *Prediction of compressive strength of concrete containing fly ash using artificial neural networks and fuzzy logic.* Computational Materials Science, 2008, vol. 41, no. 3, p. 305-311, DOI: https://doi.org/10.1016/j.commatsci.2007.04.009.

[136] C. Özel, *Prediction of compressive strength of concrete from volume ratio and Bingham parameters using adaptive neuro-fuzzy inference system (ANFIS) and data mining.* African Journal of Business Management, 2011, vol. 6, DOI: https://doi.org/10.5897/IJPS11.1181.

[137] P. Chopra, R. Sharma, and D. Kumar, *Regression models for the prediction of compressive strength of concrete with & without fly ash.* International Journal of Latest Trends in Engineering and Technology, 2014, vol. 3, p. 400-406.

[138] M. Nikoo, P. Zarfam, and H. Sayahpour, *Determination of compressive strength of concrete using Self Organization Feature Map (SOFM).* Engineering with Computers, 2015, vol. 31, no. 1, p. 113-121, DOI: https://doi.org/10.1007/s00366-013-0334-x.

[139] R. Aggarwal, M. Kumar, R. K. Sharma, and M. K. Sharma, *Predicting Compressive Strength of Concrete.* International Journal of Applied Science and Engineering, 2015, vol. 13, no. 2, p. 171-185, DOI: https://doi.org/10.6703/IJASE.2015.13(2).171.

[140] Z. R. Yang and Z. Yang, *6.01 - Artificial Neural Networks*, in *Comprehensive Biomedical Physics*, A. Brahme, Editor. 2014, Elsevier: Oxford. p. 1-17 DOI: https://doi.org/10.1016/B978-0-444-53632-7.01101-1.

[141] I. C. Yeh, *Design of High-Performance Concrete Mixture Using Neural Networks and Nonlinear Programming.* Journal of Computing in Civil Engineering, 1999, vol. 13, no. 1, p. 36-42, DOI: https://doi.org/10.1061/(ASCE)0887-3801(1999)13:1(36).

[142] M. M. Alshihri, A. M. Azmy, and M. S. El-Bisy, *Neural networks for predicting compressive strength of structural light weight concrete.* Construction and Building Materials, 2009, vol. 23, no. 6, p. 2214-2219, DOI: https://doi.org/10.1016/j.conbuildmat.2008.12.003.

[143] A. F. Bingöl, A. Tortum, and R. Gül, *Neural networks analysis of compressive strength of lightweight concrete after high temperatures.* Materials & Design (1980-2015), 2013, vol. 52, p. 258-264, DOI: https://doi.org/10.1016/j.matdes.2013.05.022.

[144] S. Das, P. Pal, and R. Singh, *Prediction of Concrete Mix Proportion using ANN Technique.* 2015, vol. 2, p. 820-825.

[145] J. A. Thompson, S. Roecker, S. Grunwald, and P. R. Owens, *Chapter 21 - Digital Soil Mapping: Interactions with and Applications for Hydropedology*, in *Hydropedology*, H. Lin, Editor. 2012, Academic Press: Boston. p. 665-709 DOI: https://doi.org/10.1016/B978-0-12-386941-8.00021-6.

[146] G. B. M. Heuvelink and R. Webster, *Modelling soil variation: past, present, and future.* Geoderma, 2001, vol. 100, no. 3, p. 269-301, DOI: https://doi.org/10.1016/S0016-7061(01)00025-8.

[147] S. Malek, C. Hui, N. Aziida, S. Cheen, et al., *Ecosystem Monitoring Through Predictive Modeling*, in *Encyclopedia of Bioinformatics and Computational Biology*, S. Ranganathan, Gribskov, M., Nakai, K., and Schönbach, C., Editors. 2019, Academic Press: Oxford. p. 1-8 DOI: https://doi.org/10.1016/B978-0-12-809633-8.20060-5.

[148] P. Shrestha Bijaya, L. Duckstein, and Z. Stakhiv Eugene, *Fuzzy Rule-Based Modeling of Reservoir Operation.* Journal of Water Resources Planning and Management, 1996, vol. 122, no. 4, p. 262-269, DOI: https://doi.org/10.1061/(ASCE)0733-9496(1996)122:4(262).

[149] D. J. Bartholomew, *Analysis and Interpretation of Multivariate Data*, in *International Encyclopedia of Education (Third Edition)*, P. Peterson, Baker, E., and McGaw, B., Editors. 2010, Elsevier: Oxford. p. 12-17 DOI: https://doi.org/10.1016/B978-0-08-044894-7.01303-8.

[150] M. F. M. Zain and S. M. Abd, *Multiple Regression Model for Compressive Strength Prediction of High Performance Concrete.* Journal of Applied Sciences, 2009, vol. 9, DOI: https://doi.org/10.3923/jas.2009.155.160.

[151] J. L. Huang, P. Y. Huang, Z. W. Li, and X. H. Zheng, *Prediction of Bond Strength of FRP-Concrete Based on Multiple Linear Regression Method.* Advanced Materials

Research, 2011, vol. 163-167, p. 3623-3628, DOI: https://doi.org/10.4028/www.scientific.net/AMR.163-167.3623.

[152] A. Omran Behzad, Q. Chen, and R. Jin, *Comparison of Data Mining Techniques for Predicting Compressive Strength of Environmentally Friendly Concrete.* Journal of Computing in Civil Engineering, 2016, vol. 30, no. 6, p. 04016029, DOI: https://doi.org/10.1061/(ASCE)CP.1943-5487.0000596.

[153] N.-D. Hoang, A.-D. Pham, Q.-L. Nguyen, and Q.-N. Pham, *Estimating Compressive Strength of High Performance Concrete with Gaussian Process Regression Model.* Advances in Civil Engineering, 2016, vol. 2016, p. 2861380, DOI: https://doi.org/10.1155/2016/2861380.

[154] M. Pal and S. Deswal, *Modelling pile capacity using Gaussian process regression.* Computers and Geotechnics, 2010, vol. 37, no. 7, p. 942-947, DOI: https://doi.org/10.1016/j.compgeo.2010.07.012.

[155] I. Lewandowski, J. C. Clifton-Brown, J. M. O. Scurlock, and W. Huisman, *Miscanthus: European experience with a novel energy crop.* Biomass and Bioenergy, 2000, vol. 19, no. 4, p. 209-227, DOI: https://doi.org/10.1016/S0961-9534(00)00032-5.

[156] N. Brosse, A. Dufour, X. Meng, Q. Sun, et al., *Miscanthus: a fast-growing crop for biofuels and chemicals production.* Biofuels, Bioproducts and Biorefining, 2012, vol. 6, no. 5, p. 580-598, DOI: https://doi.org/10.1002/bbb.1353.

[157] R. Pude, C. H. Treseler, and G. Noga, *Morphological, chemical and technical parameters of Miscanthus genotypes.* Journal of Applied Botany and Food Quality, 2004, vol. 78, no. 1, p. 58-63.

[158] M. Bołtryk and E. Pawluczuk, *Properties of a lightweight cement composite with an ecological organic filler.* Construction and Building Materials, 2014, vol. 51, p. 97-105, DOI: https://doi.org/10.1016/j.conbuildmat.2013.10.065.

[159] H. Archila, S. Kaminski, D. Trujillo, E. Zea Escamilla, et al., *Bamboo reinforced concrete: a critical review.* Materials and Structures, 2018, vol. 51, no. 4, DOI: https://doi.org/10.1617/s11527-018-1228-6.

[160] M. Bołtryk, A. Krupa, and E. Pawluczuk, *Modification of the properties of the cement composites with the organic filler*. Construction and Building Materials, 2018, vol. 167, p. 143-153, DOI: https://doi.org/10.1016/j.conbuildmat.2018.02.025.

[161] J. Page, M. Sonebi, and S. Amziane, *Design and multi-physical properties of a new hybrid hemp-flax composite material*. Construction and Building Materials, 2017, vol. 139, p. 502-512, DOI: https://doi.org/10.1016/j.conbuildmat.2016.12.037.

[162] Y. Chen, Q. L. Yu, and H. J. H. Brouwers, *Acoustic performance and microstructural analysis of bio-based lightweight concrete containing miscanthus*. Construction and Building Materials, 2017, vol. 157, p. 839-851, DOI: https://doi.org/10.1016/j.conbuildmat.2017.09.161.

[163] L. Chupin, S. Arnoult, M. Brancourt-Hulmel, C. Lapierre, et al., *Polyethylene composites made from below-ground miscanthus biomass*. Industrial Crops and Products, 2017, vol. 109, p. 523-528, DOI: https://doi.org/10.1016/j.indcrop.2017.09.007.

[164] B. Elim, W. G. Hime, and C. C. Staff, *The role of calcium chloride in concrete*, 1976 [cited 2020]; Available from: http://www.concreteconstruction.net/how-to/materials/the-role-of-calcium-chloride-in-concrete_o.

[165] X. Pang, P. Boul, and W. Cuello Jimenez, *Isothermal calorimetry study of the effect of chloride accelerators on the hydration kinetics of oil well cement*. Construction and Building Materials, 2015, vol. 77, p. 260-269, DOI: https://doi.org/10.1016/j.conbuildmat.2014.12.077.

[166] P. Rapp, *Effect of calcium chloride on portland cements and concretes*. Research of the National Bureau of Standards, 1935, vol. 14, p. 499-517.

[167] E. C. f. standardisation, *Section 5.2: Basic requirements for composition of concrete*, in *EN 206: Concrete - Specification, performance, production and conformity*. 2013: Brussels

[168] M. A. Mansur and M. A. Aziz, *A study of jute fibre reinforced cement composites*. International Journal of Cement Composites and Lightweight Concrete, 1982, vol. 4, no. 2, p. 75-82, DOI: https://doi.org/10.1016/0262-5075(82)90011-2.

[169] E. C. f. standardisation, *Section 11: Lightweight aggregate concrete structures*, in *EN 1992: Design of concrete structures - Part 1-1: General rules and rules for buildings*. 2004: Brussels

[170] E. C. f. standardisation, *Section 3.1: Concrete*, in *EN1992: Design of concrete structures - Part 1-1: General rules and rules for buildings*. 2004: Brussels

[171] S. Geräte, *Manual shrinkage drain*, 2017 [cited 2017]; Available from: http://www.schleibinger.com/cmsimple/downloads/manual_shrinkage_drain_04-07-2017.pdf.

[172] E. M. Gartner, J. F. Young, D. A. Damidot, and I. Jawed, *Hydration of Portland cement*, in *Structure and performance of cements*. 2002, Spon Press: London and New York. p. 57-113

[173] B. Sagmeister, *Optimization of the mixture of no-fines lightweight concrete*. Betonwerk + Fertigteil-Technik, 1999, vol. 65, no. 11, p. 71-77.

[174] P. Pereira Dias and D. Waldmann, *Optimisation of the mechanical properties of Miscanthus lightweight concrete.* Construction and Building Materials, 2020, vol. 258, p. 119643-119656, DOI: https://doi.org/10.1016/j.conbuildmat.2020.119643.

[175] F. Tröger, G. Wegener, and C. Seemann, *Miscanthus and flax as raw material for reinforced particleboards.* Industrial Crops and Products, 1998, vol. 8, no. 2, p. 113-121, DOI: https://doi.org/10.1016/S0926-6690(97)10017-6.

[176] A. Bourmaud and S. Pimbert, *Investigations on mechanical properties of poly(propylene) and poly(lactic acid) reinforced by miscanthus fibers.* Composites Part A: Applied Science and Manufacturing, 2008, vol. 39, no. 9, p. 1444-1454, DOI: https://doi.org/10.1016/j.compositesa.2008.05.023.

[177] J. Girones, L. Vo, S. Arnoult, M. Brancourt-Hulmel, et al., *Miscanthus stem fragment – Reinforced polypropylene composites: Development of an optimized preparation procedure at small scale and its validation for differentiating genotypes.* Polymer Testing, 2016, vol. 55, p. 166-172, DOI: https://doi.org/10.1016/j.polymertesting.2016.08.023.

[178] R. Muthuraj, M. Misra, and A. K. Mohanty, *Biocomposite consisting of miscanthus fiber and biodegradable binary blend matrix: compatibilization and performance evaluation.* RSC Advances, 2017, vol. 7, no. 44, p. 27538-27548, DOI: https://doi.org/10.1039/C6RA27987B.

[179] J. Salvadó, J. A. Velásquez, and F. Ferrando, *Binderless fiberboard from steam exploded Miscanthus Sinensis: optimization of pressing and pretreatment conditions.* Wood Science and Technology, 2003, vol. 37, no. 3, p. 279-286, DOI: https://doi.org/10.1007/s00226-003-0186-4.

[180] R. Pude, P. Banaszuk, R. Trettin, and G. Noga, *Suitability of Phragmites for lightweight concrete.* Journal of Applied Botany and Food Quality, 2005, vol. 79, p. 141-146.

[181] M. A. Kewalramani and R. Gupta, *Concrete compressive strength prediction using ultrasonic pulse velocity through artificial neural networks.* Automation in Construction, 2006, vol. 15, no. 3, p. 374-379, DOI: https://doi.org/10.1016/j.autcon.2005.07.003.

[182] F. Khademi, M. Akbari, S. M. Jamal, and M. Nikoo, *Multiple linear regression, artificial neural network, and fuzzy logic prediction of 28 days compressive strength of concrete.* Frontiers of Structural and Civil Engineering, 2017, vol. 11, no. 1, p. 90-99, DOI: https://doi.org/10.1007/s11709-016-0363-9.

[183] C.-E. 197-1:2011, *Cement Part 1: Composition, specifications and conformity criteria for common cements* 2011.

[184] C.-E. 459-1:2015, *Building lime - Part 1: Definitions, specifications and conformity criteria*. 2015.

[185] J. S. Pozo-Antonio, *Evolution of mechanical properties and drying shrinkage in lime-based and lime cement-based mortars with pure limestone aggregate.* Construction and Building Materials, 2015, vol. 77, p. 472-478, DOI: https://doi.org/10.1016/j.conbuildmat.2014.12.115.

[186] M. J. Mosquera, B. Silva, B. Prieto, and E. Ruiz-Herrera, *Addition of cement to lime-based mortars: Effect on pore structure and vapor transport.* Cement and Concrete

Research, 2006, vol. 36, no. 9, p. 1635-1642, DOI: https://doi.org/10.1016/j.cemconres.2004.10.041.

[187] C.-E. 196-1:2005, *Methods of testing cement - Part 1: Determination of strength*. 2016.

[188] B. E. 12390-7:2019, *Testing hardened concrete. Density of hardened concrete*. 2019.

[189] M. Guo and J. S. Hesthaven, *Reduced order modeling for nonlinear structural analysis using Gaussian process regression.* Computer Methods in Applied Mechanics and Engineering, 2018, vol. 341, p. 807-826, DOI: https://doi.org/10.1016/j.cma.2018.07.017.

[190] Mathworks, *Statistics and Machine Learning Toolbox*, 2021.

[191] G. ABC, *2019 Global Status Report for Buildings and Construction*. 2019, Global Alliance for Buildings and Construction. p. 12.

[192] C. Maalouf, C. Ingrao, F. Scrucca, T. Moussa, et al., *An energy and carbon footprint assessment upon the usage of hemp-lime concrete and recycled-PET façades for office facilities in France and Italy.* Journal of Cleaner Production, 2018, vol. 170, p. 1640-1653, DOI: https://doi.org/10.1016/j.jclepro.2016.10.111.

[193] G. Balčiūnas, S. Vėjelis, S. Vaitkus, and A. Kairytė, *Physical Properties and Structure of Composite Made by Using Hemp Hurds and Different Binding Materials.* Procedia Engineering, 2013, vol. 57, p. 159-166, DOI: https://doi.org/10.1016/j.proeng.2013.04.023.

[194] M. Rubenstein, *Emissions from the Cement Industry*, 2012 [cited 2020]; Available from: https://blogs.ei.columbia.edu/2012/05/09/emissions-from-the-cement-industry/.

[195] C.-F. J. Kuo, C.-H. Lin, and M.-W. Hsu, *Analysis of intelligent green building policy and developing status in Taiwan.* Energy Policy, 2016, vol. 95, p. 291-303, DOI: https://doi.org/10.1016/j.enpol.2016.04.046.

[196] F. Collet, M. Bart, L. Serres, and J. Miriel, *Porous structure and water vapour sorption of hemp-based materials.* Construction and Building Materials, 2008, vol. 22, no. 6, p. 1271-1280, DOI: https://doi.org/10.1016/j.conbuildmat.2007.01.018.

[197] J. Figala, V. Vranová, K. Rejšek, and P. Formánek, *Giant Miscanthus (Miscantus x Giganteus Greef Et Deu.) - A Promising Plant for Soil Remediation: A Mini Review*. Acta Universitatis Agriculturae et Silviculturae Mendelianae Brunensis, 2015, vol. 63, p. 2241-2246, DOI: https://doi.org/10.11118/201563062241.

[198] H. Wang, P.-C. Chiang, Y. Cai, C. Li, et al., *Application of Wall and Insulation Materials on Green Building: A Review*. Sustainability, 2018, vol. 10, no. 9, DOI: https://doi.org/10.3390/su10093331.

[199] M. Fourmentin, P. Faure, P. Pelupessy, V. Sarou-Kanian, et al., *NMR and MRI observation of water absorption/uptake in hemp shives used for hemp concrete*. Construction and Building Materials, 2016, vol. 124, p. 405-413, DOI: https://doi.org/10.1016/j.conbuildmat.2016.07.100.

[200] J. Clifton-Brown, A. Hastings, M. Mos, J. P. McCalmont, et al., *Progress in upscaling Miscanthus biomass production for the European bio-economy with seed-based hybrids*. GCB Bioenergy, 2017, vol. 9, no. 1, p. 6-17, DOI: https://doi.org/10.1111/gcbb.12357.

[201] E. C. f. standardization, *Cement -Part 1: Composition, specifications and conformity criteria for common cements*, in *DIN EN 197-1:2011-11 Cement -Part 1: Composition, specifications and conformity criteria for common cements*. 2011

[202] G. H. Tattersall and P. H. Baker, *The effect of vibration on the rheological properties of fresh concrete*. Magazine of Concrete Research, 1988, vol. 40, no. 143, p. 79-89, DOI: https://doi.org/10.1680/macr.1988.40.143.79.

[203] FUJIFILM, *Fujifilm's measurement film solution - Structure and principle*, 2020 [cited 2020]; Available from: https://www.fujifilm.com/products/measurement_film/en/prescale/feature/.

[204] E. C. f. standardisation, *Section 3.1.6: Design compressive and tensile strengths*, in *EN1992: Design of concrete structures - Part 1-1: General rules and rules for buildings*. 2004: Brussels

[205] H. Xu, W. Zhou, R. Xie, L. Da, et al., *Characterization of Rock Mechanical Properties Using Lab Tests and Numerical Interpretation Model of Well Logs*. Mathematical

Problems in Engineering, 2016, vol. 2016, p. 5967159, DOI: https://doi.org/10.1155/2016/5967159.

[206] Z. Sanal, *Stochastik/Normalverteilung*, in *Mathematik für Ingenieure*. 2015, Springer: Wiesbaden. p. 373-411 DOI: https://doi.org/10.1007/978-3-658-10642-3.

[207] K. J. Willam and E. P. Warnke, *Constitutive models for the triaxial behavior of concrete.* Proceedings of the International Assoc. for Bridge and Structural Engineering, 1975, vol. 19, p. 1-30.

[208] N. Stevulova, J. Cigasova, P. Purcz, I. Schwarzova, et al., *Water Absorption Behavior of Hemp Hurds Composites.* Materials, 2015, vol. 8, p. 2243-2257, DOI: https://doi.org/10.3390/ma8052243.

[209] H. N. Dhakal, Z. Y. Zhang, and M. O. W. Richardson, *Effect of water absorption on the mechanical properties of hemp fibre reinforced unsaturated polyester composites.* Composites Science and Technology, 2007, vol. 67, no. 7, p. 1674-1683, DOI: https://doi.org/10.1016/j.compscitech.2006.06.019.

[210] A. Célino, S. Fréour, F. Jacquemin, and P. Casari, *Characterization and modeling of the moisture diffusion behavior of natural fibers.* Journal of Applied Polymer Science, 2013, vol. 130, no. 1, p. 297-306, DOI: https://doi.org/10.1002/app.39148.

[211] P. L. Domone, *Self-compacting concrete: An analysis of 11 years of case studies.* Cement and Concrete Composites, 2006, vol. 28, no. 2, p. 197-208, DOI: https://doi.org/10.1016/j.cemconcomp.2005.10.003.

[212] V. Picadet, *Bulk Density and Compressibility*, in *Bio-aggregates Based Building Materials* A. Sofiane and Florence, C., Editors. 2017, Springer, Dordrecht. p. 111-124 DOI: https://doi.org/10.1007/978-94-024-1031-0.

[213] S. Pavía, *Effect of Testing Variables (Method of Production)*, in *Bio-aggregates Based Building Materials : State-of-the-Art Report of the RILEM Technical Committee 236-BBM*, S. Amziane and Collet, F., Editors. 2017, Springer Netherlands: Dordrecht. p. 189-201 DOI: https://doi.org/10.1007/978-94-024-1031-0_9.

[214] X. Chen, Y. Huang, C. Chen, J. Lu, et al., *Experimental study and analytical modeling on hysteresis behavior of plain concrete in uniaxial cyclic tension.* International Journal of Fatigue, 2017, vol. 96, p. 261-269, DOI: https://doi.org/10.1016/j.ijfatigue.2016.12.002.

[215] A. Sikora, *European Green Deal – legal and financial challenges of the climate change.* ERA Forum, 2021, vol. 21, no. 4, p. 681-697, DOI: https://doi.org/10.1007/s12027-020-00637-3.

[216] M. L. Smith, J. N. Bruhn, and J. B. Anderson, *The fungus Armillaria bulbosa is among the largest and oldest living organisms.* Nature, 1992, vol. 356, no. 6368, p. 428-431, DOI: https://doi.org/10.1038/356428a0.

[217] L. Courard, A. Darimont, A. Louis, and F. Michel, *Mineralization of bio-based materials: effect on cement-based mix properties.* 2011.

[218] Stowa, *From biomass to Mycelium composite: An exploration on cellulose and weed residues*, STOWA, Editor. 2019: Amersfoort - NL.

[219] M. Jones, A. Mautner, S. Luenco, A. Bismarck, et al., *Engineered mycelium composite construction materials from fungal biorefineries: A critical review.* Materials & Design, 2020, vol. 187, p. 108397, DOI: https://doi.org/10.1016/j.matdes.2019.108397.

[220] O. Robertson, F. Høgdal, L. McKay, and T. Lenau. *Fungal Future: A review of mycelium biocomposites as an ecological alternative insulation material*. 2020. Lyngby, Denmark: NordDESIGN DOI: https://doi.org/10.35199/NORDDESIGN2020.18.

[221] EOTA, *ETAG 004*, in *European Organisation for Technical Approvals*. 2013: Brussels

[222] F. Domínguez-Muñoz, B. Anderson, J. M. Cejudo-López, and A. Carrillo-Andrés, *Uncertainty in the thermal conductivity of insulation materials.* Energy and Buildings, 2010, vol. 42, no. 11, p. 2159-2168, DOI: https://doi.org/10.1016/j.enbuild.2010.07.006.

[223] L. K. Norford, L. R. Glicksman, H. S. Harvey, and J. A. Charlson, *Development of Low-Cost Wheat-Straw Insulation Board.* HVAC&R Research, 1999, vol. 5, no. 3, p. 249-263, DOI: https://doi.org/10.1080/10789669.1999.10391236.

[224] G. C. Carolina and B. S. Antonio José, *Estudio de la variación en la conductividad térmica de la cascarilla de arroz aglomerada con fibras vegetales.* Ingeniería y Desarrollo, 2002, vol. 12, p. 1-9.

[225] N. T. I. GmbH, *NETZSCH TAURUS Instruments*; Available from: https://www.taurus-instruments.de/en/product/thermal-conductivity-measuring-devices/with-guarded-hot-plate/.

[226] M. Pruteanu, *Investigations Regarding the Thermal Conductivity of Straw.* Bulletin of the Polytechnic Institute of Jassy, Constructions, Architechture Section, 2010, vol. LVI (LX)(3).

[227] F. Collet and S. Pretot, *Thermal conductivity of hemp concretes: Variation with formulation, density and water content.* Construction and Building Materials, 2014, vol. 65, p. 612-619, DOI: https://doi.org/10.1016/j.conbuildmat.2014.05.039.

[228] T. L. Bergmann, A. S. Lavine, F. P. Incropera, and D. P. DeWitt, *Fundamentals of Heat and Mass Transfer*. 2018, Hoboken, N.J.: John Wiley & Sons.

[229] EN 13501-2, *Fire classification of construction products and building elements - Part 2: Classification using data from fire resistance tests, excluding ventilation services*. 2003, EUROPEAN COMMITTEE FOR STANDARDIZATION: Brussels.

[230] Association d'assurance accident, *Recommandations de prévention (Brochure complète)*, in *Installations et réglementations de service*. Association d'assurance accident,: aaa.public.lu, 05/2011.